PATTERNS AND DRIVERS OF RIVERINE PARTICULATE ORGANIC CARBON TRANSPORT IN AN ANDEAN VALLEY



Kathryn E. Clark

Linacre College

&

School of Geography and the Environment

Thesis submitted to the University of Oxford in fulfilment of the requirements for the degree of Doctor of Philosophy.

Oxford Hilary 2014

Patterns and drivers of riverine particulate organic carbon transport in an Andean Valley

Kathryn Clark, Linacre College

Thesis submitted to the University of Oxford in fulfilment of the requirements for the degree of Doctor of Philosophy. Hilary 2014

Abstract

Physical erosion can mobilise particulate organic carbon (POC) from vegetation and soil, representing an export of primary productivity from ecosystems, and a lateral transfer of carbon recently-derived from the atmosphere. These carbon transfers are thought to be enhanced in mountain forests where erosion rates are high. However, the rates and controls on POC transfer remain poorly constrained, as does the impact of POC export on carbon cycling at regional and global scales. This thesis takes an interdisciplinary approach to address this issue, using remote sensing, river geochemistry, river hydrology, and geomorphic mapping in the Kosñipata Valley, in the Central Andes of Peru. Its main aims are to: 1) estimate stream discharge throughout the year and to evaluate the water balance and sources; 2) quantify the source of riverine POC, accounting for POC derived from sedimentary rocks (POC_{fossil}) to examine the POC eroded from soils and vegetation ($POC_{non\text{-}fossil}$); 3) quantify river POC yields; 4) assess the hillslope processes that erode POC; and 5) assess how POC export impacts the carbon balance of mountain forest, and how fluvial transfer impacts the wider carbon cycle.

Stream flow was monitored from January 2010 to February 2011 at two newly installed river gauging stations in the Kosñipata Valley at 2250 m (Wayqecha, 48.5 km^2) and 1360 m (San Pedro, 164.4 km^2). Then annual water balance for the San Pedro catchment was quantified. Rainfall inputs of 3028 mm and cloud water inputs of 308 ± 97 mm were

balanced by outputs via stream runoff (2721 mm) and actual evapotranspiration (907 mm), leaving a residual of -294 ± 97 mm (< ~10 % of water inputs).

The source of POC in river suspended sediment samples was quantified using radiocarbon ($\Delta^{14}C$, ‰), stable carbon isotopes, and the nitrogen to carbon ratio. This revealed that river $POC_{non\text{-}fossil}$ was sourced from very young organic carbon in the valley ($\Delta^{14}C$ ~50 ‰) and that POC_{fossil} comprised 43 % of total POC. Combining the hydrometric measurements with river samples, annual particulate load fluxes were quantified. The vast majority (73 % to 77 %) of the annual suspended sediment transfer and POC (both POC_{fossil} and $POC_{non\text{-}fossil}$) occurred in the wet season over a period of 4 months. The suspended sediment yield for the valley (960 – 1200 t km^{-2} yr^{-1}) was consistent with those for the Andean portion of the Madre de Dios River into which the Kosñipata River drains. The river $POC_{non\text{-}fossil}$ yield was 5.2 – 6.9 tC km^{-2} yr^{-1}.

Landslides are likely to have played an important role in the mobilisation of $POC_{non\text{-}fossil}$. A detailed landslide mapping using 25 years of remote sensing data revealed that on average 0.09 % of the valley per year is impacted by this mass-wasting process. These landslides mobilise ~28 tC km^{-2} yr^{-1} of soil and vegetation valley-wide. The discrepancy between the landslide erosional flux and fluvial $POC_{non\text{-}fossil}$ export suggests an important fraction of the $POC_{non\text{-}fossil}$ harvested by landslides is either exported as coarse debris (not quantified in the fluvial $POC_{non\text{-}fossil}$ flux), remains buried onsite, or is degraded and respired onsite. Landslides also played an important ecosystem function, turning over some sections of the mountain forest within ~625 years, with a 1200 year valley-wide mean.

On the basin scale, the Madre de Dios River drains ~ 6 % of the Amazonian Andes. This study enables estimation of the delivery of POC to the lowland Amazon Basin. Using the observation that $POC_{non\text{-}fossil}$ and POC_{fossil} fluxes were closely linked with suspended

sediment transfer, total yields of ~0.22 MtC yr^{-1} and ~0.17 MtC yr^{-1}, respectively, were estimated from this section of the Andes. The export of $POC_{non\text{-}fossil}$ from mountain forests by rivers represents 0.4 – 1.0 % yr^{-1} of the net primary productivity of Andean forest and so even if only a small portion of this is buried in sedimentary deposits, it may promote the Andes as a carbon sink. These results demonstrate the long-term influence of erosional processes in the cycling of carbon in the Amazon Basin.

Acknowledgements

My research was made possible because of the generous financial support I received from the following: the Clarendon Fund from Oxford University, the Overseas Research Scholarship from the British government (ORS), and the Natural Sciences and Engineering Research Council of Canada (NSERC). Additionally, radiocarbon analysis was carried out under a grant awarded by the National Environmental Research Council (NERC) on allocation # 1516.0910. I am extremely grateful for this funding. Finally, I appreciate the travel grants from the Environmental Change Institute (ECI), the Oxford University Centre for the Environment (OUCE), Linacre College, the Geochemical Society, the American Geophysical Union (AGU), and the Santander fund.

I would like to acknowledge the efforts of many people who provided advice and guidance throughout the duration of this research: Oxford supervisors Yadvinder Malhi and Mark New, and unofficial supervisors Bob Hilton (Durham University) and Josh West (University of Southern California). They were great mentors and helped me to become an independent researcher. Their valuable critiques and insights greatly helped shape the thesis.

My main field assistant Arturo Robles Caceres, played a pivotal role in Peru carrying out and organising field collections. Thank you to my field assistants: Laura Morales, Raul Jackson Abarca Martínez, Mags Yurca Hurtado, Rogelio Paja Yurka, Juan Alberto “Beto” Gibaja Lopez, Judit Huamán Ovalle, Israel Cuba Torres, Armando “Tomy” Alfaro-Tapia, Dante Oviedo Licona, Johny Farfan Flores, Rosalbina Butrón Loayza, David Ocampo, Yorka Gutiérrez Usca, Juan Costa Taborga, Harol Alagon Huaman, Sarah Federman, and Emeterio Nunoncca Sencia. I would like to thank ACCA (Asociación para la Conservación de la Cuenca Amazónica) at the Wayqecha and Los Amigos fieldstations, Incaterra at the San Pedro field site, and CREES (Conservation, Research and Education towards Environmental Sustainability) at the Manu Learning Centre (MLC). As well, I would like to express my

appreciation to Anna Maria Lechuga at Labquim in Cusco for providing me with many necessary supplies for the field.

Valuable comments from my transfer of status examiners Josh Fisher and Simon Dadson, and from my confirmation of status examiners Kate Halladay and Simon Dadson were appreciated.

Thank you to Darren Gröcke, Charlotte Bryant, Mark Torres, Philippa Ascough who ran my samples for geochemical analyse in their labs and to Simon Abele for working through several ArcGIS issues with me. I have several collaborators through the ABERG (Andes Biodiversity and Ecosystems Research Group) team to whom I am grateful for their input and support, especially Greg Asner, Josh Fisher, Josh Rapp, Miles Silman, Sassan Saatchi, Aline Horwath, Toby Marthews, Robin Martin, William Farfan, and Carlos “Beto” Quesada. Thank you to the students at USC and University of Durham who have used data or samples that I collected over my DPhil: Mark Torres, Yanning Rao, Natalie Ballew, and Renee Wang. Thank you to Joan Arthur and Jane Applegarth for the much appreciated help with sample shipments and equipment purchases. I thank Ruth Saxton, of the OUCE and Jackie Favarin, of Linacre College for all of the DPhil administrative work.

Fellow researchers in the Ecosystems lab provided support and encouragement throughout the duration of this research, most notably, Kate Halladay, Norma Salinas, Liana Anderson, Imma Oliveras, Terhi Riutta, Toby Marthews, Greg Goldsmith, Chris Doughty, Przemyslaw Zelazowski, David Galbraith, Josh Fisher, Stephen Heathcote, Royd Vinya, Sam Moore, Alex Morel, and Cecile Girardin.

Throughout this DPhil, my family, especially my parents Sue and Bruce Clark, and my Nana Jean Mitchell, provided emotional and financial support. Thank you especially to my mother who was very helpful in last minute thesis preparations and editing.

My time in Oxford was accompanied by many supportive friends from Linacre College, the LGBT society, and the OUAWFC (Oxford University Women's Association Football Club). I would specifically like to thank Méabh Brennan, Meghan Bailey, Katrin Wilhelm, Kate Halladay, Norma Salinas, Alex Neroth van Vogelpoel, Courtney Traub, Gaia Donati, Ben Sabatini, Maria New, Roya Haghighat-Khah, Carmel Levitan, Sarah Rouse, Lizzy Button, Rob Noble, Andrew Faull, Simon Driscoll, and Meleesa Naughton.

Finally, I would also like to thank my Peruvian contingent; I could not have survived the fieldwork frenzy in Peru without the friendship and support of *mis amigas* Rosalbina Butrón Loayza, Yolvi Valdez Tejeira, Mireya Natividad "Naty" Raurau Quisiyupanqui, Judit Huamán Ovalle, and our beloved Flor "Florcita" Zamora.

Dedicated to my parents Susan Clark and the late Bruce Clark

Table of contents

Patterns and drivers of riverine particulate organic carbon transport in an Andean Valley iii
Abstract iii
Acknowledgements vi
Table of contents xi
List of Tables xv
List of Figures xvi
Acronyms, notations and abbreviations xxii
Chapter 1 : Introduction 1
1.1. Approach 1
1.2. Aims 3
1.3. Thesis structure 4
1.4. Study area 7
Chapter 2 : Literature review 14
2.1. Introduction 14
2.2. General overview 14
2.2.1. The importance of the Andes 14
2.2.2. Mountains 15
2.2.3. The Amazon River 15
2.3. River hydrology 16
2.3.1. Amazon Basin 16
2.3.2. Tropical montane cloud forests 17
2.3.3 Groundwater 17
2.4. River suspended sediment and POC 18
2.4.1. Global perspective 18
2.4.2. Fossil POC and non-fossil POC 19
2.4.3. Mountain POC 20
2.4.4. Andean POC 20
2.4.5. Transport of $POC_{non\text{-}fossil}$ 21
2.4.6. Climate 22
2.4.7. $POC_{non\text{-}fossil}$ and the C cycle 22
2.5. Landslides 23
2.5.1. Landslide dynamics 23
2.5.2. Landslide mechanics and fluvial incision 24
2.5.3. Landslide mapping techniques 25
2.5.4. Landslides as an ecological agent 26
2.5.5. Landslides and carbon 27
2.5.6. Landslides and river POC 28
2.6. References 29
Linking statement: Chapter 2 to 3 42
Chapter 3 : The hydrological regime of a forested tropical Andean valley 44
Abstract 45
3.1. Introduction 46
3.2. Study area 49
3.3. Materials and methods 52
3.3.1. Discharge and runoff measures 52
3.3.2. Catchment wide rainfall estimates 54
3.3.3. Water isotope measurements 55

3.3.4. Actual evapotranspiration estimates *57*
3.4. Results 58
3.4.1. Discharge and runoff *58*
3.4.2. Catchment wide rainfall *59*
3.4.3. Isotopic analyses and mixing calculations *60*
3.4.4. Cloud water in streamflow *65*
3.5. Discussion 67
3.5.1. Water balance *67*
3.5.2. Quickflow, baseflow and hysteresis *70*
3.5.2.1. Quickflow *70*
3.5.2.2. Baseflow *70*
3.5.2.3. Hysteresis *71*
3.5.3. Causes for hysteresis *75*
3.5.3.1. Soil water *75*
3.5.3.2. Groundwater *77*
3.6. Conclusions 78
3.7. Acknowledgements 79
3.8. References 81
Chapter 3: Supplementary information: **90**
S3.1. Materials and methods 90
S3.1.1. Discharge and runoff measures *90*
S3.1.1.1. San Pedro gauging station *90*
S3.1.1.2. Wayqecha gauging station *95*
S3.1.2. Catchment wide rainfall estimates *96*
S3.1.3. Water isotope measurements *99*
S3.1.4. Water isotope mixing model *105*
S3.1.5. Actual evapotranspiration estimates *113*
S3.2. Results 114
S3.2.1. Isotopic analysis *114*
S3.3. Tables for supplementary information 116
S3.4. References for supplementary information 117
Linking statement: Chapter 3 to 4 ..... **120**
Chapter 4 : New views on 'old' carbon in the Amazon River: Insight from the source of organic carbon eroded from the Peruvian Andes **122**
Abstract 123
4.1. Introduction 124
4.2. Study area 126
4.3. Materials and methods 129
4.3.1. Sample collection and hydrometric measurements *129*
4.3.2. Geochemical analyses *130*
4.4. Results 133
4.4.1. Suspended load and river stage height *133*
4.4.2. Elemental geochemistry *135*
4.4.3. Isotope geochemistry *137*
4.4.4 Evidence for Mixing of POC Sources *138*
4.5. Discussion 140
4.5.1 Source of Andean POC *140*
4.5.2 Hydrologic and geomorphic controls on POC source *143*

4.5.3. Implications for Supply of Andean POC to the Amazon River *146*
4.6. Conclusions 149
4.7. Acknowledgements 150
4.8. References 151
Linking statement: Chapter 4 to 5 ..... **159**
Chapter 5 : Fluvial incision links landslides, carbon transfer and plant diversity in an Andean Valley **161**
Abstract 162
5.1. Introduction 163
5.2. Study area 165
5.3. Materials and methods 169
5.3.1. Landslide mapping *169*
5.3.2. Landslide frequency, turnover and probability *170*
5.3.3. Landslide revegetation *172*
5.4. Results and discussion 173
5.4.1. Landslide frequencies and patterns *173*
5.4.2. Link between landslide frequency and river incision and implications for the threshold hillslope model of topographic evolution *174*
5.4.3. Role of rainfall and earthquakes for spatial landslide patterns? *177*
5.4.4. Landslides and the mobilization of organic material *179*
5.4.5. Revegetation of landslide scars *183*
5.4.6. Influence of incision-driven hillslope steepening and failure on plant composition: *184*
5.5. Conclusions 187
5.6. Acknowledgements 188
5.7. References 189
Chapter 5: Supplementary information: **196**
S5.1. Materials and methods 196
S5.1.1. Landslide mapping *196*
S5.1.2. Landsat imagery limitations *197*
S5.1.3. Landslide frequencies and turnover *202*
S5.1.4. Landslide probability *204*
S5.1.5. High resolution DEM *204*
S5.1.6. STRM DEM *205*
S5.2. Tables for supplementary information 206
S5.3. Figures for supplementary information 208
S5.4. References for supplementary information 211
Linking statement: Chapter 5 to 6 ..... **213**
Chapter 6 : Export of particulate organic carbon by an Andean river and implications of its delivery to the lowland Amazon River **215**
Abstract 216
6.1. Introduction 217
6.2. Study Area 219
6.3. Materials and Methods 222
6.3.1. Sample collection and hydrometric measurements *222*
6.3.2. Geochemical analyses *223*
6.3.3. Rating curves *225*
6.3.4. Annual sediment yields *226*
6.4. Results 227

6.4.1. Elemental and isotope geochemistry *227*
6.4.2. End member mixing analysis *229*
6.4.3. Sediment and POC rating curves *230*
6.4.4. Suspended load behaviour *231*
6.4.4.1. San Pedro gauging station *231*
6.4.4.2. Wayqecha gauging station *232*
6.4.4.3. Rating curve accuracy *233*
6.4.4.4. Inter-basin comparisons *234*
6.4.5. Annual transfer *235*
6.5. Discussion 237
6.5.1. Fluvial transport of $POC_{non\text{-}fossil}$ *237*
6.5.2. Controls on sediment and POC export *239*
6.5.2.1. Climate *239*
6.5.2.2. Landslides *241*
6.5.3. Global controls on $POC_{non\text{-}fossil}$ yields in mountain river catchments *243*
6.5.4. $POC_{non\text{-}fossil}$ export and the carbon budget of Andean forest *245*
6.5.5. Andean POC export and contribution to the Amazon Basin carbon budget *247*
6.6. Conclusions 250
6.7. Acknowledgements 251
6.8. References 253
Chapter 6: Supplementary information: **263**
S6.1. Tables for supplementary information 263
S6.2. Figures for supplementary information 269
S6.3. References for supplementary information 274
Chapter 7 : Conclusions **275**
7.1. Review of main findings 275
7.1.1. River hydrology *275*
7.1.2. Fossil and non-fossil river POC *276*
7.1.3. Landslide activity *277*
7.1.4. Mobilisation of carbon due to landslide activity *277*
7.1.5. River suspended sediment and POC fluxes *278*
7.1.6. Climatic and physical forcing of river suspended load *279*
7.2. Implications of findings 279
7.3. Future research needs 283
7.4. Concluding remarks 285
7.5. References 286

List of Tables

Table 3.1: Descriptions of the Wayqecha and San Pedro catchments on the Kosñipata River.....49

Table 3.2: Seasonal and annual results for the San Pedro (SP; 164.4 km^2) and Wayqecha (WQ; 48.5 km^2) catchments. Water year considered from February 2010 to January 2011.....59

Table 3.3: Breakdown of streamflow into its sources 67

Table 4.1: Catchment descriptions 128

Table 4.2: Suspended sediment river samples.....136

Table 6.1: Descriptions of the Wayqecha and San Pedro catchments on the Kosñipata River.....221

Table 6.2: Suspended sediment and POC fluxes for the Kosñipata Valley 230

List of Figures

Figure 1.1: Kosñipata Valley around the San Pedro gauging station. Many of these landslides (brown scars) occurred in a single storm event March 4th 2010. This photo was taken by Gregory P. Asner of the Carnegie Institution for Science in 2010. 7

Figure 1.2: a) This large bedrock landslide occurred in 2007. The crown of the landslide is ~2500 masl. The landslide area is 156,400 m^2 and the debris trail cleared 90,100 m^2. b) The road was washed out by this landslide, but that didn't stop people from carrying on. Note the truck (left) and people (right). Photos were taken by a) William Farfan Rios in 2009 and b) Kathryn Clark in March 2010. .. 8

Figure 1.3: a) The Kosñipata Valley is not full of landslides. This picture was taken from the puna grasslands (~3500 masl) down into the tropical montane cloud forest valley. b) The valley is often submersed in cloud. This picture was taken at San Pedro ~1400 masl. The photos were taken by Kathryn Clark in November 2009 and February 2010. 9

Figure 1.4: a) When I arrived to San Pedro in the dry season to set everything up the river was only ~11 m wide and clear. b) I was in for a big surprise when the wet season abruptly arrived at the end of November 2009 and the rivers quickly converted from clear channels to sediment-rich flash flood and the channel was ~17 m wide and murky. David collected our biggest suspended sediment sample (~18,000 g m^{-3}) of the river campaign. c) The wet season changes the river channel completely. Besides entraining POC, the river mobilises large boulders over time. Photos by a) Kathryn Clark in August 2009, b) David Ocampo in November 2009, and c) Kathryn Clark in January 2010. 10

Figure 1.5: After two installations the river height logger was in place and worked for most of the year. Eventually the large boulder on the left moved on top of the sensor, hence why measurements stopped in February 2011. Photo taken by Kathryn Clark in September 2010. 11

Figure 1.6: a) Judit taking a river sample from the Kosñipata River at the San Pedro gauging during the 2-week experiment. b) Arturo taking a much larger volume sample in the dry season. Photos taken by Kathryn Clark in February 2010 and September 2010 respectively. 11

Figure 1.7: a) Beto and b) Dante taking samples during the 2-week wet season sampling campaign from the Wayqecha gauging station in the headwaters of the Kosñipata River. 12

Figure 1.8: a) Wet season baseline flow at Wayqecha, measured during the two-week campaign at the end of January 2010 and b) dry season baseflow flow at Wayqecha gauging station in August 2010. 12

Figure 1.9: a) Bright-eyed and bushy tailed I arrived to the valley for the first time with Arturo to do a landslide inventory. We are on the road outside the Wayqecha field station. The Kosñipata valley below with the Amazon covered in a blanket of cloud. b) Post-Peru sickness and back to the field for another month with my makeshift rope belt. I also measured all the tributaries that intersected with the road each month over the year. c) Here Arturo and I pose in front a fresh landslide. This landslide occurred around ~1300 masl during the largest storm of the year March 4th 2010. d) We are en route to collect the largest $POC_{non\text{-}fossil}$ sample of the campaign (116 g m^{-3}) at midnight. Photos by Kathryn Clark June 2009, Rosalbina Butrón October 2009, Kathryn Clark in March 2010, and Judit Huamán in February 4th 2010. 13

Figure 2.1: River suspended sediment yield versus the $POC_{non\text{-}fossil}$ yield for 11 catchments in Taiwan [*Hilton et al.*, 2012], the western Southern Alps of New Zealand [*Korup et al.*, 2004; *Hilton et al.*, 2008a], the Santa Clara and Alsea Rivers in the West Coast of the USA [*Hatten et al.*, 2012], and a headwater catchment in the Swiss Alps [*Smith et al.*, 2013]. 21

Figure 3.1: a) The study area in the Eastern Andes of Peru is in the Kosñipata River Valley. The purple lines delineate the two basins: the Wayqecha catchment is the smaller basin and the San Pedro catchment is the larger basin encompassing the Wayqecha catchment. The hydrologic gauging stations are WQ = Wayqecha and SP = San Pedro. The shaded elevation is from shuttled radar topography mission (SRTM) digital elevation model (DEM) with a 90 x 90 m resolution. The TRMM 3B43 tile used in this study (cf. Figure 3.3a) is shown by the black box outline. The met stations used for rainfall data in this study are numbered 1 – 9 (Table S3.2). b) The Kosñipata River flows into the Alto Madre de Dios (AMdD) and then into the Madre de Dios River. c) The Madre de Dios River joins the Madeira River and then flows into the Amazon River. 50

Figure 3.2: Runoff (Q; mm d^{-1}) over the study period for the Wayqecha and San Pedro gauging stations in the Kosñipata Valley. Rainfall from the Wayqecha meteorological station is on the secondary axis (mm d^{-1}). The San Pedro runoff (Q – SP) and baseline runoff (Q_b – SP) were measured nearly continuously through the year, with a 31-day gap partly in July and August that is covered by three manual measurements. The Wayqecha runoff (Q – WQ) was measured throughout the year from a daily to a monthly interval. 54

Figure 3.3: a) Available mean monthly rainfall data for the 9 meteorological stations in the Kosñipata Valley (dark dashes and light error bars) and estimated mean monthly rainfall (grey circles and dark error bars) covering the months of the 1-year study period (February 2010 to January 2011) determined using the linear regression equations for each met station derived from tropical rainfall measuring mission (TRMM) data outlined in Table S3.8. The error bars are 2 x standard error. The linear regression is derived from the mean monthly met station rainfall data derived from TRMM versus elevation (mm $month^{-1}$ = -0.1216 × elevation + 593.16). Available mean monthly rainfall for 5 meteorological stations outside of the study area but within the larger Madre de Dios Basin (triangles) [*Rapp and Silman*, 2012]. The shaded box shows the TRMM 3B43 v7a monthly mean rainfall for the 1-year study period plus 2 x standard error and with the elevational range of the 34.5 x 34.5 km tile. The altitudinal range of the study area is represented by the dashed lines at 1350 and 4000 masl. b) Linear regressions, valid only for the Kosñipata Valley (~1000 to 4000 masl), of estimated catchment wide rainfall by month from February 2010 to January 2011, color-coded by season. c) and d) The breakdown of annual rainfall contribution by season, for the San Pedro catchment (c) and Wayqecha catchment (d) at 100 m intervals following the monthly linear regressions. Note uneven distribution of rainfall throughout the valley; there is a higher rainfall rate at lower elevations (b), but because of the basin distribution the overall rainfall input is estimated to be at mid-elevations (c). The catchment-wide seasonal and annual estimated rainfall values are summarised in Table 3.2. 56

Figure 3.4: Catchment wide TRMM calibrated rainfall for the San Pedro catchment from 1998 to 2012. The red shaded area represents the 1-year study period. 61

Figure 3.5: δD (‰) and Dxs (‰) of rainwater (square symbols), dry season cloud water vapour (yellow diamonds), and river water (grey circles) from within the San Pedro catchment. Rainwater samples from the dry season (yellow) were from May to August and the wet season (green) from December to March. All error bars correspond to two standard deviations. The grey shaded regions encompass the mean δD and Dxs values and one standard deviation for each end-member (i.e. wet season rainfall, dry season rainfall, and dry season cloud water vapour). The ranges defined by these grey boxes were used to generate random sets of end-member compositions for the three end-member mixing model. 61

Figure 3.6: Time series of δD_{river}, Dxs_{river}, and the calculated mixing proportions for the San Pedro catchment. For all of the panels, the coloured backgrounds refer to seasonal changes in precipitation

with green signifying the wet season (Dec. to Mar.), blue signifying the transition from the wet to dry season (Apr.), yellow signifying the dry season (May to Aug.), and red signifying the transition from the dry to wet season (Oct. to Nov). a) The time series of δD_{river} values with error bars signifying 2 standard deviations. b) The time series of Dxs_{river} values with error bars signifying 2 standard deviations. c) Time series of the 5^{th} (lower error bar), 50^{th} (open circle), and 95^{th} percentile (upper error bar) values of the distribution of fractional contributions of wet season rain to river discharge calculated using the three end-member mixing model. d) Time series of the 5^{th} (lower error bar), 50^{th} (open square), and 95^{th} percentile (upper error bar) values of the distribution of fractional contributions of dry season rain to river discharge calculated using the three end-member mixing model. e) Time series of the 5^{th} (lower error bar), 50^{th} (open diamond), and 95^{th} percentile (upper error bar) values of the distribution of fractional contributions of cloud water vapour to river discharge calculated using the three end-member mixing model. f) Time series of the mean contributions of wet season rain (circle), dry season rain (square), and cloud water vapour (diamond) to river discharge.. 64

Figure 3.7: Variation in the isotopic composition of river water a) deuterium excess (Dxs_{river}, %) and b) hydrogen isotope ratio (δD_{river}, ‰) plotted versus discharge ($m^3\ s^{-1}$). Variation in the mean contributions to river flow as a function of water discharge for wet season rain (c), dry season rain (d), and cloud water vapour (e) as calculated by the end member mixing analysis, also plotted versus discharge. Refer to source data in Table S3.7..... 66

Figure 3.8: Cumulative water input and output (mm $month^{-1}$) over the 1-year study period (February 2010 to January 2011) as well as for February 2011. Water input comprises rainfall and cloud water interception. Water output comprises runoff, actual evapotranspiration, and residual. The residual was calculated per month from a rearrangement of equation 1. The residual shows that rainfall is stored (positive residual) particularly during January and February, and then subsequently released (negative residual) in the wet-dry transition season (April) and throughout most of the dry season (May to August) when rainfall it is lowest. Hence runoff exceeds rainfall throughout this period. 72

Figure 3.9: Monthly rainfall - runoff plots for the Kosñipata Valley, showing anticlockwise hysteresis. Plots show runoff at San Pedro versus a) catchment wide and b) meteorological station rainfall for the Wayqecha met station; baseflow at San Pedro versus c) catchment wide and d) meteorological station rainfall at Wayqecha; and quickflow at San Pedro versus e) catchment wide and f) meteorological station rainfall at Wayqecha. Monthly-averaged values for daily discharge and met station rainfall were determined by summing daily flux (mm d^{-1}) and taking the mean for each month over the 1-year study period. Days with zero rainfall at Wayqecha station were removed from mean rainfall calculations. Rainfall estimated for the San Pedro catchment was determined by month (see materials and methods). Error bars represent 2 * standard error. Months are numbers 1-12. The months are numbered chronologically and colour coded by season (Table S3.1). The one-to-one line for discharge to rainfall is represented by the grey dashed line. Months with runoff to the left of this line indicate dominance of groundwater discharge. Groundwater dominance (via baseflow) occurs from April to June when compared to catchment wide rainfall (a & c) and from February to July when compared to Wayqecha met station rainfall (b & d). Rainfall at the Wayqecha met station located at 2900 masl (Table S3.2) was lower than the catchment rainfall especially during the latter part of the wet season (February and March), suggesting the importance of rainfall at lower elevations during the wet season. Quickflow was variable throughout the year with a general linear trend with rainfall. 74

Figure 4.1: a) Geological Map of study region in Peru [*Schenk et al.*, 1999] with an inset map of the Amazon Basin with the map area indicated. The stars represent the locations of gauging stations on the Kosñipata River valley (this study) and locations of published Andean POC data are shown by

other symbols [*Mayorga et al.*, 2005]. b) Kosñipata River valley, Peru with elevation (SRTM) and locations of hydrometric and sampling gauging stations. 127

Figure 4.2: River stage height (grey line, m) over the study period for a) San Pedro (161 km^2 watershed area), and b) Wayqecha (50 km^2 watershed area) gauging stations (Figure 4.1b). Samples for geochemical analysis shown as circles with suspended sediment concentration (SSC, mg L^{-1}), where dark fill indicates the sample was also analysed for ^{14}C content. 132

Figure 4.3: Exceedance probability (%) for hydrometric measurements from the Kosñipata River. a) Mean river height (6 hr) over the longer-term study period as light grey dashes, with suspended sediment samples from the yearlong study as dark grey dashes, and with suspended sediment samples from this study as black circles. b) Suspended sediment concentration (mg L^{-1}) of samples collected over the yearlong study as grey dashes and samples from this study as black circles. 135

Figure 4.4: Elemental and isotopic composition of POC in suspended load (circles) from the Kosñipata River. Samples collected from San Pedro as black circles and from Wayqecha as grey circles,, with analytical uncertainties smaller than the point size. a) The stable isotopes of POC ($\delta^{13}C_{org}$, ‰) versus the nitrogen to organic ratio (N/C) , b) $\delta^{13}C_{org}$ (‰) versus the radiocarbon content ($\Delta^{14}C_{org}$, ‰). For display, river materials plotted at the radiocarbon depleted end member ($\Delta^{14}C_{org}$ = -1000 ‰ see main text for discussion). Boxes show ranges from published sources [Zimmermann et al., 2009; Rao, 2011], where O_H and A are soil horizons. 139

Figure 4.5: Organic carbon concentration (C_{org} %) versus modern C_{org} % (C_{org}% × Fraction Modern, F_{mod}) for San Pedro and Wayqecha river POC samples for a single hydrological event. Linear fit is the solid line and 95 % confidence intervals as dashed lines, (r^2 = 0.99, P < 0.0001, n =16). At modern C_{org} = 0 % the fossil contribution can be determined. 142

Figure 4.6: a) The fraction non-fossil POC (F_{nf}) during flood events plotted as circles, with river stage height (m) shown as grey line. The first storm sampled over the study period is shown for San Pedro and other sampled events (Figure 4.2) show a similar pattern. F_{nf} increases as stage height increases. b) F_{nf} versus rate of change of river height over the 6 hours preceding sample collection, with samples from San Pedro as black circles and Wayqecha as grey circles. Positive rate of change indicate the rising limb of flood hydrographs and negative rate of change show the falling limb. In all parts, whiskers show errors on F_{nf} values. 144

Figure 4.7: Stable isotopic composition ($\delta^{13}C_{org}$, ‰) and radiocarbon content ($\Delta^{14}C_{org}$, ‰) of POC for published data and those collected in this study. Andean headwater samples from high altitude sites collected at low turbidity from *Mayorga et al.* [2005] are shown as squares, and from *Townsend-Small et al.* [2007] are shown as squares with crosses. All other samples were collected during the wet season, with Andean samples from the Kosñipata River in this study (black circles), Andean sourced Amazon River samples (dark grey triangles), Amazon River tributaries with no Andean source (light grey triangles), with samples re-classified from *Mayorga et al.* [2005] based on their upstream contributing area. 149

Figure 5.1: a) Ecosystem types in the eastern Andes of Peru [*Consbio*, 2011]. Bare areas are cities, agriculture, glaciers and riverbed, with the Kosñipata Valley field site magnified in the inset. Areas delimited by red polygons are regions of high annual cloud cover > 74 % [*Halladay et al.*, 2012]. b) Georectified geological map [*Mendívil Echevarría and Dávila Manrique*, 1994; *Carlotto Caillaux et al.*, 1996; *Vargas Vilchez and Hipolito Romero*, 1998; *INGEMMET*, 2013], where the sedimentary rocks are on a scale ranging from dark to light colour within each era. Active faults [*Sébrier et al.*, 1985; *Cabrera et al.*, 1991] and documented earthquakes since 1975 [*USGS*, 2013]. 167

Figure 5.2: a) Landslide distribution in the Kosñipata Valley over the 25-year study period mapped from Landsat satellite images with annual resolution, with Landsat topographic shadow regions in light grey. b) Landslide frequency (L_f, % yr^{-1}), and c) forest slope turnover (τ_{ls}, yr) by year on a 1km^2 grid. Grid cells with > 50 % Landsat topographic shadow were removed from the analysis in (b) and (c). 171

Figure 5.3: The proportion of catchment area as a function of elevation for the basin (dotted line) and mapped landslides (dashed line) with the resultant landslide probability (P_{ls}, % yr^{-1}) (solid line). a) Landslide occurrence by pixel, calculated over 300m elevation bin sizes from the 3 m x 3 m DEM, is elevated at low elevations (dashed line is higher than dotted line) and reduced at higher elevations (dashed line lower than dotted line). The non-uniform spatial distribution is reflected in landslide probability (solid line). b) Landslide probability by pixel (at one degree bin size from the slope map created from the same DEM) is greatest at high slopes. Vertical line at 38 ° delineates threshold slope angle where slopes have significantly higher landslide probability. 172

Figure 5.4: Landslide recovery time as percent area recovered by 2011, evaluated from a WorldView-2 pan-sharpened satellite image at 2m x 2m resolution. Each data point represents the landslides from a single year during the study period (black and grey circles; n = 23). Landslides occurring at least 4 years prior to 2011 (black circles) were used to determine equation 1 (area of recovered landslides (%) = 4.394±0.735 × year of landslide origin prior to 2011 – 23.406±10.196), where the mean estimated time for 100 % recovery of all the landslides of a given year is ~28 yrs (r^2 = 0.7, n = 18)..... 173

Figure 5.5: Downstream profiles over 0.44 km^2 swath along the Kosñipata River. a) Stream channel (blue) and min., max., and mean catchment topography (black and grey dashed lines), along with landslide frequencies (red line). Grey box indicates region of incision downstream of prominent knickzone in the river channel at ~1700 m elevation which coincides with significant increase in landslide frequency. b) Inset of the knickzone shown in (a). c) Landslide frequency (red line) with mean normalised precipitation from meteorological station data (dashed light blue), wet season 2B31 TRMM precipitation (dark blue line), and annual 2B31 TRMM precipitation (grey line). 2B31 TRMM is at 4 x 4 km resolution from *Bookhagen* [in review]. 176

Figure 5.6: a) Area-normalised mobilisation of organic carbon (tC km^{-2} yr^{-1}) and b) total mobilisation of carbon by landslides (tC yr^{-1}) over the altitudinal gradient contributed by the soil organic carbon stock (brown line), vegetation carbon stock (dashed line) and sum of soil + vegetation (total, green line). Landslide probability is highest at low elevations so the yield is highest there (a), but the total flux due to landslides is dominated by mid-elevations that comprise the majority of basin area (b). These estimates are for the forested portion of the valley only. See Figure S5.6 for estimates that include puna grasslands. c) Plant species richness (circles) from the Kosñipata forest plots as a function of elevation compared to landslide probability (red line)..... 182

Figure 6.1: a) An altitudinal map, using shuttle radar topographic mission (SRTM) digital elevation model at 90 x 90 m resolution, showing the Wayqecha and San Pedro gauging stations (red triangles) along the Kosñipata River. b) The Kosñipata River feeds the Madre de Dios River a tributary of the Amazon. The Madre de Dios Basin (red outline) at the Miraflores river gauging station (MI, yellow circle) is 124,000 km^2 and the Andean portion of the Madre de Dios Basin (red region) > 550 masl is 35,600 km^2. The river network was produced from HydroSHEDS (hydrological data and maps based on shuttle elevation derivatives at multiple scales) [*Lehner et al.*, 2008]. c) The Amazon River network with the two river gauging stations in the Andes (red triangle) and the Miraflores river gauging station (yellow dot) in Amazonia. The Andean portion of Amazonia (light green) and

Amazonia *sensu stricto* (dark green) from [*Eva et al.*, 2005] fall mostly within the Amazon Basin (within black outline) [*Lehner et al.*, 2008]. 220

Figure 6.2: River discharge (Q_w, $m^3\ s^{-1}$) over the study period for a) San Pedro (164.4 km^2 watershed area), and b) Wayqecha (48.5 km^2 watershed area) gauging stations (Figure 6.1a), with suspended sediment samples (SS), POC_{fossil} and $POC_{non\text{-}fossil}$ concentrations (g m^{-3}) on the secondary axis. 225

Figure 6.3: Elemental and isotopic composition of POC in suspended load (circles) from the Kosñipata River. Samples collected from San Pedro as black circles and from Wayqecha as grey circles, with analytical uncertainties small than the point size. a) The stable isotopes of POC ($\delta^{13}C_{org}$, ‰) versus the nitrogen to organic carbon ratio (N/C). Boxes show ranges from published sources [*Zimmermann et al.*, 2009; *Rao*, 2011], where O_H and A are soil horizons.....228

Figure 6.4: Seasonal variation of POC $\delta^{13}C_{org}$ (‰) and measured Q_w ($m^3\ s^{-1}$) over the sampling period for the a) San Pedro gauging station (n = 67) and for the b) Wayqecha gauging station (n = 42). Several suspended sediment samples at low flow in the dry season did not yield a $\delta^{13}C_{org}$ result (SP n = 3 and WQ n = 3; Table S6.1). ^{13}C-depleted POC dominates the dry season POC. 229

Figure 6.5: Annual breakdown by month of a) suspended sediment flux, and b) $POC_{non\text{-}fossil}$ and POC_{fossil} fluxes for the San Pedro catchment. 235

Figure 6.6: Suspended sediment yield versus the $POC_{non\text{-}fossil}$ yield for this study, 11 catchments in Taiwan [*Hilton et al.*, 2012], the western Southern Alps of New Zealand [*Korup et al.*, 2004; *Hilton et al.*, 2008a], the Santa Clara and Alsea Rivers in the West Coast of the USA [*Hatten et al.*, 2012], and a headwater catchment in the Swiss Alps [*Smith et al.*, 2013].....236

Figure 6.7: a) Cumulative flux of river discharge (Q_w) and the associated $POC_{non\text{-}fossil}$, POC_{fossil}, and suspended sediment (SS) against total daily Q_w (mm hr^{-1}) over the course of the year study period at the San Pedro river gauging station. Mean Q_w was 0.32 mm hr^{-1} (black vertical line). Samples are well distributed over the different hydrologic conditions (black dashes). b) Cumulative flux as in a) ranked by day (n = 335) where 1 is the largest Q_w day and 335 is the lowest Q_w day, demonstrating the important role of flood events in the flux of $POC_{non\text{-}fossil}$, POC_{fossil} and suspended sediment in the Kosñipata Valley. 250

Acronyms, notations and abbreviations

ABERG	Andes Biodiversity and Ecosystems Research Group
ACCA	Asociación para la Conservación de la Cuenca Amazónica
AET	Actual evapotranspiration
AGLB	Above ground living biomass
AMdD	Alto Madre de Dios
AMS	American Meteorological Society
AToMS	Airborne Taxonomic Mapping System
BFI	Base flow index
BGLB	Below ground living biomass
C	Carbon
C3	C_3 carbon fixation
CAO	Carnegie Airborne Observatory
cm	Centimetre
C_{org}	Organic carbon (%)
CW	Cloud water
CWI	Cloud water interception
d	Day
D	Deuterium (^2H)
dbh	Diameter at breast height
DEM	Digital elevation model
DSM	Digital surface model
DTM	Digital terrain model
Dxs	D-excess ($\delta D - 8 \times \delta^{18}O$, ‰)
ea	Water vapour pressure
EA	Elemental analyser
ED	Excess discharge
ET	Evapotranspiration
F_f	Fraction fossil
$F_{f\text{-}N/C}$	Fraction fossil derived from N/C
$F_{landslide}$	Fraction covered by landslides
F_{mod}	Fraction modern
F_{nf}	Fraction non-fossil
$F_{nf\text{-}N/C}$	Fraction non-fossil derived from N/C
g	Gramme
GF/F	Glass fibre filters
GLS	Global Land Survey
GPS	Global positioning system
H	Hydrogen (^1H)
ha	Hectre
HDPE	High-density polyethylene

hPa	Hectopascal
hr	Hour
IAEA	International Atomic Energy Agency
IPCC	Intergovernmental Panel on Climate Change
IRMS	Isotope-ratio mass spectrometry
km	Kilometre
L	Litre
LE_c	Canopy transpiration
LE_i	Interception evaporation
LE_s	Soil evaporation
LiDAR	Airborne Light Detection and Ranging
LMCF	Lower montane cloud forest
LMRF	Lower montane rain forest
L_f	Landslide frequency (% yr^{-1} or occurrence yr^{-1})
LTRF	Lower tropical rainforest
m	Metre
Ma	Million years
masl	Metres above sea level
MdD	Madre de Dios
mg	Milligrams
Mg	Megagram
min	Minute
mL	Millilitre
mm	Millimetre
Mt	Megatonne
N	Nitrogen
N/C	Nitrogen to organic carbon ratio
NASA	National Aeronautics and Space Administration
NDVI	Normalised difference vegetation index
NEP	Net ecosystem productivity
NERC	Natural Environment Research Council
NIR	Near infrared
NPP	Net primary production
NSERC	Natural Sciences and Engineering Research Council of Canada
O_H	Organic soil horizon
PAR	Photosynthetically active radiation (μmol PAR m^{-2} s^{-1})
Pg	Petagram
P_{ls}	Landslide probability
POC	Particulate organic carbon
POC_{fossil}	Fossil particulate organic carbon
$POC_{non\text{-}fossil}$	Non-fossil particulate organic carbon
PT-JPL	Priestley and Taylor - Jet Propulsion Laboratory

Q_b	Baseflow
Q_w	River discharge ($m^3 s^{-1}$)
R	Hydraulic radius (m)
R_c	Runoff coefficient (%)
R_h	Heterotrophic respiration
RH	Relative humidity
R_n	Net radiation ($W m^{-2}$)
R_s	Solar radiation ($W m^{-2}$)
S	Slope (%)
s	Second
SALLJ	South American Low Level Jet
SAVI	Soil adjusted vegetation index
sec	Second
SENAMHI	Servicio Nacional de Meterología e Hidrología del Perú
SP	San Pedro
SPA	Soil-Plant-Atmospheric
SRTM	Shuttle Radar Topography Mission
SS	Suspended sediment
SSC	Suspended sediment concentration
SUERC	Scottish Universities Environmental Research Centre
t	Metric tonne
T_{max}	Maximum daily air temperature
TMCF	Tropical montane cloud forest
TRMM	Tropical Rainfall Measuring Mission
UMCF	Upper montane cloud forest
VIS	Visible
VPDB	Vienna Pee Dee Belemnite
VSLAP	Vienna standard light Antarctic precipitation
VSMOW	Vienna standard mean ocean water
VSWIR	Visible-to-shortwave infrared
WD	Woody debris
WGS	World Geodetic System
WQ	Wayqecha
yr	Year
$\delta^{13}C_{org}$	Organic delta 13-carbon ($^{13}C/^{12}C$, ‰)
$\Delta^{14}C_{org}$	Organic Delta 14-carbon or radiocarbon ($^{14}C/^{12}C$, ‰)
$\delta^{18}O$	Delta 18-oxygen ($^{18}O/^{16}O$, ‰)
δD	Delta deuterium (D/H, ‰)
τ_{ls}	Slope turnover (yr)
µm	Micrometre

Chapter 1 : Introduction

1.1. Approach

Organic carbon transport in rivers is interesting because it evaluates movement of carbon from one ecosystem to another, and it provides a significant bridge between modern and geologic carbon cycles. In montane forests, carbon is mobilised by erosional forces, such as landslides and overland surface flow, and is delivered to the river channel. If this soil and vegetation carbon is transported downriver and buried in sedimentary deposits, it is effectively removing CO_2 from the modern carbon cycle. The effect of rivers constantly transporting carbon from land to the ocean floor may play an important link in the global carbon cycle.

In order to appreciate and measure the carbon sink, one must first evaluate the carbon source. Mountain regions are excellent locations to study high rates of erosion significant on a global scale. Landslides act as an excellent driver of erosion of soil and vegetation in these mountain systems. Monitoring landslide rates, turnover, and the carbon they mobilise provides an insight into the material transported in the river. In some regions, however, the bedrock is sedimentary containing fossil organic carbon trapped for millions of years. Fossil organic carbon represents a different pool of carbon, one that is currently in the geological carbon cycle and, if oxidised, represents an addition of CO_2 to the atmosphere – an introduction to the modern carbon cycle. Since the fates of both the fossil and the non-fossil (sourced from soil and vegetation) carbon are juxtaposed, it is imperative to distinguish between these two sources in river particulate organic carbon (POC). The best location to carry out the separation of POC into fossil and non-fossil carbon is in the mountains, where onsite evaluation of source types can be carried out (i.e. testing soil layers, vegetation, bedrock outcrops and riverbed materials). Once in the lowlands or in marine environments, the POC signature changes as it mixes with additional sources and undergoes various levels

of decomposition/oxidation complicating the original mountain POC signal. Monitoring river POC in mountain settings is an efficient way to understand and evaluate carbon sources (fossil vs. non-fossil), to examine the potential role that landslides play, and to estimate the amount of carbon that is mobilised and transported downriver.

Knowledge of streamflow and annual runoff is imperative for a full river carbon study. Without knowing runoff, it is impossible to scale up from limited spot POC collections to produce an annual flux. As well, storms contribute large amounts of sediment and carbon transported into the river. Thus, continual discharge measures are extremely beneficial to capture these events which may occur < two weeks of the year. Seasonality in stream runoff also plays a role in sediment and POC transport and thus needs to be monitored in a river POC study.

An improved understanding of Andean hydrological cycle, POC sources and flux, and landslide rates and carbon mobilisation would significantly advance scientific understanding of the Andes and provide insight to other mountain locations around the world. Such understanding could also help identify important parameters that could be eventually incorporated into biogeochemical modelling of the Andes and the Amazon Basin. Finally, understanding of the source of a potentially large portion of the lowland and ocean carbon in sedimentary deposits would help further the understanding of this important aspect of the global carbon cycle.

1.2. Aims

In mountain catchments, erosion delivers sediment and organic material to the river channel and is transported downstream. The principal aim of this thesis was to determine POC sources and to evaluate drivers that deliver and transport POC in an Andean river Valley. There are several aims of each chapter which contribute a pivotal component to the principal aim of the thesis. Finally, the data collected throughout this study is valuable to the growing knowledge of the Kosñipata Valley ecosystem and to the broader literature interested in the understanding of montane hydrology, river POC, and landslide carbon dynamics.

The main aims of this study were to:

- Determine the hydrological budget and therefore quantify the seasonal and annual stream runoff. (Chapter 3)
- Evaluate the importance of storms in river POC transport, and to partition between POC_{fossil} and $POC_{non\text{-}fossil}$ sources. (Chapter 4)
- Examine landslide rates and slope turnover times for the Kosñipata Valley using remote sensing, and estimate the amount of soil and vegetation mobilised by landslides. (Chapter 5)
- Quantify annual fluxes of suspended sediment, and non-fossil and fossil POC in the river. (Chapter 6)
- Compare the contribution of landslide-derived soil and vegetation carbon to river $POC_{non\text{-}fossil}$ fluxes. (Chapter 6)

1.3. Thesis structure

This thesis follows the requirements for the University of Oxford's D.Phil. by submitted papers route; therefore, chapters 3 to 6 have been prepared and structured for submission to peer reviewed journals. Chapter 4 was published in 2013, chapter 5 was submitted in 2013, and chapter 3 submitted in 2014, and chapter 6 will be submitted in 2015. This introductory chapter discusses why this study is important and states the overall aims of the research.

Chapter 2 provides a literature review of the key topics of the thesis, highlighting gaps in the research and setting a background for the subsequent chapters:

1. The nature of hydrological regimes in forested montane environments which promote high rates of river POC and sediment transfer.

2. The importance of mountain systems in the erosion of sediment and POC.

3. The fate of non-fossil and fossil particulate organic carbon in the carbon cycle.

4. The role that landslides play in the mountain landscape, with particular focus on what causes them and the effect they have on the ecosystem.

Chapter 3 (*The hydrological regime of a forested tropical Andean valley*) presents river discharge results collected from two gauging station in an Andean catchment over a year time period. The water balance is assessed by evaluating inputs (rainfall and cloud water) and outputs (runoff and actual evapotranspiration) over the year. The rainfall-runoff relationship is evaluated monthly providing insight into seasonal hydrological variability. A seasonal lag in river runoff is discussed, focusing on role of groundwater as the source.

Chapter 4 (*New views on 'old' carbon in the Amazon River: Insight from the source of organic carbon eroded from the Peruvian Andes*) presents river particulate organic carbon

(POC) samples collected over 2 storms measured in an Andean catchment. Stable ($\delta^{13}C_{org}$ ‰ and $\delta^{15}N$ ‰), element concentrations (C_{org} % and N %), and radiocarbon ($\Delta^{14}C_{org}$ ‰) were utilised to carry out two end-member mixing modelling, allowing for fossil from non-fossil POC to be partitioned. The importance of fossil and non-fossil POC in the carbon cycle is discussed. The influence of storms on the transfer of sediment and POC is evaluated. Finally, the prevalence of Andean POC was evaluated in the lowland Amazon River.

Chapter 5 (*Fluvial incision links landslides, carbon transfer and plant diversity in an Andean valley*) presents analysis of Landsat satellite imagery (Landsat 4 and 7) every year over a 25-year period to map landslides in the Kosñipata Valley, Peru. Landslide rates and slope turnover were determined and spatial and temporal trends and causes assessed. A compilation of available biomass and carbon stock data (above ground, below ground and soil) made it possible to assess the mobilisation of carbon through landslide activity. The Landsat imagery (30 x 30 m) dataset allowed for a time series analysis to be carried out from 1988 to 2012. High resolution satellite imagery, Quickbird (2.4 x 2.4 m) and Worldview (2 x 2 m), could be utilised to verify landslides.

Chapter 6 (*Export of particulate organic carbon by an Andean river and implications of its delivery to the lowland Amazon River*) presents annual yields of river suspended sediment, $POC_{non\text{-}fossil}$ and POC_{fossil}, using a calibration method developed in chapter 4 and stream runoff determined in chapter 3. Sediment samples were collected weekly to monthly over the span of a year from two river gauging stations in the Kosñipata Valley. The impact and role of seasonality on sediment load was determined. The $POC_{non\text{-}fossil}$ yield was determined and compared to the landslide mobilised $OC_{non\text{-}fossil}$ yield (chapter 5). Andean-derived suspended sediment and POC yields from this study were compared to regional estimates derived from lowland Amazonia river yields. The impact of Andean river $POC_{non\text{-}}$

$_{fossil}$ on Andean net primary productivity was determined and impact of this lateral transfer in Amazonia was discussed.

Chapter 7, the concluding chapter, reviews the main findings, discusses implications of findings, outlines future research needs, and provides concluding remarks. The aims of this thesis are revisited including whether or not they have been achieved and what they mean for the literature of river POC composition and transport, montane river hydrology, and landslide carbon dynamics. The main contributions of this interdisciplinary thesis are:

1) assessing the stream runoff and water balance for the Kosñipata valley;

2) separating river $POC_{non\text{-}fossil}$ and POC_{fossil} and determining their end members;

3) evaluating landslide rates and slope turnover; estimating carbon mobilised by landslides;

4) determining annual flux of suspended sediment, $POC_{non\text{-}fossil}$ and POC_{fossil};

5) demonstrating the role of landslides, storms and seasonality on sediment and POC transport in rivers;

6) estimating regional suspended sediment and POC fluxes and discussing their fate in the Amazon lowlands.

A discussion regarding the need for onsite landslide work to understand carbon dynamics better, scaling-up landslide mapping to determine rates in the larger Andean region, and tracking Andean river organic carbon into the lowland Amazon are identified as future research needs. The objective of this research was identified due to a shortage of information about landslides and river POC in the Eastern Andes. The main outcome is to provide knowledge for future geochemical and geomorphological studies in the Andes and the Amazon, and to provide insight into Andean erosional processes.

1.4. Study area

The following is an informal introduction to the Kosñipata Valley study area in Peru through the use of photos and short captions, with more thorough study area sections in each of the 4 papers (Chapters 3 to 6).



Figure 1.1: Kosñipata Valley around the San Pedro gauging station. Many of these landslides (brown scars) occurred in a single storm event March 4th 2010. This photo was taken by Gregory P. Asner of the Carnegie Institution for Science in 2010.



Figure 1.2: a) This large bedrock landslide occurred in 2007. The crown of the landslide is ~2500 masl. The landslide area is 156,400 m^2 and the debris trail cleared 90,100 m^2. b) The road was washed out by this landslide, but that didn't stop people from carrying on. Note the truck (left) and people (right). Photos were taken by a) William Farfan Rios in 2009 and b) Kathryn Clark in March 2010.

a)



b)



Figure 1.3: a) The Kosñipata Valley is not full of landslides. This picture was taken from the puna grasslands (~3500 masl) down into the tropical montane cloud forest valley. b) The valley is often submersed in cloud. This picture was taken at San Pedro ~1400 masl. The photos were taken by Kathryn Clark in November 2009 and February 2010.



Figure 1.4: a) When I arrived to San Pedro in the dry season to set everything up the river was only ~11 m wide and clear. b) I was in for a big surprise when the wet season abruptly arrived at the end of November 2009 and the rivers quickly converted from clear channels to sediment-rich flash flood and the channel was ~17 m wide and murky. David collected our biggest suspended sediment sample (~18,000 g m^{-3}) of the river campaign. c) The wet season changes the river channel completely. Besides entraining POC, the river mobilises large boulders over time. Photos by a) Kathryn Clark in August 2009, b) David Ocampo in November 2009, and c) Kathryn Clark in January 2010.



Figure 1.5: After two installations the river height logger was in place and worked for most of the year. Eventually the large boulder on the left moved on top of the sensor, hence why measurements stopped in February 2011. Photo taken by Kathryn Clark in September 2010.

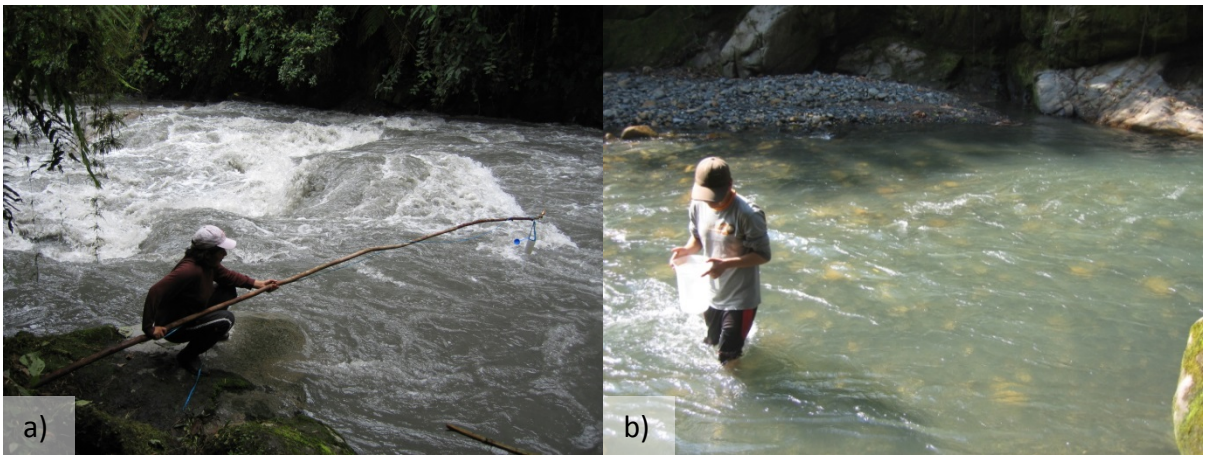


Figure 1.6: a) Judit taking a river sample from the Kosñipata River at the San Pedro gauging during the 2-week experiment. b) Arturo taking a much larger volume sample in the dry season. Photos taken by Kathryn Clark in February 2010 and September 2010 respectively.



Figure 1.7: a) Beto and b) Dante taking samples during the 2-week wet season sampling campaign from the Wayqecha gauging station in the headwaters of the Kosñipata River.



Figure 1.8: a) Wet season baseline flow at Wayqecha, measured during the two-week campaign at the end of January 2010 and b) dry season baseflow flow at Wayqecha gauging station in August 2010.



Figure 1.9: a) Bright-eyed and bushy tailed I arrived to the valley for the first time with Arturo to do a landslide inventory. We are on the road outside the Wayqecha field station. The Kosñipata valley below with the Amazon covered in a blanket of cloud. b) Post-Peru sickness and back to the field for another month with my makeshift rope belt. I also measured all the tributaries that intersected with the road each month over the year. c) Here Arturo and I pose in front a fresh landslide. This landslide occurred around ~1300 masl during the largest storm of the year March 4th 2010. d) We are en route to collect the largest $POC_{non\text{-}fossil}$ sample of the campaign (116 g m^{-3}) at midnight. Photos by Kathryn Clark June 2009, Rosalbina Butrón October 2009, Kathryn Clark in March 2010, and Judit Huamán in February 4th 2010.

Chapter 2 : Literature review

2.1. Introduction

This thesis is concerned with evaluating the river particulate carbon cycle and landslides in a tropical montane cloud forest (TMCF) in southern Peru. More specifically, it seeks to characterise: 1) river hydrological variability, 2) river particulate organic carbon (POC) sources, 3) landslide dynamics and carbon mobilisation, and 4) river POC and sediment yields in the Kosñipata Valley of Peru. Therefore, this review will address literature relevant to the aforementioned topics. This will aid in the interpretation of the results within the study with respect to the possible controlling mechanisms, and place the study area in the context of the wider region of the Andes and around the globe.

2.2. General overview

2.2.1. The importance of the Andes

Intact ecosystems have become increasingly important as concerns over climate change, anthropogenic impacts, modification of the carbon and hydrological cycles, and loss of biodiversity have emerged. The forested slopes of the Eastern Andes, for example, contain rich biodiversity and many of the world's endemic species [*Young*, 1992; *Gentry and Ortiz,* 1993; *Still et al.*, 1999]. It is a biodiversity hotspot with $1/6^{th}$ of all plant and vertebrate species [*Myers et al.*, 2000]. The Andes contain a large amount of tropical montane cloud forest (TMCF) ecosystems [*Mulligan*, 2010; *Bruijnzeel et al.*, 2011]. Tropical montane cloud forests, however, are one of the least studied terrestrial ecosystems and one of the most vulnerable in a changing climate [*Pounds et al.*, 1999; *Still et al.*, 1999; *Foster*, 2001].

Andean sediment transport, hydrological and nutrient cycling contribute to the health of Amazonian ecosystems [*McClain and Naiman*, 2008]. In light of a changing climate, land use pressures, and possible Amazon die-back projected by some models [*Cox et al.*, 2004], it

becomes even more pressing to understand the role that the Andean slopes play in the Amazon Basin [*Malhi et al.*, 2010].

2.2.2. Mountains

Mountain rivers are an important component of the world's major river basins and play a crucial role in lowland river biogeochemistry and carbon cycling [*Gibbs*, 1967; *Hedges et al.*, 2000; *Galy et al.*, 2008b; *McClain and Naiman*, 2008]. High rates of physical erosion [*Larsen et al.*, 2014] can result in the efficient transfer of particulate organic carbon (POC) [*Kao and Liu*, 1996; *Stallard*, 1998; *Hilton et al.*, 2012] and sediment [*Milliman and Syvitski*, 1992; *Kao and Liu*, 1997; *Hicks et al.*, 2000; *Lyons et al.*, 2002; *Korup et al.*, 2004] to rivers. The highest sediments yields are from the mountains of Taiwan, New Zealand, and Southeast Asia [*Milliman and Farnsworth*, 2011]. Mountain-derived sediment provides the majority of sediment found on the lowland continents [*Gibbs*, 1967; *Milliman and Syvitski*, 1992; *Milliman and Farnsworth*, 2011], significant because mountain regions dominate erosion on earth [*Larsen et al.*, 2014] impacting the lowland regions they drain into.

2.2.3. The Amazon River

The Amazon River is the world's largest fluvial system in terms of drainage area and runoff [*Meybeck and Ragu*, 1997]. It delivers 550-1500 Mt yr^{-1} of sediment to the Atlantic [*Meade et al.*, 1979; *Richey et al.*, 1986; *Dunne et al.*, 1998; *Guyot et al.*, 2005; *Martinez et al.*, 2009] and is the largest point source of POC to the oceans, at ~15 MtC yr^{-1} [*Richey et al.*, 1990b; *Beusen et al.*, 2005]. The mountain headwaters, of the Andes, impart a strong signature on the inorganic chemistry of the particulate load [*Allegre et al.*, 1996; *Gaillardet et al.*, 1997; *Bouchez et al.*, 2011]. They are also thought to supply ~80-90 % of the Amazon River's sediment flux [*Gibbs*, 1967; *Meade et al.*, 1985; *Richey et al.*, 1986; *Wittmann et al.*, 2011]. In contrast, the majority of POC carried in the lowland Amazon River is thought to derive from floodplain sources [*Mayorga et al.*, 2005], which implies substantial replacement

or consumption of Andean POC contributing to outgassing [*Richey et al.*, 2002]. Recently, *Bouchez et al.* [*2010*]; *Bouchez et al.* [2014] have demonstrated using river POC that the Andes indeed contribute to Amazonian river POC yields, but the extent to which has yet to be determined.

2.3. River hydrology

2.3.1. Amazon Basin

The Amazon River has the highest discharge of all of the world's rivers, at 6,300 $km^3 yr^{-1}$, with a very high runoff of 1000 mm yr^{-1} [*Milliman and Farnsworth*, 2011] over its watershed, contributing 20 % of world's water discharge to oceans [*Richey et al.*, 1990b; *Beighley et al.*, 2009]. The Andean portion (> 500 m) of the Amazon basin represents an area of 623 217 km^2 and covers ~10 % of the Amazon River Basin [*McClain and Naiman*, 2008]. Water input from the Andes to the Amazon is approximately proportional to areal coverage (10%) [*Dunne et al.*, 1998; *McClain and Naiman*, 2008]. The routing of water from the eastern flank of the Andes determines the quantity and quality of this economically and ecologically valuable resource for the region [*Barnett et al.*, 2005; *Postel and Thompson*, 2005; *Célleri and Feyen*, 2009] and impacts the biogeochemical cycles and ecology of the lowland Amazon, by providing nutrient and sediment rich waters to the river [*Stallard and Edmond*, 1983; *Allegre et al.*, 1996; *McClain and Naiman*, 2008]. Information about Andean river discharge, flow sources, and flow routing is thus critical for understanding the suspended sediment fluxes, biogeochemical cycles, aquatic ecology, and chemical weathering processes of the Andes-Amazon system, and how these may respond to changes in climate and land-use.

2.3.2. Tropical montane cloud forests

Andean Tropical Montane Cloud Forests (TMCF) comprise a small area but are likely to contribute disproportionately to the overall water balance of the region due to its topographic position [*Killeen et al.*, 2007; *Bruijnzeel et al.*, 2011]. The hydrology of TMCFs is of particular interest because these forests host valuable and diverse ecosystems [*Myers et al.*, 2000; *Bruijnzeel et al.*, 2010] and have been shown to provide a steady supply of water to downstream regions, due in large part to their relatively high water yield, i.e. high stream water output for a given precipitation input [*Zadroga*, 1981; *Tognetti et al.*, 2010]. Despite the importance of Andean TMCFs, their hydrology remains to be thoroughly evaluated.

Prior research on the hydrology of TMCFs has focused on hydrometeorological and forest canopy level studies [*Mulligan*, 2010; *Bruijnzeel et al.*, 2011]. The stability of TMCF stream flow is frequently attributed to a combined effect of water input from cloud water interception (CWI) and reduced water output due to low water use and evapotranspiration [*Zadroga*, 1981; *McJannet et al.*, 2010; *Giambelluca and Gerold*, 2011]. Rainfall is often thought to be quickly exported via overland flow and shallow subsurface stormflow, leading to rapid rainfall-response times [*Schellekens et al.*, 2004; *Goller et al.*, 2005; *Boy et al.*, 2008].

2.3.3 Groundwater

Transient groundwater storage may also play a significant role in mountain hydrological systems [*Tipper et al.*, 2006; *Calmels et al.*, 2011; *Andermann et al.*, 2012]. At peak discharge, in a Mexican TMCF, a high percentage of storm river runoff was pre-event groundwater, where precipitation recharged groundwater reserves [*Blume et al.*, 2008; *Muñoz-Villers et al.*, 2012]. In TMCFs groundwater residence times have been shown to be up to 3 years using water isotope analysis [*Muñoz-Villers and McDonnell*, 2012]. There was also evidence for deep vertical infiltration where there were porous soils and bedrock

[*Muñoz-Villers and McDonnell*, 2012]. Modelling Andean TMCF runoff has shown that inclusion of deeper reservoirs (flow in bedrock, the weathered top of bedrock, and C-horizon) improved streamflow predictions during storm peaks and during low flow [*Crespo et al.*, 2012].

Improved understanding of the extent to which groundwater stabilizes Andean TMCF hydrology, by reducing streamflow variation throughout the year, is likely to be important for accurately assessing how environmental change, such as land use change or shifting cloud base, might affect hydrological functioning in the Andes and downstream in the Amazon [*Ataroff and Rada*, 2000; *Mulligan*, 2010; *Bruijnzeel et al.*, 2011; *Crespo et al.*, 2012; *Rapp and Silman*, 2014].

2.4. River suspended sediment and POC

2.4.1. Global perspective

Mountain rivers are key to providing suspended sediment and POC to the world's rivers [*Milliman*, 1995; *Kao and Liu*, 1997; *Hicks et al.*, 2000; *Lyons et al.*, 2002; *Hilton et al.*, 2008a; *Hilton et al.*, 2008b; *Wheatcroft et al.*, 2010; *Milliman and Farnsworth*, 2011; *Goñi et al.*, 2013; *Larsen et al.*, 2014]. Globally, river carbon comprises an important part of the carbon cycle transferring ~1.7 PgC yr^{-1} terrestrial carbon from soils to headwater streams [*IPCC*, 2013]. The fate of this carbon may be one of the following: 1) it is released as CO_2 in freshwater outgassing, 2) it is buried in organic inland sediment stores, or 3) it is delivered by rivers to the coastal ocean. Carbon delivered from land to ocean occurs as dissolved inorganic carbon (0.3 PgC yr^{-1}), dissolved organic carbon (0.2 PgC yr^{-1}), or particulate organic carbon (POC; 0.1 to 0.4 PgC yr^{-1} [*Seitzinger et al.*, 2005; *Syvitski et al.*, 2005; *Mayorga et al.*, 2010; *IPCC*, 2013].

2.4.2. Fossil POC and non-fossil POC

In river POC there are two different source components. There is the non-fossil component which is comprised of biosphere carbon from terrestrial soil and vegetation. There is also, the fossil component which is comprised of ancient organic carbon from sedimentary bedrock. $POC_{non\text{-}fossil}$ contains recent atmospheric CO_2 fixed via photosynthesis (e.g. *Hilton et al.* [2008b]). $POC_{non\text{-}fossil}$ transfer exports a fraction of primary productivity [*Hilton et al.*, 2012] and, if it escapes oxidation during transport [*Mayorga et al.*, 2005; *Cole et al.*, 2007; *Tranvik et al.*, 2009] and is buried in long-lived floodplain sediments (e.g. *Stallard* [1998]; *Aalto et al.* [2003]) or offshore deposits (e.g. *Galy et al.* [2007b]), can be a net sink of atmospheric CO_2 [*France-Lanord and Derry*, 1997]. If the river $POC_{non\text{-}fossil}$ is oxidised however, recently sequestered CO_2 would be rereleased into the atmosphere, resulting in no net change of atmospheric CO_2 levels [*Hilton et al.*, 2011a].

At the same time, physical erosion can mobilise fossil POC [*Galy and Eglinton*, 2011; *Hilton et al.*, 2011a; *Pawson et al.*, 2012] which, if oxidised, may counter contemporary CO_2 drawdown, adding ancient carbon to the atmosphere (e.g. *Galy et al.* [2008a]; *Bouchez et al.* [2010]). If the POC_{fossil} is reburied however, it results in no net change to atmospheric CO_2 [*Blair et al.*, 2003; *Hilton et al.*, 2011a]. River POC_{fossil} can be significant (15 to 70 % total POC) [*Kao and Liu*, 1996; *Blair et al.*, 2003; *Leithold et al.*, 2006; *Hilton et al.*, 2011a], with a marked impact on the elemental and isotopic composition of particulate organic matter [*Komada et al.*, 2004; *Galy et al.*, 2007a; *Hilton et al.*, 2010; *Bouchez et al.*, 2014]. Thus, special care must be taken to separate out the non-fossil sources (soil and vegetation) from the fossil sources (ancient organic carbon) because their fates in the carbon cycle are juxtaposed [*Hilton et al.*, 2008b; *Hilton et al.*, 2011a; *Hovius et al.*, 2011]. Constraining the source of this POC is therefore fundamental to understanding how its erosion and transfer impacts carbon cycling.

2.4.3. Mountain POC

In many mountain settings around the world, physical erosion mobilises soil and vegetation, and sedimentary bedrock and transfers them into the river system [*Hilton et al.*, 2008a; *Galy and Eglinton*, 2011]. The association of POC with mineral sediment can inhibit its degradation during transport and deposition [*Canfield*, 1994; *Hedges and Keil*, 1995]. As a result, mountain rivers can contribute notably to the transfer of POC to large river systems [*Hedges et al.*, 1986; *Galy and Eglinton*, 2011] and to the delivery of POC to the ocean [*Lyons et al.*, 2002]. Mountain $POC_{non\text{-}fossil}$ yields range from 1.2 to 74 tC km^{-2} yr^{-1} [*Hilton et al.*, 2008a; *Hatten et al.*, 2012; *Hilton et al.*, 2012; *Smith et al.*, 2013] and POC_{fossil} yields range from 10 to 246 tC km^{-2} yr^{-1} [*Hilton et al.*, 2011a; *Hatten et al.*, 2012; *Smith et al.*, 2013]. A comparison of suspended sediment yield with $POC_{non\text{-}fossil}$ yield suggests that sediment yield is a dominant control on $POC_{non\text{-}fossil}$ yield in mountain river catchments around the world [*Hilton et al.*, 2012] (Figure 2.1). A global compilation of $POC_{non\text{-}fossil}$ yields versus suspended sediment yields indicates that the Taiwan samples are not distinct from global river suspended load yields [*Galy*, in prep].

2.4.4. Andean POC

Although, it has been established that the role of the Andes is in biogeochemical cycles is vital for the function of Amazonia, research involving river POC and suspended sediment has mostly revolved around the lowland Amazon [*Gibbs*, 1967; *Meade et al.*, 1985; *Richey et al.*, 1986]. Despite this recognition, the rates of POC transfer from the Andes remain poorly constrained [*Richey et al.*, 1990a; *Moreira-Turcq et al.*, 2003; *Bouchez et al.*, 2014].

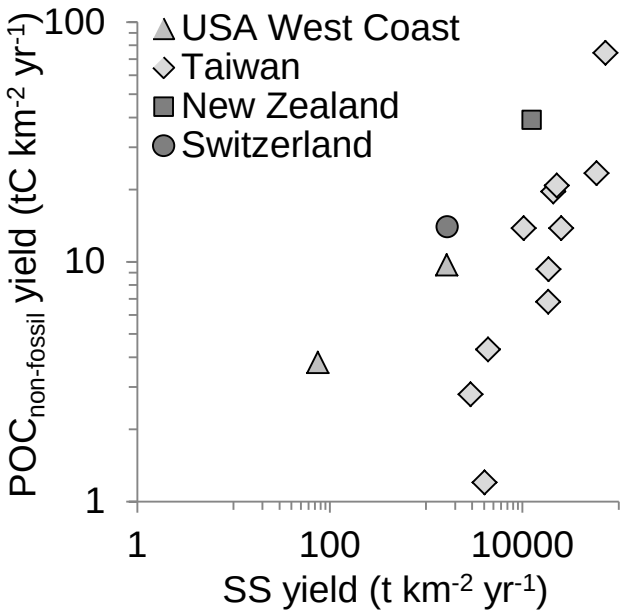


Figure 2.1: River suspended sediment yield versus the $POC_{non\text{-}fossil}$ yield for 11 catchments in Taiwan [*Hilton et al.*, 2012], the western Southern Alps of New Zealand [*Korup et al.*, 2004; *Hilton et al.*, 2008a], the Santa Clara and Alsea Rivers in the West Coast of the USA [*Hatten et al.*, 2012], and a headwater catchment in the Swiss Alps [*Smith et al.*, 2013].

Andean riverine POC has been sampled in the Upper Ucayali and Upper Beni rivers [*Hedges et al.*, 2000; *Mayorga et al.*, 2005; *Aufdenkampe et al.*, 2007; *Townsend-Small et al.*, 2007; *Townsend-Small et al.*, 2008], however large portions of the Andes remain un-sampled (e.g. the Madre de Dios River draining the Peruvian Andes). It is clear that there is a growing need to constrain the source of POC, with recent work highlighting the importance of rock-derived POC input to Andean fed rivers [*Bouchez et al.*, 2010; *Bouchez et al.*, 2014].

2.4.5. Transport of $POC_{non\text{-}fossil}$

The supply of soil and vegetation material comes from two main geomorphic processes. First, bedrock landslides can clear entire tracks of mountain forest and deliver this material to the river channel network [*Hilton et al.*, 2008a; *West et al.*, 2011]. This process mobilises $POC_{non\text{-}fossil}$ ranging from fine grained, mineral associated $POC_{non\text{-}fossil}$, to entire tree trunks [*Hilton et al.*, 2011b; *West et al.*, 2011]. Second, overland surface flow and

shallow landsliding can mobilise loose material and $POC_{non\text{-}fossil}$ from surface soils [*Gomi et al.*, 2008] and the rate of transport depends on hillslope steepness [*Roering et al.*, 2001]. Rainfall can drive both landslide activity and overland surface flow, resulting in efficient hillslope-channel coupling and delivery of $POC_{non\text{-}fossil}$ to river channels [*Hilton et al.*, 2012].

2.4.6. Climate

Individual storm events and the associated rainfall-driven changes in suspended load and POC transport (e.g. *Hilton et al.* [2012]) suggest a strong climate control on the mobilisation and transport of material. Thus, it is important to evaluate river POC during episodic rainfall events, as it is a time when the vast majority of sediment and POC is transported in the Andes [*Townsend-Small et al.*, 2008] and elsewhere [*Hilton et al.*, 2008b; *Hilton et al.*, 2012]. Until now, there has been very little research into the role that the export of soil and vegetation (non-fossil organic carbon) plays over the course of storms [*Hilton et al.*, 2008b]. The exact extent of soil and vegetation OC transfer to rivers during storm activity is not known for the Andes, but would give immense insight into the understanding of $POC_{non\text{-}fossil}$ flow into the Amazon.

2.4.7. $POC_{non\text{-}fossil}$ and the C cycle

Erosion and fluvial transport of $POC_{non\text{-}fossil}$ represents an export of organic matter from the forest ecosystem [*Hilton et al.*, 2012; *Ciais et al.*, 2013]. Organic carbon that is laterally transferred from one ecosystem to another via rivers, influences the carbon budget of the ecosystem, but is largely ignored or discounted from C budget analyses [*Ciais et al.*, 2013]. This erosion and transfer of river $POC_{non\text{-}fossil}$ transports forest productivity out of the ecosystem [*Hilton et al.*, 2008a; *Hilton et al.*, 2008b]. Although the flux transferred is small compared to forest productivity, it is important over longer-timescales, because erosion and burial of $POC_{non\text{-}fossil}$ can contribute to CO_2 sequestration [*Stallard*, 1998; *Galy et al.*, 2007b; *Kao et al.*, 2014].

2.5. Landslides

2.5.1. Landslide dynamics

Landslides can cover 1.2 to 17 % of mountain regions [*Wilcke et al.*, 2003; *Blodgett and Isacks*, 2007; *Tsutsui et al.*, 2007]. Implications for landslide activity are vast in mountain systems as they impact ecology, plant biodiversity, soil dynamics, and carbon and nutrient cycling [*Bussmann et al.*, 2008; *Restrepo et al.*, 2009].

In tropical montane forests landslides play a fundamental role in maintaining a dynamic ecosystem promoting nutrient cycling by creating open spaces and turning over and exposing nutrients in soil and bedrock [*Schrumpf et al.*, 2001]. Surprisingly, considering the vast expanse of the Andes and the clear benefits that landslides provide, there have been only a few studies focusing on the Eastern Andes, addressing landslide-derived sediment rates [*Blodgett and Isacks*, 2007] and modelling of forest recovery rates on landslide scars [*Dislich and Huth*, 2012].

Conceptual models of montane forest dynamics suggest that geomorphic disturbance could influence the structure of ecosystems [*Kessler*, 1999; *Restrepo et al.*, 2009; *Walker et al.*, 2013]. These patterns should be present at the same scale as the spatial patterns of landslide dynamics, acting over tens to thousands of km^2 [*Hovius et al.*, 2000; *Larsen and Montgomery*, 2012]. Moreover, spatial variability in geomorphic processes persists on timescales of 10^5-10^6 years, while forest turnover occurs over 10^2-10^3 years [*Restrepo and Alvarez*, 2006; *Restrepo et al.*, 2009; *Hilton et al.*, 2011b; *Ramos Scharrón et al.*, 2012], such that geomorphic heterogeneity is likely to be maintained over repeated cycles of forest turnover. This is long enough to influence ecosystem development.

New landslides are often a reactivation of existing landslides and often triggered by rainfall [*Guzzetti et al.*, 1994; *Iiritano et al.*, 1998; *Guzzetti*, 2000; *Calcaterra and Santo*, 2004]. Monitoring of landslide reactivation can be evaluated using tree-ring records [*Lopez*

Saez et al., 2012] or mapping using highly temporal satellite imagery [*Kamp et al.*, 2008; *van Westen et al.*, 2008]. The velocity of a landslide depends on the volume of material being moved and friction on the sliding surface [*Scheidegger*, 1973]. Landslide volume to area fit a power-law relationship [*Guzzetti et al.*, 2009], with a greater exponent when bedrock landslides are evaluated and a smaller exponent when soil landslides are evaluated [*Larsen et al.*, 2010].

2.5.2. Landslide mechanics and fluvial incision

Mountain topography is generated by the interaction of rock uplift and erosion. In the basic conceptual model for topographic evolution, fluvial incision into uplifted rock steepens slopes, while landslides, that are triggered once slopes reach a critical failure angle [*Burbank et al.*, 1996; *Montgomery*, 2001], reduce slope angle and lower the terrain [*Carson and Petley*, 1970; *Hovius et al.*, 2000; *Korup*, 2005; *Korup et al.*, 2010; *Larsen and Montgomery*, 2012]. Over time, these processes reach a steady state both topographically and in the balance between rates of uplift and erosion [*Willett and Brandon*, 2002].

The threshold hillslope model indicates that there is a critical slope known as a threshold angle or maximum stable slope that steep mountain slopes can obtain until slope failure occurs [*Burbank et al.*, 1996; *Montgomery*, 2001]. In active mountain ranges, landscape evolution depends on the maintenance of hillslopes at their threshold angles. Mean threshold angle varies between mountain ranges around 30-40 ° [*Scheidegger*, 1973; *Blodgett and Isacks*, 2007; *Lin et al.*, 2008; *Clarke and Burbank*, 2010] and landslide rates increase once the threshold has been passed [*Lin et al.*, 2008]. In the Himalayas, landslide rates spatially track river incision and rapid uplift [*Larsen and Montgomery*, 2012]. This demonstrates that the primary mechanism that mountain systems employ to counteract uplift and river incision is to increase landslide rates [*Larsen and Montgomery*, 2012].

Through modelling mountain erosion, *Egholm et al.* [2013] found that the key to understanding erosion rates in tectonically active and inactive mountain ranges was a bidirectional coupling between bedrock river incision and landslides. Landslides produce sediment providing clastic material for abrasion of the bedrock river channel, but they also produce a high volume of material buffering the bedrock and preventing erosion of the river bedrock.

2.5.3. Landslide mapping techniques

Landslides are an essential erosional process that displaces and transports sediment and organic carbon in mountain systems [*Hilton et al.*, 2008a]. Knowledge of past landslide disturbance and landslide rates is imperative to understand ecological and geomorphological phenomena in mountain systems [*Hilton et al.*, 2008a; *Hilton et al.*, 2012]. To properly understand river POC source in mountainous environment, it is of upmost importance to study spatial and temporal landslide rates.

High resolution image mapping and field surveys, where time and money permits, are an extremely beneficial way to inventory landslides. Aerial photographs taken from airplanes, and high resolution satellite images such as Quickbird and Ikonos are useful in landslide monitoring and mapping [*Hervás et al.*, 2003; *Delacourt et al.*, 2004]. The hit and miss ratio depends on the resolution of the satellite imagery used and the level of expertise of the person carrying out the analysis [*Petley et al.*, 2002; *Gold et al.*, 2004; *van den Eeckhaut et al.*, 2005]. Despite potential errors in landslide inventories, the use of remote sensed data to carry out landslide inventories is often preferred over a field survey due to the high cost, time, and logistical problems of field surveys.

For regional scale analysis, researchers use remotely sensed data, such as Aster, Landsat TM, IRS, Spot and microwave ERS, Radarsat, Envisat, to map qualitative properties like the number, distribution, and types of landslides [*Metternicht et al.*, 2005]. The imagery

is inexpensive or free, multi-temporal, and covers large areas, but only large landslides can be mapped at this level [*Singhroy*, 2004].

2.5.4. Landslides as an ecological agent

Landslides mobilise sediment [*Hovius et al.*, 1997; *Dadson et al.*, 2004; *Korup et al.*, 2005; *Hilton et al.*, 2008a] and biomass [*Hilton et al.*, 2011b; *West et al.*, 2011]. They provide important ecological services. They force slope turnover [*Hilton et al.*, 2011b], influence vegetation dynamics [*Restrepo et al.*, 2009; *Walker et al.*, 2013], deliver important nutrients and minerals downriver [*Kalliola et al.*, 1993], uncover and mix nutrients [*Porder et al.*, 2007; *Peltzer et al.*, 2010], rejuvenate soils and microbial biomass [*Peltzer et al.*, 2010], provide bare ground to undergo colonisation [*Walker et al.*, 1996; *Restrepo et al.*, 2009], provide nesting and feeding habitats for birds[*Bussmann et al.*, 2008], promote dynamic forests [*Wells et al.*, 2001; *Grau et al.*, 2003], and promote an increase in biodiversity [*Kessler*, 1999]. Landslides are thought to provide an intermediate level of disturbance which allows species richness and diversity to flourish [*Kessler*, 2001]. It is possible that landslides contribute to the maintenance of high biodiversity of the tropical forests [*Garwood et al.*, 1979; *Guariguata*, 1990]. Landslide disturbance rates are estimated at 0.1-20 % per century [*Garwood et al.*, 1979; *Guariguata*, 1990; *Restrepo et al.*, 2003; *Hilton et al.*, 2011a]. This geomorphic process may significantly alter successional trajectories, transforming the ecosystem dynamics on a centennial to millennia time scale [*Restrepo et al.*, 2009; *Hilton et al.*, 2011a].

Landslides are characteristic of the Peruvian Andes, but the extent of their role in slope turnover and soil carbon export has not yet been determined. Andean montane forests and the adjacent lowlands are home to one of the richest biodiversities on Earth [*Myers et al.*, 2000; *Malhi et al.*, 2006; *Malhi et al.*, 2008].

2.5.5. Landslides and carbon

Landslides are known to remove whole sections of the forest and transporting materials downslope [*Restrepo and Alvarez*, 2006; *Hilton et al.*, 2011b; *West et al.*, 2011]. Landslides mobilise biomass and soil layers depositing them into the river channel or onto the valley-sides [*Hilton et al.*, 2011b]. Respiration of the landslide material returns recently sequestered CO_2 back to the atmosphere, but a portion of this carbon is transported by the river and buried in long-lived sedimentary basins [*Galy et al.*, 2007b]. Thus, landslide dynamics aid in the sequestering and removal of atmospheric CO_2 and play an important role in the carbon cycle on geological time scales [*Galy et al.*, 2007b].

Landslides influence the carbon cycle, not only though mobilisation biomass and soil [*Garwood et al.*, 1979; *Restrepo and Alvarez*, 2006; *Hilton et al.*, 2011b; *West et al.*, 2011], but also, by mobilising carbon rich organic bedrock [*Hilton et al.*, 2011a]. The erosion through landslide activity of organic carbon rich bedrock is important and does have an impact in the regional carbon cycle [*Hilton et al.*, 2011a].

Detailed studies on carbon stocks and biomass can be utilised to map terrestrial carbon along an altitudinal gradient. These can then be compared to landslide rates to estimate the carbon mobilised through landslide activity. The amount of carbon landslides mobilise in different mountain ranges varies from 2 to 33 tC km^{-2} yr^{-1} [*Hilton et al.*, 2011b; *Ramos Scharrón et al.*, 2012]. This is due to varying landslide rates coupled with varying total carbon stocks. In the Kosñipata Valley, there is a vast wealth of knowledge of vegetation (tree stems, epiphytes, course woody debris, and roots) and soil carbon stocks [*Girardin et al.*, 2010; *Zimmermann et al.*, 2010; *Horwath*, 2011; *Gurdak et al.*, 2013]. Up scaling carbon dynamics from the local to the catchment level has not been done before [*Malhi*, 2012]. A carbon map in the Andes, in conjunction with landslide rates, would make it possible to determine the mobilisation of organic carbon due to landslide activity.

Additionally, spatially heterogeneous landslide patterns in the landscape would selectively sample soil and vegetation; thus, landslides may be expected to have an important influence both on the carbon budget and on biomarker records. While landslides and consequent ecosystem modification occur at local scales, their key role in mobilising carbon may also have critical effects on the carbon cycle at regional and even global scales.

2.5.6. Landslides and river POC

Once the structure and composition of the POC and fluxes are known, the next logical question would be to think about where the carbon is coming from. Landslide debris rich in carbon and nutrients is often deposited directly into river channels and eventually transported downstream. Landslides are responsible for a large portion of the sediment and carbon contained in mountains river systems [*Johnson et al.*, 2006; *Hilton et al.*, 2008a; *Hilton et al.*, 2008b]. In the Eastern Andes of Bolivia, *Blodgett and Isacks* [2007] estimated that 90% of landslide material eventually reaches rivers, as landslides evaluated in the field had approximately 100% direct delivery to streams. Thus, this suggests that landslide debris delivered to the river system is eventually transferred by the river. Along similar lines, *Hovius et al.* [2000] suggested that the resident time of landslide debris in the watershed was dependent on the frequency and magnitude of large floods. Understanding the source, particle size and yield of landslide mobilised sediment and organic carbon within catchments is important for assessing its potential entrainment into rivers, and for determining the resulting preservation efficiency of the eroded organic carbon. This ultimately determines the carbon balance of erosional processes (e.g., [*Hilton et al.*, 2008b; *Galy and Eglinton*, 2011; *West et al.*, 2011]).

2.6. References

Aalto, R., Maurice-Bourgoin, L., Dunne, T., Montgomery, D. R., Nittrouer, C. A., and Guyot, J. L. (2003), Episodic sediment accumulation on Amazonian flood plains influenced by El Nino/Southern Oscillation, *Nature*, *425*(6957), 493-497, doi: http://dx.doi.org/10.1038/nature02002.

Allegre, C. J., Dupre, B., Negrel, P., and Gaillardet, J. (1996), Sr-Nd-Pb isotope systematics in Amazon and Congo River systems: Constraints about erosion processes, *Chemical Geology, 131*(1-4), 93-112, doi: http://dx.doi.org/10.1016/0009-2541(96)00028-9.

Andermann, C., Longuevergne, L., Bonnet, S., Crave, A., Davy, P., and Gloaguen, R. (2012), Impact of transient groundwater storage on the discharge of Himalayan rivers, *Nature Geoscience*, *5*(2), 127-132, doi: http://dx.doi.org/10.1038/NGEO1356.

Ataroff, M., and Rada, F. (2000), Deforestation impact on water dynamics in a Venezuelan Andean cloud forest, *AMBIO: A Journal of the Human Environment, 29*(7), 440-444, doi: http://dx.doi.org/10.1579/0044-7447-29.7.440.

Aufdenkampe, A. K., Mayorga, E., Hedges, J. I., Llerena, C., Quay, P. D., Gudeman, J., Krusche, A. V., and Richey, J. E. (2007), Organic matter in the Peruvian headwaters of the Amazon: Compositional evolution from the Andes to the lowland Amazon mainstem, *Organic Geochemistry, 38*(3), 337-364, doi: http://dx.doi.org/10.1016/j.orggeochem.2006.06.003.

Barnett, T. P., Adam, J. C., and Lettenmaier, D. P. (2005), Potential impacts of a warming climate on water availability in snow-dominated regions, *Nature*, *438*(7066), 303-309, doi: http://dx.doi.org/10.1038/nature04141.

Beighley, R. E., Eggert, K. G., Dunne, T., He, Y., Gummadi, V., and Verdin, K. L. (2009), Simulating hydrologic and hydraulic processes throughout the Amazon River Basin, *Hydrological Processes*, *23*(8), 1221-1235, doi: http://dx.doi.org/10.1002/hyp.7252.

Beusen, A. H. W., Dekkers, A. L. M., Bouwman, A. F., Ludwig, W., and Harrison, J. (2005), Estimation of global river transport of sediments and associated particulate C, N, and P, *Global Biogeochemical Cycles, 19*(4), doi: http://dx.doi.org/10.1029/2005gb002453.

Blair, N. E., Leithold, E. L., Ford, S. T., Peeler, K. A., Holmes, J. C., and Perkey, D. W. (2003), The persistence of memory: The fate of ancient sedimentary organic carbon in a modern sedimentary system, *Geochimica et Cosmochimica Acta, 67*(1), 63-73, doi: http://dx.doi.org/10.1016/s0016-7037(02)01043-8.

Blodgett, T. A., and Isacks, B. L. (2007), Landslide erosion rate in the eastern cordillera of northern Bolivia, *Earth Interactions, 11*, 1-30, doi: http://dx.doi.org/10.1175/2007EI222.1.

Blume, T., Zehe, E., Reusser, D. E., Iroumé, A., and Bronstert, A. (2008), Investigation of runoff generation in a pristine, poorly gauged catchment in the Chilean Andes I: A multi-method experimental study, *Hydrological Processes, 22*(18), 3661-3675, doi: http://dx.doi.org/10.1002/hyp.6971.

Bouchez, J., Beyssac, O., Galy, V., Gaillardet, J., France-Lanord, C., Maurice, L., and Moreira-Turcq, P. (2010), Oxidation of petrogenic organic carbon in the Amazon floodplain as a source of atmospheric CO_2, *Geology, 38*(3), 255-258, doi: http://dx.doi.org/10.1130/g30608.1.

Bouchez, J., Gaillardet, J., France-Lanord, C., Maurice, L., and Dutra-Maia, P. (2011), Grain size control of river suspended sediment geochemistry: Clues from Amazon River depth profiles, *Geochemistry Geophysics Geosystems, 12*, doi: http://dx.doi.org/10.1029/2010gc003380.

Bouchez, J., Galy, V., Hilton, R. G., Gaillardet, J., Moreira-Turcq, P., Pérez, M. A., France-Lanord, C., and Maurice, L. (2014), Source, transport and fluxes of Amazon River particulate organic carbon: insights from river sediment depth-profiles, *Geochimica et Cosmochimica Acta*, (133), 280-298, doi: http://dx.doi.org/10.1016/j.gca.2014.02.032.

Boy, J., Valarezo, C., and Wilcke, W. (2008), Water flow paths in soil control element exports in an Andean tropical montane forest, *European Journal of Soil Science, 59*(6), 1209-1227, doi: http://dx.doi.org/10.1111/j.1365-2389.2008.01063.x.

Bruijnzeel, L. A., Kappelle, M., Mulligan, M., and Scatena, F. N. (2010), Tropical montane cloud forests: state of knowledge and sustainability perspectives in a changing world, in *Tropical Montane Cloud Forests. Science for Conservation and Management*, edited by L. S. Hamilton, L. A. Bruijnzeel and F. N. Scatena, pp. 691-740, Cambridge University Press, Cambridge, UK.

Bruijnzeel, L. A., Mulligan, M., and Scatena, F. N. (2011), Hydrometeorology of tropical montane cloud forests: emerging patterns, *Hydrological Processes, 25*(3), 465-498, doi: http://dx.doi.org/10.1002/hyp.7974.

Burbank, D. W., Leland, J., Fielding, E., Anderson, R. S., Brozovic, N., Reid, M. R., and Duncan, C. (1996), Bedrock incision, rock uplift and threshold hillslopes in the northwestern Himalayas, *Nature*, *379*(6565), 505-510.

Bussmann, R. W., Wilcke, W., and Richter, M. (2008), Landslides as important disturbance regimes - Causes and regeneration, in *Gradients in a tropical mountain ecosystem of Ecuador*, edited by E. Beck, J. Bendix, I. Kottke, F. Makeschin and R. Mosandl, pp. 321-330, Springer-Verlag, Berlin Heildelburg.

Calcaterra, D., and Santo, A. (2004), The January 10, 1997 Pozzano landslide, Sorrento Peninsula, Italy, *Engineering Geology*, *75*(2), 181-200.

Calmels, D., Galy, A., Hovius, N., Bickle, M., West, A. J., Chen, M. C., and Chapman, H. (2011), Contribution of deep groundwater to the weathering budget in a rapidly eroding mountain belt, Taiwan, *Earth and Planetary Science Letters, 303*(1), 48-58, doi: http://dx.doi.org/10.1016/j.epsl.2010.12.032.

Canfield, D. E. (1994), Factors Influencing organic-carbon preservation in marine-sediments, *Chemical Geology*, *114*(3-4), 315-329.

Carson, M. A., and Petley, D. J. (1970), The existence of threshold hillslopes in the denudation of the landscape, *Transactions of the Institute of British Geographers*, *49*, 71-95.

Célleri, R., and Feyen, J. (2009), The hydrology of tropical Andean ecosystems: importance, knowledge status, and perspectives, *Mountain Research and Development, 29*(4), 350-355, doi: http://dx.doi.org/10.1659/mrd.00007.

Ciais, P., Dolman, A. J., Bombelli, A., Duren, R., Peregon, A., Rayner, P. J., Miller, C., Gobron, N., Kinderman, G., and Marland, G. (2013), Current systematic carbon cycle observations and

needs for implementing a policy-relevant carbon observing system, *Biogeosciences Discussions, 10*(7), doi: http://dx.doi.org/10.5194/bgd-10-11447-2013.

Clarke, B. A., and Burbank, D. W. (2010), Bedrock fracturing, threshold hillslopes, and limits to the magnitude of bedrock landslides, *Earth and Planetary Science Letters, 297*(3), 577-586, doi: http://dx.doi.org/10.1016/j.epsl.2010.07.011.

Cole, J. J., Prairie, Y. T., Caraco, N. F., McDowell, W. H., Tranvik, L. J., Striegl, R. G., Duarte, C. M., Kortelainen, P., Downing, J. A., and Middelburg, J. J. (2007), Plumbing the global carbon cycle: integrating inland waters into the terrestrial carbon budget, *Ecosystems, 10*(1), 172-185, doi: http://dx.doi.org/10.1007/s10021-006-9013-8.

Cox, P. M., Betts, R. A., Collins, M., Harris, P. P., Huntingford, C., and Jones, C. D. (2004), Amazonian forest dieback under climate-carbon cycle projections for the 21st century, *Theoretical and Applied Climatology, 78*(1-3), 137-156, doi: http://dx.doi.org/10.1007/s00704-004-0049-4.

Crespo, P. J., Feyen, J., Buytaert, W., Célleri, R., Frede, H.-G., Ramírez, M., and Breuer, L. (2012), Development of a conceptual model of the hydrologic response of tropical Andean micro-catchments in Southern Ecuador, *Hydrology and Earth System Sciences Discussions, 9*(2), 2475-2510, doi: http://dx.doi.org/10.5194/hessd-9-2475-2012.

Dadson, S. J., Hovius, N., Chen, H., Dade, W. B., Lin, J.-C., Hsu, M.-L., Lin, C.-W., Horng, M.-J., Chen, T.-C., Milliman, J., and Stark, C. P. (2004), Earthquake-triggered increase in sediment delivery from an active mountain belt, *Geology, 32*, 733-736, doi: http://dx.doi.org/10.1130/G20639.1

Delacourt, C., Alleman, P., Casson, B., and Vadon, H. (2004), Velocity field of the 'La Clapiere' landslide measured by the correlation of aerial and Quickbird satellite images, *Geophysical Research Letters, 31*(15), 15619.

Dislich, C., and Huth, A. (2012), Modelling the impact of shallow landslides on forest structure in tropical montane forests, *Ecological Modelling, 239*, 40-53, doi: http://dx.doi.org/10.1016/j.ecolmodel.2012.04.016.

Dunne, T., Mertes, L. A. K., Meade, R. H., Richey, J. E., and Forsberg, B. R. (1998), Exchanges of sediment between the flood plain and channel of the Amazon River in Brazil, *Geological Society of America Bulletin, 110*(4), 450-467.

Egholm, D. L., Knudsen, M. F., and Sandiford, M. (2013), Lifespan of mountain ranges scaled by feedbacks between landsliding and erosion by rivers, *Nature, 498*(7455), 475-478, doi: http://dx.doi.org/10.1038/nature12218.

Foster, P. (2001), The potential negative impacts of global climate change on tropical montane cloud forests, *Earth-Science Reviews, 55*(1-2), 73-106, doi: http://dx.doi.org/10.1016/S0012-8252(01)00056-3.

France-Lanord, C., and Derry, L. A. (1997), Organic carbon burial forcing of the carbon cycle from Himalayan erosion, *Nature, 390*(6655), 65-67.

Gaillardet, J., Dupre, B., Allegre, C. J., and Negrel, P. (1997), Chemical and physical denudation in the Amazon River basin, *Chemical Geology, 142*(3-4), 141-173.

Galy, V., Bouchez, J., and France-Lanord, C. (2007a), Determination of total organic carbon content and delta C-13 in carbonate-rich detrital sediments, *Geostandards and Geoanalytical Research, 31*(3), 199-207, doi: http://dx.doi.org/10.1111/j.1751-908X.2007.00864.x.

Galy, V., France-Lanord, C., Beyssac, O., Faure, P., Kudrass, H., and Palhol, F. (2007b), Efficient organic carbon burial in the Bengal fan sustained by the Himalayan erosional system, *Nature, 450*(7168), 407-U406, doi: http://dx.doi.org/10.1038/nature06273.

Galy, V., Beyssac, O., France-Lanord, C., and Eglinton, T. (2008a), Recycling of graphite during Himalayan erosion: A geological stabilization of carbon in the crust, *Science, 322*(5903), 943-945, doi: http://dx.doi.org/10.1126/science.1161408.

Galy, V., France-Lanord, C., and Lartiges, B. (2008b), Loading and fate of particulate organic carbon from the Himalaya to the Ganga-Brahmaputra delta, *Geochimica et Cosmochimica Acta, 72*(7), 1767-1787, doi: http://dx.doi.org/10.1016/j.gca.2008.01.027.

Galy, V., and Eglinton, T. (2011), Protracted storage of biospheric carbon in the Ganges-Brahmaputra basin, *Nature Geoscience, 4*(12), 843-847, doi: http://dx.doi.org/10.1038/ngeo1293.

Galy, V. (in prep).

Garwood, N. C., Janos, D. P., and Brokaw, N. (1979), Earthquake-caused landslides: a major disturbance to tropical forests, *Science*, *205*(4410), 997-999.

Gentry, S., and Ortiz, S. R. (1993), Patrones de composición florística en la Amazonia Peruana, in *Amazona Peruana Vegetación humeda tropical en la llano subandino*, edited by R. Kalliola, M. Puhakka and W. Danjoy, pp. 155-166, PAUT and ONERN, Jyvaskyla, Finland.

Giambelluca, T. W., and Gerold, G. (2011), Hydrology and biogeochemistry of tropical montane cloud forests, in *Forest Hydrology and Biogeochemistry*, edited by F. L. Levia, D. Carlyle-Moses and T. Tanaka, pp. 221-259, Springer, Netherlands.

Gibbs, R. J. (1967), Amazon River - Environmental factors that control its dissolved and suspended load, *Science*, *156*(3783), 1734-1737.

Girardin, C. A. J., Malhi, Y., Aragao, L. E. O. C., Mamani, M., Huasco, W. H., Durand, L., Feeley, K. J., Rapp, J., Silva-Espejo, J. E., Silman, M., Salinas, N., and Whittaker, R. J. (2010), Net primary productivity allocation and cycling of carbon along a tropical forest elevational transect in the Peruvian Andes, *Global Change Biology, 16*(12), 3176-3192, doi: http://dx.doi.org/10.1111/j.1365-2486.2010.02235.x.

Gold, R. D., Wegmann, K. W., Palmer, S. P., Carson, R. J., and Spencer, P. K. (2004), A comparative study of aerial photographs and LIDAR imagery for landslide detection in the Puget Lowland, Washington *Rep.*, Washington Division of Geology and Earth Resources, Washington.

Goller, R., Wilcke, W., Leng, M. J., Tobschall, H. J., Wagner, K., Valarezo, C., and Zech, W. (2005), Tracing water paths through small catchments under a tropical montane rain forest in south Ecuador by an oxygen isotope approach, *Journal of hydrology, 308*(1), 67-80, doi: http://dx.doi.org/10.1016/j.jhydrol.2004.10.022.

Gomi, T., Sidle, R. C., Ueno, M., Miyata, S., and Kosugi, K. (2008), Characteristics of overland flow generation on steep forested hillslopes of central Japan, *Journal of Hydrology, 361*(3), 275-290, doi: http://dx.doi.org/10.1029/2007WR005894.

Goñi, M. A., Hatten, J. A., Wheatcroft, R. A., and Borgeld, J. C. (2013), Particulate organic matter export by two contrasting small mountainous rivers from the Pacific Northwest, U.S.A, *Journal of Geophysical Research: Biogeosciences, 118*(1), 112-134, doi: http://dx.doi.org/10.1002/jgrg.20024.

Grau, H. R., Easdale, T. A., and Paolini, L. (2003), Subtropical dendroecology—dating disturbances and forest dynamics in northwestern Argentina montane ecosystems, *Forest Ecology and Management, 177*(1–3), 131-143, doi: http://dx.doi.org/10.1016/S0378-1127(02)00316-X.

Guariguata, M. R. (1990), Landslide disturbance and forest regeneration in the upper Luquillo mountains of Puerto Rico *The Journal of Ecology*, *78*(3), 814-832.

Gurdak, D. J., Aragao, L. E. O. C., Rozas-Dávila, A., Huaraca Huasco, W., García Cabrera, K., Doughty, C. E., Farfan-Rios, W., Silva-Espejo, J. E., Metcalfe, D. B., Silman, M. R., and Malhi, Y. (2013), Assessing above-ground woody debris dynamics along a gradient of elevation in Amazonian cloud forests in Peru: balancing above-ground inputs and respriation outputs, *Plant Ecology and Diversity, 7*(1-2), 143-160, doi: http://dx.doi.org/10.1080/17550874.2013.818073.

Guyot, J. L., Filizola, N., and Laraque, A. (2005), The suspended sediment flux of the River Amazon at Obidos, Brazil, 1995-2003, in *Sediment Budgets 1*, edited by D. E. Walling and A. J. Horowitz, pp. 347-354, International Association of Hydrological Sciences, Wallingford, UK.

Guzzetti, F., Cardinali, M., and Reichenbach, P. (1994), The AVI project - A bibliographical and archive inventory of landslides and floods in Italy, *Environmental Management*, *18*(4), 623.

Guzzetti, F. (2000), Landslide fatalities and the evaluation of landslide risk in Italy, *Engineering Geology*, *58*(2), 89-107.

Guzzetti, F., Ardizzone, F., Cardinali, M., Rossi, M., and Valigi, D. (2009), Landslide volumes and landslide mobilization rates in Umbria, central Italy, *Earth and Planetary Science Letters, 279*(3–4), 222-229, doi: http://dx.doi.org/10.1016/j.epsl.2009.01.005.

Hatten, J. A., Goñi, M. A., and Wheatcroft, R. A. (2012), Chemical characteristics of particulate organic matter from a small, mountainous river system in the Oregon Coast Range, USA, *Biogeochemistry*, 1-24, doi: http://dx.doi.org/10.1007/s10533-010-9529-z.

Hedges, J. I., Clark, W. A., Quay, P. D., Richey, J. E., Devol, A. H., and Santos, U. d. M. (1986), Compositions and Fluxes of Particulate Organic Material in the Amazon River, *Limnology and Oceanography*, *31*(4), 717-738.

Hedges, J. I., and Keil, R. G. (1995), Sedimentary organic-matter preservation - an assessment and speculative systhesis, *Marine Chemistry*, *49*(2-3), 81-115.

Hedges, J. I., Mayorga, E., Tsamakis, E., McClain, M. E., Aufdenkampe, A., Quay, P., Richey, J. E., Benner, R., Opsahl, S., Black, B., Pimentel, T., Quintanilla, J., and Maurice, L. (2000), Organic matter in Bolivian tributaries of the Amazon River: A comparison to the lower mainstream, *Limnology and Oceanography*, *45*(7), 1449-1466.

Hervás, J., Barredo, J. I., Rosin, P. L., Pasuto, A., Mantovani, F., and Silvano, S. (2003), Monitoring landslides from optical remotely sensed imagery: the case history of Tessina landslide, Italy, *Geomorphology*, *54*(1-2), 63-75, doi: http://dx.doi.org/10.1016/S0169-555X(03)00056-4.

Hicks, D. M., Gomez, B., and Trustrum, N. A. (2000), Erosion thresholds and suspended sediment yields, Waipaoa River Basin, New Zealand, *Water Resources Research, 36*(4), 1129-1142, doi: http://dx.doi.org/10.1029/1999WR900340.

Hilton, R. G., Galy, A., and Hovius, N. (2008a), Riverine particulate organic carbon from an active mountain belt: Importance of landslides, *Global Biogeochemical Cycles, 22*, BG1017, doi: http://dx.doi.org/10.1029/2006GB002905.

Hilton, R. G., Galy, A., Hovius, N., Chen, M.-C., Horng, M.-J., and Chen, H. (2008b), Tropical-cyclone-driven erosion of the terrestrial biosphere from mountains, *Nature Geoscience, 1*(11), 759-762, doi: http://dx.doi.org/10.1038/ngeo333.

Hilton, R. G., Galy, A., Hovius, N., Horng, M.-J., and Chen, H. (2010), The isotopic composition of particulate organic carbon in mountain rivers of Taiwan, *Geochimica et Cosmochimica Acta, 74*(11), 3164-3181, doi: http://dx.doi.org/10.1016/j.gca.2010.03.004.

Hilton, R. G., Galy, A., Hovius, N., Horng, M.-J., and Chen, H. (2011a), Efficient transport of fossil organic carbon to the ocean by steep mountain rivers: An orogenic carbon sequestration mechanism, *Geology, 39*(1), 71-74, doi: http://dx.doi.org/10.1130/g31352.1.

Hilton, R. G., Meunier, P., Hovius, N., Bellingham, P. J., and Galy, A. (2011b), Landslide impact on organic carbon cycling in a temperate montane forest, *Earth Surface Processes and Landforms, 36*(12), 1670-1679, doi: http://dx.doi.org/10.1002/esp.2191.

Hilton, R. G., Galy, A., Hovius, N., Kao, S.-J., Horng, M.-J., and Chen, H. (2012), Climatic and geomorphic controls on the erosion of terrestrial biomass from subtropical mountain forest, *Global Biogeochemical Cycles, 26*(3), GB3014, doi: http://dx.doi.org/10.1029/2012gb004314.

Horwath, A. (2011), Epiphytic bryophytes as cloud forest indicators: Stable isotopes, biomass and diversity along an altitudinal gradient in Peru, 260 pp, Plant Sciences, University of Cambridge, Cambridge.

Hovius, N., Stark, C. P., and Allen, P. A. (1997), Sediment flux from a mountain belt derived by landslide mapping, *Geology, 25*(3), 231-234.

Hovius, N., Stark, C. P., Chu, H. T., and Lin, J. C. (2000), Supply and removal of sediment in a landslide-dominated mountain belt: Central Range, Taiwan, *Journal of Geology, 108*(1), 73-89, doi: http://dx.doi.org/10.1086/314387.

Hovius, N., Galy, A., Hilton, R. G., Sparkes, R., Smith, J., Shuh-Ji, K., Hongey, C., In-Tian, L., and West, A. J. (2011), Erosion-driven drawdown of atmospheric carbon dioxide: The organic pathway, *Applied Geochemistry, 26*, S285-S287, doi: http://dx.doi.org/10.1016/j.apgeochem.2011.03.082.

Iiritano, G., Versace, P., and Sirangelo, B. (1998), Real-time estimation of hazard for landslides triggered by rainfall, *Environmental Geology, 35*(2-3), 175-183.

IPCC (2013), Climate change 2013: The physical science basis. Contribution of Working Group I to the fifth Assessment Report of the Intergovernmental Panel on Climage Change *Rep.*, 1535 pp, Cambridge, UK and New York, NY, USA.

Johnson, J. S., Lehmann, J., Couto, E. G., and Riha, S. J. (2006), DOC and DIC in flowpaths of Amazonian headwater catchments with hydrologically contrasting soils, *Biogeochemistry, 81*, 45-57, doi: http://dx.doi.org/10.1007/s10533-006-9029-3.

Kalliola, R., Puhakka, M., Salo, J., Linna, A., and Räsänen, M. (1993), Mineral nutrients in fluvial sediments from the Peruvian Amazon, *Catena*, *20*(3), 333-349.

Kamp, U., Growley, B. J., Khattak, G. A., and Owen, L. A. (2008), GIS-based landslide susceptibility mapping for the 2005 Kashmir earthquake region, *Geomorphology*, *101*(4), 631-642, doi: http://dx.doi.org/10.1016/j.geomorph.2008.03.003.

Kao, S. J., and Liu, K.-K. (1996), Particulate organic carbon export from a subtropical mountainous river (Lanyang Hsi) in Taiwan, *Limnology and Oceanography, 41*(8), 1749-1757.

Kao, S. J., and Liu, K. K. (1997), Fluxes of dissolved and nonfossil particulate organic carbon from an Oceania small river (Lanyang Hsi) in Taiwan, *Biogeochemistry*, *39*(3), 255-269.

Kao, S. J., Hilton, R. G., Selvaraj, K., Dai, M., Zehetner, F., Huang, J. C., Hsu, S. C., Sparkes, R., Liu, J. T., Lee, T. Y., Yang, J. Y. T., Galy, A., Xu, X., and Hovius, N. (2014), Preservation of terrestrial organic carbon in marine sediments offshore Taiwan: mountain building and atmospheric carbon dioxide sequestration, *Earth Surface Dynamics, 2*(1), 127-139, doi: http://dx.doi.org/10.5194/esurf-2-127-2014.

Kessler, M. (1999), Plant species richness and endemism during natural landslide succession in a perhumid montane forest in the Bolivian Andes, *Ecotropica, 5*, 123-136.

Kessler, M. (2001), Patterns of diversity and range size of selected plant groups along an elevational transect in the Bolivian Andes, *Biodiversity & Conservation, 10*(11), 1897-1921, doi: http://dx.doi.org/10.1023/A:1013130902993.

Killeen, T. J., Douglas, M., Consiglio, T., Jørgensen, P. M., and Mejia, J. (2007), Dry spots and wet spots in the Andean hotspot, *Journal of Biogeography, 34*(8), 1357-1373, doi: http://dx.doi.org/10.1111/j.1365-2699.2006.01682.x.

Komada, T., Druffel, E. R. M., and Trumbore, S. E. (2004), Oceanic export of relict carbon by small mountainous rivers, *Geophysical Research Letters, 31*(7), L07504, doi: http://dx.doi.org/10.1029/2004gl019512.

Korup, O., McSaveney, M. J., and Davies, T. R. H. (2004), Sediment generation and delivery from large historic landslides in the Southern Alps, New Zealand, *Geomorphology, 61*(1–2), 189-207, doi: http://dx.doi.org/10.1016/j.geomorph.2004.01.001.

Korup, O. (2005), Distribution of landslides in southwest New Zealand, *Landslides, 2*(1), 43-51, doi: http://dx.doi.org/10.1007/s10346-004-0042-0.

Korup, O., Schmidt, J., and McSaveney, M. J. (2005), Regional relief characteristics and denudation pattern of the western Southern Alps, New Zealand, *Geomorphology, 71*(3), 402-423, doi: http://dx.doi.org/10.1016/j.geomorph.2005.04.013.

Korup, O., Densmore, A. L., and Schlunegger, F. (2010), The role of landslides in mountain range evolution, *Geomorphology, 120*(1), 77-90, doi: http://dx.doi.org/10.1016/j.geomorph.2009.09.017.

Larsen, I. J., Montgomery, D. R., and Korup, O. (2010), Landslide erosion controlled by hillslope material, *Nature Geoscience, 3*(4), 247-251, doi: http://dx.doi.org/10.1038/ngeo776.

Larsen, I. J., and Montgomery, D. R. (2012), Landslide erosion coupled to tectonics and river incision, *Nature Geoscience, 5*(7), 468-473, doi: http://dx.doi.org/10.1038/ngeo1479.

Larsen, I. J., Montgomery, D. R., and Greenberg, H. M. (2014), The contribution of mountains to global denudation, *Geology*, G35136. 35131, doi: http://dx.doi.org/10.1130/G35136.1

Leithold, E. L., Blair, N. E., and Perkey, D. W. (2006), Geomorphologic controls on the age of particulate organic carbon from small mountainous and upland rivers, *Global Biogeochemical Cycles, 20*(3), doi: http://dx.doi.org/10.1029/2005gb002677.

Lin, G.-W., Chen, H., Hovius, N., Horng, M.-J., Dadson, S., Meunier, P., and Lines, M. (2008), Effects of earthquake and cyclone sequencing on landsliding and fluvial sediment transfer in a mountain catchment, *Earth Surface Processes and Landforms, 33*(9), 1354-1373, doi: http://dx.doi.org/10.1002/esp.1716.

Lopez Saez, J., Corona, C., Stoffel, M., Schoeneich, P., and Berger, F. (2012), Probability maps of landslide reactivation derived from tree-ring records: Pra Bellon landslide, southern French Alps, *Geomorphology, 138*(1), 189-202, doi: http://dx.doi.org/10.1016/j.geomorph.2011.08.034.

Lyons, W. B., Nezat, C. A., Carey, A. E., and Hicks, D. M. (2002), Organic carbon fluxes to the ocean from high-standing islands, *Geology, 30*(5), 443-446, doi: http://dx.doi.org/10.1130/0091-7613(2002)030<0443:ocftto>2.0.co;2.

Malhi, Y., Wood, D., Baker, T. R., Wright, J., Phillips, O. L., Cochrane, T., Meir, P., Chave, J., Almeida, S., and Arroyo, L. (2006), The regional variation of aboveground live biomass in old-growth Amazonian forests, *Global Change Biology, 12*(7), 1107-1138, doi: http://dx.doi.org/10.1111/j.1365-2486.2006.01120.x.

Malhi, Y., Roberts, J. T., Betts, R. A., Killeen, J. T., Li, W., and Nobre, C. A. (2008), Climate change, deforestation, and the fate of the Amazon, *Science, 319*, 169-172, doi: http://dx.doi.org/10.1126/science.1146961

Malhi, Y., Silman, M., Salinas, N., Bush, M., Meir, P., and Saatchi, S. (2010), Introduction: Elevation gradients in the tropics: laboratories for ecosystem ecology and global change research, *Global Change Biology, 16*(12), 3171-3175, doi: http://dx.doi.org/10.1111/j.1365-2486.2010.02323.x.

Malhi, Y. (2012), The productivity, metabolism and carbon cycle of tropical forest vegetation, *Journal of Ecology, 100*(1), 65-75, doi: http://dx.doi.org/10.1111/j.1365-2745.2011.01916.x.

Martinez, J. M., Guyot, J. L., Filizola, N., and Sondag, F. (2009), Increase in suspended sediment discharge of the Amazon River assessed by monitoring network and satellite data, *Catena, 79*(3), 257-264, doi: http://dx.doi.org/10.1016/j.catena.2009.05.011.

Mayorga, E., Aufdenkampe, A. K., Masiello, C. A., Krusche, A. V., Hedges, J. I., Quay, P. D., Richey, J. E., and Brown, T. A. (2005), Young organic matter as a source of carbon dioxide outgassing from Amazonian rivers, *Nature, 436*(7050), 538-541, doi: http://dx.doi.org/10.1038/nature03880.

Mayorga, E., Seitzinger, S. P., Harrison, J. A., Dumont, E., Beusen, A. H. W., Bouwman, A. F., Fekete, B. M., Kroeze, C., and Van Drecht, G. (2010), Global Nutrient Export from WaterSheds 2 (NEWS 2): Model development and implementation, *Environmental Modelling & Software, 25*(7), 837-853, doi: http://dx.doi.org/10.1016/j.envsoft.2010.01.007.

McClain, M. E., and Naiman, R. J. (2008), Andean influences on the biogeochemistry and ecology of the Amazon River, *Bioscience, 58*(4), 325-338, doi: http://dx.doi.org/10.1641/b580408.

McJannet, D. L., Wallace, J. S., and Reddell, P. (2010), Comparative water budgets of a lower and an upper montane cloud forest in the Wet Tropics of northern Australia, in *Tropical Montane Cloud Forests. Science for Conservation and Management*, edited by L. A. Bruijnzeel and F. N. Scatena, pp. 479-490, Cambrige University Press, Cambridge, UK.

Meade, R. H., Nordin, C. F., Curtis, W. F., Costarodrigues, F. M., Dovale, C. M., and Edmond, J. M. (1979), Sediment loads in the Amazon River, *Nature, 278*(5700), 161-163.

Meade, R. H., Dunne, T., Richey, J. E., Santos, U. D., and Salati, E. (1985), Storage and remobilisation of suspended sediment in the lower Amazon River of Brazil, *Science, 228*(4698), 488-490.

Metternicht, G., Hurni, L., and Gogu, R. (2005), Remote sensing of landslides: An analysis of the potential contribution to geo-spatial systems for hazard assessment in mountainous environments, *Remote Sensing of Environment, 98*(2-3), 284-303, doi: http://dx.doi.org/10.1016/j.rse.2005.08.004.

Meybeck, M., and Ragu, A. (1997), River discharges to the oceans: An assessment of suspended solids, major ions and nutrients *Rep.*, 245 pp, United Nations Environmental Programme, World Health Organization, Nairobi, Kenya.

Milliman, J. D., and Syvitski, J. P. M. (1992), Geomorphic tectonic control of sediment discharge to the ocean - the importance of small mountain rivers, *Journal of Geology, 100*(5), 525-544.

Milliman, J. D. (1995), Sediment discharge to the ocean from small mountainous rivers: The New Guinea example, *Geo-Marine Letters, 15*(3-4), 127-133.

Milliman, J. D., and Farnsworth, K. L. (2011), Runoff, erosion, and delivery to the coastal ocean, in *River discharge to the coastal ocean: a global synthesis*, edited, pp. 13-69, Cambridge University Press, Cambridge, UK.

Montgomery, D. R. (2001), Slope distributions, threshold hillslopes, and steady-state topography, *American Journal of Science, 301*(4-5), 432-454, doi: http://dx.doi.org/10.2475/ajs.301.4-5.432.

Moreira-Turcq, P., Seyler, P., Guyot, J. L., and Etcheber, H. (2003), Exportation of organic carbon from the Amazon River and its main tributaries, *Hydrological Processes, 17*(7), 1329-1344, doi: http://dx.doi.org/10.1002/hyp.1287.

Mulligan, M. (2010), Modelling the tropics-wide extent and distribution of cloud forest and cloud forest loss, with implications for conservation priority, in *Tropical Montane Cloud Forests. Science for Conservation and Management*, edited by L. A. Bruijnzeel, F. N. Scatena and L. S. Hamilton, pp. 14-38, Cambridge University Press, Cambridge, UK.

Muñoz-Villers, L. E., Holwerda, F., Gómez-Cárdenas, M., Equihua, M., Asbjornsen, H., Bruijnzeel, L. A., Marín-Castro, B. E., and Tobón, C. (2012), Water balances of old-growth and

regenerating montane cloud forests in central Veracruz, Mexico, *Journal of Hydrology, 462*, 53-66, doi: http://dx.doi.org/10.1016/j.jhydrol.2011.01.062.

Muñoz-Villers, L. E., and McDonnell, J. J. (2012), Runoff generation in a steep, tropical montane cloud forest catchment on permeable volcanic substrate, *Water Resources Research, 48*(9), W09528, doi: http://dx.doi.org/10.1029/2011WR011316.

Myers, N., Mittermeier, R. A., Mittermeier, C. G., Da Fonseca, G. A. B., and Kent, J. (2000), Biodiversity hotspots for conservation priorities, *Nature, 403*(6772), 853-858, doi: http://dx.doi.org/10.1038/35002501.

Pawson, R. R., Evans, M. G., and Allott, T. E. H. A. (2012), Fluvial carbon flux from headwater peatland streams: significance of particulate carbon flux, *Earth Surface Processes and Landforms*, doi: http://dx.doi.org/10.10002/esp.3257.

Peltzer, D. A., Wardle, D. A., Allison, V. J., Baisden, W. T., Bardgett, R. D., Chadwick, O. A., Condron, L. M., Parfitt, R. L., Porder, S., Richardson, S. J., Turner, B. L., Vitousek, P. M., Walker, J., and Walker, L. R. (2010), Understanding ecosystem retrogression, *Ecological Monographs, 80*(4), 509-529, doi: http://dx.doi.org/10.1890/09-1552.1.

Petley, D. N., Crick, W. D. O., and Hart, A. B. (2002), The use of satellite imagery in landslide studies in high mountain areas, in *23rd Asian Conference on Remote Sensing (ACRS)*, edited, Kathmandu.

Porder, S., Vitousek, P. M., Chadwick, O. A., Chamberlain, C. P., and Hilley, G. E. (2007), Uplift, erosion, and phosphorus limitation in terrestrial ecosystems, *Ecosystems, 10*(1), 159-171, doi: http://dx.doi.org/10.1007/s10021-006-9011-x.

Postel, S. L., and Thompson, B. H. (2005), Watershed protection: Capturing the benefits of nature's water supply services, *Natural Resources Forum, 29*(2), 98-108, doi: http://dx.doi.org/10.1111/j.1477-8947.2005.00119.x.

Pounds, J. A., Fogden, M. P. L., and Campbell, J. H. (1999), Biological response to climate change on a tropical mountain, *Nature, 398*(6728), 611-615, doi: http://dx.doi.org/10.1038/19297.

Ramos Scharrón, C. E., Castellanos, E. J., and Restrepo, C. (2012), The transfer of modern organic carbon by landslide activity in tropical montane ecosystems, *Journal of Geophysical Research: Biogeosciences (2005–2012), 117*(G3), doi: http://dx.doi.org/10.1029/2011JG001838.

Rapp, J. M., and Silman, M. R. (2014), Epiphyte response to drought and experimental warming [v1; ref status: approved 1, approved with reservations 1, http://f1000r.es/2oy], *F1000Research, 3*(7), doi: http://dx.doi.org/10.12688/f1000research.3-7.v1.

Restrepo, C., Vitousek, P., and Neville, P. (2003), Landslides significantly alter land cover and the distribution of biomass: an example from the Ninole ridges of Hawai'i, *Plant Ecology, 166*(1), 131-143, doi: http://dx.doi.org/10.1023/A:1023225419111.

Restrepo, C., and Alvarez, N. (2006), Landslides and their contribution to land-cover change in the mountains of Mexico and Central America, *Biotropica, 38*(4), 446-457, doi: http://dx.doi.org/10.1111/j.1744-7429.2006.00178.x.

Restrepo, C., Walker, L. R., Shiels, A. B., Bussmann, R., Claessens, L., Fisch, S., Lozano, P., Negi, G., Paolini, L., and Poveda, G. (2009), Landsliding and its multiscale influence on mountainscapes, *Bioscience, 59*(8), 685-698, doi: http://dx.doi.org/10.1525/bio.2009.59.8.10.

Richey, J. E., Meade, R. H., Salati, E., Devol, A. H., Nordin, C. F., and Dossantos, U. (1986), Water discharge and suspended sediment concentrations in the Amazon River 1982-1984, *Water Resources Research, 22*(5), 756-764.

Richey, J. E., Hedges, J. I., Devol, A. H., Quay, P. D., Victoria, R., Martinelli, L., and Forsberg, B. R. (1990a), Biogeochemistry of carbon in the Amazon River, *Limnol. Oceanogr, 35*(2), 352-371.

Richey, J. E., Valarezo, C., Valarezo, C., and Valarezo, C. (1990b), Biogeochemistry of carbon in the Amazon River, *Limnology and Oceanography, 35*, 352-371.

Richey, J. E., Melack, J. M., Aufdenkampe, A. K., Ballester, V. M., and Hess, L. L. (2002), Outgassing from Amazonian rivers and wetlands as a large tropical source of atmospheric CO_2, *Nature, 416*(617-620), doi: http://dx.doi.org/10.1038/416617a.

Roering, J. J., Kirchner, J. W., and Dietrich, W. E. (2001), Hillslope evolution by nonlinear, slope-dependent transport: Steady state morphology and equilibrium adjustment timescales, *Journal of Geophysical Research, 106*(B8), 16499-16513, doi: http://dx.doi.org/10.1029/2001jb000323.

Scheidegger, A. E. (1973), On the prediction of the reach and velocity of catastrophic landslides, *Rock mechanics, 5*(4), 231-236, doi: http://dx.doi.org/10.1007/BF01301796.

Schellekens, J., Scatena, F. N., Bruijnzeel, L. A., van Dijk, A. I. J. M., Groen, M. M. A., and van Hogezand, R. J. P. (2004), Stormflow generation in a small rainforest catchment in the Luquillo Experimental Forest, Puerto Rico, *Hydrological Processes, 18*(3), 505-530, doi: http://dx.doi.org/10.1002/hyp.1335.

Schrumpf, M., Guggenberger, G., Valrezo, C., and Zech, W. (2001), Development and nutrient status along an altitudinal gradient in the south Ecuadorian Andes, *Die Erde, 132*, 43-59.

Seitzinger, S. P., Harrison, J. A., Dumont, E., Beusen, A. H. W., and Bouwman, A. F. (2005), Sources and delivery of carbon, nitrogen, and phosphorus to the coastal zone: An overview of Global Nutrient Export from Watersheds (NEWS) models and their application, *Global Biogeochemical Cycles, 19*(4), GB4S01, doi: http://dx.doi.org/10.1029/2005GB002606.

Singhroy, V. (2004), Remote Sensing of Landslides, in *Landslide Hazard and Risk*, edited by T. Glade, M. Anderson and M. J. Crozier, pp. 469-492, Wiley & Sons, Chichester, England.

Smith, J. C., Galy, A., Hovius, N., Tye, A. M., Turowski, J. M., and Schleppi, P. (2013), Runoff-driven export of particulate organic carbon from soil in temperate forested uplands, *Earth and Planetary Science Letters, 365*, 198-208, doi: http://dx.doi.org/10.1016/j.epsl.2013.01.027.

Stallard, R. F., and Edmond, J. M. (1983), Geochemistry of the Amazon: 2. The influence of geology and weathering environment on the dissolved load, *Journal of Geophysical Research: Oceans, 88*(C14), 9671-9688.

Stallard, R. F. (1998), Terrestrial sedimentation and the carbon cycle: Coupling weathering and erosion to carbon burial, *Global Biogeochemical Cycles, 12*(2), 231-257.

Still, C. J., Foster, P. N., and Schneider, S. H. (1999), Simulating the effects of climate change on tropical montane cloud forests, *Nature, 398*(6728), 608-610, doi: http://dx.doi.org/10.1038/19293.

Syvitski, J. P. M., Vörösmarty, C. J., Kettner, A. J., and Green, P. (2005), Impact of Humans on the Flux of Terrestrial Sediment to the Global Coastal Ocean, *Science, 308*(5720), 376-380, doi: http://dx.doi.org/10.1126/science.1109454.

Tipper, E. T., Bickle, M. J., Galy, A., West, A. J., Pomiès, C., and Chapman, H. J. (2006), The short term climatic sensitivity of carbonate and silicate weathering fluxes: insight from seasonal variations in river chemistry, *Geochimica Et Cosmochimica Acta, 70*(11), 2737-2754, doi: http://dx.doi.org/10.1016/j.gca.2006.03.005.

Tognetti, S., Aylward, B., and Bruijnzeel, L. A. (2010), Assessment needs to support the development of arrangements for payments for ecosystem services from tropical montane cloud forests, in *Tropical Montane Cloud Forests. Science for Conservation and Management*, edited by L. A. Bruijnzeel, F. N. Scatena and L. S. Hamilton, pp. 671-685, Cambridge University Press, Cambridge, UK.

Townsend-Small, A., Noguera, J. L., McClain, M. E., and Brandes, J. A. (2007), Radiocarbon and stable isotope geochemistry of organic matter in the Amazon headwaters, Peruvian Andes, *Global Biogeochemical Cycles, 21*(2), doi: http://dx.doi.org/10.1029/2006gb002835.

Townsend-Small, A., McClain, M. E., Hall, B., Noguera, J. L., Llerena, C. A., and Brandes, J. A. (2008), Suspended sediments and organic matter in mountain headwaters of the Amazon River: Results from a 1-year time series study in the central Peruvian Andes, *Geochimica et Cosmochimica Acta, 72*(3), 732-740, doi: http://dx.doi.org/10.1016/j.gca.2007.11.020.

Tranvik, L. J., Downing, J. A., Cotner, J. B., Loiselle, S. A., Striegl, R. G., Ballatore, T. J., Dillon, P., Finlay, K., Fortino, K., and Knoll, L. B. (2009), Lakes and reservoirs as regulators of carbon cycling and climate, *Limnology and Oceanography, 54*(6), 2298-2314.

Tsutsui, K., Rokugawa, S., Nakagawa, H., Miyazaki, S., Cheng, C.-T., Shiraishi, T., and Yang, S.-D. (2007), Detection and volume estimation of large-scale landslides based on elevation-change analysis using DEMs extracted from high-resolution satellite stereo imagery, *IEEE Transactions on Geoscience and Remote Sensing, 45*(6), 1681-1696, doi: http://dx.doi.org/10.1109/TGRS.2007.895209.

van den Eeckhaut, M., Poesen, J., Verstraeten, G., Vanacker, V., Moeyersons, J., Nyssen, J., and van Beek, L. P. H. (2005), The effectiveness of hillshade maps and expert knowledge in mapping old deep-seated landslides, *Geomorphology, 67*, 351-363, doi: http://dx.doi.org/10.1016/j.geomorph.2004.11.001.

van Westen, C. J., Castellanos, E., and Kuriakose, S. L. (2008), Spatial data for landslide susceptibility, hazard, and vulnerability assessment: An overview, *Engineering Geology, 102*(3–4), 112-131, doi: http://dx.doi.org/10.1016/j.enggeo.2008.03.010.

Walker, L. R., Zarin, D. J., Fetcher, N., Myster, R. W., and Johnson, A. H. (1996), Ecosystem development and plant succession on landslides in the Caribbean, *Biotropica, 28*(4a), 566-576.

Walker, L. R., Shiels, A. B., Bellingham, P. J., Sparrow, A. D., Fetcher, N., Landau, F. H., and Lodge, D. J. (2013), Changes in abiotic influences on seed plants and ferns during 18 years of

primary succession on Puerto Rican landslides, *Journal of Ecology, 101*(3), 650-661, doi: http://dx.doi.org/10.1111/1365-2745.12071.

Wells, A., Duncan, R. P., and Stewart, G. H. (2001), Forest dynamics in Westland, New Zealand: the importance of large, infrequent earthquake-induced disturbance, *Journal of Ecology, 89*(6), 1006-1018, doi: http://dx.doi.org/10.1111/j.1365-2745.2001.00594.x.

West, A. J., Lin, C. W., Lin, T. C., Hilton, R. G., Liu, S. H., Chang, C. T., Lin, K. C., Galy, A., Sparkes, R. B., and Hovius, N. (2011), Mobilization and transport of coarse woody debris to the oceans triggered by an extreme tropical storm, *Limnology and Oceanography, 56*(1), 77-85, doi: http://dx.doi.org/10.4319/lo.2011.56.1.0077.

Wheatcroft, R. A., Goni, M. A., Hatten, J. A., Pasternack, G. B., and Warrick, J. A. (2010), The role of effective discharge in the ocean delivery of particulate organic carbon by small, mountainous river systems, *Limnology and Oceanography, 55*(1), 161.

Wilcke, W., Valladarez, H., Stoyan, R., Yasin, S., Valarezo, C., and Zech, W. (2003), Soil properties on a chronosequence of landslides in montane rain forest, Ecuador, *Catena, 53*, 79-95, doi: http://dx.doi.org/10.1016/S0341-8162(02)00196-0.

Willett, S. D., and Brandon, M. T. (2002), On steady states in mountain belts, *Geology, 30*(2), 175-178, doi: http://dx.doi.org/10.1130/0091-7613(2002)030<0175:OSSIMB>2.0.CO;2.

Wittmann, H., von Blanckenburg, F., Maurice, L., Guyot, J.-L., Filizola, N., and Kubik, P. W. (2011), Sediment production and delivery in the Amazon River basin quantified by in situ-produced cosmogenic nuclides and recent river loads, *Geological Society of America Bulletin, 123*(5-6), 934-950, doi: http://dx.doi.org/10.1130/b30317.1.

Young, K. R. (1992), Biogeography of the montane forest zone of the eastern slopes of Peru, edited, U. N. M. S. M., Lima, Peru.

Zadroga, F. (1981), The hydrological importance of a montane cloud forest area of Costa Rica, *Tropical agricultural hydrology*, 59-73.

Zimmermann, M., Meir, P., Silman, M., Fedders, A., Gibbon, A., Malhi, Y., Urrego, D. H., Bush, M. B., Feeley, K. J., Garcia, K., Farfan, W., Goetz, B. P., Johnson, W. T., Kline, K. M., Modi, A. T., Rurau, Q. N. M., Staudt, B. T., and Zamora, F. (2010), No differences in soil carbon stocks across the tree line in the Peruvian Andes, *Ecosystems*, (13), 62-74, doi: http://dx.doi.org/10.1007/s10021-009-9300-2.

Linking statement: Chapter 2 to 3

I start my research chapters by looking at streamflow over a one year period in the Kosñipata Valley. This paper addresses the first research aim: **to determine the hydrologic budget and therefore assess the seasonal and annual stream runoff**. It does so by carrying out onsite river gauging measurements over a year, with an additional analysis of catchment-wide rainfall, actual evapotranspiration, and cloud water.

In later chapters, I will determine POC and sediment fluxes, and the role of seasonality and storms on sediment yield. To do this however, we must first determine stream runoff in conjunction with the suspended sample collections. Thus, two gauging stations (one in a smaller catchment nested within the larger catchment) were set-up in the Kosñipata Valley in order to determine streamflow and particulate organic carbon and suspended sediment transport.

I was the main author and wrote the paper, and also designed the structure of the research, conducted and organised the field work with the help of research assistants, and carried out all of the data analysis with the exception of the cloud water mixing modelling. Additionally several people contributed to various parts of this paper. Mark Torres carried out the lab analysis of the water isotope samples and carried out the 3-end member mixing modelling using stable isotopes in water to determine the importance of cloud water in streamflow. Josh West provided the main supervision. Specifically, he advised on the design and set-up of the nested catchment river gauging stations, aided in the outline of the paper, aided in the interpretation of the data, and was the main editor. Bob Hilton aided in the design of the river gauging stations, assisted with the paper concept and provided general guidance. Mark New provided advice on the catchment wide-rainfall, evapotranspiration, and the water balance uncertainties. Aline Horwath provided the cloud vapour and some of the rainfall isotope data necessary to constrain the cloud water mixing model. Josh Fisher created the

evapotranspiration model used and provided guidance for its use. Josh Rapp collected a large proportion of the rainfall data used in the catchment-wide rainfall analysis. Arturo Robles was the main field assistant. In addition to aiding in the editing, Yadvinder Malhi provided overall general advice on and data analysis of the paper.

This paper was submitted in June 2014 to *Hydrology and Earth System Science* (HESS).

Chapter 3 : The hydrological regime of a forested tropical Andean valley

Kathryn E. Clark[1], Mark A. Torres[2], A. Joshua West[2], Robert G. Hilton[3], Mark New[4,1], Aline B. Horwath[5], Joshua B. Fisher[6], Joshua M. Rapp[7,8], Arturo Robles Caceres[9], and Yadvinder Malhi[1]

[1] School of Geography and the Environment, University of Oxford, UK.
(*correspondence: kathryn.clark23@gmail.com)

[2] Department of Earth Sciences, University of Southern California, Los Angeles, USA.

[3] Department of Geography, Durham University, UK.

[4] African Climate and Development Initiative, University of Cape Town, South Africa.

[5] Department of Plant Sciences, University of Cambridge, UK.

[6] Water & Carbon Cycles Group, NASA Jet Propulsion Laboratory, USA.

[7] Department of Biology, Wake Forest University, Winston Salem, USA.

[8] Current address: Department of Biology, Tufts Unviersity, USA.

[9] Facultad de Ciencias Biológicas, Universidad Nacional de San Antonio Abad del Cusco, Peru.

Abstract

The hydrology of tropical mountain catchments plays a central role in ecological function, geochemical and biogeochemical cycles, erosion and sediment production, and water supply in globally important environments. Yet many questions remain unanswered about tropical mountain hydrology, and there have been few studies quantifying the seasonal and annual water budgets of these environments. In this study, the hydrologic regime was investigated in the Kosñipata River catchment, which lies in the eastern Andes and is dominated by tropical montane cloud forest with some high elevation *puna* grasslands. Field river height measurements were made and calibrated to discharge for a period of one year (February 2010 to January 2011) at two nested gauging stations, at San Pedro (with the larger upstream catchment area of 164.4 km^2) and Wayqecha (with the smaller upstream area of 48.5 km^2). River runoff was estimated to be 2721 mm yr^{-1} for the San Pedro catchment, and baseflow comprised ~80 % of streamflow. Catchment wide rainfall estimates were 3028 mm yr^{-1} for the San Pedro basin, calculated by calibrating TRMM 3B43 rainfall data with rainfall data from 9 meteorological stations in the valley. Relationships between monthly rainfall and river runoff in the Kosñipata Valley follow an anti-clockwise hysteresis through the year, with a persistence of high runoff after the end of the wet season. Isotope studies indicate that cloud water interception was a minor contributor (11 ± 4 %) to runoff in this catchment, and the size of the soil- and shallow ground-water reservoir is most likely insufficient to explain sustained dry season flow. Thus, the observed hysteresis in rainfall-runoff relationships is best explained by sustained groundwater flow in the dry season. These results demonstrate the importance of transient groundwater storage in stabilizing the annual hydrograph in this tropical montane cloud forest (TMCF) in the Andes.

3.1. Introduction

The routing of water from the eastern flank of the Andes determines the quantity and quality of this economically and ecologically valuable resource for the region [*Barnett et al.*, 2005; *Postel and Thompson*, 2005; *Célleri and Feyen*, 2009] and impacts the biogeochemical cycles and ecology of the lowland Amazon [*Stallard and Edmond*, 1983; *Allegre et al.*, 1996; *McClain and Naiman*, 2008]. The Amazon River has the highest discharge of all of the world's rivers, at 6 300 $km^3 yr^{-1}$, with a very high runoff of 1000 mm yr^{-1} [*Milliman and Farnsworth*, 2011] over its watershed, contributing 20% of world's water discharge to oceans [*Richey et al.*, 1990; *Beighley et al.*, 2009]. The Andean portion (> 500 m) of the Amazon Basin represents an area of 623 217 km^2 and covers ~10 % of the Amazon River Basin [*McClain and Naiman*, 2008]. Although the water input from the Andes to the Amazon is approximately proportional to areal coverage (10 %) [*Dunne et al.*, 1998; *McClain and Naiman*, 2008], the Andes are the dominant source of the Amazon's dissolved load [*Guyot et al.*, 1996; *McClain and Naiman*, 2008], and contribute 80-90 % of its suspended sediment [*Gibbs*, 1967; *Meade et al.*, 1985; *Richey et al.*, 1986]. Information about Andean river discharge, flow sources, and flow routing is thus critical for understanding the suspended sediment fluxes, biogeochemical cycles, aquatic ecology, and chemical weathering processes of the Andes-Amazon system, and how these may respond to changes in climate and land-use.

Despite this importance, the dynamics of Andean hydrology remain to be completely resolved. This is especially true in Andean Tropical Montane Cloud Forest (TMCF), which comprises a small area but is likely to contribute disproportionately to the overall water balance of the region due to its topographic position [*Killeen et al.*, 2007; *Bruijnzeel et al.*, 2011]. The hydrology of TMCFs is of particular interest because these forests host valuable and diverse ecosystems [*Myers et al.*, 2000; *Bruijnzeel et al.*, 2010]

and have been shown to provide a steady supply of water to downstream regions, due in large part to their relatively high water yield, i.e. high stream water output for a given precipitation input [*Zadroga*, 1981; *Tognetti et al.*, 2010]. TMCFs are unique hydrologic systems because of the additional water input from cloud water interception (CWI) and because frequent fog occurrence may lower incoming solar radiation, increasing humidity and potentially lowering evapotranspiration (ET) [*Zadroga*, 1981; *McJannet et al.*, 2010; *Giambelluca and Gerold*, 2011]. Nonetheless, in many TMCFs, high annual rainfall dominates over CWI [*Eugster et al.*, 2006; *McJannet et al.*, 2007; *Holwerda et al.*, 2010a; *Holwerda et al.*, 2010b; *McJannet et al.*, 2010; *Schmid et al.*, 2010] implying that rainfall is the primary source of TMCF streamflow. However, rainfall is often thought to be quickly exported via overland flow and shallow subsurface stormflow, leading to rapid rainfall-response times [*Schellekens et al.*, 2004; *Goller et al.*, 2005; *Boy et al.*, 2008].

However, transient groundwater storage may also play a significant role in mountain hydrological systems [*Tipper et al.*, 2006; *Calmels et al.*, 2011; *Andermann et al.*, 2012]. The importance of groundwater in TMCF hydrology has recently been highlighted by studies in a Mexican TMCF, where groundwater was shown to stabilize the rainfall-runoff response [*Muñoz-Villers and McDonnell*, 2012], and in an Andean TMCF in Ecuador, where considering the effect of groundwater reservoirs was important for accurately predicting streamflow [*Crespo et al.*, 2012]. Improved understanding of the extent to which groundwater stabilizes Andean TMCF hydrology is likely to be important for accurately assessing how environmental change, such as land use change or shifting cloud base, might affect hydrological functioning in the Andes and downstream in the Amazon [*Ataroff and Rada*, 2000; *Mulligan*, 2010; *Bruijnzeel et al.*, 2011; *Crespo et al.*, 2012; *Rapp and Silman*, 2014].

In this paper we evaluate river discharge at two gauging stations in the Kosñipata River, in a well-studied region in the eastern Andes of Peru [*Girardin et al.*, 2010; *Malhi et al.*, 2010; *Salinas et al.*, 2011; *Halladay et al.*, 2012b; *van de Weg et al.*, 2012; *Rapp and Silman*, 2014], over a one year period. We compare discharge data to rainfall estimates in order to assess the water balance and hydrologic variability throughout the study year. We use the distinct water isotope composition of cloud and rain water to constrain the role of cloud water input. Stable water isotopes, i.e. δD (‰) and $\delta^{18}O$ (‰), can be used to distinguish water sources due to distinct fractionation that occurs during evaporation and condensation [*Craig*, 1961; *Rozanski et al.*, 1993; *Gat*, 1996; *Froehlich et al.*, 2002; *Scholl et al.*, 2011]. Stable water isotopes have been used in studies of cloud forest hydrology to estimate local water recycling [*Rhodes et al.*, 2006; *Scholl et al.*, 2007], trace water paths through soil layers in a catchment [*Goller et al.*, 2005], evaluate water sources in stormflow [*Muñoz-Villers and McDonnell*, 2012], evaluate water mean transit time [*Timbe et al.*, 2014] and examine ecohydrology [*Dawson*, 1998; *Goldsmith et al.*, 2012]. We extend this application to constrain the contributions of different precipitation sources to annual streamflow, and in the process we add valuable new water isotope data for a widely studied TMCF in the Andes.

We focus our attention on the following questions: 1) How well can the annual water budget be closed and what are the uncertainties? 2) How is stream runoff partitioned between quickflow and baseflow? 3) Are there any significant seasonal lags between rainfall and stream runoff, and what are the causes of these lags? 4) What is the relative importance of rainfall and cloud water in sustaining streamflow throughout the year? and 5) What are the roles of soil and groundwater in determining seasonal patterns of river flow?

3.2. Study area

In this study we focus on the Kosñipata Valley (13°3'37" S, 71°32'40" W) with evaluation ranging from 1360 to 4000 meters above sea level (masl) (Figure 3.1a). We consider two nested catchments in the Kosñipata: the San Pedro Catchment, which drains an area of 164.4 km^2, and its headwater sub-catchment at Wayqecha, with an area of 48.5 km^2. Downstream of the study region, the Kosñipata River flows into the Alto Madre de Dios River which feeds the Madre de Dios River (Figure 3.1b), a major tributary of the Amazon River (Figure 3.1c). The geology of the study area is dominated by meta-sedimentary mudstones covering ~80% and 100% of the San Pedro and Wayqecha catchments respectively, with a plutonic intrusion comprising ~20 % of the San Pedro catchment (Table 3.1) [*Carlotto Caillaux et al.*, 1996]. The geological characteristics and vegetation of the valley are generally representative of the larger eastern Andean region of southern Peru and northern Bolivia [*Carlotto Caillaux et al.*, 1996; *Consbio*, 2011; *INGEMMET*, 2013]. The region is particularly prone to landslides (refer to chapter 5).

Table 3.1: Descriptions of the Wayqecha and San Pedro catchments on the Kosñipata River.

Catchment	Area (km^2)	Mean slope* (°)	Mean elevation* (masl)	Elevation range (masl)	Landcover type¤ (~ %)	Geology^ (~ %)	Gauge lat/long (S, W)	Gauge elevation (masl)
Wayqecha	48.5	26	3195	2260 to 3930	TMCF (50), puna /transition (50)	mudstones (100)	13°9'46", 71°35'21"	2250
San Pedro	164.4	28	2805	1355 to 4000	TMCF (80), puna /transition (20)	mudstones (80), pluton intrusions (20)	13°3'37", 71°32'40"	1360

* Based on Shuttle Radar Topography Mission (SRTM) data with a 90 x 90 m resolution.
^ Basin geology derived from [*Carlotto Caillaux et al.*, 1996].
¤ Landcover types were determined using 2009 Quickbird 2 imagery.

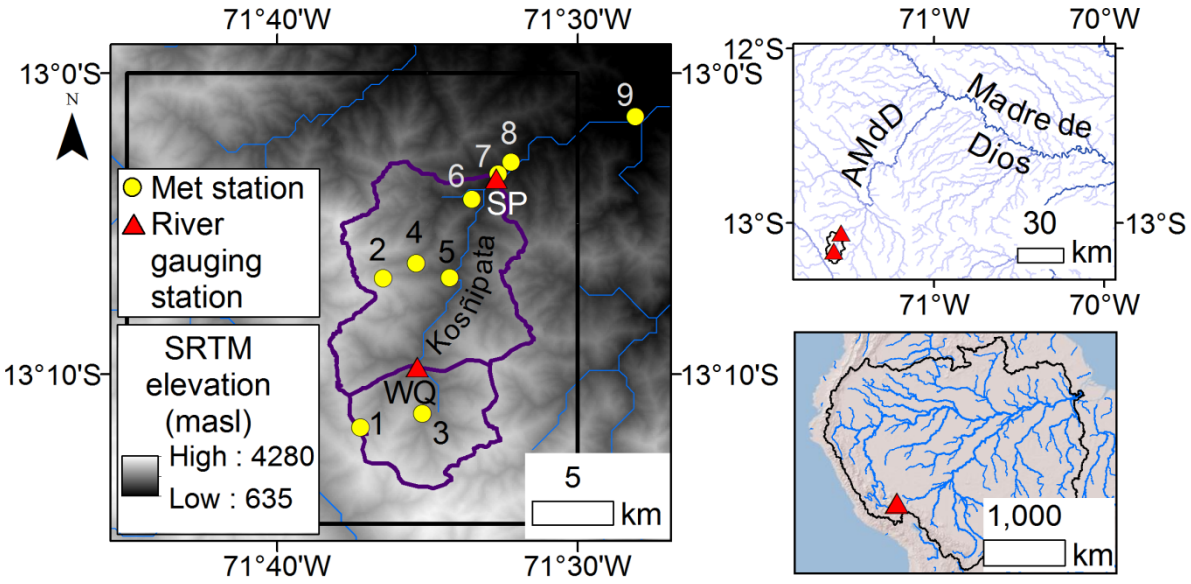


Figure 3.1: a) The study area in the Eastern Andes of Peru is in the Kosñipata River Valley. The purple lines delineate the two basins: the Wayqecha catchment is the smaller basin and the San Pedro catchment is the larger basin encompassing the Wayqecha catchment. The hydrologic gauging stations are WQ = Wayqecha and SP = San Pedro. The shaded elevation is from shuttled radar topography mission (SRTM) digital elevation model (DEM) with a 90 x 90 m resolution. The TRMM 3B43 tile used in this study (cf. Figure 3.3a) is shown by the black box outline. The met stations used for rainfall data in this study are numbered 1 – 9 (Table S3.2). b) The Kosñipata River flows into the Alto Madre de Dios (AMdD) and then into the Madre de Dios River. c) The Madre de Dios River joins the Madeira River and then flows into the Amazon River.

The climate of the Eastern Andes is influenced by the South American Low Level Jet (SALLJ), which carries humid winds west over Amazonia [*Marengo et al.*, 2004]. The Kosñipata Valley sits in a band of persistent cloudiness that runs along the Eastern Andes [*Halladay et al.*, 2012b] and lies within in a "wet-spot" with particularly high rainfall relative to the Andean regions to the north and to the south [*Killeen et al.*, 2007]. Within the valley, rainfall decreases with an increase of elevation, from 5300 mm yr^{-1} at 1500 masl down to 1560 mm yr^{-1} at 3025 masl, near the treeline [*Girardin et al.*, 2013; *Huaraca Huasco et al.*, 2013], where down-valley winds collide with most air from Amazonia [*Halladay et al.*, 2012b]. Rainfall also decreases at lower elevations in the Andes foothills, below the San Pedro gauging station; highest rainfall is observed

between 1000 and 1500 masl [*Rapp and Silman*, 2012] due to orographic effects. Note that lower total annual rainfall amounts were reported previously for this region [*Lambs et al.*, 2012], but the data used is this previous study were incomplete for the locations where we recorded highest rainfall. Orographic fog (cf. *Scholl et al.* [2011]) plays an important role in the Kosñipata Valley. Cloud base varies in height throughout the year, with the cloud base at its lowest in the dry season (June to August) [*Halladay et al.*, submitted]. In July (mid-dry season) the cloud base is >60 % of the time >1800 masl and 30% of the time between 1500 – 1800 masl [*Rapp and Silman*, 2014]. Cloud water interception has not been directly quantified in the valley, but ranges from ~20 to ~2000 mm yr^{-1} in other tropical montane cloud forest catchments [*Bruijnzeel et al.*, 2011]; similar ranges are expected in the Kosñipata Valley. Annual mean temperatures in the Kosñipata range from ~19 °C at low elevations to ~12 °C at high elevations [*Girardin et al.*, 2013; *Huaraca Huasco et al.*, 2013] with an adiabatic air temperature lapse rate of 4.94 °C km^{-1} of altitude [*Girardin et al.*, 2010]. The wet season is generally defined to be December to March, the wet-dry transition season to be April, the dry season to be May to September, and the dry-wet transition season to be October and November (Table S3.1). These terms are used in a relative sense in the Andes, since precipitation is still significant in the dry season.

The valley is dominated by forest (~80 % in the San Pedro catchment and ~50 % in the Wayqecha sub-catchment; Table 3.1) with the remainder of the catchments being high elevation grasslands called wet *puna* [*Squeo et al.*, 2006]. Small areas of bare bedrock are exposed at the highest elevations. In the forested area, vegetation consists of sub-alpine cloud forest at high elevations (3400 to 3600 masl), upper montane cloud forest between 2000 to 3400 masl, and lower montane cloud forest and sub-montane tropical rainforest between 1200 to 2000 masl [*Horwath*, 2011]. The Kosñipata Valley is

partially contained in Manu National Park, where logging is prohibited. The soils in the forested parts of the catchment are predominantly Inceptisols [*Asner et al.*, 2014] with a soil water content > 25 % throughout the year [*Girardin et al.*, 2013; *Huaraca Huasco et al.*, 2013]. Soils show little evidence of seasonal moisture stress except at the highest treeline sites [*Girardin et al.*, 2013]. At lower altitudes there are only short periods at mid-day at the driest time of year which show some signs of moisture stress [*Rapp*, 2010]. The timberline occurs at 3300 ± 250 masl with *puna* grasslands and some shrubland above the timberline (See chapter 5). The soils in the *puna* grasslands in the valley are usually saturated for ~8 months of the year (November to June; I. Oliveras personal communication) due to relatively high precipitation and low temperatures [*Wilcox et al.*, 1988].

3.3. Materials and methods

3.3.1. Discharge and runoff measures

This study focuses on runoff measurements made over a one year period of study at two in-stream gauging stations we established along the Kosñipata River (Figure 3.1a). Field measurements consisted of river height, flow velocity and cross-sectional area measurements, which together allowed us to estimate discharge and runoff over the study period. For full details of the cross-sectional area and river velocity measurements and corrections, and the corresponding stage height to discharge rating curves for both the Wayqecha and San Pedro catchments, see the supplementary section. A brief summary is provided here.

The San Pedro in-stream automatic gauging station is situated at 13°3'37"S, 71°32'40"W, at 1360 masl. River stage height at the San Pedro gauge station was measured from November 2009 to April 2011 using a river logger (WL16 Data Logger,

range 0 – 9 m, Global Water), recording river level every ~15 min. The instantaneous discharge associated with each height measurement was calculated using equation S2. This was based on calibrated stage-discharge relationships. Total monthly discharge was determined by summing over each month, and the monthly totals were converted into an instantaneous discharge ($m^3 s^{-1}$) for each month. Seasonal discharges ($m^3 s^{-1}$) and annual discharge ($m^3 s^{-1}$) were determined by taking the mean of the monthly instantaneous discharges over the appropriate time period ($m^3 s^{-1}$). There was a gap in the logger data of 31 days in the dry season between mid-July and early-August (Figure 3.2) because the batteries were not functioning in the logger. These gaps were filled by extrapolation, where the known runoff per day was corrected for the total days in the month. Baseflow (Q_b) at the San Pedro gauging station was determined from mean daily discharge ($m^3 s^{-1}$) using the method outlined in *Gustard et al.* [1992]. Base flow index (BFI) was calculated as the ratio of the total volume of baseflow divided by the total volume of streamflow.

The Wayqecha in-stream manual gauging station is located at 13°9'46"S, 71°35'21"W, at 2250 masl (Figure 3.1a, Table 3.1). Field measurements were taken weekly to monthly at the Wayqecha gauging station over the one year study period (n = 44, with a two week intensive wet season study period from the end of January to mid-February 2010 (n = 15; Figure 3.2). River height was manually recorded using a measuring stick. Available instantaneous discharge ($m^3 s^{-1}$) measurements were used to determine mean monthly discharge. Since there were no field measurements in September, the mean for this month was linearly extrapolated from the August and October mean monthly discharges. There are significant uncertainties associated with the discharge and runoff at the Wayqecha gauging station because 1) the data comes from only 59 spot measurements throughout the year and 2) the river bed was changing locations and 4 river profiles were used over the year.

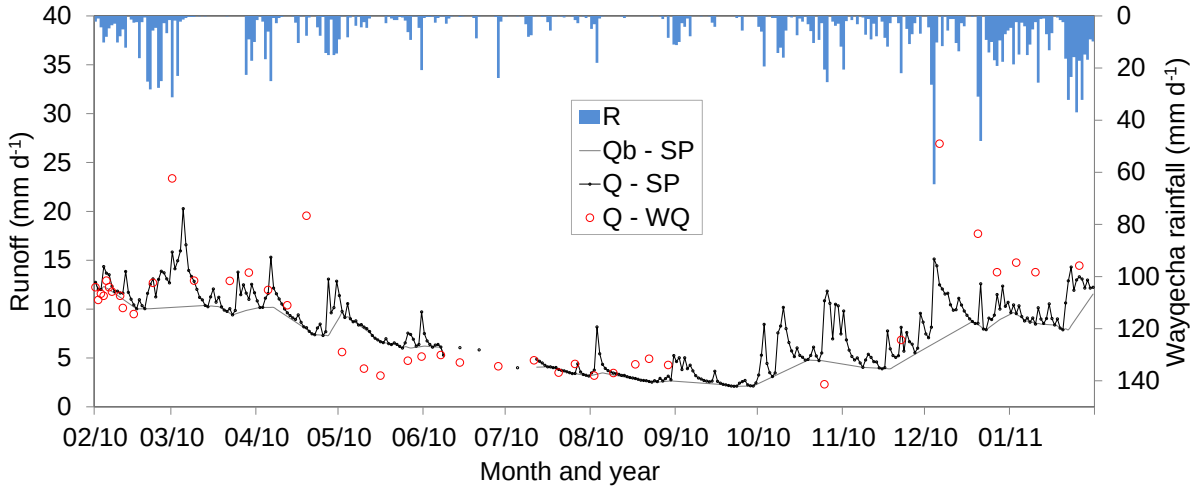


Figure 3.2: Runoff (Q; mm d^{-1}) over the study period for the Wayqecha and San Pedro gauging stations in the Kosñipata Valley. Rainfall from the Wayqecha meteorological station is on the secondary axis (mm d^{-1}). The San Pedro runoff (Q – SP) and baseline runoff (Q_b – SP) were measured nearly continuously through the year, with a 31-day gap partly in July and August that is covered by three manual measurements. The Wayqecha runoff (Q – WQ) was measured throughout the year from a daily to a monthly interval.

3.3.2. Catchment wide rainfall estimates

Meteorological stations are located throughout the valley along an altitudinal gradient from 887 to 3460 masl (Figures 3.1 & 3.3a), distributed in various landcover types and on a range of slopes and aspects (Table S3.2). Only data from the Wayqecha meteorological station was recorded over the full length of this river study, so rainfall was estimated for both catchments using the long-term monthly record from 0.25 ° x 0.25 ° merged Tropical Rainfall Measuring Mission (TRMM) data [*TRMM*, 2013] together with the long-term monthly rainfall data from nine meteorological stations [*ACCA*, 2012; *Rapp and Silman*, 2012; *SENAMHI*, 2012; *Girardin et al.*, 2013; *Huaraca Huasco et al.*, 2013].

The 3B43 v7a TRMM is a third level product with outputs in mm d^{-1}, which have been converted to mm $month^{-1}$ with an output each month from 1998 to 2012. Both the Wayqecha and the San Pedro basins are encompassed in one 3B43 TRMM tile with an area of ~730 km^2 centred at 12°7'48"S, 71°38'6"W (Figure 3.1a). The raw TRMM 3B43

data is known to underestimate rainfall in the Andes [*Bookhagen and Strecker*, 2008; *Scheel et al.*, 2011]. Indeed, in the case of the Kosñipata, TRMM 3B43 rainfall is an underestimate compared to nearly all of the data from met station rainfall gauges in the valley and is most comparable to the met stations at high elevations with low rainfall (Figure 3.3a). Because of the apparent systematic bias, we did not use the TRMM data directly but instead calibrated the TRMM data using meteorological data to make robust catchment wide rainfall estimates. This has the advantage of allowing us to use the long-term TRMM record that covers periods of time when data is not available from the Kosñipata met stations, which only have sporadic temporal coverage, ranging from 13 to 79 months of rainfall data (Table S3.2). For complete methods on catchment wide rainfall estimates see the supplementary section.

3.3.3. Water isotope measurements

River water, rainfall, and cloud water were collected from 2009 to 2011 from a range of elevations throughout the valley. River water was collected from the river surface, passed through a 0.2 μm nylon filter, and stored unpreserved in containers that prevented evaporative loss (see supplement). Rainfall samples were collected at the time of river water collection near the river gauge, with additional samples collected along an altitudinal transect in the valley between 1500 to 3600 masl (Table S3.3a). Cloud vapour was collected along the altitudinal transect below the canopy using a cryogenic pump (Table S3.3b).

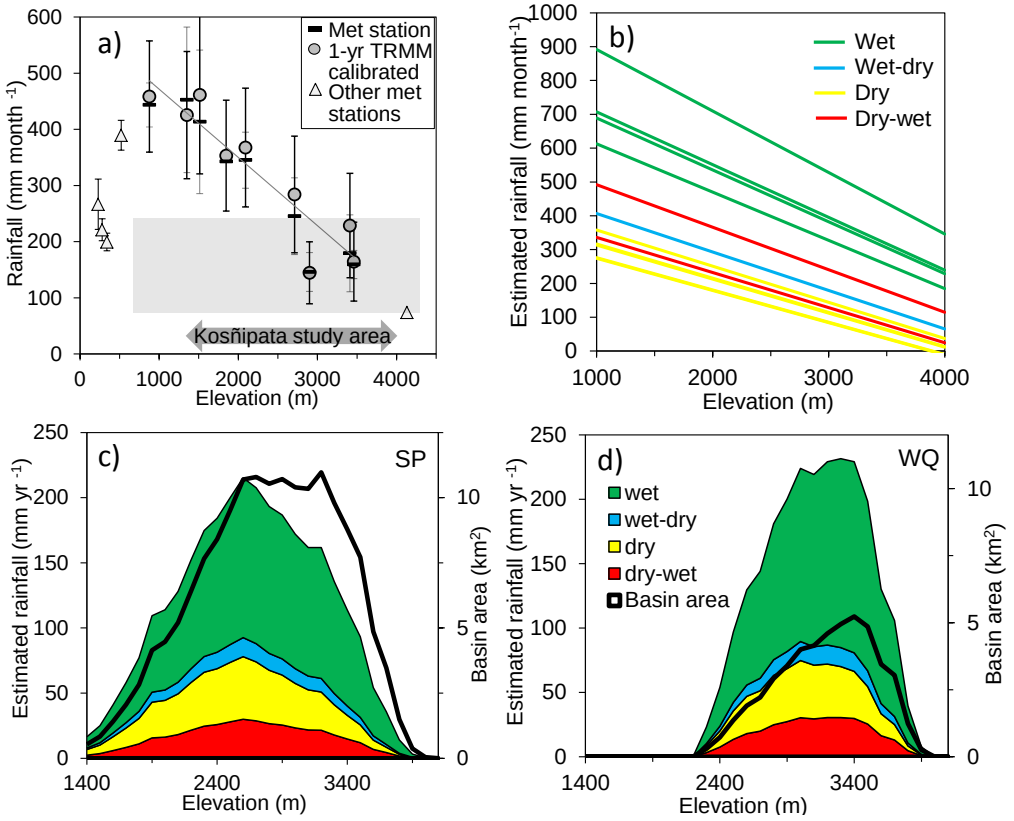


Figure 3.3: a) Available mean monthly rainfall data for the 9 meteorological stations in the Kosñipata Valley (dark dashes and light error bars) and estimated mean monthly rainfall (grey circles and dark error bars) covering the months of the 1-year study period (February 2010 to January 2011) determined using the linear regression equations for each met station derived from tropical rainfall measuring mission (TRMM) data outlined in Table S3.8. The error bars are 2 x standard error. The linear regression is derived from the mean monthly met station rainfall data derived from TRMM versus elevation (mm month^{-1} = -0.1216 × elevation + 593.16). Available mean monthly rainfall for 5 meteorological stations outside of the study area but within the larger Madre de Dios Basin (triangles) [*Rapp and Silman*, 2012]. The shaded box shows the TRMM 3B43 v7a monthly mean rainfall for the 1-year study period plus 2 x standard error and with the elevational range of the 34.5 x 34.5 km tile. The altitudinal range of the study area is represented by the dashed lines at 1350 and 4000 masl. b) Linear regressions, valid only for the Kosñipata Valley (~1000 to 4000 masl), of estimated catchment wide rainfall by month from February 2010 to January 2011, color-coded by season. c) and d) The breakdown of annual rainfall contribution by season, for the San Pedro catchment (c) and Wayqecha catchment (d) at 100 m intervals following the monthly linear regressions. Note uneven distribution of rainfall throughout the valley; there is a higher rainfall rate at lower elevations (b), but because of the basin distribution the overall rainfall input is estimated to be at mid-elevations (c). The catchment-wide seasonal and annual estimated rainfall values are summarised in Table 3.2.

Isotopic analysis was carried out on the samples to determine δD (delta deuterium, ‰), and $\delta^{18}O$ (delta 18-oxygen, ‰), and deuterium excess (defined as Dxs = δD – 8 × $\delta^{18}O$, in ‰). Deuterium excess (Dxs), representing the offset from the meteoric water line (see supplement), and provides information about the source conditions of water vapour [*Dansgaard,* 1964]. Dxs is controlled by kinetic effects during evaporation, where a larger Dxs value is an indicator of enhanced moisture recycling and a lower value indicates an enhanced evaporative loss [*Salati et al.,* 1979; *Cappa et al.*, 2003].

River water, rainfall, and water vapour samples were analysed with a Picarro L1102-i cavity ring down spectrometer (CRDS). River water and rainfall from 2011 were injected 5 times and the final 3 samples averaged. Precision (1σ) was 0.2 ‰ for $\delta^{18}O$ and 1 ‰ for δD, though some samples showed larger uncertainties. VSMOW and VSLAP standards were analysed at the same time and were used to assess accuracy and precision of the instrument between runs. Rainfall from 2009 and water vapour were injected 9 times and the final 6 samples averaged. Precision (1σ) was <0.1 ‰ for $\delta^{18}O$ and 1 ‰ for δD. Calibration of results to VSMOW was achieved by analysing internal standards before and after each set of 7 to 8 samples. Internal standards SPIT, BOTTY, and DELTA were used to calibrate against VSMOW. Additional analyses using IRMS were used as a check on the CRDS results (see supplement).

3.3.4. Actual evapotranspiration estimates

Actual evapotranspiration (AET) was estimated using the PT-JPL (Priestley and Taylor – Jet Propulsion Laboratory) AET method developed by *Fisher et al.* [2008]. The model is based on ecophysiological theory using traits that are measurable in the field or remotely. The model uses a bio-meteorological approach incorporating the radiation based model from Priestley and Taylor [1972] to determine rates of actual

evapotranspiration. The model requires only four variables: normalised difference vegetation index (NDVI), net radiation (R_n), maximum air temperature (T_{max}), and minimum relative humidity (RH_{min}). For complete methods on actual evapotranspiration estimates for the San Pedro catchment, see the supplementary section.

3.4. Results

3.4.1. Discharge and runoff

The San Pedro basin, with a mean elevation of 2805 masl and a catchment area of 164.4 km^2, was estimated to have a mean annual discharge of 14 ± 4 $m^3 s^{-1}$ and an annual runoff of 2721 mm yr^{-1} (~7.5 mm d^{-1}; Table 3.2). This compares with a microcatchment in the Ecuadorian Andes, with very similar vegetation cover and elevation ranges, which had a runoff of 3068 mm yr^{-1}, equivalent to 8.4 mm d^{-1} [*Crespo et al.*, 2011]. At San Pedro, 50 % of the annual flow was during the wet season, which covers only 33 % of the year (Table 3.2). Quickflow estimated for the San Pedro catchment was 440 ± 15 mm yr^{-1} (1.2 ± 0.5 mm d^{-1}). Baseflow estimated for the San Pedro catchment was 2337 ± 50 mm yr^{-1} (6.4 ± 1.7 mm d^{-1}) (Table 3.2).

The Wayqecha basin, with a mean elevation 3195 masl and a catchment area of 48.5 km^2, was estimated to have a mean annual discharge of 4.7 $m^3 s^{-1}$ with an annual runoff of 3065 mm yr^{-1} (8.0 mm d^{-1}; Table 3.2). The catchment had a seasonal range in monthly mean values of 2.3 to 8.8 $m^3 s^{-1}$, or 4.1 to 14.1 mm d^{-1}. There are significant uncertainties in these annual totals for Wayqecha as they are based on only 59 spot measurements of discharge. The seasonal variation in flow was greater in amplitude at Wayqecha compared to San Pedro. This suggests that the discharge and runoff in the Wayqecha sub-basin follows a similar pattern to the larger San Pedro catchment that it is nested in, but may be subjected to more short-term variations.

Table 3.2: Seasonal and annual results for the San Pedro (SP; 164.4 km^2) and Wayqecha (WQ; 48.5 km^2) catchments. Water year considered from February 2010 to January 2011.

Monthly mean	WQ Q m^3s^{-1}	SP Q $m^3 s^{-1}$	WQ Runoff mm d^{-1} (%)	SP Runoff mm d^{-1} (%)	SP Baseflow runoff mm d^{-1} (%)	SP Quick-flow runoff mm d^{-1} (%)	SP BFI*	WQ Catch-ment wide rainfall^ mm d^{-1} (%)	SP Catch-ment wide rainfall^ mm d^{-1} (%)	SP P-Q ¤ mm d^{-1}	SP R_C § %
Wet	8.0 ±1.1	21.4 ±2.2	14.1±2.4 (56.5)	11.3±1.1 (50)	9.4±1.3 (49)	1.8±0.5 (50.5)	0.84	12.6 (62)	14.7 (58)	3.4	12.2
Wet-dry	7.8	18.8	14.4 (13.5)	9.9 (11)	8.8 (11)	1.1 (7.5)	0.89	5.3 (6.5)	6.8 (7)	-3.1	16.2
Dry	2.3 ±0.3	8.5 ±3.9	4.1± 0.6 (21)	4.5± 1.7 (25)	4.4±1.9 (29)	0.4±0.2 (14)	0.91	3.0 (18)	4.3 (21)	-0.2	9.3
Dry-wet	2.6 ±2.6	12.1 ±1.0	4.6± 3.4 (9)	6.2± 0.7 (14)	4.2±0.4 (11)	2.0±1.2 (28)	0.82	5.4 (13.5)	7.0 (14)	0.8	29.6
Annual	4.7	14.3	8.4 (100)	7.5 (100)	6.4 (100)	1.2 (100)	0.84	6.7 (100)	8.3 (100)	0.8	14.5

Seasonal contribution as percentage of total annual in parenthesis. Error values are 2 x standard error based on monthly data.
* Base flow index (BFI) is the ratio of the total volume of baseflow divided by the total volume of discharge following the method outlined in *Gustard et al.* [1992].
^ Catchment-wide rainfall is reported for February 2010 to January 2011, with the contribution from each season as a percentage in parenthesis.
¤ Catchment wide rainfall (mm d^{-1}) minus runoff (mm d^{-1}) is P – Q.
§ The runoff coefficient (R_c) is a measure of rainfall-runoff response. It is the total quickflow divided by the total precipitation as described in *Blume et al.* [2007].

3.4.2. Catchment wide rainfall

The estimated annual rainfall for the study period (February 2010 to January 2011) was 3028 mm yr^{-1} (8.3 mm d^{-1}) and 2444 mm yr^{-1} (6.7 mm d^{-1}) for the San Pedro and Wayqecha and catchments respectively (Table 3.2). Based on the long-term calibrated TRMM record, the 15-year (1998 to 2012) mean annual rainfall was 2811 ± 124 mm yr^{-1} and 2243 ± 115 mm yr^{-1} and for the San Pedro and Wayqecha catchments respectively, indicating that our river discharge measurements were made in a year with higher than average rainfall (Figure 3.4; Table S3.4).

The Wayqecha sub-catchment had lower catchment wide rainfall than in the San Pedro catchment. This was apparent in the distribution of rainfall throughout the valley (Figure 3.3) and reflects variation in annual rainfall as a function of elevation (Table S3.2). Seasonal differences suggest that the wet season is slightly more dominant in the

Wayqecha catchment (+4 % compared to the same period in the San Pedro catchment) and that the dry season rainfall is slightly more dominant in the San Pedro catchment (+3 % compared to the same period in the Wayqecha catchment; Table 3.2).

The total rainfall contribution over the study period was divided into 100 m altitudinal bins to demonstrate how rainfall was distributed over the valley (Figure 3.3c & d). In the San Pedro catchment, although most of the surface area is located at mid to high elevation ranges (~2400-3400 masl), the rainfall is predominantly sourced from ~ 2400 masl (Figure 3.3c).

3.4.3. Isotopic analyses and mixing calculations

Rainwater δD and $\delta^{18}O$ values display considerable seasonal variation whereas variation with elevation during a given season is less pronounced Table S3.3a; Figure 3.5). Rainwater δD and $\delta^{18}O$ values are highest during the dry season. Seasonal variation in Dxs is minimal (Figure 3.5). The $\delta^{18}O$ and δD of Kosñipata cloud water vapours are not clearly distinct from rainwaters. This result departs from the isotopic enrichment found in cloud waters in non-orographic settings, but similarity between cloud and rainwater isotopes has also been found in the few cases of orographic cloud formation that have been studied [*Scholl et al.*, 2011]. Despite the overlap in $\delta^{18}O$ and δD, the cloud water vapour samples have higher and more variable Dxs values than all of the rainwater samples (Figure 3.5).

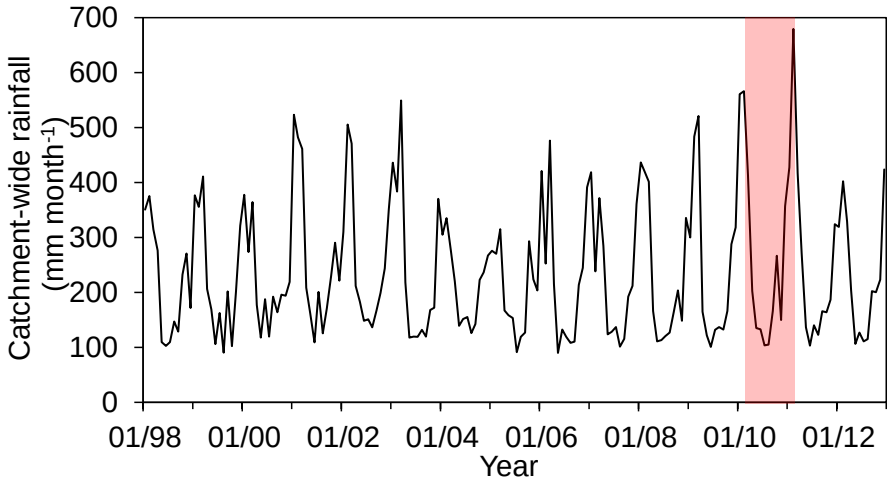


Figure 3.4: Catchment wide TRMM calibrated rainfall for the San Pedro catchment from 1998 to 2012. The red shaded area represents the 1-year study period.

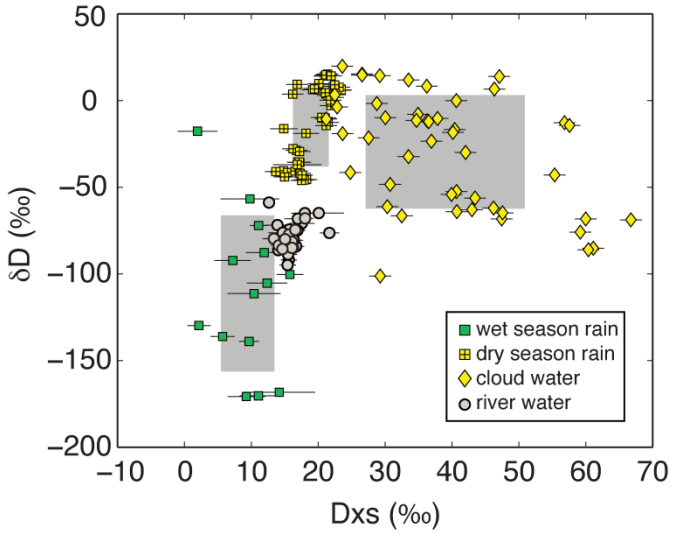


Figure 3.5: δD (‰) and Dxs (‰) of rainwater (square symbols), dry season cloud water vapour (yellow diamonds), and river water (grey circles) from within the San Pedro catchment. Rainwater samples from the dry season (yellow) were from May to August and the wet season (green) from December to March. All error bars correspond to two standard deviations. The grey shaded regions encompass the mean δD and Dxs values and one standard deviation for each end-member (i.e. wet season rainfall, dry season rainfall, and dry season cloud water vapour). The ranges defined by these grey boxes were used to generate random sets of end-member compositions for the three end-member mixing model.

For the Kosñipata River at the San Pedro gauging station, δD, $\delta^{18}O$, and Dxs values ranged from -94.8 to -64.9 ‰, -14.5 to -10.9 ‰, and 19.1 to 22.6 ‰ respectively (Table S3.5). A slight seasonality is apparent in stream water isotopic composition, with slightly higher δD values during the dry season and dry-to-wet season transition (Figure 3.6a). A significant seasonal variation in Dxs in streamwater is not apparent (Figure 3.6b). See the supplementary section for full details on the δD, $\delta^{18}O$, and Dxs isotope results.

At the Wayqecha gauging station, δD and $\delta^{18}O$ values were more depleted than at the San Pedro gauging station as a result of altitude effects on water isotope ratios (cf. *Lambs et al.* [2012]; *Ponton et al.* [in review]). Values for δD, $\delta^{18}O$, and Dxs ranged from -107.0 to -88.9 ‰, -15.9 to -13.5 ‰, and 18.3 to 20.5 ‰ (Table S3.6). Relative to samples collected at the San Pedro gauging station, seasonality at the Wayqecha gauging station is less pronounced.

Qualitative comparison between the river water isotope data from San Pedro and the rainwater and cloud water isotope data suggests that, throughout the year, wet season precipitation is the dominant contributor to river discharge (Figure 3.5). As discussed below, this probably results from the storage of wet season precipitation in groundwater that is released to the stream over time. It is possible that isotopic enrichment may take place via evaporation as water makes its way from precipitation to streamflow, either associated with throughfall (e.g. *Brodersen et al.* [2000]) or in soils (e.g. *Thorburn et al.* [1993]; *Dawson and Ehleringer* [1998]). Such isotopic enrichment could bias inferences about water sources using isotopic signatures. However, we note that any evaporative enrichment would act to decrease the relative contribution from wet season rainfall (the depleted source), supporting the qualitative inference that wet season rainfall is the dominant source of streamflow throughout the year. Moreover, the Kosñipata

streamwaters appear to have little geochemical imprint of evaporation. Chloride concentrations provide a conservative tracer that should be enriched during evaporation; in the Kosñipata samples, Cl concentrations are similar in rainwater (2-20 μM) and streamwater (2-12 μM) [*Torres et al.*, in prep.]. Kosñipata stream waters also lie on the same local meteoric water line as rainwater, with no evidence for relative D-depletion that may be expected during evaporation (see supplement).

To quantitatively constrain the relative contributions of different water sources to river discharge, a three end-member mixing model was used (see supplementary info for details). In this model, mixing between wet season precipitation, dry season precipitation, and dry season cloud water vapour is considered along with observed variability in the isotopic compositions of each of these end-members (i.e. *Phillips and Gregg* [2001]). Since we assume minimal evaporative enrichment of water isotopes during runoff generation, the results of this model provide a minimum constraint on the contribution from wet season rainfall. Results of the three end-member mixing calculations are distributions of possible end-member contributions (Figure 3.6c to f). For individual samples, mean contributions of wet season rainfall, dry season rainfall, and cloud water vapour to river discharge range from 46-67 %, 19-33 %, and 7-31 % respectively (Figure 3.6f; Table S3.7). Similarly, the maximum likely contributions of each source to a single sample, which we define as the 95^{th} percentile value of the distribution, range from 66-87 %, 38-60 %, and 19-5 2% for wet season precipitation, dry season precipitation, and cloud water vapour respectively (Figure 3.6c to f). It is worth noting that only two samples (n = 62) show mean and maximum likely contributions of cloud water vapour greater than 18 % and 40 % respectively (Figure 3.6f; Table S3.7). These contributions calculated from the water isotope mixing model reflect the ultimate source of the water to

stream runoff, with storage and mixing in groundwater likely to be an important intermediary but one which would not affect the source partitioning.

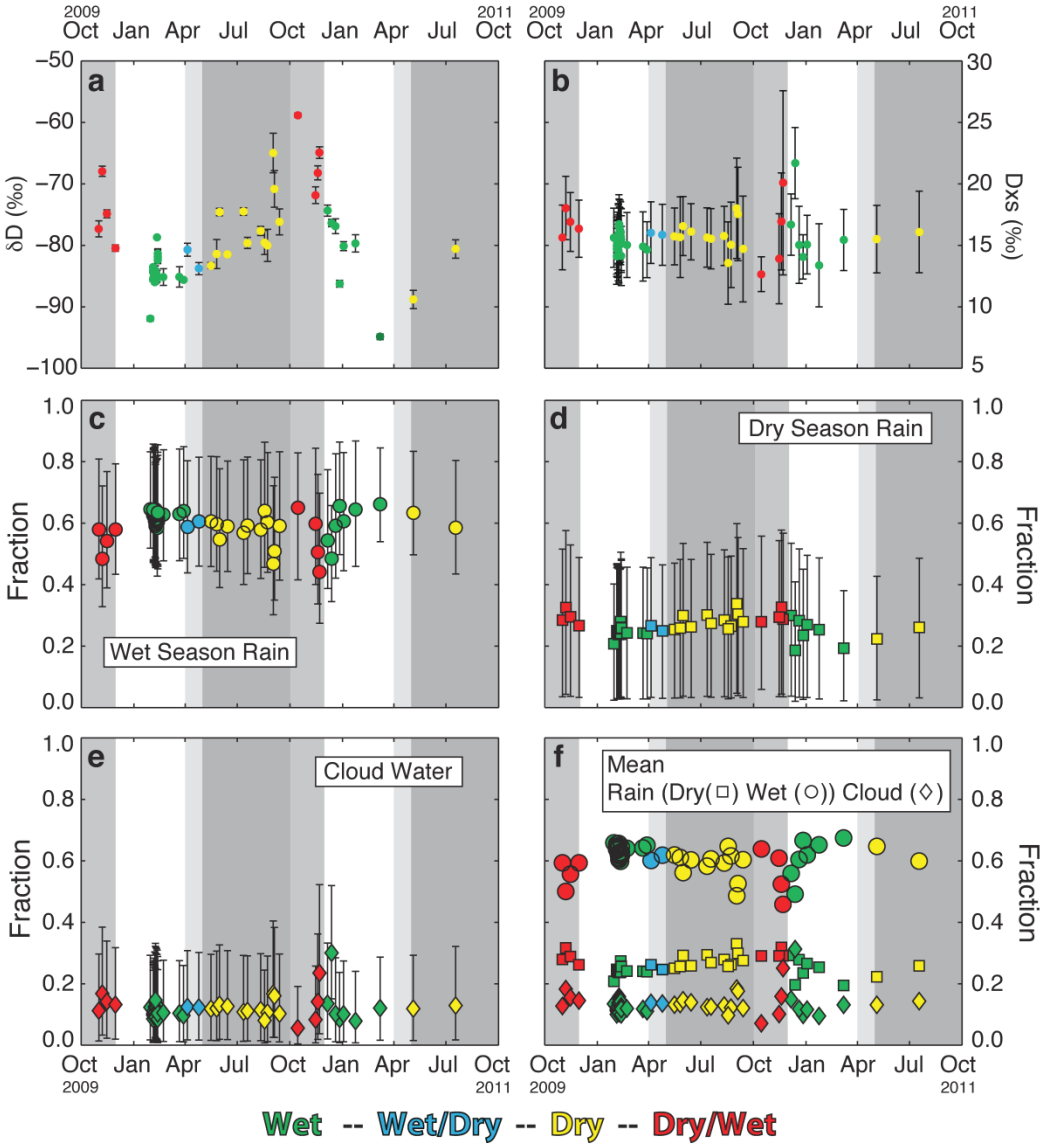


Figure 3.6: Time series of δD_{river}, Dxs_{river}, and the calculated mixing proportions for the San Pedro catchment. For all of the panels, the coloured backgrounds refer to seasonal changes in precipitation with green signifying the wet season (Dec. to Mar.), blue signifying the transition from the wet to dry season (Apr.), yellow signifying the dry season (May to Aug.), and red signifying the transition from the dry to wet season (Oct. to Nov). a) The time series of δD_{river} values with error bars signifying 2 standard deviations. b) The time series of Dxs_{river} values with error bars signifying 2 standard deviations. c) Time series of the 5^{th} (lower error bar), 50^{th} (open circle), and 95^{th} percentile (upper error bar) values of the distribution of fractional contributions of wet season rain to river discharge calculated using the three end-member mixing model. d) Time series of the 5^{th} (lower error bar), 50^{th} (open square), and 95^{th} percentile (upper error bar) values of the distribution of fractional contributions of dry season rain to river discharge calculated

using the three end-member mixing model. e) Time series of the 5th (lower error bar), 50th (open diamond), and 95th percentile (upper error bar) values of the distribution of fractional contributions of cloud water vapour to river discharge calculated using the three end-member mixing model. f) Time series of the mean contributions of wet season rain (circle), dry season rain (square), and cloud water vapour (diamond) to river discharge.

3.4.4. Cloud water in streamflow

In addition to rainfall, cloud water (CW) also contributes to Kosñipata streamflow. Isotopic mixing calculations constrain the likely cloud water vapour contribution to between 10 and 18 % of streamflow, even in the dry season, based on the mean values from the mixing model (Table S3.7). It is worth noting that all samples except for the two with the highest analytical uncertainties show this range of cloud water vapour contribution regardless of collection season (Figures 3.6f and 3.7c). Based on our estimated monthly total river discharge and the average values for cloud water contribution in each month, we estimate that total cloud water contribution to streamflow was 308 ± 97 mm yr $^{-1}$, using the 50th percentile values of the cloud water fraction and confidence intervals defined by the 5th and 95th percentiles (Tables 3.3 & S3.7). Compared to our annual discharge of 2721 mm, this means cloud water contributed 11 ± 4 % of annual streamflow. Our estimated cloud water flux to the river falls within the (admittedly very broad) range of CW interception fluxes measured in TMCFs ranging from ~50 to 1950 mm yr^{-1} [*Bendix et al.*, 2008; *Bruijnzeel et al.*, 2011].

Our results suggest that cloud water appears to play a non-negligible but secondary role in stream runoff in the Kosñipata River even during the dry season when rainfall was at its lowest and cloud immersion is most frequent. Cloud frequency is high in the valley, with cloud cover > 70 % year round [*Halladay et al.*, 2012b]. In the dry season (July) 40 % of the time the cloud base was > 1800 masl [*Rapp and Silman*, 2014].

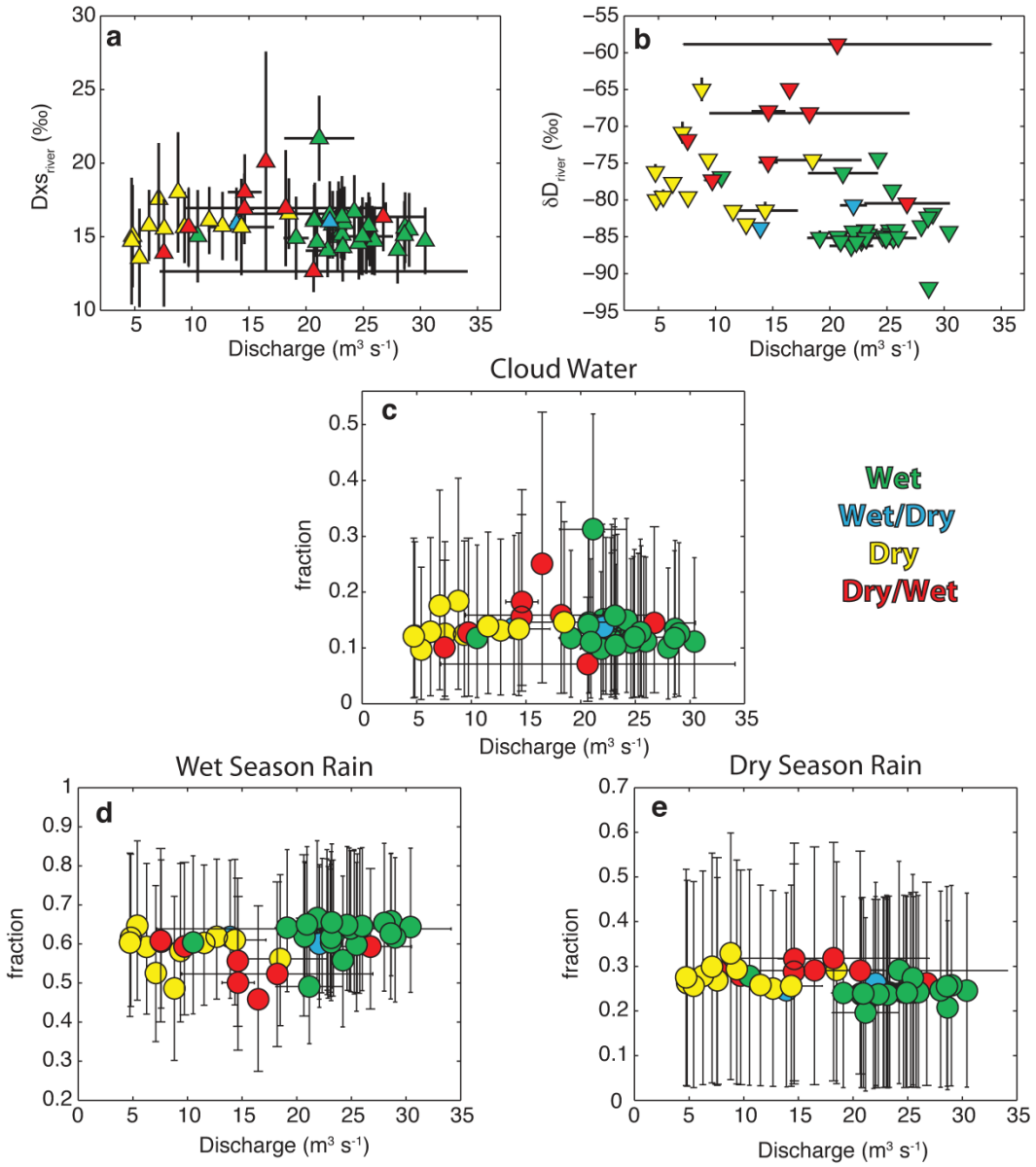


Figure 3.7: Variation in the isotopic composition of river water a) deuterium excess (Dxs_{river}, ‰) and b) hydrogen isotope ratio (δD_{river}, ‰) plotted versus discharge ($m^3\ s^{-1}$). Variation in the mean contributions to river flow as a function of water discharge for wet season rain (c), dry season rain (d), and cloud water vapour (e) as calculated by the end member mixing analysis, also plotted versus discharge. Refer to source data in Table S3.7.

Cloud immersion is a key characteristic of tropical montane cloud forest [*Bruijnzeel et al.*, 2011], and provides an important water source to the forest canopy and the diverse epiphyte community [*Bruijnzeel et al.*, 2011; *Giambelluca and Gerold*, 2011; *Rapp and Silman*, 2014]. However, it is possible that much of the intercepted water is transpired or evaporated directly from the canopy. Overall, cloud water contribution to stream runoff supplies a relatively constant proportion of total flow throughout the year and never dominates water inputs to the Kosñipata River, even during times of the lowest flow (Table 3.3).

Table 3.3: Breakdown of streamflow into its sources

	n	Fraction wet season rainfall	Fraction dry season rainfall	Fraction cloud water	Wet season rain as a source (mm month^{-1})	Dry season rain as a source (mm month^{-1})	Cloud water as a source (mm month^{-1})	Total stream runoff, as measured (mm month^{-1})
Feb-10	28	0.62±0.04	0.24±0.04	0.11±0.03	212±13	83±14	37±11	241
Mar-10	2	0.62±0.15	0.25±0.16	0.10±0.12	237±58	96±60	40±46	382
Apr-10	2	0.65±0.14	0.21±0.14	0.11±0.12	192±41	63±42	33±35	296
May-10	3	0.61±0.12	0.25±0.13	0.11±0.10	146±29	60±31	27±24	238
Jun-10	1	0.63±0.20	0.22±0.20	0.12±0.17	89±28	32±29	17±25	141
Jul-10	2	0.58±0.13	0.28±0.14	0.12±0.11	65±28	30±15	14±12	110
Aug-10	3	0.58±0.13	0.27±0.14	0.12±0.10	62±14	29±15	12±11	106
Sep-10	3	0.59±0.13	0.26±0.23	0.12±0.11	52±12	24±12	10±10	88
Oct-10	1	0.64±0.22	0.26±0.23	0.08±0.16	131±46	52±48	16±35	204
Nov-10	3	0.52±0.14	0.30±0.15	0.14±0.12	92±25	53±27	24±22	176
Dec-10	4	0.56±0.12	0.30±0.13	0.10±0.09	179±36	93±42	33±28	317
Jan-11	2	0.55±0.16	0.29±0.18	0.14±0.14	177±53	94±58	44±46	322
Wet		0.59±0.07	0.27±0.07	0.11±0.05				
Wet-dry		0.65±0.14	0.21±0.14	0.11±0.12				
Dry		0.60±07	0.25±0.07	0.12±0.06				
Dry-wet		0.59±0.14	0.28±0.14	0.11±0.11				
Annual		0.60±0.04	0.26±0.05	0.11±0.04				

Error bars are propagated uncertainty (1σ) from individual samples per month.
Derived from the Monte Carlo mixing modelling (Table S3.7)

3.5. Discussion

3.5.1. Water balance

The annual water balance for the Kosñipata Valley at the San Pedro gauging station can be described by the following equation (water inputs to the catchment on the left, losses from the catchment on the right):

$$Rainfall + CW = AET + Runoff + Residual \quad (1)$$

Stream runoff was 2721 mm yr^{-1} and catchment wide rainfall was 3028 mm yr^{-1}. Using the PT-JPL model [*Fisher et al.*, 2008] we estimate actual evapotranspiration (AET) to be 909 mm yr^{-1}. Based on the isotope mixing model results, we estimate cloud water (CW) contribution to be 308 ± 97 mm yr^{-1}. The residual is the amount of water not accounted for by this water balance and gives an estimate of overall uncertainty in our calculation. We calculate from equation (1) a residual of -294 ± 97 mm, equivalent to 9 ± 3 % of total annual water inputs through precipitation and CW, indicating that any imbalance within our budget is within the uncertainties of the water balance components. In other TMCF catchment studies it has also been difficult to fully close the water budget, although the <~10 % imbalance within our budget is almost certainly within the uncertainties in individual components of the water balance calculation. There are several uncertainties in the water balance, including in our estimates of:

Evapotranspiration: The actual evapotranspiration could be lower than what the PT-JPL model [*Fisher et al.*, 2008] predicts. In lowland tropical forests, evapotranspiration (ET) is 1000-1300 mm yr^{-1} [*Fisher et al.*, 2009; *Bruijnzeel et al.*, 2011], but given that the valley is in a tropical montane cloud forest, lower ET values between 800 and 1200 mm yr^{-1} are possible [*Bruijnzeel et al.*, 2011]. For one month from mid-July to mid-August 2008 sap flow was predicted to be 53 mm $month^{-1}$ using the Soil-Plant-Atmospheric (SPA) model based on Wayqecha forest canopy sap flow measurements (2900 masl) [*van de Weg et al.*, 2014]. Sap flow is a proxy for canopy transpiration. For the same time period when the sap flow measurements were made, the PT-JPL model predicted canopy transpiration at 49 mm $month^{-1}$ for the Wayqecha met station nearby the plot. This suggests that even though the PT-JPL model has not been deployed in TMCF previously, it provides a reasonable canopy transpiration result.

Rainfall: Rainfall was estimated for the catchment by calibrating TRMM rainfall with actual rainfall collected from 9 gauging stations. In the Kosñipata Valley there was a decrease of rainfall with an increase of elevation, corresponding to an average annual rainfall gradient of ~148 mm per hundred metres (Figure 3.3a). It is possible that rainfall deviates from this trend along the altitudinal gradient because our results are limited to 9 meteorological stations dispersed over a large area (Figure 3.1a). Intense localised storm activity also increases the chance of underestimating precipitation. Additionally, the types of rain gauges used in the valley (Table S3.2) are not ideal for cloud forests due to an underestimation of wind driven precipitation on steep slopes [*Bruijnzeel et al.*, 2011; *Frumau et al.*, 2011]. Thus underestimation of precipitation may contribute significant uncertainty in our measurements.

Cloud water: CW contribution to stream flow was estimated from water isotope data and mixing modelling (see section 3.3 & 4.3), suggesting a likely input that is approximately 11 ± 4 % of streamflow (Figures 3.6f and 3.7c; Table 3.3). Variation within this range would not considerably affect the water balance, since it is a small component overall, but it may introduce some additional uncertainty.

Stream runoff: Stream runoff can be easily overestimated especially in mountain rivers due to an overestimation of velocity [*Thome and Zevenbergen*, 1985; *Chen and Chiu*, 2004]. We have taken this under consideration at the San Pedro gauging station and corrected surface velocity to estimate mean channel velocity following equation S1, but it is possible that our runoff values remain overestimated.

It is also possible that deep groundwater input from a surrounding catchment could account for some of the residual in our water budget calculation for the Kosñipata. In a

TMCF in Mexico, for example, a residual on the water budget of +700 mm yr^{-1} was attributed to deep groundwater leakage out of the study area [*Muñoz-Villers et al.*, 2012].

3.5.2. Quickflow, baseflow and hysteresis

3.5.2.1. Quickflow

The runoff coefficient [*Blume et al.*, 2007] measures the rainfall response, in terms of the proportion of rainfall that enters the stream as quickflow and can be calculated as an annual, seasonal or event based measurement. Over the year that was studied, the mean runoff coefficient (R_c) was 14.5 % (Table 3.2). The dry-wet transition season had the highest rainfall-runoff response with a R_c of ~30 %, indicating that in the dry-wet season rainfall is more likely to contribute to quickflow rather than to be absorbed into the soil, in comparison to other seasons with lower R_c. Since half of the quickflow occurred in the wet season, this was, unsurprisingly, the most important period in the annual cycle for storm-flow discharge (Table 3.2). The sources of the storm streamflow are unknown, but it is possible that a large proportion was pre-event water as measured in other TMCFs [*Muñoz-Villers and McDonnell*, 2012]. Overall, the strong rainfall-runoff responses produce conditions that aid in the exportation of sediment and associated particulate carbon and nutrients from the eastern Andes [*Townsend-Small et al.*, 2008; *Clark et al.*, 2013]. See chapters 4 and 6 for further details.

3.5.2.2. Baseflow

While quickflow is important for material export, baseflow appears to be important in supporting sustained flow over the course of the year. The annual BFI was high in the Kosñipata Valley (0.834, or 83 %) and comparable to catchments with permeable bedrock [*Gustard et al.*, 1992] and the presence of groundwater. The value we found for the Kosñipata is consistent with a Mexican TMCF where 90 % of the annual flow was attributed to baseflow [*Muñoz-Villers et al.*, 2012] and an Ecuadorian TMCF

microcatchment where 70 % of annual flow was baseflow [*Crespo et al.*, 2011]. The BFI for the Kosñipata was the highest in the wet-dry transition season (0.90) and the dry season (0.91), and lowest in the dry-wet transition season (0.82) and the wet season (0.84) indicating a larger importance of baseflow in the wet-dry transition and the dry seasons (Table 3.2), as expected.

3.5.2.3. Hysteresis

A monthly breakdown of the water balance shows the distribution of annual residual when water is going into storage (+) and when water is coming out of storage (- ; Figure 3.8). The mid-wet season (January & February) was a time of recharge with positive residual values. This store was subsequently drained as discharge to stream runoff in the wet-dry transitional season (April) and most of the dry season (May to August), both of which showed negative residual values (Figure 3.8). This illustrates how rainfall stored during the wet season plays an important role in sustaining steady dry season runoff. The results of the isotope mixing analysis confirms this inference by showing that wet season rainfall is still prominent in contributing to streamflow in the dry season: sources of streamflow during May to September 2010 were 60 ± 7 % from wet season rainfall, 25 ± 7 % was from dry season rainfall and 12 ± 6 % from cloud water (Table 3.3).

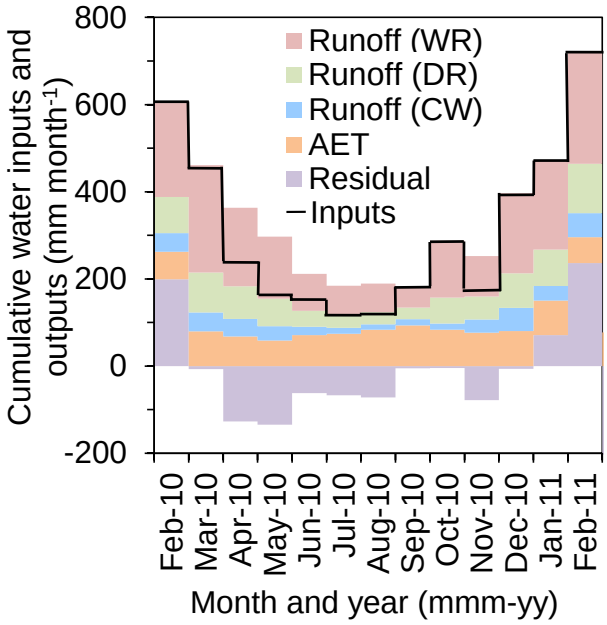


Figure 3.8: Cumulative water input and output (mm month^{-1}) over the 1-year study period (February 2010 to January 2011) as well as for February 2011. Water input comprises of wet season rainfall (WR) and dry season rainfall (DR), and cloud water interception (CW). Water output comprises runoff, actual evapotranspiration, and residual. The residual was calculated per month from a rearrangement of equation 1. The residual shows that rainfall is stored (positive residual) particularly during January and February, and then subsequently released (negative residual) in the wet-dry transition season (April) and throughout most of the dry season (May to August) when rainfall it is lowest. Hence runoff exceeds rainfall throughout this period.

At a seasonal timescale, the San Pedro catchment, in the Peruvian Andes, total streamflow and baseflow both follow an annual anti-clockwise hysteresis pattern (Figure 3.9a-d). This is similar to that observed by *Andermann et al.* [2012] in the Nepalese Himalaya. In the wet season in the Kosñipata Valley (December to March), the catchment wide rainfall was greater than streamflow and baseflow. During the wet-dry transition season (April), however, there was a switch and streamflow and baseflow were greater than rainfall. At the start of the dry season (May and June) the trend continued and the rainfall was still lower than streamflow and baseflow. By the middle of the dry season (July and August) rainfall was equal to streamflow and baseflow. By the time of the late dry season (September), rainfall started to increase and was greater than streamflow and

baseflow. Overall, the dry-wet transition season (October and November) had higher rainfall than streamflow and baseflow. Finally, in the early wet season (December to January) the cycle was completed where the contribution of rainfall dominated streamflow and baseflow (Figure 3.9a & c). The annual anti-clockwise hysteresis was even more pronounced when the San Pedro streamflow is compared to the rainfall gathered over the study period at the Wayqecha meteorological station at 2900 masl (Figure 3.9b & d).

The water isotope data support the indication of seasonal hysteresis observed in the water balance estimates. The relationship between river discharge and δD showed a seasonal clockwise hysteresis, but this was not observed in Dxs (Figure 3.7a & b). Considering the observed end-member δD and Dxs compositions, this implies that there was seasonal variation in the relative contributions of wet and dry season rainfall but not cloud water vapour (Figure 3.7c to e). The Monte-Carlo derived confidence intervals on the mixing results provide large ranges. However, the mean results (Figure 3.7), which best represent each end-member composition, show a seasonal anti-clockwise hysteresis between river discharge and the mean contribution of wet-season precipitation that is consistent with the hysteresis observed in the water balance. Dry season and dry-wet transitional season runoff appear to be sustained by relatively lower, but still dominant, contributions from wet season precipitation (Figure 3.7d). A corresponding variation in the contribution of dry season precipitation with discharge is also evident, whereby dry season and dry-wet transitional season runoff is composed of a larger proportion of dry season rainfall (Figure 3.7e). The hysteresis in the mixing model results is attributable to the seasonal hysteresis in streamwater δD. No seasonal hysteresis in the contribution of cloud water interception to river discharge is apparent (Figure 3.7c), consistent with no seasonal pattern in the streamwater Dxs.

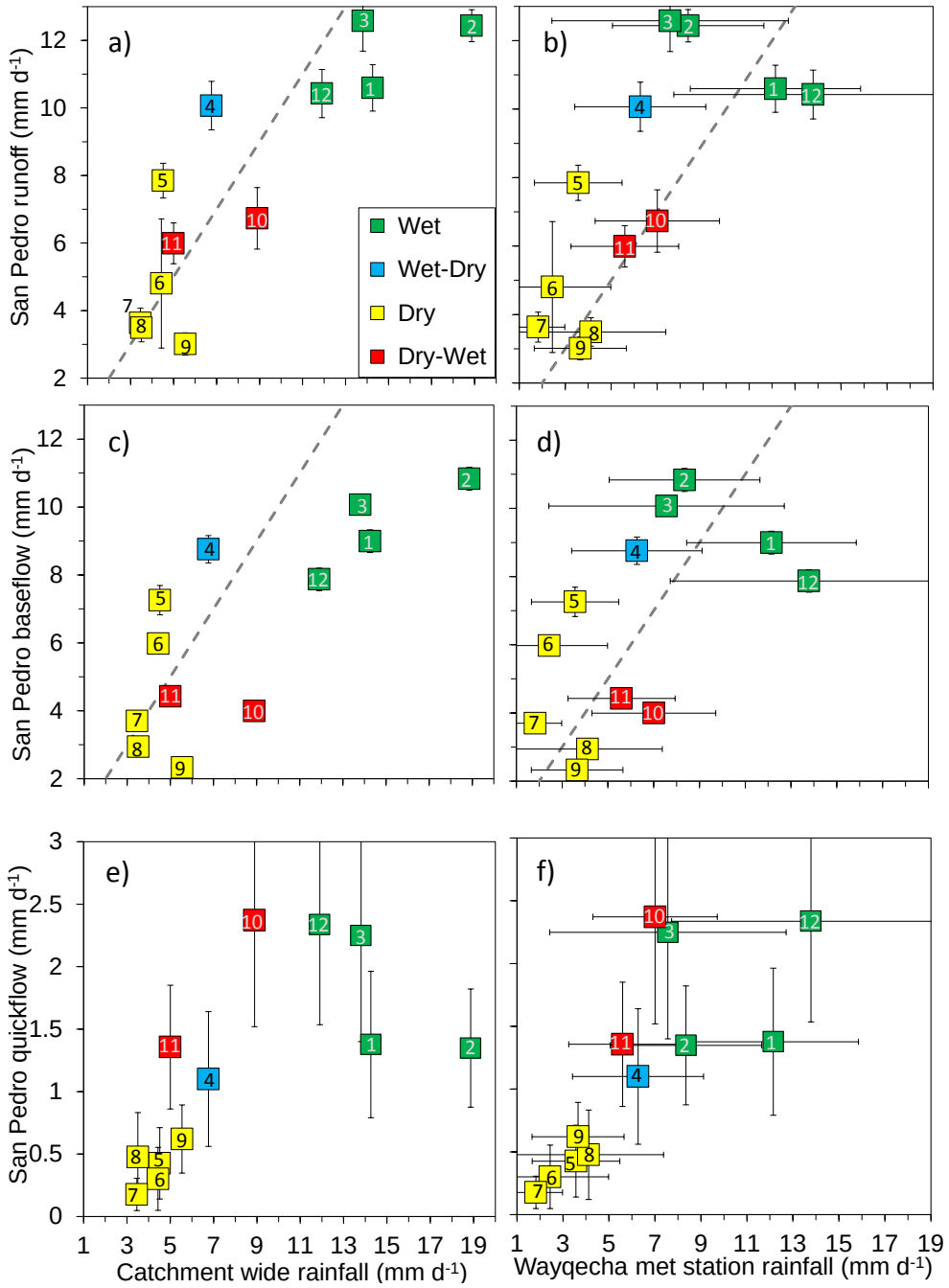


Figure 3.9: Monthly rainfall - runoff plots for the Kosñipata Valley, showing anticlockwise hysteresis. Plots show runoff at San Pedro versus a) catchment wide and b) meteorological station rainfall for the Wayqecha met station; baseflow at San Pedro versus c) catchment wide and d) meteorological station rainfall at Wayqecha; and quickflow at San Pedro versus e) catchment wide and f) meteorological station rainfall at Wayqecha. Monthly-averaged values for daily discharge and met station rainfall were determined by summing daily flux (mm d^{-1}) and taking the mean for each month over the 1-year study period. Days with zero rainfall at Wayqecha station were removed from mean rainfall calculations. Rainfall estimated for the San Pedro catchment was determined by month (see materials and methods). Error bars represent 2 * standard error. Months are numbers 1-12. The months are numbered chronologically and colour coded

by season (Table S3.1). The one-to-one line for discharge to rainfall is represented by the grey dashed line. Months with runoff to the left of this line indicate dominance of groundwater discharge. Groundwater dominance (via baseflow) occurs from April to June when compared to catchment wide rainfall (a & c) and from February to July when compared to Wayqecha met station rainfall (b & d). Rainfall at the Wayqecha met station located at 2900 masl (Table S3.2) was lower than the catchment rainfall especially during the latter part of the wet season (February and March), suggesting the importance of rainfall at lower elevations during the wet season. Quickflow was variable throughout the year with a general linear trend with rainfall.

The consistent, annual anti-clockwise hysteresis in both the water balance and the contribution from different sources inferred from the water isotopes indicates that there are important factors other than the storm runoff response that influenced hydrologic variability throughout the year in the Kosñipata Valley. The lag in runoff can be explained by a significant portion of wet season rainfall being stored, and then several months later discharged as runoff in the wet-dry transition and dry seasons (Figure 3.9a & Table 2). The delay in rainfall to streamflow runoff helps provide water in the catchment at times of lower rainfall, stabilising dry season runoff.

3.5.3. Causes for hysteresis

3.5.3.1. Soil water

There are several potential mechanisms causing a seasonal lag in streamflow. The water isotope data points to rainfall as the primary ultimate source of water, i.e. rather than cloud water, but it is still unclear how rainfall is stored temporarily over the year. Shallow groundwater (i.e., lateral flow through soil layers) derived from accumulation of water in soils during the wet season may contribute to the delayed stream runoff. In the Kosñipata Valley, shallow groundwater may be sourced from drainage of saturated *puna* grassland soils. In Paramo wetlands (which are a similar but wetter mountain top biome) in the northern Andes of Ecuador, delayed groundwater has been shown to play an important role in dry season runoff [*Buytaert and Beven*, 2011]. Tropical montane cloud

forest soils in a similar forest in Ecuador can also be a potential source for delayed runoff over shorter periods of 3.7 to 9.2 weeks [*Timbe et al.*, 2014], but soil water supply over these timescales is too brief to explain the seasonal lag observed in the Kosñipata.

In order to evaluate whether seasonal variations in soil water content are sufficient to entirely account for the variability that would be needed to explain the seasonal lag in runoff in the Kosñipata, we use the following equation:

$$A_{catchment} \times ED = A_{storage} \times d \times \Delta V \quad (2)$$

where $A_{catchment}$ is the area of the drainage basin (m^2), ED is the excess discharge (mm) consisting of the sum of the negative monthly residual values from the wet-dry transitional season to the dry season (April to September; Figure 3.8), $A_{storage}$ is the area of the basin covered in soil (m^2), d is depth of soil layer (m), and ΔV is the variation in soil water content that needs to occur to account for the excess discharge. Since the area of the catchment and area covered in soil are approximately the same, the area variables in Equation (2) cancel out. Equation (2) can be rearranged to solve for the variability in soil water:

$$\Delta V = \frac{ED}{d} \quad (3)$$

For our order-of-magnitude calculation, we assume mean soil depth (*d*) to be ~0.5 m, consistent with data from the Kosñipata catchment [*Zimmermann et al.*, 2009; *Gibbon et al.*, 2010]. Using the mean CW monthly input into streamflow (Table 3.3), the excess discharge (ED) from April to September was 468 mm. Hence, from equation (3), volumetric water content would need to have a seasonal range of 94 % to fully account for the seasonal excess discharge. Typical soil water content is around 40 % and shows a

seasonal variation of < 5 % [*Girardin et al.*, 2013; *Huaraca Huasco et al.*, 2013] in both cloud forests and puna soils. This variability in soil moisture is an order of magnitude smaller than required to explain sustained streamflow. Hence the excess dry season discharge cannot be accounted for by seasonal storage and drainage of soils.

3.5.3.2. Groundwater

If soil water content changes are insufficient to account for the excess dry season discharge, the source of this excess discharge is likely to be deep groundwater, stored within the fractured bedrock below the shallow soil layer. In central eastern Mexico, groundwater in the TMCF was found to be an important component of dry season runoff [*Muñoz-Villers et al.*, 2012]. Groundwater occurs mostly in permeable bedrock and within fractures of impermeable bedrock [*Todd and Mays*, 1980; *Gascoyne and Kamineni*, 1994; *Jardine et al.*, 1999]. In the Nepal Himalayas, deep-groundwater recharges through fractured bedrock containing aquifers several tens of meters deep and has a storage residence time of ~45 days [*Andermann et al.*, 2012]. Fracturing and the exposure of bedding planes through the process of uplift and erosion in the Kosñipata Valley [*Carlotto Caillaux et al.*, 1996] could provide conduits that aid in deep-groundwater flow. In the San Pedro catchment ~80 % of the valley consists of sedimentary mudstones and shale, and ~20 % of plutonic intrusions (Table 3.1). Shale has a very low porosity and permeability [*Morris and Johnson*, 1967; *Domenico and Schwartz*, 1990], but when fractured its porosity is greatly increased [*Jardine et al.*, 1999]. Plutonic intrusions, as found in lower parts of the catchment, also have increased porosity as a result of fracturing [*Gascoyne and Kamineni*, 1994]. Thus we viewed deep fractured bedrock as the likely transient storage reservoir explaining the annual hydrograph in the Kosñipata.

The observation of a significant role for seasonal groundwater storage and release in Kosñipata River has implications for understanding Andean water resources, predicting flooding, and quantifying biogeochemical fluxes, and particularly for assessing how these may respond to changing climate. The rate of warming over the next 100 years in the region of the Kosñipata Valley is expected to proceed an order of magnitude faster than the 1 °C increase in temperature per 1000 years during the Pleistocene-Holocene [*Bush et al.*, 2004]. The observation of upslope migration of plant species already indicates a dramatic pace of change in the Kosñipata [*Hillyer and Silman*, 2010; *Feeley et al.*, 2011; *Tovar et al.*, 2013]. It remains unclear how patterns of rainfall and cloud frequency have been changing and will change in the future [*Halladay et al.*, 2012a; *Rapp and Silman*, 2012], much less how the hydrologic system will respond, both to changes in magnitude and in seasonality of precipitation sources. The baseline of water isotope data, the partitioning of precipitation sources, and the conceptual framework presented in this study offer the potential to help understand what hydrologic responses might be expected to changes in precipitation (e.g. as in Puerto Rico, [*Scholl and Murphy*, 2014]. Further exploration and verification of the observations in this study, for example by considering longer-term water budgets [*Andermann et al.*, 2012] and/or detailed analysis of stream hydrochemistry [*Tipper et al.*, 2006; *Calmels et al.*, 2011], would strengthen understanding of how Andean TMCFs function hydrologically today and how this function may evolve in the future.

3.6. Conclusions

We estimated runoff for the Kosñipata Valley, a catchment in the Peruvian Andes with an area of 164.4 km^2 at the San Pedro gauging site, to be 2721 mm yr^{-1}. Annual stream runoff was composed of wet season rainfall 60 ± 4 %, dry season rainfall 26 ± 5 %, and cloud water 11 ± 4 %. Baseflow contributed 83 % of the streamflow over the one

year of study. Runoff followed an annual anti-clockwise hysteresis with respect to rainfall, exhibiting a lag in stream runoff that maintained stream water flow in the early dry season. Dry season runoff was composed of 60 ± 7 % of wet season rainfall. An annual water budget indicated that 3028 mm was contributed to the catchment by rainfall, 308 ± 97 mm was supplied by cloud water, and 909 mm was lost through actual evapotranspiration. The contribution from cloud water, although important to the TMCF ecology, plays a secondary role in river streamflow (~10 %) in this catchment, even during the low flow of the dry season. The annual water budget balanced within ~10 %, which likely reflects uncertainties in our measurements. Excess discharge measured throughout the wet-dry transitional season and dry season (April to September) was ~470 mm over the study year. Deep groundwater in fractured rock is probably the cause of this seasonal lag in stream runoff, as seasonal variation in soil water content would be insufficient.

3.7. Acknowledgements

This paper is a product of the Andes Biodiversity and Ecosystems Research Group (ABERG). KEC was funded by the Natural Sciences and Engineering Research Council of Canada (NSERC) and Clarendon Fund PhD scholarships. AJW is supported to work in the Kosñipata by NSF-EAR 1227192. YM is supported by the Jackson Foundation and a European Research Council Advanced Investigator Grant. We thank ACCA Peru (Wayqecha) and Incaterra (San Pedro) for field support; L.V. Morales, R.J. Abarca Martínez, M.H. Yucra Hurtado, R. Paja Yurca, J. A. Gibaja Lopez, I. Cuba Torres, J. Huamán Ovalle, A. Alfaro-Tapia, R. Butrón Loayza, J. Farfan Flores, D. Ocampo, and D. Oviedo Licona for field assistance. We thank L. Anderson for the TRMM 3B43 v7a data; K. Halladay for the GL model data; S. Abele for the SENAMHI data; M. Palace for the

2009 Quickbird image; G.P. Asner for use of the Carnegie Airborne Observatory (CAO) DEM.

3.8. References

ACCA (2012), Weather data San Pedro station, edited by Asociación para la concervación de la cuenca Amazónica, Botanical Reseach Institute of Texas, http://atrium.andesamazon.org/index.php.

Allegre, C. J., Dupre, B., Negrel, P., and Gaillardet, J. (1996), Sr-Nd-Pb isotope systematics in Amazon and Congo River systems: Constraints about erosion processes, *Chemical Geology, 131*(1-4), 93-112, doi: http://dx.doi.org/10.1016/0009-2541(96)00028-9.

Andermann, C., Longuevergne, L., Bonnet, S., Crave, A., Davy, P., and Gloaguen, R. (2012), Impact of transient groundwater storage on the discharge of Himalayan rivers, *Nature Geoscience, 5*(2), 127-132, doi: http://dx.doi.org/10.1038/NGEO1356.

Asner, G. P., Anderson, C. B., Martin, R. E., Knapp, D. E., Tupayachi, R., Sinca, F., and Malhi, Y. (2014), Landscape-scale changes in forest structure and functional traits along an Andes-to-Amazon elevation gradient, *Biogeosciences, 11*(3), 843-856, doi: http://dx.doi.org/10.5194/bg-11-843-2014.

Ataroff, M., and Rada, F. (2000), Deforestation impact on water dynamics in a Venezuelan Andean cloud forest, *AMBIO: A Journal of the Human Environment, 29*(7), 440-444, doi: http://dx.doi.org/10.1579/0044-7447-29.7.440.

Barnett, T. P., Adam, J. C., and Lettenmaier, D. P. (2005), Potential impacts of a warming climate on water availability in snow-dominated regions, *Nature, 438*(7066), 303-309, doi: http://dx.doi.org/10.1038/nature04141.

Beighley, R. E., Eggert, K. G., Dunne, T., He, Y., Gummadi, V., and Verdin, K. L. (2009), Simulating hydrologic and hydraulic processes throughout the Amazon River Basin, *Hydrological Processes, 23*(8), 1221-1235, doi: http://dx.doi.org/10.1002/hyp.7252.

Bendix, J., Rollenbeck, R., Richter, M., Fabian, P., and Emck, P. (2008), Climate Gradients in a Tropical Mountain Ecosystem of Ecuador, in *Gradients in a tropical mountain ecosystem of Ecuador*, edited by E. Beck, J. Bendix, I. Kottke, F. Makeschin and R. Mosandl, pp. 63-73, Springer Berlin Heidelberg.

Blume, T., Zehe, E., and Bronstert, A. (2007), Rainfall—runoff response, event-based runoff coefficients and hydrograph separation, *Hydrological Sciences Journal, 52*(5), 843-862, doi: http://dx.doi.org/10.1623/hysj.52.5.843.

Bookhagen, B., and Strecker, M. R. (2008), Orographic barriers, high-resolution TRMM rainfall, and relief variations along the eastern Andes, *Geophysical Research Letters, 35*(6), L06403, doi: http://dx.doi.org/10.1029/2007GL032011.

Boy, J., Valarezo, C., and Wilcke, W. (2008), Water flow paths in soil control element exports in an Andean tropical montane forest, *European Journal of Soil Science, 59*(6), 1209-1227, doi: http://dx.doi.org/10.1111/j.1365-2389.2008.01063.x.

Brodersen, C., Pohl, S., Lindenlaub, M., Leibundgut, C., and Wilpert, K. v. (2000), Influence of vegetation structure on isotope content of throughfall and soil water, *Hydrological Processes, 14*(8), 1439-1448, doi: http://dx.doi.org/10.1002/1099-1085(20000615)14:8<1439::AID-HYP985>3.0.CO;2-3.

Bruijnzeel, L. A., Kappelle, M., Mulligan, M., and Scatena, F. N. (2010), Tropical montane cloud forests: state of knowledge and sustainability perspectives in a changing world, in *Tropical Montane Cloud Forests. Science for Conservation and Management*, edited by L. S. Hamilton, L. A. Bruijnzeel and F. N. Scatena, pp. 691-740, Cambridge University Press, Cambridge, UK.

Bruijnzeel, L. A., Mulligan, M., and Scatena, F. N. (2011), Hydrometeorology of tropical montane cloud forests: emerging patterns, *Hydrological Processes, 25*(3), 465-498, doi: http://dx.doi.org/10.1002/hyp.7974.

Bush, M. B., Silman, M. R., and Urrego, D. H. (2004), 48,000 Years of Climate and Forest Change in a Biodiversity Hot Spot, *Science, 303*(5659), 827-829, doi: http://dx.doi.org/10.1126/science.1090795.

Buytaert, W., and Beven, K. (2011), Models as multiple working hypotheses: Hydrological simulation of tropical alpine wetlands, *Hydrological Processes, 25*(11), 1784-1799, doi: http://dx.doi.org/10.1002/hyp.7936.

Calmels, D., Galy, A., Hovius, N., Bickle, M., West, A. J., Chen, M. C., and Chapman, H. (2011), Contribution of deep groundwater to the weathering budget in a rapidly eroding mountain belt, Taiwan, *Earth and Planetary Science Letters, 303*(1), 48-58, doi: http://dx.doi.org/10.1016/j.epsl.2010.12.032.

Cappa, C. D., Hendricks, M. B., DePaolo, D. J., and Cohen, R. C. (2003), Isotopic fractionation of water during evaporation, *Journal of Geophysical Research: Atmospheres, 108*(D16), 4525, doi: http://dx.doi.org/10.1029/2003JD003597.

Carlotto Caillaux, V. S., Rodriguez, G., Fernando, W., Roque, C., Dionicio, J., and Chávez, R. (1996), Geología de los cuadrángulos de Urubamba y Calca, Instituto Geológica Nacional, Lima, Peru.

Célleri, R., and Feyen, J. (2009), The hydrology of tropical Andean ecosystems: importance, knowledge status, and perspectives, *Mountain Research and Development, 29*(4), 350-355, doi: http://dx.doi.org/10.1659/mrd.00007.

Chen, Y.-C., and Chiu, C.-L. (2004), A fast method of flood discharge estimation, *Hydrological Processes, 18*(9), 1671-1684, doi: http://dx.doi.org/10.1002/hyp.1476.

Clark, K. E., Hilton, R. G., West, A. J., Malhi, Y., Gröcke, D. R., Bryant, C. L., Ascough, P. L., Robles Caceres, A., and New, M. (2013), New views on "old" carbon in the Amazon River: Insight from the source of organic carbon eroded from the Peruvian Andes, *Geochemistry, Geophysics, Geosystems, 14*(5), 1644-1659, doi: http://dx.doi.org/10.1002/ggge.20122.

Consbio (2011), Ecosistemas Terrestres de Peru (Data Basin Dataset) for ArcGIS, edited by The Nature Conservancy/NatureServe.

Craig, H. (1961), Standard for Reporting Concentrations of Deuterium and Oxygen-18 in Natural Waters, *Science, 133*(3467), 1833-1834, doi: http://dx.doi.org/10.1126/science.133.3467.1833.

Crespo, P. J., Feyen, J., Buytaert, W., Bücker, A., Breuer, L., Frede, H. G., and Ramírez, M. (2011), Identifying controls of the rainfall–runoff response of small catchments in the

tropical Andes (Ecuador), *Journal of Hydrology*, *407*(1), 164-174, doi: http://dx.doi.org/10.1016/j.jhydrol.2011.07.021.

Crespo, P. J., Feyen, J., Buytaert, W., Célleri, R., Frede, H.-G., Ramírez, M., and Breuer, L. (2012), Development of a conceptual model of the hydrologic response of tropical Andean micro-catchments in Southern Ecuador, *Hydrology and Earth System Sciences Discussions*, *9*(2), 2475-2510, doi: http://dx.doi.org/10.5194/hessd-9-2475-2012.

Dansgaard, W. (1964), Stable isotopes in precipitation, *Tellus*, *16*(4), 436-468, doi: http://dx.doi.org/10.1111/j.2153-3490.1964.tb00181.x.

Dawson, T. E. (1998), Fog in the California redwood forest: ecosystem inputs and use by plants, *Oecologia*, *117*(4), 476-485, doi: http://dx.doi.org/10.1007/s004420050683.

Dawson, T. E., and Ehleringer, J. R. (1998), Plants, isotopes and water use: a catchment-scale perspective, in *Isotope tracers in catchment hydrology*, edited by C. Kendall and J. J. McDonnell, pp. 165-202, Elsevier, Amsterdam.

Domenico, P. A., and Schwartz, F. W. (1990), *Physical and chemical hydrogeology*, 2 ed., John Wiley & Sons, New York.

Dunne, T., Mertes, L. A. K., Meade, R. H., Richey, J. E., and Forsberg, B. R. (1998), Exchanges of sediment between the flood plain and channel of the Amazon River in Brazil, *Geological Society of America Bulletin*, *110*(4), 450-467.

Eugster, W., Burkard, R., Holwerda, F., Scatena, F. N., and Bruijnzeel, L. A. (2006), Characteristics of fog and fogwater fluxes in a Puerto Rican elfin cloud forest, *Agricultural and Forest Meteorology*, *139*(3–4), 288-306, doi: http://dx.doi.org/10.1016/j.agrformet.2006.07.008.

Feeley, K. J., Silman, M. R., Bush, M. B., Farfan, W., Cabrera, K. G., Malhi, Y., Meir, P., Revilla, N. S., Quisiyupanqui, M. N. R., and Saatchi, S. (2011), Upslope migration of Andean trees, *Journal of Biogeography*, *38*(4), 783-791, doi: http://dx.doi.org/10.1111/j.1365-2699.2010.02444.x.

Fisher, J. B., Tu, K. P., and Baldocchi, D. D. (2008), Global estimates of the land–atmosphere water flux based on monthly AVHRR and ISLSCP-II data, validated at 16 FLUXNET sites, *Remote Sensing of Environment*, *112*(3), 901-919, doi: http://dx.doi.org/10.1016/j.rse.2007.06.025.

Fisher, J. B., Malhi, Y., Bonal, D., Da Rocha, H. R., De Araujo, A. C., Gamo, M., Goulden, M. L., Hirano, T., Huete, A. R., and Kondo, H. (2009), The land–atmosphere water flux in the tropics, *Global Change Biology*, *15*(11), 2694-2714, doi: http://dx.doi.org/10.1111/j.1365-2486.2008.01813.x.

Froehlich, K., Gibson, J. J., and Aggarwal, P. (2002), Deuterium excess in precipitation and its climatological significance, paper presented at Study of Environmental Change Using Isotope Techniques. Proc. Intern. Conf, Citeseer.

Frumau, K. F. A., Bruijnzeel, L. A., and Tobón, C. (2011), Precipitation measurement and derivation of precipitation inclination in a windy mountainous area in northern Costa Rica, *Hydrological Processes*, *25*(3), 499-509, doi: http://dx.doi.org/10.1002/hyp.7860.

Gascoyne, M., and Kamineni, D. (1994), The hydrogeochemistry of fractured plutonic rocks in the Canadian Shield, *Applied Hydrogeology*, *2*(2), 43-49.

Gat, J. R. (1996), Oxygen and hydrogen isotopes in the hydrologic cycle, *Annual Review of Earth and Planetary Sciences*, *24*(1), 225-262.

Giambelluca, T. W., and Gerold, G. (2011), Hydrology and biogeochemistry of tropical montane cloud forests, in *Forest Hydrology and Biogeochemistry*, edited by F. L. Levia, D. Carlyle-Moses and T. Tanaka, pp. 221-259, Springer, Netherlands.

Gibbon, A., Silman, M. R., Malhi, Y., Fisher, J. B., Meir, P., Zimmermann, M., Dargie, G. C., Farfan, W. R., and Garcia, K. C. (2010), Ecosystem carbon storage across the grassland-forest transition in the high Andes of Manu National Park, Peru, *Ecosystems*, *13*(7), 1097-1111, doi: http://dx.doi.org/10.1007/s10021-010-9376-8.

Gibbs, R. J. (1967), Amazon River - Environmental factors that control its dissolved and suspended load, *Science*, *156*(3783), 1734-1737.

Girardin, C. A. J., Malhi, Y., Aragao, L. E. O. C., Mamani, M., Huasco, W. H., Durand, L., Feeley, K. J., Rapp, J., Silva-Espejo, J. E., Silman, M., Salinas, N., and Whittaker, R. J. (2010), Net primary productivity allocation and cycling of carbon along a tropical forest elevational transect in the Peruvian Andes, *Global Change Biology*, *16*(12), 3176-3192, doi: http://dx.doi.org/10.1111/j.1365-2486.2010.02235.x.

Girardin, C. A. J., Silva-Espejo, J. E., Doughty, C. E., Huaraca Huasco, W., Metcalfe, D. B., Durand-Baca, L., Marthews, T. R., Aragao, L. E. O. C., Farfan Rios, W., García Cabrera, K., Halladay, K., Fisher, J. B., Galiano-Cabrera, D. F., Huaraca-Quispe, L. P., Alzamora-Taype, I., Equiluz-Mora, L., Salinas-Revilla, N., Silman, M., Meir, P., and Malhi, Y. (2013), Productivity and carbon allocation in a tropical montane cloud forest of the Peruvian Andes, *Plant Ecology and Diversity*, *7*(1-2), 107-123, doi: http://dx.doi.org/10/1080/17550874.2013.820222.

Goldsmith, G. R., Muñoz-Villers, L. E., Holwerda, F., McDonnell, J. J., Asbjornsen, H., and Dawson, T. E. (2012), Stable isotopes reveal linkages among ecohydrological processes in a seasonally dry tropical montane cloud forest, *Ecohydrology*, *5*(6), 779-790, doi: http://dx.doi.org/10.1002/eco.268.

Goller, R., Wilcke, W., Leng, M. J., Tobschall, H. J., Wagner, K., Valarezo, C., and Zech, W. (2005), Tracing water paths through small catchments under a tropical montane rain forest in south Ecuador by an oxygen isotope approach, *Journal of hydrology*, *308*(1), 67-80, doi: http://dx.doi.org/10.1016/j.jhydrol.2004.10.022.

Gustard, A., Bullock, A., and Dixon, J. (1992), Low flow estimation in the United Kingdom*Rep.*, Institute of Hydrology, Wallingford, UK.

Guyot, J. L., Fillzola, N., Quintanilla, J., and Cortez, J. (1996), Dissolved solids and suspended sediment yields in the Rio Madeira basin, from the Bolivian Andes to the Amazon, *IAHS Publication*, 55-64.

Halladay, K., Malhi, Y., and New, M. (2012a), Cloud frequency climatology at the Andes/Amazon transition: 2. Trends and variability, *Journal of geophysical research*, *117*, D23103, doi: http://dx.doi.org/10.1029/2012JD017789.

Halladay, K., Malhi, Y., and New, M. (2012b), Cloud frequency climatology at the Andes/Amazon transition: 1. Seasonal and diurnal cycles, *Journal of geophysical research, 117*, D23102, doi: http://dx.doi.org/10.1029/2012JD017770.

Halladay, K., New, M., and *et al.* (submitted), Atmospheric structure and cloud depth in a tropical montane cloud forest.

Hillyer, R., and Silman, M. R. (2010), Changes in species interactions across a 2.5 km elevation gradient: effects on plant migration in response to climate change, *Global Change Biology, 16*(12), 3205-3214, doi: http://dx.doi.org/10.1111/j.1365-2486.2010.02268.x.

Holwerda, F., Bruijnzeel, L. A., Muñoz-Villers, L. E., Equihua, M., and Asbjornsen, H. (2010a), Rainfall and cloud water interception in mature and secondary lower montane cloud forests of central Veracruz, Mexico, *Journal of Hydrology, 384*(1–2), 84-96, doi: http://dx.doi.org/10.1016/j.jhydrol.2010.01.012.

Holwerda, F., Bruijnzeel, L. A., Oord, A. L., and Scatena, F. N. (2010b), Fog interception in a Puerto Rican elfin cloud forest: a Wet-canopy Water budget approach, in *Tropical Montane Cloud Forests: Science for Conservation and Management*, edited by L. A. Bruijnzeel, F. N. Scatena and L. S. Hamilton, pp. 282-292, Cambridge University Press, Cambridge, UK.

Horwath, A. (2011), Epiphytic bryophytes as cloud forest indicators: Stable isotopes, biomass and diversity along an altitudinal gradient in Peru, 260 pp, Plant Sciences, University of Cambridge, Cambridge.

Huaraca Huasco, W., Girardin, C. A. J., Doughty, C. E., Metcalfe, D. B., Baca, L. D., Silva-Espejo, J. E., Cabrera, D. G., Aragão, L. E. O., Davila, A. R., Marthews, T. R., Huaraca-Quispe, L. P., Alzamora-Taype, I., Eguiluz-Mora, L., Farfan-Rios, W., Cabrera, K. G., Halladay, K., Salinas-Revilla, N., Silman, M., Meir, P., and Malhi, Y. (2013), Seasonal production, allocation and cycling of carbon in two mid-elevation tropical montane forest plots in the Peruvian Andes, *Plant Ecology and Diversity, 7*(1-2), doi: http://dx.doi.org/10.1080/17550874.2013.819042.

INGEMMET (2013), GEOCATMIN - Geologia integrada por proyectos regionales, edited by Instituto Geológico Minero Metalúrgico.

Jardine, P. M., Sanford, W. E., Gwo, J. P., Reedy, O. C., Hicks, D. S., Riggs, J. S., and Bailey, W. B. (1999), Quantifying diffusive mass transfer in fractured shale bedrock, *Water Resources Research, 35*(7), 2015-2030.

Killeen, T. J., Douglas, M., Consiglio, T., Jørgensen, P. M., and Mejia, J. (2007), Dry spots and wet spots in the Andean hotspot, *Journal of Biogeography, 34*(8), 1357-1373, doi: http://dx.doi.org/10.1111/j.1365-2699.2006.01682.x.

Lambs, L., Horwath, A., Otto, T., Julien, F., and Antoine, P. O. (2012), Isotopic values of the Amazon headwaters in Peru: comparison of the wet upper Río Madre de Dios watershed with the dry Urubamba-Apurimac river system, *Rapid Communications in Mass Spectrometry, 26*(7), 775-784, doi: http://dx.doi.org/10.1002/rcm.6157.

Malhi, Y., Silman, M., Salinas, N., Bush, M., Meir, P., and Saatchi, S. (2010), Introduction: Elevation gradients in the tropics: laboratories for ecosystem ecology and global change research, *Global Change Biology, 16*(12), 3171-3175, doi: http://dx.doi.org/10.1111/j.1365-2486.2010.02323.x.

Marengo, J. A., Soares, W. R., Saulo, C., and Nicolini, M. (2004), Climatology of the low-level jet east of the Andes as derived from the NCEP-NCAR reanalyses: Characteristics and temporal variability, *Journal of climate, 17*(12), 2261-2280.

McClain, M. E., and Naiman, R. J. (2008), Andean influences on the biogeochemistry and ecology of the Amazon River, *Bioscience, 58*(4), 325-338, doi: http://dx.doi.org/10.1641/b580408.

McJannet, D., Wallace, J., and Reddell, P. (2007), Precipitation interception in Australian tropical rainforests: II. Altitudinal gradients of cloud interception, stemflow, throughfall and interception, *Hydrological Processes, 21*(13), 1703-1718, doi: http://dx.doi.org/10.1002/hyp.6346.

McJannet, D. L., Wallace, J. S., and Reddell, P. (2010), Comparative water budgets of a lower and an upper montane cloud forest in the Wet Tropics of northern Australia, in *Tropical Montane Cloud Forests. Science for Conservation and Management*, edited by L. A. Bruijnzeel and F. N. Scatena, pp. 479-490, Cambrige University Press, Cambridge, UK.

Meade, R. H., Dunne, T., Richey, J. E., Santos, U. D., and Salati, E. (1985), Storage and remobilisation of suspended sediment in the lower Amazon River of Brazil, *Science, 228*(4698), 488-490.

Milliman, J. D., and Farnsworth, K. L. (2011), Runoff, erosion, and delivery to the coastal ocean, in *River discharge to the coastal ocean: a global synthesis*, edited, pp. 13-69, Cambridge University Press, Cambridge, UK.

Morris, D. A., and Johnson, A. I. (1967), Summary of Hydrologic and Physical Properties of Rock and Soil Materials, as Analyzed by the Hydrologic Laboratory of the US Geological Survey 1948-60*Rep.*, 46 pp, US Government Printing Office, Washington, USA.

Mulligan, M. (2010), Modelling the tropics-wide extent and distribution of cloud forest and cloud forest loss, with implications for conservation priority, in *Tropical Montane Cloud Forests. Science for Conservation and Management*, edited by L. A. Bruijnzeel, F. N. Scatena and L. S. Hamilton, pp. 14-38, Cambridge University Press, Cambridge, UK.

Muñoz-Villers, L. E., Holwerda, F., Gómez-Cárdenas, M., Equihua, M., Asbjornsen, H., Bruijnzeel, L. A., Marín-Castro, B. E., and Tobón, C. (2012), Water balances of old-growth and regenerating montane cloud forests in central Veracruz, Mexico, *Journal of Hydrology, 462*, 53-66, doi: http://dx.doi.org/10.1016/j.jhydrol.2011.01.062.

Muñoz-Villers, L. E., and McDonnell, J. J. (2012), Runoff generation in a steep, tropical montane cloud forest catchment on permeable volcanic substrate, *Water Resources Research, 48*(9), W09528, doi: http://dx.doi.org/10.1029/2011WR011316.

Myers, N., Mittermeier, R. A., Mittermeier, C. G., Da Fonseca, G. A. B., and Kent, J. (2000), Biodiversity hotspots for conservation priorities, *Nature, 403*(6772), 853-858, doi: http://dx.doi.org/10.1038/35002501.

Phillips, D. L., and Gregg, J. W. (2001), Uncertainty in source partitioning using stable isotopes, *Oecologia, 127*(2), 171-179, doi: http://dx.doi.org/10.1007/s004420000578.

Ponton, C., West, A. J., Feakins, S. J., and Galy, V. (in review), Biomarkers in transit reveal the nature of fluvial integration.

Postel, S. L., and Thompson, B. H. (2005), Watershed protection: Capturing the benefits of nature's water supply services, *Natural Resources Forum*, *29*(2), 98-108, doi: http://dx.doi.org/10.1111/j.1477-8947.2005.00119.x.

Priestley, C. H. B., and Taylor, R. J. (1972), On the Assessment of Surface Heat Flux and Evaporation Using Large-Scale Parameters, *Monthly Weather Review*, *100*(2), 81-92.

Rapp, J. M. (2010), Climate control on plant performance across an Andean altitudinal gradient, 253 pp, Biology, Wake Forest University, Winston-Salem, North Carolina.

Rapp, J. M., and Silman, M. R. (2012), Diurnal, seasonal, and altitudinal trends in microclimate across a tropical montane cloud forest, *Climate research, 55*(1), 17-32, doi: http://dx.doi.org/10.3354/cr01127.

Rapp, J. M., and Silman, M. R. (2014), Epiphyte response to drought and experimental warming [v1; ref status: approved 1, approved with reservations 1, http://f1000r.es/2oy], *F1000Research, 3*(7), doi: http://dx.doi.org/10.12688/f1000research.3-7.v1.

Rhodes, A. L., Guswa, A. J., and Newell, S. E. (2006), Seasonal variation in the stable isotopic composition of precipitation in the tropical montane forests of Monteverde, Costa Rica, *Water Resources Research, 42*(11), W11402, doi: http://dx.doi.org/10.1029/2005WR004535.

Richey, J. E., Meade, R. H., Salati, E., Devol, A. H., Nordin, C. F., and Dossantos, U. (1986), Water discharge and suspended sediment concentrations in the Amazon River 1982-1984, *Water Resources Research*, *22*(5), 756-764.

Richey, J. E., Valarezo, C., Valarezo, C., and Valarezo, C. (1990), Biogeochemistry of carbon in the Amazon River, *Limnology and Oceanography*, *35*, 352-371.

Rozanski, K., Araguás-Araguás, L., and Gonfiantini, R. (1993), Isotopic Patterns in Modern Global Precipitation, in *Climate Change in Continental Isotopic Records*, edited by P. K. Swart, K. C. Lohman, J. McKenzie and S. Savin, pp. 1-36, American Geophysical Union, Washington, DC.

Salati, E., Dall'Olio, A., Matsui, E., and Gat, J. R. (1979), Recycling of water in the Amazon basin: an isotopic study, *Water resources research, 15*(5), 1250-1258, doi: http://dx.doi.org/10.1029/WR015i005p01250.

Salinas, N., Malhi, Y., Meir, P., Silman, M., Roman Cuesta, R., Huaman, J., Salinas, D., Huaman, V., Gibaja, A., Mamani, M., and Farfan, F. (2011), The sensitivity of tropical leaf litter decomposition to temperature: results from a large-scale leaf translocation experiment along an elevation gradient in Peruvian forests, *New Phytologist*, *189*(4), 967-977, doi: http://dx.doi.org/10.1111/j.1469-8137.2010.03521.x.

Scheel, M. L. M., Rohrer, M., Huggel, C., Santos Villar, D., Silvestre, E., and Huffman, G. J. (2011), Evaluation of TRMM Multi-satellite Precipitation Analysis (TMPA) performance in the Central Andes region and its dependency on spatial and temporal resolution, *Hydrology and Earth System Sciences*, *15*(8), 2649-2663, doi: http://dx.doi.org/10.5194/hess-15-2649-2011.

Schellekens, J., Scatena, F. N., Bruijnzeel, L. A., van Dijk, A. I. J. M., Groen, M. M. A., and van Hogezand, R. J. P. (2004), Stormflow generation in a small rainforest catchment in the

Luquillo Experimental Forest, Puerto Rico, *Hydrological Processes, 18*(3), 505-530, doi: http://dx.doi.org/10.1002/hyp.1335.

Schmid, S., Burkard, R., Frumau, K. F. A., Tobon, C., Bruijnzeel, L. A., Siegwolf, R., and Eugster, W. (2010), The wet-canopy water balance of a Costa Rican cloud forest during the dry season, in *Tropical Montane Cloud Forests: Science for Conservation and Management*, edited by L. A. Bruijnzeel, F. N. Scatena and L. S. Hamilton, pp. 302-308, Cambridge University Press, Cambridge, UK.

Scholl, M., Eugster, W., and Burkard, R. (2011), Understanding the role of fog in forest hydrology: stable isotopes as tools for determining input and partitioning of cloud water in montane forests, *Hydrological Processes, 25*(3), 353-366, doi: http://dx.doi.org/10.1002/hyp.7762.

Scholl, M. A., Giambelluca, T. W., Gingerich, S. B., Nullet, M. A., and Loope, L. L. (2007), Cloud water in windward and leeward mountain forests: The stable isotope signature of orographic cloud water, *Water Resources Research, 43*(12), W12411, doi: http://dx.doi.org/10.1029/2007WR006011.

Scholl, M. A., and Murphy, S. F. (2014), Precipitation isotopes link regional climate patterns to water supply in a tropical mountain forest, eastern Puerto Rico, *Water Resources Research, 50*(5), 4305-4322, doi: http://dx.doi.org/10.1002/2013WR014413.

SENAMHI (2012), Clima: Datos históricos Peru, edited, Servicio Nacional de Meteorologia e Hidrologia del Peru, Lima, Peru.

Squeo, F. A., Warner, B. G., Aravena, R., and Espinoza, D. (2006), Bofedales: high altitude peatlands of the central Andes, *Revista Chilena de Historia Natural, 79*(2), 245-255.

Stallard, R. F., and Edmond, J. M. (1983), Geochemistry of the Amazon: 2. The influence of geology and weathering environment on the dissolved load, *Journal of Geophysical Research: Oceans, 88*(C14), 9671-9688.

Thome, C. R., and Zevenbergen, L. W. (1985), Estimating mean velocity in mountain rivers, *Journal of Hydraulic Engineering, 111*(4), 612-624.

Thorburn, P. J., Hatton, T. J., and Walker, G. R. (1993), Combining measurements of transpiration and stable isotopes of water to determine groundwater discharge from forests, *Journal of Hydrology, 150*(2–4), 563-587, doi: http://dx.doi.org/10.1016/0022-1694(93)90126-T.

Timbe, E., Windhorst, D., Crespo, P., Frede, H. G., Feyen, J., and Breuer, L. (2014), Understanding uncertainties when inferring mean transit times of water trough tracer-based lumped-parameter models in Andean tropical montane cloud forest catchments, *Hydrol. Earth Syst. Sci., 10*(12), 15871-15914, doi: http://dx.doi.org/10.5194/hess-18-1503-2014.

Tipper, E. T., Bickle, M. J., Galy, A., West, A. J., Pomiès, C., and Chapman, H. J. (2006), The short term climatic sensitivity of carbonate and silicate weathering fluxes: insight from seasonal variations in river chemistry, *Geochimica Et Cosmochimica Acta, 70*(11), 2737-2754, doi: http://dx.doi.org/10.1016/j.gca.2006.03.005.

Todd, D. K., and Mays, L. W. (1980), *Groundwater Hydrology*, 625 pp., Wiley.

Tognetti, S., Aylward, B., and Bruijnzeel, L. A. (2010), Assessment needs to support the development of arrangements for payments for ecosystem services from tropical montane cloud forests, in *Tropical Montane Cloud Forests. Science for Conservation and Management*, edited by L. A. Bruijnzeel, F. N. Scatena and L. S. Hamilton, pp. 671-685, Cambridge University Press, Cambridge, UK.

Torres, M. A., Clark, K. E., and West, A. J. (in prep.), Variation in the hydrologic influence on chemical weathering across a mountain-to-floodplain transition in the Peruvian Amazon.

Tovar, C., Arnillas, C. A., Cuesta, F., and Buytaert, W. (2013), Diverging responses of tropical Andean biomes under future climate conditions, *PloS one, 8*(5), e63634, doi: http://dx.doi.org/10.1371/journal.pone.0063634.

Townsend-Small, A., McClain, M. E., Hall, B., Noguera, J. L., Llerena, C. A., and Brandes, J. A. (2008), Suspended sediments and organic matter in mountain headwaters of the Amazon River: Results from a 1-year time series study in the central Peruvian Andes, *Geochimica et Cosmochimica Acta*, *72*(3), 732-740, doi: http://dx.doi.org/10.1016/j.gca.2007.11.020.

TRMM (2013), Tropical Rainfall Measuring Mission product 3B43 v7a, edited, NASA.

van de Weg, M. J., Meir, P., Grace, J., and Ramos, G. D. (2012), Photosynthetic parameters, dark respiration and leaf traits in the canopy of a Peruvian tropical montane cloud forest, *Oecologia*, *168*(1), 23-34.

van de Weg, M. J., Meir, P., Williams, M., Girardin, C., Malhi, Y., Silva-Espejo, J., and Grace, J. (2014), Gross primary productivity of high elevation tropical montane cloud forest, *Ecosystems*, 1-14, doi: http://dx.doi.org/10.1007/s10021-014-9758-4.

Wilcox, B. P., Allen, B., and Bryant, F. (1988), Description and classification of soils of the high-elevation grasslands of central Peru, *Geoderma*, *42*(1), 79-94.

Zadroga, F. (1981), The hydrological importance of a montane cloud forest area of Costa Rica, *Tropical agricultural hydrology*, 59-73.

Zimmermann, M., Meir, P., Bird, M. I., Malhi, Y., and Ccahuana, A. J. Q. (2009), Climate dependence of heterotrophic soil respiration from a soil-translocation experiment along a 3000 m tropical forest altitudinal gradient, *European Journal of Soil Science, 60*(6), 895-906, doi: http://dx.doi.org/10.1111/j.1365-2389.2009.01175.x.

Chapter 3: Supplementary information:

The hydrological regime of a forested tropical Andean valley

Kathryn E. Clark[1], Mark A. Torres[2], A. Joshua West[2], Robert G. Hilton[3], Mark New[4,1], Aline B. Horwath[5], Joshua B. Fisher[6], Joshua M. Rapp[7,8], Arturo Robles Caceres[9], and Yadvinder Malhi[1]

S3.1. Materials and methods

S3.1.1. Discharge and runoff measures

The cross-sectional area of the Kosñipata River was determined by measuring in-stream river profiles and out-of-stream bank area at low flow several times over the span of the study. River depths were taken every 50 cm along the width of the river using a measuring stick. The out-of-stream banks of the river profile were measured with a laser range finder (TruPulse 200 Rangefinder, Laser Technologies Inc.). The cross-sectional areas of active flow were calculated using river height and the river profile (low flow cross-sectional area + out-of-stream area up to the measured river height).

River velocity was measured using a float method and handheld velocity meters. For the majority of the year it was too dangerous to enter the river, so surface velocity was measured using the stick float method with 5 replicates. The stick float method consisted of tossing a stick into the middle of the river channel from the river bank and recording the time for the stick to travel a specified distance [*McMahon*, 1957; *Baud et al.*, 2005]. In the late dry season, when it was possible to enter the river, flow meters were used to measure stream velocity.

S3.1.1.1. San Pedro gauging station

At the San Pedro gauging station metered stream velocity was measured with a Flow Probe (FP101 Global Water); this probe records average and maximum stream

velocity across the full cross-section of the river. The stick float method produced results that overlapped with the maximum stream velocity measurements using the flow meter (Figure S3.1a) but both the float and maximum velocities were systematically offset from the average velocities due to velocity variations with depth [*Smart*, 1999].

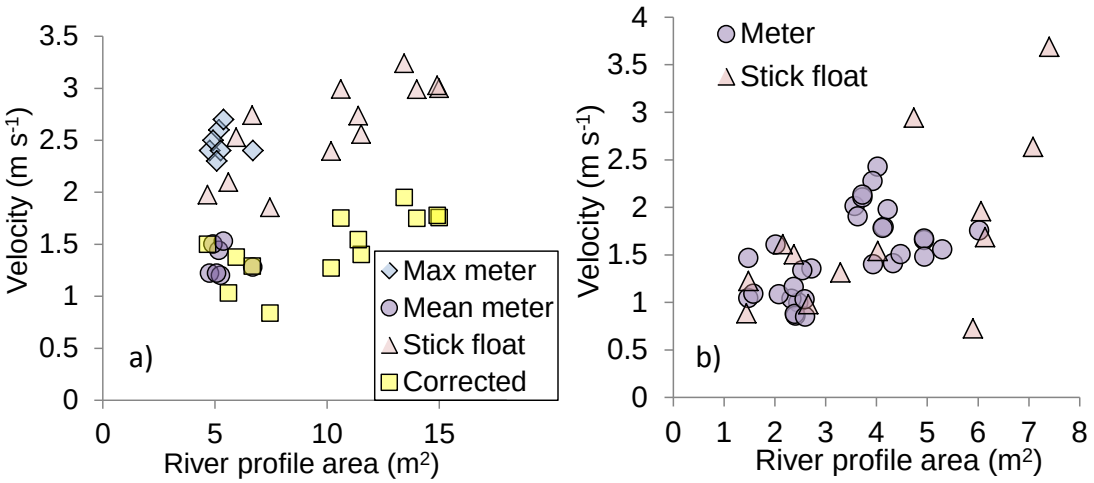


Figure S3.1: River velocity (m s^{-1}) against flow profile area (m^2) at (a) the San Pedro gauging station and (b) the Wayqecha gauging station. At San Pedro gauging station (a) the mean meter velocity and max. meter velocity were measured at the same time along the river cross-sectional profile using a flow meter. The mean and max. meter velocities were used to correct the stick float velocity using equation S1. The corrected velocity was used to determine the discharge river height rating curve for the San Pedro gauging station. At Wayqecha gauging station (b), the meter velocity was measured at the middle of the river channel or close to the middle of the river channel with a flow meter at ~0.75 vertical depth to capture mean velocity. The stick float velocity was used especially at higher discharges. The river is small at Wayqecha and the meter and stick float overlap. This suggests little variation in velocity along the vertical profile and thus no correction was made to the stick float velocity.

We calibrated a linear regression of mean velocity and max velocity measures as: (based on n = 12 measurements).

$$mean\ channel\ velocity\ \left(\frac{m}{s}\right) = surface\ velocity\ \left(\frac{m}{s}\right) \times 0.803\ - 0.6522 \qquad (S1)$$

This regression implies that there is a larger correction of velocity in the Kosñipata River than predicted for a simple logarithmic vertical velocity profiles typical of lowland rivers [*Sukhodolov et al.*, 1998; *Smart*, 1999], but this is expected since mountain rivers have a more s-shaped vertical velocity profile due to drag [*Jarrett*, 1990]. To yield representative mean velocities, float stick velocities were corrected using Equation S1, on the basis that the maximum velocity is at the surface and is measured by the float method. We validated this velocity correction by comparison to theoretical velocities.

We compared our corrected maximum velocity with a theoretical hydrodynamic velocity. For the theoretical calculation, we adopted the Jarrett [1984] modification of Manning's Equation for mountain rivers in Colorado, in which river channel slope (S) and hydraulic radius (R) were the only input variables. The slope of the Kosñipata River channel at San Pedro is 0.04 (m m^{-1}), determined in ArcGIS using GPS waypoints made in the field upstream and downstream of the San Pedro gauging station, and an orthorectified pan-sharpened Quickbird image from 2009. The horizontal distance between the two waypoints following the river thalweg in the Quickbird image was 812 m. The vertical difference between the two points was 35 m (channel slope S = 4.3 %). This measurement was confirmed using the Carnegie Airborne Observatory (CAO) [*Asner et al.*, 2012] LiDAR-based digital elevation model resampled at 3 m x 3 m grid cells from 1.12 m x 1.12 m grid cells [*Asner*, unpublished data] , which gives a horizontal distance of 92.9 m and the vertical distance of 3.9 m across the gauging site (S = 4.2 %). The hydraulic radius (R) is the cross-section river profile area (m^2) divided by the wetted parameter (the length of the cross-section profile in contact with the banks, m); onsite river profile measurements varied between R = 0.40 m and 0.49 m (n = 8). The difference between the empirical velocity measurements and those determined from theory using equation 10 from Jarrett [1984] was less than 2 0 %, with a mean of offset 0.65 %

(ranging from -9.7 to 13.1 %; n = 7). Given the range of assumptions in both the theoretical and empirical values, we view this similarity as encouraging validation of our methods.

Discharge was calculated by multiplying corrected velocity by the river cross-sectional area. Discharge and river stage height were used to construct a power-law stage-discharge rating curve for the San Pedro gauging station, as (n=20; r^2 = 0.86; Figure S3.2):

$$Discharge\left(\frac{m^3}{s}\right) = 30.228 \times Stage\ ht\ (m)^{0.8492} \qquad (S2)$$

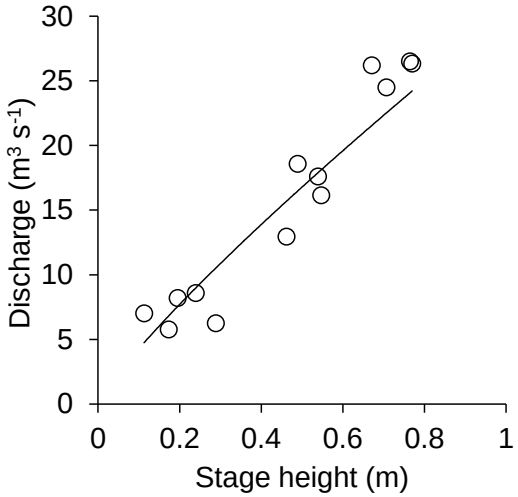


Figure S3.2: Stage height (m) to river discharge (m^3 s^{-1}) rating curve for the San Pedro gauging station, with a power-law regression (Equation S2).

The San Pedro gauging station had an almost continuous river height record for the study year, with the river logger recording river height every 15 minutes. The instantaneous discharge associated with each height measurement was calculated using equation S2. The months of each season were derived from Table S3.1 and from Figure 3.4. The

monthly and annual streamflow results were calculated by summing the total streamflow for each month and the total over the year and were converted into mean seasonal runoff (mm d^{-1}) and annual runoff (mm d^{-1} and mm yr^{-1}).

Table S3.1. Catchment-wide mean monthly estimated rainfall (mm $month^{-1}$) 1998 to 2012 showing seasonality.

Sub-catchment	Jan.	Feb.	March	April	May	June	July	Aug.	Sept.	Oct.	Nov.	Dec.
Wayqecha	330±40	342±57	346±38	167±18	92±13	89±12	92±13	87±11	111±14	158±22	173±22	256±36
San Pedro	389±43	401±64	406±41	213±20	132±14	127±13	132±14	126±12	152±15	203±23	219±23	309±39
Months	15	15	15	15	15	15	15	15	15	15	15	15
Season*	wet	wet	wet	wet-dry	dry	dry	dry	dry	dry	dry-wet	dry-wet	wet

*Rainfall patterns indicate that the wet season runs from December to March (green), the wet-dry transition season runs throughout April (blue), the dry season runs from May until September (yellow), and the dry-wet transition season runs through October and November (red).

There was a gap in the logger data of 31 days in the dry season between mid-July and early-August (Figure 3.2). This gap is due to issues with the battery in the logger. During this gap three manual river height measures were taken. Total daily discharge (m^3 d^{-1}) and total daily runoff (mm d^{-1}) were determined from these measurements. A correction for the average discharge values for July and August was made based on these point measurements, because these months only had 10 and 21 days of measurements, respectively. First, the mean daily runoff (mm d^{-1}) was determined for the available days including the days with the manual measurements. Secondly, the mean daily runoff was multiplied by the number of days in the months with 30 and 31 days respectively to give a corrected total runoff (mm $month^{-1}$) for those months.

Baseflow (Q_b) was determined for the San Pedro gauging station mean daily discharge (m^3 s^{-1}) using the method outlined in *Gustard et al.* [1992]: (1) First, the 5-day minimum mean daily discharge was determined for non-overlapping 5 day blocks over the study period. (2) Second, the 5-day minima were multiplied by 0.9 and if this value

was less than either the preceding or subsequent 5-day minimum, it was assigned to be part of the baseflow. (3) Third, mean daily discharge values were linearly interpolated in between the selected 5-day minimum discharge values selected in step two. (4) Finally, if the linearly interpolated daily baseflow discharge value was less than the actual mean daily discharge value, the actual value was replaced by the interpolated value for that day. This determined the daily baseflow discharge ($m^3 s^{-1}$) for the duration of the study period. Daily quickflow (Q_d) ($m^3 s^{-1}$) was calculated as the difference between the actual daily discharge flow ($m^3 s^{-1}$) and the calculated daily baseflow (Q_b) ($m^3 s^{-1}$). Base flow index (BFI) was calculated as the ratio of the total volume of baseflow divided by the total volume of streamflow.

S3.1.1.2. Wayqecha gauging station

At the Wayqecha gauging station, stream flow was measured using an MJP Student Stream Flow Meter as close as possible to the middle of the channel, at 75 % of the total vertical depth down from the water surface. Revolutions per minute measured from the flow meter were converted to velocity ($m s^{-1}$) using the flow meter calibration. When it was not possible to enter the river due to fast flow conditions, measurements were made from the bank, making it possible to measure faster velocities. The float stick method was used for 30 % of the measurements, following the same protocol as at the San Pedro gauging station. At the Wayqecha gauging station there was no evidence of velocity variation across the vertical profile (Figure S3.1b), perhaps because the river channel at this site is small, and no corrections were applied to the measured float velocities. Discharge was calculated by multiplying velocity by the river cross-sectional area; four river profiles were used over the course of the study year because of the changing channel morphology. Power-law stage-discharge rating curves (cf. Eq. S2) were made for each profile [*Wooding*, 1965; *Petersen-Øverleir*, 2005; *McMillan et al.*, 2010].

Seasonal discharge was determined by taking the mean of the monthly discharges that fell within each season (based on seasonal divisions outlined in Table S3.1). The annual discharge was calculated as the mean of the monthly discharge rates. Monthly runoff was determined from the mean monthly discharge divided by catchment area (48.5 km^2) and is reported as a mean daily runoff for each month (mm d^{-1}). Seasonal runoff was determined by taking the mean of the monthly runoffs that fell within each season.

S3.1.2. Catchment wide rainfall estimates

The calibration of the TRMM data and calculation of catchment wide rainfall for the Wayqecha and San Pedro catchments was done using the following series of steps: (1) For individual met stations, monthly rainfall (mm $month^{-1}$) was compared to the TRMM data (mm $month^{-1}$) and a linear regression was determined (Table S3.8). (2) These regression equations were used to estimate a calibrated monthly rainfall (mm $month^{-1}$) for the 9 meteorological stations for each TRMM month from 1998 to 2012 (n = 180). The mean annual estimated rainfall (mm yr^{-1}) ranged from 1600 to 5260 mm yr^{-1} for the various met stations (Table S3.2). (3) For each TRMM month (n = 180) a new linear regression was determined between the elevation of each met station and the estimated rainfall for each met station (from step 2). The mean monthly estimated rainfall for the study period coincided well with the met station rainfall (Figure 3.3a). (4) The elevation distribution and its proportion at 1 masl intervals were determined in ArcGIS at a 90 m x 90 m pixel resolution using Shuttle Radar Topography Mission (SRTM) digital elevation model (DEM) for each catchment using the boundaries in Figure 3.1a.

Table S3.2: Station descriptions for meteorological data from the Kosñipata Valley.

# in Fig. 3.1a[◊]	Met station	Gauge type	Elevation (masl)	Lat/long coordinates (S, W)	Land cover type	Landscape description	Aspect	Slope (°)	n	T_{max} (°C)	RH_{min} (%)	R_n (W m^{-2})	Met station annual rainfall (mm yr^{-1})	TRMM calibrated rainfall[§] (1998 to 2012) (mm yr^{-1})	Estimated AET
1	Acjanaco	manual	3460	13°11'45.674", 71°37'14.818"	Puna grassland	rolling mountain top	140	8.6	79	12.1	65.0[^]	N/A	1908[a]	1800	N/A
2	TU 3450	Smart Sensors/ HOBO	3450	13°6'48.749", 71°36'27.306"	Transition & Scrub-land	rolling mountain top/peak of a mountain ridge	356	26.7	16	11.9	72.3	92*	2148[b]	2516	744
3	Wayqecha	Campbell Scientific	2900	13°11'18.434", 71°35'9.667"	UMCF	mountain slope just below tree line, far from ridge	122	32.8	45	16.2	70.0	84[#]	1752[c]	1600	732
4	TU 2750	Smart Sensors/ HOBO	2750	13°6'18.537", 71°35'22.26"	UMCF	mountain ridge	319	28	19	16.0	75.7	87*	2940[b]	3154	780
5	Rocotal	manual	2090	13°6'47.575", 71°34'14.673"	UMCF/ LMCF	mountain slope near road	70.5	32.9	97	20.6	76.4[^]	N/A	4140[a]	4152	N/A
6	TU 1800	Smart Sensors/ HOBO	1850	13°4'11.331", 71°33'30.215"	LMCF	Mid –mountain slope	321	30.6	18	20.3	72.4	100*	4116[b]	3998	948
7	San Pedro[≠]	Vantage Pro 2 Plus, Davis Instruments	1450	13°3'21.219", 71°32'48.841"	LMRF	mountain slope near the river	183	13.6	13	23.7	77.0	98[#]	5436[d]	4831	984
	San Pedro[≠]	Skye Instruments	1360	13°3'20.191", 71°32'38.305"	LMRF	mountain slope near the river	183	4							
8	SP 1500	Smart Sensors/ HOBO	1500	13°2'57.577", 71°32'11.579"	LMRF	mountain slope	170	29.5	13	22.0	74.9	95*	4956[b]	5191	936
9	Chonta-chaca	manual	887	13°1'26.091", 71°28'4.887"	LTRF	low mountains near road and river	-1	2.1	80	27.3	83.6[^]	N/A	5316[a]	5260	N/A

[◊] Stations 2, 3, 4, 6, 7 and 8 are run by the ABERG consortium.
[a] data from [*SENAMHI*, 2012]
[b] data from [*Rapp and Silman*, 2012]
[c] data from [*Girardin et al.*, 2013]
[d] data from [*ACCA*, 2012; *Huaraca Huasco et al.*, 2013]
[≠] Data for the two San Pedro met stations were merged since they were located close to one another and totalled only 13 months of data.
[§]TRMM calibrated rainfall (mm yr^{-1}) from 1998 to 2012 (n = 180 months) was determined for each met station as described in the text.
UMCF = Upper montane cloud forest, LMCF = Lower montane cloud forest, LMRF = Lower montane rain forest, LTRF = Lower tropical rainforest. Aspect and slope were determined by using SRTM DEM at 90 x 90 m resolution. n = available months of meteorological station data. T_{max} = mean max daily temperature averaged monthly, RH_{min} = mean daily minimum relative humidity averaged monthly, [^] estimated RH_{min} using dry and wet bulb temperatures assuming atmospheric pressure was 1013 hPa, and R_n = mean daily net radiation averaged monthly.
* Photosynthetic active radiation (PAR) (µmol PAR m^{-2} s^{-1}) was converted to estimate R_n by first dividing it by 2.1 to convert it to solar radiation (R_s) (W m^{-2}) [*Monteith and Unsworth*, 2008] and then converted to R_n.
[#] Solar radiation was converted to estimate net radiation (R_n) by multiplying R_s by 0.75 [*Malhi et al.*, 2002; *Fisher et al.*, 2010] Actual evapotranspiration (AET) estimated using met station data in the PT-JPL model developed by *Fisher et al.* [2008].

(5) For each month, the linear regression equation developed in step 3 was applied to the elevation distributions in order to estimate rainfall by month (mm month^{-1}), yielding valley-averaged monthly rainfall estimates over the duration of the TRMM record. (6) For our study period the monthly data were summed to yield seasonal and annual estimated rainfall. The estimated catchment wide monthly rainfall data from the TRMM study period (1998 to 2012) was summed to yield annual results (mm yr^{-1}).

Table S3.8: TRMM-met station rainfall regressions used to estimate rainfall

Station number (Figure 3.1a)	Met station name	Rainfall estimate (mm month^{-1})	R^2
1	Acjanaco	0.8395 × TRMM + 35.315	0.73
2	3450 TU	1.1091 × TRMM + 58.255	0.89
3	Wayqecha	0.6606 × TRMM + 43.022	0.67
4	2750 TU	1.239 × TRMM + 93.704	0.84
5	Rocotal	1.264 × TRMM + 173.4	0.31
6	1800 TU	1.1793 × TRMM + 172.08	0.79
7	San Pedro	1.354 × TRMM + 217.35	0.73
8	1500 TU	1.6807 ×TRMM + 203.07	0.83
9	Chontachaca	1.183 × TRMM + 276.69	0.63

S3.1.3. Water isotope measurements

Samples for the determination of the stable isotopic composition of hydrogen and oxygen in water from the Kosñipata River were collected from the river surface with a clean polypropylene graduated cylinder, filtered onsite with a 0.2 μm nylon filter, and stored unpreserved in a 60 mL HDPE bottles.

To test the suitability of storing the samples in HDPE bottles, a subset of the samples were also collected into 15 mL glass exetainers with rubber septa after filtration and stored unpreserved. Upon returning the laboratory, all of the samples were stored at 3 °C until analysis. Comparisons between the two different collection methods (i.e. HDPE bottles vs. glass exetainers) did not reveal any systematic differences and agreed within the analytical uncertainties.

Isotopic analyses of samples collected in HDPE bottles were performed with a Picarro L1102-i cavity ring down spectrometer at the University of Southern California. Each sample or standard was injected into the cavity and measured 5 times. The first two injections were discarded to eliminate cross-contamination between samples and the values of the remaining three injections were averaged. Values are reported in delta notation relative to the VSMOW standard where

$$\delta D = \left(\left(\frac{D/H_{sample}}{D/H_{VSMOW}} \right) - 1 \right) * 1000 \qquad (S3)$$

and

$$\delta^{18}O = \left(\left(\frac{^{18}O/^{16}O_{sample}}{^{18}O/^{16}O_{VSMOW}} \right) - 1 \right) * 1000 \qquad (S4)$$

Both the average value and the standard deviation of the three replicate injections are reported in Tables S3.3, S3.5, and S3.6. Typical precision (1σ) was 0.2 ‰ for $\delta^{18}O$ and 1 ‰ for δD, though some samples showed larger uncertainties. Regular analysis (i.e. every 15 samples) of an in-house water standard calibrated with VSMOW and VSLAP was used to assess drift in the accuracy and precision of the instrument during and between sample runs. Additionally, an external standard (LGR Water #2 – sealed 11/20/07) was analysed for calibration purposes. Isotopic analyses of river water samples collected in glass exetainers were performed with either a Los-Gatos DLT-100 Liquid Water Isotope Analyzer at the California Institute of Technology or a Delta V Advantage IRMS equipped with a Gasbench II system at the University of Oxford.

Data on rain water isotopes include both samples collected in this study, and data from *Horwath* [2011]. For samples collected in this study, rainwater was collected in a rinsed plastic container left out in an open area near the San Pedro River gauging station and Wayqecha River gauging station during river water sample collection from June 2010 to June

2011. Additional rainfall samples were taken February 2011 from at elevations of 2050, 2130, 2300 and 2400. Samples were transferred into 15 mL glass exetainers with rubber septa after filtration and stored refrigerated and unpreserved. These samples were analysed as described above for the river waters (Table S3.3). Rain water samples from *Horwath* [2011] consisted of fresh precipitation as well as rainwater pools on leaves and were collected at elevations of 1500, 2000, 2500, 3000, and 3600 masl over the course of ~1 week in April 2009, July 2009, and September 2009 (Table S3.3).

Cloud water vapour samples are from [*Horwath*, 2011]. Detailed description of the collection are presented in *Horwath* [2011]. Cloud water vapour samples were collected below the tree canopy using a 'double action hand pump' (Galert) to draw ambient air into a cryogenic trap (liquid N_2) continuously over the course of 15-20 minutes.Cloud water vapour samples were collected at the same elevations and during the same time periods as the rainwater with the exception that there were no cloud water vapour samples collected during April 2009. Isotopic analyses for all rain and cloud water samples collected by *Horwath* [2011] were made using a Picarro L1102-i cavity ring down spectrometer.

Table S3.3a: Water isotope data for rainfall collected in the Kosñipata Valley

Season	Date (dd-mmm-yy)	Elevation (m)	$\delta^{18}O$ (‰)	σ $\delta^{18}O$ (‰)	δD (‰)	σ δD (‰)	Dxs (‰)	σ Dxs (‰)
Dry season	13-Jun-11	1360	-4.63	0.10	-18.89	0.57	18.18	0.98
Wet season	19-Dec-10	1360	-2.46	0.14	-17.70	0.98	1.95	1.46
Wet season	22-Mar-11	1360	-12.44	0.16	-92.29	0.45	7.22	1.36
Wet season	27-Dec-10	1360	-15.22	0.24	-111.36	0.45	10.40	1.98
Wet season	24-Jan-11	1360	-16.49	0.06	-129.76	0.74	2.16	0.87
Wet season	21-Feb-11	1360	-18.58	0.08	-138.96	0.41	9.66	0.75
Dry season	06-Jul-09	1500	-7.19	0.08	-40.73	0.50	16.82	0.81
Dry season	06-Jul-09	1500	-7.18	0.08	-40.69	0.50	16.71	0.81
Dry season	06-Jul-09	1500	-7.16	0.08	-40.73	0.50	16.52	0.81
Dry season	07-Jul-09	1500	-7.39	0.08	-41.90	0.50	17.25	0.81
Dry season	07-Jul-09	1500	-7.41	0.08	-42.00	0.50	17.30	0.81
Dry season	07-Jul-09	1500	-7.57	0.08	-42.96	0.50	17.58	0.81
Dry season	14-Sep-09	1500	-2.55	0.08	1.81	0.50	22.19	0.81
Dry season	14-Sep-09	1500	-2.08	0.08	4.46	0.50	21.08	0.81
Dry season	14-Sep-09	1500	-1.93	0.08	7.70	0.50	23.13	0.81
Dry season	15-Sep-09	1500	-1.56	0.08	3.72	0.50	16.19	0.81
Dry season	16-Sep-09	1500	-2.70	0.08	0.21	0.50	21.84	0.81
Dry season	16-Sep-09	1500	-0.94	0.08	9.36	0.50	16.85	0.81
Dry season	05-Jul-09	2000	-6.62	0.08	-35.67	0.50	17.26	0.81
Dry season	05-Jul-09	2000	-6.57	0.08	-35.59	0.50	16.95	0.81
Dry season	05-Jul-09	2000	-6.58	0.08	-35.49	0.50	17.17	0.81
Dry season	12-Sep-09	2000	-1.61	0.08	6.26	0.50	19.17	0.81
Dry season	12-Sep-09	2000	-3.10	0.08	-2.88	0.50	21.89	0.81
Dry season	12-Sep-09	2000	-1.75	0.08	6.11	0.50	20.08	0.81
Dry season	12-Sep-09	2000	-1.59	0.08	6.70	0.50	19.42	0.81
Wet season	20-Feb-11	2040	-22.81	0.29	-168.28	1.34	14.18	2.65
Wet season	20-Feb-11	2050	-22.50	0.14	-170.76	0.87	9.25	1.39
Wet season	20-Feb-11	2130	-14.71	0.16	-105.35	0.77	12.35	1.51
Dry season	28-Jun-10	2290	-3.88	0.06	-16.21	0.91	14.86	1.03
Dry season	28-Jun-10	2290	-6.73	0.20	-36.95	0.82	16.86	1.80
Wet season	22-Mar-10	2290	-8.32	0.27	-56.74	0.52	9.80	2.19
Wet season	19-Feb-11	2290	-10.40	0.07	-72.11	0.33	11.08	0.64
Wet season	27-Dec-10	2290	-17.72	0.08	-136.09	0.60	5.70	0.89
Wet season	19-Feb-11	2300	-14.52	0.09	-100.38	0.70	15.77	0.99
Wet season	19-Feb-11	2400	-12.46	0.17	-87.71	0.32	11.93	1.37
Dry season	03-Jul-07	2500	-5.69	0.08	-28.75	0.50	16.76	0.81
Dry season	03-Jul-07	2500	-5.50	0.08	-27.76	0.50	16.24	0.81
Dry season	03-Jul-07	2500	-5.82	0.08	-29.33	0.50	17.22	0.81
Dry season	03-Jul-07	2500	-7.97	0.08	-45.49	0.50	18.25	0.81
Dry season	03-Jul-07	2500	-7.96	0.08	-45.77	0.50	17.90	0.81

Dry season	03-Jul-07	2500	-7.95	0.08	-46.08	0.50	17.51	0.81
Dry season	08-Sep-09	2500	-0.85	0.08	14.33	0.50	21.16	0.81
Dry season	08-Sep-09	2500	-0.89	0.08	14.32	0.50	21.48	0.81
Dry season	08-Sep-09	2500	-0.75	0.08	15.40	0.50	21.41	0.81
Dry season	08-Sep-09	2500	-0.85	0.08	14.12	0.50	20.93	0.81
Dry season	08-Sep-09	2500	-0.78	0.08	14.90	0.50	21.17	0.81
Dry season	08-Sep-09	2500	-0.96	0.08	14.23	0.50	21.93	0.81
Dry season	10-Sep-09	2500	-2.19	0.08	3.70	0.50	21.18	0.81
Dry season	10-Sep-09	2500	-4.25	0.08	-12.50	0.50	21.47	0.81
Dry season	10-Sep-09	2500	-3.89	0.08	-10.05	0.50	21.08	0.81
Dry season	10-Sep-09	2500	-2.32	0.08	2.95	0.50	21.47	0.81
Dry season	10-Sep-09	2500	-4.45	0.08	-14.42	0.50	21.19	0.81
Dry season	10-Sep-09	2500	-3.78	0.08	-9.74	0.50	20.54	0.81
Dry season	01-Jul-09	3000	-7.00	0.08	-41.47	0.50	14.51	0.81
Dry season	01-Jul-09	3000	-6.92	0.08	-40.57	0.50	14.83	0.81
Dry season	01-Jul-09	3000	-6.83	0.08	-40.99	0.50	13.66	0.81
Dry season	01-Jul-09	3000	-7.15	0.08	-42.20	0.50	15.03	0.81
Dry season	01-Jul-09	3000	-7.11	0.08	-41.47	0.50	15.42	0.81
Dry season	01-Jul-09	3000	-7.38	0.08	-44.05	0.50	14.97	0.81
Dry season	09-Sep-09	3000	-1.76	0.08	8.20	0.50	22.24	0.81
Dry season	09-Sep-09	3000	-1.68	0.08	9.05	0.50	22.47	0.81
Dry season	09-Sep-09	3000	-2.17	0.08	5.89	0.50	23.21	0.81
Dry season	09-Sep-09	3000	-2.15	0.08	6.22	0.50	23.43	0.81
Dry season	09-Sep-09	3000	-1.29	0.08	9.82	0.50	20.10	0.81

Table S3.3b: Water isotope data for cloud water collected in the Kosñipata Valley

	Date	Elevation	$\delta^{18}O$*	σ $\delta^{18}O$	δD*	σ δD	Dxs*	σ Dxs
	(dd-mmm-yy)	(m)	(‰)	(‰)	(‰)	(‰)	(‰)	(‰)
Cloud water	14-Sep-09	1500	-1.40	0.08	15.34	0.50	26.57	0.81
Cloud water	14-Sep-09	1500	-0.47	0.08	19.81	0.50	23.60	0.81
Cloud water	14-Sep-09	1500	-1.48	0.08	14.71	0.50	26.56	0.81
Cloud water	14-Sep-09	1500	-1.86	0.08	14.35	0.50	29.21	0.81
Cloud water	14-Sep-09	1500	-5.09	0.08	-0.04	0.50	40.65	0.81
Cloud water	14-Sep-09	1500	-2.71	0.08	11.87	0.50	33.51	0.81
Cloud water	12-Sep-09	2000	-3.81	0.08	-1.71	0.50	28.76	0.81
Cloud water	12-Sep-09	2000	-2.40	0.08	3.30	0.50	22.48	0.81
Cloud water	12-Sep-09	2000	-7.32	0.08	-18.41	0.50	40.15	0.81
Cloud water	12-Sep-09	2000	-5.77	0.08	-11.47	0.50	34.69	0.81
Cloud water	12-Sep-09	2000	-6.09	0.08	-12.16	0.50	36.53	0.81
Cloud water	03-Jul-07	2500	-8.29	0.08	-41.50	0.50	24.80	0.81
Cloud water	03-Jul-07	2500	-16.04	0.08	-68.33	0.50	60.00	0.81
Cloud water	03-Jul-07	2500	-16.94	0.08	-68.80	0.50	66.75	0.81
Cloud water	03-Jul-07	2500	-12.28	0.08	-42.91	0.50	55.36	0.81

Cloud water	03-Jul-07	2500	-11.65	0.08	-52.50	0.50	40.68	0.81
Cloud water	03-Jul-07	2500	-13.10	0.08	-64.09	0.50	40.74	0.81
Cloud water	10-Sep-09	2500	-4.99	0.08	-9.89	0.50	30.04	0.81
Cloud water	10-Sep-09	2500	-3.31	0.08	-3.67	0.50	22.83	0.81
Cloud water	10-Sep-09	2500	-3.99	0.08	-10.70	0.50	21.21	0.81
Cloud water	10-Sep-09	2500	-7.55	0.08	-23.47	0.50	36.93	0.81
Cloud water	10-Sep-09	2500	-5.36	0.08	-7.96	0.50	34.92	0.81
Cloud water	10-Sep-09	2500	-7.14	0.08	-16.74	0.50	40.40	0.81
Cloud water	01-Jul-09	3000	-12.38	0.08	-66.54	0.50	32.50	0.81
Cloud water	01-Jul-09	3000	-18.29	0.08	-85.17	0.50	61.14	0.81
Cloud water	01-Jul-09	3000	-16.31	0.08	-101.23	0.50	29.27	0.81
Cloud water	01-Jul-09	3000	-18.31	0.08	-86.05	0.50	60.40	0.81
Cloud water	01-Jul-09	3000	-12.46	0.08	-56.25	0.50	43.45	0.81
Cloud water	01-Jul-09	3000	-16.89	0.08	-75.90	0.50	59.19	0.81
Cloud water	09-Sep-09	3000	-6.02	0.08	-10.35	0.50	37.85	0.81
Cloud water	09-Sep-09	3000	-6.00	0.08	-11.65	0.50	36.33	0.81
Cloud water	09-Sep-09	3000	-9.00	0.08	-29.96	0.50	42.03	0.81
Cloud water	09-Sep-09	3000	-8.23	0.08	-32.36	0.50	33.50	0.81
Cloud water	09-Sep-09	3000	-6.13	0.08	-21.52	0.50	27.54	0.81
Cloud water	09-Sep-09	3000	-5.34	0.08	-19.10	0.50	23.64	0.81
Cloud water	30-Jun-09	3600	-9.89	0.08	-48.36	0.50	30.76	0.81
Cloud water	30-Jun-09	3600	-11.76	0.08	-54.14	0.50	39.94	0.81
Cloud water	30-Jun-09	3600	-13.24	0.08	-62.96	0.50	42.99	0.81
Cloud water	30-Jun-09	3600	-13.53	0.08	-62.00	0.50	46.21	0.81
Cloud water	30-Jun-09	3600	-14.47	0.08	-68.30	0.50	47.43	0.81
Cloud water	30-Jun-09	3600	-14.04	0.08	-64.77	0.50	47.57	0.81
Cloud water	07-Sep-09	3600	-3.49	0.08	8.30	0.50	36.23	0.81
Cloud water	07-Sep-09	3600	-4.96	0.08	6.66	0.50	46.34	0.81
Cloud water	07-Sep-09	3600	-8.70	0.08	-12.75	0.50	56.83	0.81
Cloud water	07-Sep-09	3600	-4.16	0.08	13.84	0.50	47.08	0.81
Cloud water	07-Sep-09	3600	-8.99	0.08	-14.35	0.50	57.57	0.81
Cloud water	07-Sep-09	3600	-11.45	0.08	-61.24	0.50	30.34	0.81

* Characteristic analytical uncertainties reported by *Horwath* [2011]

S3.1.4. Water isotope mixing model

We used an isotope mixing model to distinguish contributions to river runoff from wet season rainfall, dry season rainfall, and cloud water. In order to use the water isotope data to make quantitative estimates of the water sources to river flow, three end-member isotopic mixing was simulated with the mixing equations:

$$\delta D_{river} = f_1(\delta D_1) + f_2(\delta D_2) + f_3(\delta D_3) \quad (S5)$$

$$Dxs_{river} = f_1(Dxs_1) + f_2(Dxs_2) + f_3(Dxs_3) \quad (S6)$$

and

$$1 = f_1 + f_2 + f_3 \quad (S7)$$

where

$$Dxs_{river} = \delta D_{river} - (\delta^{18}O_{river} \times 8) \quad (S8)$$

To calculate the mixing proportions (i.e. f_1,f_2, and f_3), the matrix inversion function of MATLAB 2013a was used. Due to the observed variability in the three end-members (Figure 3.5 in main text), which is known to significantly influence the results of end-member mixing calculations [*Phillips and Gregg*, 2001], 10,000 random end-member δD and Dxs values were generated using the observed ranges for each end-member. For each sample, the mixing proportions were determined for all of the 10,000 end member combinations, but only a fraction of the combinations (18-72 %) yielded realistic results (i.e. mixing proportions between 0 and 1). The mean, 5th percentile, 50th percentile, and 95th percentile of all possible ($0 \leq \Sigma f \leq 1$) mixing proportions are presented in Table S3.7. The effect of the analytical uncertainty on the individual rainwater samples on the calculated mixing proportions was

considered by generating 1000 pseudo-random synthetic data for each sample and determining the mixing portions for each of the 10,000 end member combinations (i.e. 10^7 simulations per sample). For each sample, the pseudo-random values were generated from a normal distribution with the measured sample mean and standard deviation. To assess whether or not 10^7 simulations per sample yielded re-producible results given the large number of possible end-member and sample composition combinations, replicate model calculations using different randomly generated datasets for the same input parameters were performed. These replicate calculations yielded between 0.1 and 5 % variation in the statistical parameters (i.e. mean, median, and 5^{th} and 95^{th} percentiles) of the distribution of fractional contributions for each end-member.

End-member compositions were defined based on observed precipitation data for selected time intervals. The wet season rainfall end-member was determined based on the average and standard deviation of the December 2010, March 2010, January 2011, February 2011, and March 2011 rainwater data (Figure 3.5). For dry season precipitation, the average and standard deviation of the September 2009, July 2009, June 2010, and June 2011 rainwater data was used. The cloud water vapour was defined by the average and standard deviation of the July and September 2009 cloud water data, which was the only available data (Table S3.3b).

Table S3.7: Results of Monte Carlo analysis of mixing fractions for stream water isotope samples from San Pedro

Date and hour (dd-mmm-yy hr)	Wet Rain				Dry Rain				Cloud Water				# of real
	Mean	5%	50%	95%	Mean	5%	50%	95%	Mean	5%	50%	95%	simulations
01-Nov-09	0.56	0.39	0.54	0.77	0.29	0.04	0.30	0.54	0.15	0.020	0.14	0.33	6.27E+06
07-Nov-09	0.49	0.34	0.48	0.66	0.20	0.02	0.19	0.41	0.31	0.151	0.30	0.52	4.70E+06
15-Nov-09	0.67	0.50	0.66	0.86	0.24	0.03	0.24	0.45	0.10	0.008	0.09	0.24	4.05E+06
30-Nov-09	0.60	0.42	0.59	0.83	0.28	0.03	0.28	0.52	0.12	0.011	0.10	0.28	4.98E+06
30-Jan-10 00	0.62	0.45	0.61	0.83	0.27	0.03	0.27	0.50	0.12	0.011	0.10	0.27	5.00E+06
04-Feb-10 03	0.66	0.52	0.65	0.83	0.21	0.02	0.21	0.40	0.13	0.017	0.12	0.29	4.34E+06
04-Feb-10 09	0.65	0.46	0.64	0.87	0.25	0.03	0.25	0.49	0.09	0.007	0.08	0.24	3.48E+06
04-Feb-10 15	0.65	0.48	0.64	0.86	0.25	0.03	0.25	0.47	0.10	0.008	0.09	0.24	4.12E+06
04-Feb-10 21	0.64	0.48	0.63	0.85	0.25	0.03	0.25	0.46	0.11	0.010	0.10	0.26	4.57E+06
05-Feb-10 09	0.64	0.47	0.63	0.84	0.25	0.03	0.25	0.47	0.12	0.011	0.10	0.27	4.74E+06
05-Feb-10 15	0.64	0.48	0.63	0.84	0.24	0.03	0.24	0.45	0.12	0.012	0.10	0.27	4.65E+06
05-Feb-10 21	0.64	0.48	0.63	0.84	0.24	0.03	0.25	0.46	0.12	0.011	0.10	0.27	4.64E+06
06-Feb-10 09	0.64	0.47	0.63	0.84	0.25	0.03	0.25	0.47	0.11	0.011	0.10	0.26	4.60E+06
06-Feb-10 15	0.63	0.48	0.62	0.83	0.24	0.03	0.24	0.46	0.12	0.014	0.11	0.28	4.87E+06
07-Feb-10	0.65	0.48	0.63	0.85	0.24	0.03	0.24	0.46	0.11	0.011	0.10	0.26	4.54E+06
07-Feb-10 03	0.65	0.48	0.63	0.85	0.24	0.03	0.24	0.46	0.11	0.011	0.10	0.26	4.52E+06
07-Feb-10 09	0.62	0.47	0.61	0.81	0.24	0.03	0.25	0.46	0.14	0.017	0.12	0.30	5.13E+06
07-Feb-10 15	0.64	0.48	0.63	0.84	0.24	0.03	0.25	0.46	0.12	0.012	0.11	0.28	4.76E+06
07-Feb-10 21	0.65	0.48	0.64	0.85	0.24	0.03	0.24	0.46	0.11	0.010	0.10	0.26	4.40E+06
08-Feb-10 03	0.62	0.47	0.61	0.82	0.24	0.03	0.24	0.46	0.14	0.017	0.13	0.30	5.09E+06
08-Feb-10 09	0.66	0.49	0.65	0.86	0.24	0.03	0.24	0.45	0.11	0.010	0.09	0.25	4.27E+06
08-Feb-10 15	0.61	0.46	0.60	0.80	0.24	0.03	0.24	0.45	0.15	0.023	0.14	0.32	5.25E+06
08-Feb-10 21	0.60	0.46	0.59	0.79	0.24	0.03	0.24	0.46	0.16	0.025	0.15	0.33	5.29E+06
09-Feb-10 03	0.66	0.49	0.64	0.86	0.24	0.03	0.24	0.46	0.10	0.009	0.09	0.25	4.21E+06
09-Feb-10 09	0.61	0.46	0.60	0.80	0.24	0.03	0.24	0.46	0.15	0.023	0.14	0.32	5.28E+06
09-Feb-10 15	0.62	0.47	0.61	0.82	0.24	0.03	0.24	0.46	0.13	0.017	0.12	0.30	5.06E+06
10-Feb-10 03	0.62	0.47	0.60	0.80	0.24	0.03	0.24	0.45	0.15	0.022	0.14	0.32	5.16E+06

11-Feb-10 09	0.63	0.47	0.61	0.82	0.24	0.03	0.24	0.45	0.13	0.017	0.12	0.30	5.01E+06
11-Feb-10 21	0.62	0.47	0.61	0.81	0.24	0.03	0.24	0.45	0.15	0.020	0.13	0.31	5.12E+06
12-Feb-10 05	0.60	0.43	0.58	0.81	0.27	0.03	0.28	0.51	0.13	0.014	0.11	0.29	5.53E+06
12-Feb-10 09	0.62	0.47	0.61	0.81	0.24	0.03	0.24	0.45	0.14	0.019	0.13	0.31	5.11E+06
12-Feb-10 14	0.62	0.45	0.60	0.82	0.26	0.03	0.26	0.48	0.13	0.013	0.11	0.29	5.12E+06
22-Feb-10	0.64	0.46	0.64	0.86	0.26	0.03	0.26	0.48	0.10	0.008	0.09	0.25	4.19E+06
22-Mar-10	0.63	0.46	0.61	0.83	0.26	0.03	0.26	0.48	0.12	0.012	0.10	0.27	4.92E+06
29-Mar-10	0.64	0.48	0.63	0.84	0.24	0.03	0.24	0.46	0.12	0.012	0.11	0.28	4.64E+06
05-Apr-10	0.67	0.54	0.66	0.85	0.19	0.02	0.19	0.38	0.13	0.016	0.12	0.29	4.01E+06
25-Apr-10	0.64	0.48	0.63	0.84	0.24	0.03	0.24	0.46	0.12	0.012	0.10	0.27	4.55E+06
16-May-10	0.65	0.49	0.64	0.85	0.24	0.03	0.24	0.45	0.11	0.010	0.10	0.26	4.45E+06
26-May-10	0.60	0.44	0.59	0.80	0.26	0.03	0.27	0.49	0.14	0.017	0.12	0.31	5.47E+06
31-May-10	0.62	0.46	0.61	0.81	0.25	0.03	0.25	0.46	0.14	0.016	0.12	0.30	5.15E+06
14-Jun-10	0.65	0.50	0.63	0.83	0.22	0.03	0.22	0.43	0.13	0.015	0.12	0.29	4.54E+06
12-Jul-10	0.62	0.46	0.61	0.82	0.25	0.03	0.25	0.47	0.13	0.015	0.12	0.30	5.18E+06
19-Jul-10	0.61	0.44	0.60	0.82	0.26	0.03	0.26	0.48	0.13	0.014	0.12	0.31	5.08E+06
11-Aug-10	0.56	0.39	0.55	0.78	0.29	0.04	0.30	0.53	0.15	0.019	0.13	0.33	6.23E+06
18-Aug-10	0.60	0.44	0.59	0.80	0.26	0.03	0.26	0.48	0.14	0.018	0.13	0.31	5.47E+06
23-Aug-10	0.58	0.40	0.57	0.81	0.29	0.04	0.30	0.54	0.12	0.013	0.11	0.29	5.71E+06
02-Sep-10	0.61	0.44	0.59	0.82	0.27	0.03	0.27	0.50	0.13	0.013	0.11	0.29	5.33E+06
04-Sep-10	0.60	0.43	0.59	0.80	0.26	0.03	0.26	0.49	0.14	0.017	0.13	0.32	5.30E+06
13-Sep-10	0.59	0.42	0.58	0.81	0.28	0.03	0.28	0.51	0.13	0.014	0.11	0.30	5.60E+06
15-Oct-10	0.62	0.44	0.60	0.83	0.26	0.03	0.27	0.49	0.12	0.012	0.11	0.29	4.78E+06
15-Nov-10	0.65	0.46	0.64	0.86	0.26	0.03	0.26	0.49	0.10	0.007	0.08	0.24	3.63E+06
19-Nov-10	0.49	0.30	0.47	0.72	0.33	0.05	0.34	0.60	0.18	0.026	0.17	0.40	7.14E+06
22-Nov-10	0.53	0.35	0.51	0.75	0.30	0.04	0.30	0.55	0.18	0.025	0.16	0.38	6.52E+06
06-Dec-10	0.60	0.41	0.59	0.83	0.28	0.03	0.28	0.52	0.12	0.010	0.10	0.30	4.55E+06
13-Dec-10	0.64	0.42	0.65	0.83	0.29	0.06	0.28	0.56	0.07	0.004	0.06	0.19	1.88E+06
20-Dec-10	0.59	0.42	0.58	0.81	0.28	0.03	0.28	0.52	0.13	0.013	0.11	0.30	5.50E+06

27-Dec-10	0.50	0.33	0.48	0.72	0.32	0.04	0.33	0.58	0.18	0.033	0.17	0.38	7.23E+06
03-Jan-11	0.56	0.39	0.54	0.77	0.29	0.04	0.29	0.53	0.16	0.023	0.14	0.34	6.31E+06
24-Jan-11	0.59	0.43	0.58	0.79	0.26	0.03	0.27	0.49	0.14	0.020	0.13	0.32	5.63E+06
08-Mar-11	0.52	0.34	0.51	0.76	0.32	0.04	0.33	0.58	0.16	0.019	0.14	0.36	6.49E+06
05-May-11	0.46	0.27	0.44	0.70	0.29	0.03	0.29	0.57	0.25	0.037	0.23	0.52	6.43E+06
18-Jul-11	0.61	0.40	0.60	0.84	0.29	0.04	0.29	0.54	0.10	0.008	0.08	0.26	3.97E+06

Table S3.5: Water isotope data of stream water collected from the San Pedro gauging station

Date and hour (dd-mmm-yy hr)[1]	$\delta^{18}O$ (‰)	σ $\delta^{18}O$ (‰)	δD (‰)	σ δD (‰)	Dxs	σ Dxs
01-Nov-09	-11.62	0.14	-77.33	0.65	15.64	1.32
07-Nov-09	-10.75	0.15	-67.95	0.42	18.03	1.29
15-Nov-09	-11.47	0.14	-74.89	0.32	16.89	1.20
30-Nov-09	-12.10	0.14	-80.46	0.25	16.34	1.16
30-Jan-10 00	-13.44	0.15	-91.94	0.19	15.61	1.20
04-Feb-10 03	-12.39	0.14	-84.13	0.21	14.96	1.15
04-Feb-10 09	-12.56	0.14	-85.54	0.19	14.97	1.15
04-Feb-10 15	-12.21	0.14	-83.56	0.11	14.10	1.14
04-Feb-10 21	-12.38	0.14	-84.32	0.03	14.72	1.13
05-Feb-10 09	-12.57	0.14	-85.21	0.29	15.35	1.17
05-Feb-10 15	-12.45	0.14	-84.67	0.42	14.90	1.21
05-Feb-10 21	-12.35	0.14	-84.08	0.28	14.75	1.17
06-Feb-10 09	-12.47	0.14	-85.04	0.29	14.72	1.17
06-Feb-10 15	-12.48	0.14	-85.09	0.31	14.75	1.18
07-Feb-10	-12.55	0.14	-86.01	0.16	14.41	1.15
07-Feb-10 03	-12.44	0.14	-84.94	0.48	14.56	1.23
07-Feb-10 09	-12.58	0.14	-84.71	0.51	15.91	1.25
07-Feb-10 15	-12.55	0.14	-84.50	0.33	15.90	1.18
07-Feb-10 21	-12.52	0.14	-85.04	0.28	15.12	1.17
08-Feb-10 03	-12.44	0.14	-85.22	0.29	14.29	1.17
08-Feb-10 09	-12.59	0.14	-84.27	0.07	16.48	1.14
08-Feb-10 15	-12.63	0.14	-84.58	0.09	16.47	1.14
08-Feb-10 21	-12.60	0.14	-84.10	0.39	16.71	1.20
09-Feb-10 03	-12.60	0.14	-85.03	0.22	15.79	1.16
09-Feb-10 09	-12.69	0.14	-85.19	0.25	16.33	1.17
09-Feb-10 15	-12.69	0.14	-85.71	0.13	15.80	1.15
10-Feb-10 03	-12.68	0.14	-85.25	0.43	16.22	1.22
11-Feb-10 09	-12.63	0.14	-85.00	0.46	16.08	1.23
11-Feb-10 21	-11.80	0.14	-78.70	0.11	15.72	1.15
12-Feb-10 05	-11.93	0.14	-81.34	0.39	14.12	1.20
12-Feb-10 09	-12.18	0.14	-82.38	0.22	15.10	1.15
12-Feb-10 14	-12.17	0.14	-81.88	0.54	15.46	1.26
22-Feb-10	-12.53	0.14	-85.18	0.68	15.03	1.32
22-Mar-10	-12.51	0.14	-85.15	0.83	14.90	1.41
29-Mar-10	-12.53	0.14	-85.63	0.07	14.64	1.14
05-Apr-10	-12.09	0.14	-80.72	0.53	16.03	1.25
25-Apr-10	-12.46	0.14	-83.80	0.50	15.85	1.24
16-May-10	-12.38	0.14	-83.30	0.24	15.72	1.16
26-May-10	-12.14	0.14	-81.43	1.18	15.65	1.64
31-May-10	-11.39	0.15	-74.59	0.30	16.56	1.20
14-Jun-10	-12.20	0.14	-81.47	0.13	16.10	1.14
12-Jul-10	-11.27	0.15	-74.51	0.31	15.63	1.21
19-Jul-10	-11.89	0.14	-79.62	0.45	15.53	1.22

Cont. next page…

Table S3.5, cont.: Water isotope data of stream water collected from the San Pedro gauging station

Date and hour (dd-mmm-yy hr)	$\delta^{18}O$ (‰)	σ $\delta^{18}O$ (‰)	δD (‰)	σ δD (‰)	Dxs	σ Dxs
11-Aug-10	-11.68	0.14	-77.67	0.37	15.76	1.20
18-Aug-10	-11.64	0.17	-79.54	0.98	13.55	1.67
23-Aug-10	-11.88	0.14	-80.02	1.31	15.04	1.74
02-Sep-10	-10.37	0.16	-64.99	1.61	18.01	2.04
04-Sep-10	-11.05	0.15	-70.85	1.49	17.55	1.90
13-Sep-10	-11.36	0.23	-76.20	1.06	14.70	2.15
15-Oct-10	-8.94	0.09	-58.85	0.17	12.64	0.71
15-Nov-10	-10.72	0.21	-71.86	0.68	13.90	1.83
19-Nov-10	-10.64	0.24	-68.22	0.57	16.94	1.97
22-Nov-10	-10.63	0.46	-64.93	0.47	20.09	3.74
06-Dec-10	-11.38	0.15	-74.37	0.46	16.68	1.25
13-Dec-10	-12.26	0.18	-76.37	0.31	21.68	1.45
20-Dec-10	-11.49	0.18	-76.90	0.60	15.03	1.57
27-Dec-10	-12.54	0.11	-86.25	0.28	14.05	0.90
03-Jan-11	-11.90	0.14	-80.14	0.36	15.05	1.19
24-Jan-11	-11.63	0.19	-79.70	0.70	13.38	1.69
08-Mar-11	-13.79	0.15	-94.88	0.23	15.43	1.24
05-May-11	-13.04	0.14	-88.81	0.74	15.49	1.37
18-Jul-11	-12.09	0.18	-80.61	0.75	16.08	1.66

Mean isotope values and σ (standard deviation) were from 3 replicate sample injections (see description of methods in Supplementary Text)
[1] hour not reported when only one sample collected on a given date

Only the samples collected at the San Pedro gauging samples were used in the mixing calculations, because there is a noticeable isotopic offset between the San Pedro and Wayqecha samples (Tables S3.5 & S3.6). The isotopic offset is most likely the result of the different sampling elevations, but it is not possible to separate quantitatively the effect of elevation on the isotopic composition of rainfall with the currently available data.

Table S3.6: Water isotope data of stream water collected from the Wayqecha gauging station

Date and hour (dd-mmm-yy hr)[1]	$\delta^{18}O$ (‰)	σ $\delta^{18}O$ (‰)	δD (‰)	σ δD (‰)	Dxs	σ Dxs
29-Jan-10 09	-13.93	0.16	-98.40	0.74	13.03	1.46
29-Jan-10 15	-14.02	0.16	-98.93	0.22	13.24	1.28
30-Jan-10 03	-14.33	0.16	-101.49	0.29	13.13	1.30
30-Jan-10 09	-14.17	0.16	-100.22	0.54	13.11	1.37
30-Jan-10 15	-14.21	0.16	-99.83	0.27	13.81	1.29
31-Jan-10 03	-14.08	0.16	-99.04	0.72	13.61	1.45
31-Jan-10 15	-13.85	0.16	-98.16	0.66	12.62	1.42
01-Feb-10 15	-13.83	0.16	-97.25	0.86	13.38	1.52
01-Feb-10 21	-13.84	0.16	-96.81	0.47	13.88	1.34
02-Feb-10 03	-13.85	0.16	-97.03	0.84	13.81	1.51
02-Feb-10 15	-13.67	0.16	-96.45	0.77	12.92	1.47
03-Feb-10 03	-13.77	0.16	-97.41	0.53	12.76	1.36
03-Feb-10 09	-13.74	0.16	-96.05	1.16	13.85	1.70
03-Feb-10 15	-13.73	0.16	-96.48	0.38	13.37	1.31
04-Feb-10 03	-13.75	0.16	-96.33	0.29	13.71	1.28
04-Feb-10 09	-13.80	0.16	-96.08	0.93	14.29	1.56
04-Feb-10 15	-13.65	0.16	-95.33	0.27	13.83	1.28
04-Feb-10 21	-13.75	0.16	-96.22	0.33	13.79	1.29
05-Feb-10 09	-13.80	0.16	-96.72	0.84	13.66	1.51
05-Feb-10 15	-13.87	0.16	-97.55	0.58	13.43	1.38
05-Feb-10 21	-13.76	0.16	-96.59	0.32	13.51	1.29
06-Feb-10 03	-13.81	0.16	-96.85	1.15	13.61	1.70
06-Feb-10 09	-13.63	0.16	-96.75	0.16	12.33	1.26
06-Feb-10 15	-13.68	0.16	-96.55	0.21	12.92	1.27
06-Feb-10 21	-13.80	0.16	-96.14	0.23	14.27	1.27
07-Feb-10 03	-13.70	0.16	-96.27	0.76	13.37	1.46
07-Feb-10 09	-13.73	0.16	-96.22	0.24	13.59	1.27
07-Feb-10 15	-13.70	0.16	-96.26	0.05	13.36	1.25
07-Feb-10 21	-13.74	0.16	-96.25	0.73	13.63	1.45
08-Feb-10 03	-13.65	0.16	-95.85	0.42	13.37	1.32
08-Feb-10 09	-13.73	0.16	-96.81	0.74	12.99	1.45
08-Feb-10 21	-13.68	0.16	-96.28	0.18	13.19	1.26
09-Feb-10 03	-13.65	0.16	-95.84	0.16	13.33	1.26
09-Feb-10 09	-13.87	0.16	-97.70	0.39	13.26	1.31
09-Feb-10 15	-13.71	0.16	-96.45	0.46	13.20	1.33
09-Feb-10 21	-13.75	0.16	-96.34	0.19	13.62	1.26
10-Feb-10 03	-13.77	0.16	-96.28	1.26	13.86	1.78
10-Feb-10 09	-13.68	0.16	-96.19	0.16	13.24	1.26
10-Feb-10 15	-13.70	0.16	-96.43	0.55	13.15	1.36
10-Feb-10 21	-13.47	0.16	-94.13	0.26	13.66	1.27
11-Feb-10 15	-13.66	0.16	-95.57	0.39	13.69	1.31
11-Feb-10 21	-13.50	0.16	-94.56	0.53	13.45	1.35
22-Feb-10	-13.81	0.16	-98.09	0.05	12.38	1.25

Cont. next page…

Table S3.6, cont.: Water isotope data of stream water collected from the Wayqecha gauging station

Date and hour (dd-mmm-yy hr)	$\delta^{18}O$ (‰)	σ $\delta^{18}O$ (‰)	δD (‰)	σ δD (‰)	Dxs	σ Dxs
01-Mar-10	-13.83	0.16	-97.81	0.57	12.86	1.37
05-Apr-10	-13.58	0.16	-95.45	0.27	13.22	1.27
12-Apr-10	-13.57	0.16	-95.24	0.24	13.31	1.27
19-Apr-10	-13.23	0.15	-93.21	0.37	12.62	1.29
10-May-10	-13.45	0.16	-94.45	0.13	13.16	1.25
16-May-10	-13.33	0.15	-93.77	0.25	12.85	1.27
07-Jun-10	-13.31	0.15	-93.80	0.33	12.71	1.28
28-Jun-10	-12.83	0.15	-88.97	0.37	13.66	1.29
11-Jul-10	-13.05	0.15	-90.93	0.17	13.44	1.25
26-Jul-10	-13.07	0.15	-91.66	0.50	12.89	1.33
22-Aug-10	-13.05	0.15	-91.25	0.30	13.14	1.27
29-Aug-10	-13.10	0.15	-90.49	0.31	14.29	1.27
25-Oct-10	-12.89	0.15	-89.90	0.34	13.21	1.28
20-Dec-10	-13.20	0.15	-91.93	0.25	13.64	1.26
03-Jul-11	-13.37	0.16	-94.66	0.67	12.29	1.41
18-Feb-11	-13.81	0.16	-96.92	0.28	13.58	1.28
21-Mar-11	-14.01	0.16	-99.00	0.51	13.09	1.36

Mean isotope values and σ (standard deviation) were from 3 replicate sample injections (see description of methods in Supplementary Text)
[1] hour not reported when only one sample collected on a given date

S3.1.5. Actual evapotranspiration estimates

Evapotranspiration (ET) was calculated as the sum of soil evaporation (LE_s), canopy transpiration (LE_c), and evaporation of canopy intercepted water (LE_i). The five most important parameters for calculating ET via this method are net radiation (R_n), normalised difference vegetation index (NDVI), soil adjusted vegetation index (SAVI), maximum air temperature (T_{max}), and water vapour pressure (ea). NDVI was used to predict SAVI and RH_{min} and T_{max} were used to predict water vapour pressure. The PT-JPL model was applied to all meteorological stations with RH_{min}, T_{max}, and R_n data. R_n was estimated from solar radiation (R_s) or photosynthetically active radiation (PAR) data (Table S3.2). PAR was divided by 2.1 to estimate solar radiation (R_s) which is largely a conversion from μmol PAR m^{-2} s^{-1} to total radiation R_s W m^{-2} [*Monteith and Unsworth*, 2008]. R_n was estimated by multiplying R_s by 0.75, a typical fraction for tropical forests [*Malhi et al.*, 2002; *Fisher et al.*,

2010]. AET metrological station results (Table S3.2) were in agreement with estimates of AET for other montane cloud forests [*Bruijnzeel et al.*, 2011]. The model was applied at the catchment level, on a monthly basis for the study period. To extrapolate to the catchment scale, a linear regression was run between met station RH_{min} or T_{max} and elevation. Values for the wet season and the dry season were determined for each catchment based on mean catchment elevation and the linear regression equations. The input values were: T_{max_wet} = 15.8 °C, RH_{min_wet} = 0.790, and T_{max_dry} = 15.9 °C, RH_{min_dry} = 0.679. Solar radiation (R_s) from meteorological stations was found to be comparable to results from GL model v1.2 which models mean daily solar radiation (R_s) averaged per month [*INPE*, 2012]. The solar radiation estimated by the GL model was converted to net radiation (R_n). For the mean catchment elevation for San Pedro (2805 masl; Table 3.1), a valley-wide NDVI of 0.85 was determined using an elevation-based linear regression for NDVI [*Asner et al.*, 2014]. Carnegie Airborne Observatory (CAO) AToMS includes a visible-to-shortwave Infrared (VSWIR) imaging spectrometer [*Asner et al.*, 2012] with collection including near infrared (NIR at 800 nm) and visible (VIS at 680 nm) wavelengths that were used to generate a high resolution NDVI along the altitudinal gradient in the Kosñipata Valley [*Asner et al.*, 2014]. Soil water content in the valley is > 25 % throughout the year [*Girardin et al.*, 2013; *Huaraca Huasco et al.*, 2013].

S3.2. Results

S3.2.1. Isotopic analysis

Rainwater δD and $\delta^{18}O$ values display considerable seasonal variation whereas variation with elevation during a given season is less pronounced (Table S3.3a; Figure S3.3). Rainwater δD and $\delta^{18}O$ values are enriched during the dry season. Kosñipata rainwaters fall on a local meteoric water line (LMWL, the relationship between δD and $\delta^{18}O$ in precipitation; Figure S3.3) defined by $\delta D = 8.6561 \times \delta^{18}O + 21.119$, close to the global

meteoric water line (GMWL) of $\delta D = 8.20 \times \delta^{18}O + 11.27$ [*Craig*, 1961; *Rozanski et al.*, 1993]. Dxs, which is the deviation from the GMWL, shows minimal seasonal variation in the Kosñipata rainfall samples (Figure 3.5).

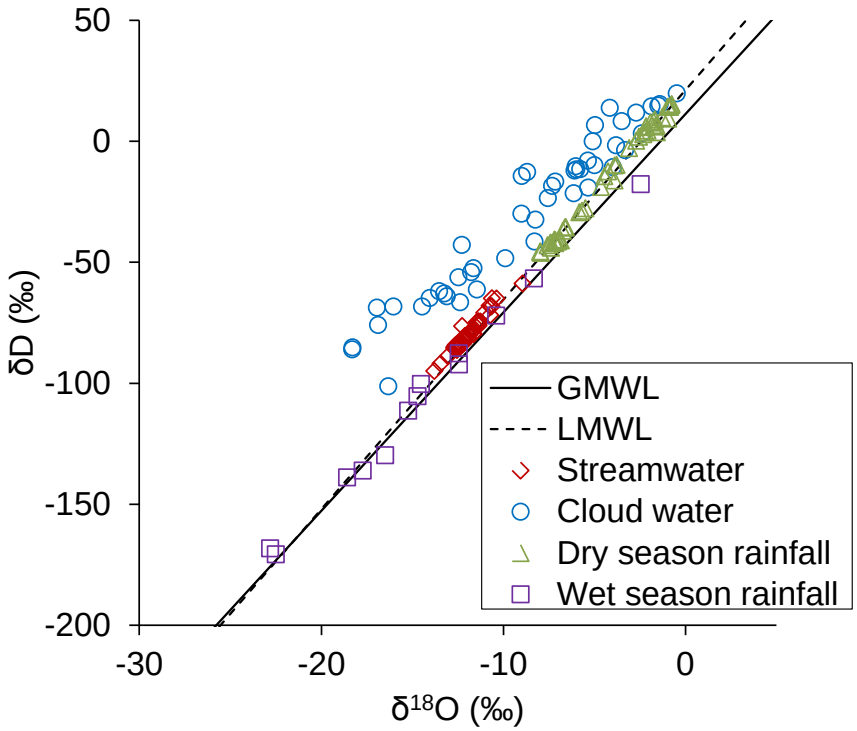


Figure S3.3: Hydrogen isotope ratio **(**δD, ‰) plotted versus oxygen isotope ratio **(**$\delta^{18}O$, ‰) of rainwater, dry season cloud water vapour (blue circles), and river water (red diamonds) from the Kosñipata Valley. Rainwater samples are from the dry season (May to August, green triangles) and from the wet season (December to March, purple squares). The global meteoric water line (GMWL, $\delta D = 8.20 \times \delta^{18}O + 11.27$) is shown as the solid line [*Craig*, 1961; *Rozanski et al.*, 1993]. The local meteoric water line (LMWL, $\delta D = 8.6561 \times \delta^{18}O + 21.119$) is shown as the dashed line.

The Kosñipata cloud water vapour has similar dD and $\delta^{18}O$ to rainwater (Figure S3.3) probably because of the orographic mechanism of cloud formation at this site [*Scholl et al.*, 2011]. Kosñipata cloud water has slightly depleted $\delta^{18}O$ and slightly enriched δD (i.e. higher Dxs, by > +20 ‰) compared to the LMWL. The deviation of cloud water from the LMWL is probably due to local water recycling [*Froehlich et al.*, 2002]. The higher and more variable Dxs of the cloud water vapour samples separates this cloud source from the rainfall samples

and is the main isotopic characteristic that allows them to be differentiated in the mixing model (Figure S3.3; Table S3.3b). Dxs has been used as a tool to evaluate water recycling in other tropical montane cloud forests [*Rhodes et al.*, 2006; *Scholl et al.*, 2007] and tropical forests such as the Amazon [*Salati et al.*, 1979; *Martinelli et al.*, 1996], and to evaluate the sources of fog [*Liu et al.*, 2007], but as far as we are aware, this is its first use as a fingerprint of cloud inputs to streamflow.

Streamwater samples fall along the LMWL defined by the rainfall samples, suggesting that evaporation most likely is not a major determinant of stream water isotopic composition (Figure S3.3). This is consistent with similar Cl concentrations in rainwater (2 – 20 μM) and streamflow (2 – 12 μM) [*Torres et al.*, in prep.]. Stream water isotopes in the Kosñipata River are consistent with other samples measured from the Amazon and Andes [*Lambs et al.*, 2007; *Lambs et al.*, 2012], i.e. they are similar to values previously measured from high Andean sites that are relatively depleted compared to the lowland Amazon due to Rayleigh distillation during orographic rain-out [*Gat*, 1996].

S3.3. Tables for supplementary information

Table S3.4: Catchment-wide annual rainfall estimates (mm yr^{-1})

Rank	Year	Wayqecha Catchment	San Pedro Catchment
1	2001	2589	3185
2	2010	2567	3161
3	2011	2547	3139
4	2002	2490	3078
5	2003	2332	2908
6	2009	2294	2865
7	2006	2210	2776
8	2012	2199	2764
9	2008	2184	2748
10	1999	2145	2705
11	2007	2126	2684
12	1998	2033	2590
13	2000	2033	2585
14	2004	2029	2580
15	2005	1861	2399
Mean	1998-2012	2243 ± 115	2811 ± 124

S3.4. References for supplementary information

ACCA (2012), Weather data San Pedro station, edited by Asociación para la concervación de la cuenca Amazónica, Botanical Reseach Institute of Texas, http://atrium.andesamazon.org/index.php.

Asner, G. P., Knapp, D. E., Boardman, J., Green, R. O., Kennedy-Bowdoin, T., Eastwood, M., Martin, R. E., Anderson, C., and Field, C. B. (2012), Carnegie Airborne Observatory-2: Increasing science data dimensionality via high-fidelity multi-sensor fusion, *Remote Sensing of Environment, 124*(0), 454-465, doi: http://dx.doi.org/10.1016/j.rse.2012.06.012.

Asner, G. P., Anderson, C. B., Martin, R. E., Knapp, D. E., Tupayachi, R., Sinca, F., and Malhi, Y. (2014), Landscape-scale changes in forest structure and functional traits along an Andes-to-Amazon elevation gradient, *Biogeosciences, 11*(3), 843-856, doi: http://dx.doi.org/10.5194/bg-11-843-2014.

Asner, G. P. (unpublished data).

Baud, O., Hager, W. H., and Minor, H. E. (2005), Toward nonintrusive flood discharge measurement, *Journal of Hydraulic Engineering, 131*(12), 1031-1035.

Bruijnzeel, L. A., Mulligan, M., and Scatena, F. N. (2011), Hydrometeorology of tropical montane cloud forests: emerging patterns, *Hydrological Processes, 25*(3), 465-498, doi: http://dx.doi.org/10.1002/hyp.7974.

Craig, H. (1961), Standard for Reporting Concentrations of Deuterium and Oxygen-18 in Natural Waters, *Science, 133*(3467), 1833-1834, doi: http://dx.doi.org/10.1126/science.133.3467.1833.

Fisher, J. B., Tu, K. P., and Baldocchi, D. D. (2008), Global estimates of the land–atmosphere water flux based on monthly AVHRR and ISLSCP-II data, validated at 16 FLUXNET sites, *Remote Sensing of Environment, 112*(3), 901-919, doi: http://dx.doi.org/10.1016/j.rse.2007.06.025.

Fisher, J. B., Whittaker, R. J., and Malhi, Y. (2010), ET come home: potential evapotranspiration in geographical ecology, *Global Ecology and Biogeography, 20*(1), 1-18, doi: http://dx.doi.org/10.1111/j.1466-8238.2010.00578.x.

Froehlich, K., Gibson, J. J., and Aggarwal, P. (2002), Deuterium excess in precipitation and its climatological significance, paper presented at Study of Environmental Change Using Isotope Techniques. Proc. Intern. Conf, Citeseer.

Gat, J. R. (1996), Oxygen and hydrogen isotopes in the hydrologic cycle, *Annual Review of Earth and Planetary Sciences, 24*(1), 225-262.

Girardin, C. A. J., Silva-Espejo, J. E., Doughty, C. E., Huaraca Huasco, W., Metcalfe, D. B., Durand-Baca, L., Marthews, T. R., Aragao, L. E. O. C., Farfan Rios, W., García Cabrera, K., Halladay, K., Fisher, J. B., Galiano-Cabrera, D. F., Huaraca-Quispe, L. P., Alzamora-Taype, I., Equiluz-Mora, L., Salinas-Revilla, N., Silman, M., Meir, P., and Malhi, Y. (2013), Productivity and carbon allocation in a tropical montane cloud forest of the Peruvian Andes, *Plant Ecology and Diversity, 7*(1-2), 107-123, doi: http://dx.doi.org/10/1080/17550874.2013.820222.

Gustard, A., Bullock, A., and Dixon, J. (1992), Low flow estimation in the United Kingdom*Rep.*, Institute of Hydrology, Wallingford, UK.

Horwath, A. (2011), Epiphytic bryophytes as cloud forest indicators: Stable isotopes, biomass and diversity along an altitudinal gradient in Peru, 260 pp*,* Plant Sciences, University of Cambridge, Cambridge.

Huaraca Huasco, W., Girardin, C. A. J., Doughty, C. E., Metcalfe, D. B., Baca, L. D., Silva-Espejo, J. E., Cabrera, D. G., Aragão, L. E. O., Davila, A. R., Marthews, T. R., Huaraca-Quispe, L. P., Alzamora-Taype, I., Eguiluz-Mora, L., Farfan-Rios, W., Cabrera, K. G., Halladay, K., Salinas-Revilla, N., Silman, M., Meir, P., and Malhi, Y. (2013), Seasonal production, allocation and cycling of carbon in two mid-elevation tropical montane forest plots in the Peruvian Andes, *Plant Ecology and Diversity*, *7*(1-2), doi: http://dx.doi.org/10.1080/17550874.2013.819042.

INPE (2012), Radiacion solar y terrestre, edited by Division de satelite y sistemas ambientales: Ministerio de ciencia y tecnologia Instituto national de investigacion espacial, Brazil.

Jarrett, R. D. (1984), Hydraulics of high-gradient streams, *Journal of Hydraulic Engineering*, *110*(11), 1519-1539.

Jarrett, R. D. (1990), Hydrologic and hydraulic research in mountain rivers 1, *JAWRA Journal of the American Water Resources Association*, *26*(3), 419-429.

Lambs, L., Muller, E., and Fromard, F. (2007), The Guianese paradox: How can the freshwater outflow from the Amazon increase the salinity of the Guianan shore?, *Journal of Hydrology*, *342*(1–2), 88-96, doi: http://dx.doi.org/10.1016/j.jhydrol.2007.05.022.

Lambs, L., Horwath, A., Otto, T., Julien, F., and Antoine, P. O. (2012), Isotopic values of the Amazon headwaters in Peru: comparison of the wet upper Río Madre de Dios watershed with the dry Urubamba-Apurimac river system, *Rapid Communications in Mass Spectrometry*, *26*(7), 775-784, doi: http://dx.doi.org/10.1002/rcm.6157.

Liu, W. J., Liu, W. Y., Li, P. J., Gao, L., Shen, Y. X., Wang, P. Y., Zhang, Y. P., and Li, H. M. (2007), Using stable isotopes to determine sources of fog drip in a tropical seasonal rain forest of Xishuangbanna, SW China, *Agricultural and Forest Meteorology*, *143*(1–2), 80-91.

Malhi, Y., Pegoraro, E., Nobre, A. D., Pereira, M. G. P., Grace, J., Culf, A. D., and Clement, R. (2002), Energy and water dynamics of a central Amazonian rain forest, *Journal of geophysical research*, *107*(D20), 45- 41-17, doi: http://dx.doi.org/10.1029/2001JD000623.

Martinelli, L. A., Victoria, R. L., Sternberg, L. S. L., Ribeiro, A., and Moreira, M. Z. (1996), Using stable isotopes to determine sources of evaporated water to the atmosphere in the Amazon basin, *Journal of Hydrology*, *183*(3–4), 191-204.

McMahon, J. P. (1957), DDT-treatment of rivers for eradication of Simuliidae, *Bulletin of the World Health Organization*, *16*(3), 541.

McMillan, H., Freer, J., Pappenberger, F., Krueger, T., and Clark, M. (2010), Impacts of uncertain river flow data on rainfall-runoff model calibration and discharge predictions, *Hydrological Processes*, *24*(10), 1270-1284, doi: http://dx.doi.org/10.1002/hyp.7587.

Monteith, J. L., and Unsworth, M. H. (2008), *Principles of environmental physics*, Academic Press.

Petersen-Øverleir, A. (2005), A hydraulics perspective on the power-law stage-discharge rating curve*Rep.*, 1-28 pp, Norges vassdrags - og energidirektorat, Oslo, Norway.

Phillips, D. L., and Gregg, J. W. (2001), Uncertainty in source partitioning using stable isotopes, *Oecologia*, *127*(2), 171-179, doi: http://dx.doi.org/10.1007/s004420000578.

Rapp, J. M., and Silman, M. R. (2012), Diurnal, seasonal, and altitudinal trends in microclimate across a tropical montane cloud forest, *Climate research, 55*(1), 17-32, doi: http://dx.doi.org/10.3354/cr01127.

Rhodes, A. L., Guswa, A. J., and Newell, S. E. (2006), Seasonal variation in the stable isotopic composition of precipitation in the tropical montane forests of Monteverde, Costa Rica, *Water Resources Research, 42*(11), W11402, doi: http://dx.doi.org/10.1029/2005WR004535.

Rozanski, K., Araguás-Araguás, L., and Gonfiantini, R. (1993), Isotopic Patterns in Modern Global Precipitation, in *Climate Change in Continental Isotopic Records*, edited by P. K. Swart, K. C. Lohman, J. McKenzie and S. Savin, pp. 1-36, American Geophysical Union, Washington, DC.

Salati, E., Dall'Olio, A., Matsui, E., and Gat, J. R. (1979), Recycling of water in the Amazon basin: an isotopic study, *Water resources research, 15*(5), 1250-1258, doi: http://dx.doi.org/10.1029/WR015i005p01250.

Scholl, M., Eugster, W., and Burkard, R. (2011), Understanding the role of fog in forest hydrology: stable isotopes as tools for determining input and partitioning of cloud water in montane forests, *Hydrological Processes, 25*(3), 353-366, doi: http://dx.doi.org/10.1002/hyp.7762.

Scholl, M. A., Giambelluca, T. W., Gingerich, S. B., Nullet, M. A., and Loope, L. L. (2007), Cloud water in windward and leeward mountain forests: The stable isotope signature of orographic cloud water, *Water Resources Research, 43*(12), W12411, doi: http://dx.doi.org/10.1029/2007WR006011.

SENAMHI (2012), Clima: Datos históricos Peru, edited, Servicio Nacional de Meteorologia e Hidrologia del Peru, Lima, Peru.

Smart, G. M. (1999), Turbulent velocity profiles and boundary shear in gravel bed rivers, *Journal of Hydraulic Engineering, 125*(2), 106-116.

Sukhodolov, A., Thiele, M., and Bungartz, H. (1998), Turbulence structure in a river reach with sand bed, *Water Resources Research, 34*(5), 1317-1334.

Torres, M. A., Clark, K. E., and West, A. J. (in prep.), Variation in the hydrologic influence on chemical weathering across a mountain-to-floodplain transition in the Peruvian Amazon.

Wooding, R. A. (1965), A hydraulic model for the catchment-stream problem: I. Kinematic-wave theory, *Journal of Hydrology, 3*(3), 254-267.

Linking statement: Chapter 3 to 4

The first step in assessing the role of stormflow on river suspended sediment and particulate organic carbon transport is to evaluate streamflow during storms at a high temporal resolution. This will insure an accurate measurement of the rising, peak, and falling limbs of the storm hydrograph. The previous chapter (3) presented the streamflow data at both the Wayqecha and San Pedro gauging stations over a one year period, and covered the period examined in this current chapter (4).

This chapter addresses the second research aim **to evaluate the importance of storms in river particulate organic carbon (POC) transport, and to partition between POC_{fossil} and $POC_{non\text{-}fossil}$ sources**. It addresses this aim by carrying out a field experiment to evaluate (POC) and suspended sediment at both Wayqecha and San Pedro gauging stations simultaneously every three hours over a span of two weeks in the wet season. Several storms were targeted to evaluate carbon content under changing hydrological conditions and erosional processes, and to capture conditions that drive annual sediment yield – addressed later in chapter 6.

I was the main author and wrote the paper, and also designed the structure, conducted and organised the field work with the help of research assistants, and carried out most of data analysis (except running samples for stable and radiocarbon isotope analysis). Bob Hilton, who was the main supervisor on this paper, helped to design the field experiment, provided the protocol for sediment sample preparation, gave guidance and instruction on data analysis, and was the main editor of the paper. Josh West provided direction in the experimental set-up and river collections. Darren Gröcke ran the samples for stable isotopes and elemental concentrations. Charlotte Bryant oversaw the radiocarbon analysis of the POC samples and aided in the methods section on the radiocarbon analysis. Philippa Ascough ran the samples

for radiocarbon isotopes. Arturo Robles was the main field assistant. Yadvinder Malhi and Mark New provided general guidance throughout. Josh, Charlotte, Yadvinder, and Philippa also provided comments on the manuscript before submission.

This chapter was published in 2013:

Clark, K. E., Hilton, R. G., West, A. J., Malhi, Y., Gröcke, D. R., Bryant, C. L., Ascough, P. L., Robles Caceres, A., and New, M. (2013), New views on "old" carbon in the Amazon River: Insight from the source of organic carbon eroded from the Peruvian Andes, *Geochemistry, Geophysics, Geosystems, 14*(5), 1644-1659.

Chapter 4 : New views on 'old' carbon in the Amazon River: Insight from the source of organic carbon eroded from the Peruvian Andes

K.E. Clark[1*], R. G. Hilton[2], A.J. West[3], Y. Malhi[1], D.R. Gröcke[4], C.L. Bryant[5], P.L. Ascough[6], A. Robles Caceres[7], and M. New[1]

[1] School of Geography and the Environment, University of Oxford, UK.
(*correspondence: kathryn.clark@ouce.ox.ac.uk)

[2] Department of Geography, Durham University, Durham, DH1 3LE, UK.
(r.g.hilton@durham.ac.uk)

[3]Department of Earth Sciences, University of Southern California, Los Angeles, USA.
(joshwest@usc.edu)

[4] Department of Earth Sciences, Durham University, DH1 3LE, UK
(d.r.grocke@durham.ac.uk)

[5] NERC Radiocarbon Facility, East Kilbride, Scotland, G75 OQF, UK
(c.bryant@nercrcl.gla.ac.uk).

[6] Scottish Universities Environmental Research Centre, East Kilbride, G75 0QF, Scotland, U.K (p.ascough@gla.ac.uk).

[7] Facultad de Ciencias Biológicas, Universidad Nacional de San Antonio Abad del Cusco, Cusco, Peru

Abstract

Mountain rivers play a key role in the delivery of particulate organic carbon (POC) to large river systems and the ocean. Due to the extent of its drainage area and runoff, the Amazon River is one of Earth's most important biogeochemical systems. However the source of POC eroded from the humid region of the Eastern Andes and the input of fossil POC from sedimentary rocks (POC_{fossil}) remains poorly constrained. Here we collected suspended sediments from the Kosñipata River during flood events to better characterise Andean POC, measuring the nitrogen to organic carbon ratio (N/C), stable carbon isotopes ($\delta^{13}C_{org}$) and radiocarbon ($\Delta^{14}C_{org}$). $\Delta^{14}C_{org}$ values ranged from -711 ‰ to -15 ‰ and significant linear trends between $\Delta^{14}C_{org,}$ N/C and $\delta^{13}C_{org}$ suggested that this reflects the mixing of POC_{fossil} with very young organic matter ($\Delta^{14}C_{org}$ ~ 50 ‰) from the terrestrial biosphere ($POC_{non\text{-}fossil}$). Using N/C and $\Delta^{14}C_{org}$ in an end member mixing analysis, we quantify the fraction of POC_{fossil} (to within 0.1) and find that it contributes a constant proportion of the suspended sediment mass (0.37 ± 0.03 %) and up to 80 % of total POC. In contrast, the relative contribution of $POC_{non\text{-}fossil}$ was variable, being most important during the rising limb and peak discharges of flood-events. The new data shed light on published measurements of 'old' POC (low $\Delta^{14}C_{org}$) in Andean-fed tributaries of the Amazon River, with their $\Delta^{14}C_{org}$ and $\delta^{13}C_{org}$ values consistent with variable addition of POC_{fossil}. The findings suggest a greater persistence of Andean POC in the lowland Amazon than previously recognised.

4.1. Introduction

Mountain rivers are an important component of the world's major river basins and play a crucial role in lowland river biogeochemistry and carbon cycling [*Gibbs*, 1967; *Hedges et al.*, 2000; *Galy et al.*, 2008b; *McClain and Naiman*, 2008]. High rates of physical erosion can result in the efficient transfer of particulate organic carbon (POC) by rivers [*Kao and Liu*, 1996; *Stallard*, 1998; *Hilton et al.*, 2012] which are also dominant sources of clastic sediment from the continents [*Milliman and Syvitski*, 1992]. The association of POC with mineral sediment can inhibit its degradation during transport and deposition [*Canfield*, 1994; *Hedges and Keil*, 1995]. As a result, mountain rivers can contribute importantly to the transfer of POC to large river systems [*Hedges et al.*, 1986a; *Galy and Eglinton*, 2011] and in the delivery of POC to the ocean [*Lyons et al.*, 2002]. Constraining the source of this POC is fundamental to understanding how its erosion and transfer impacts carbon cycling. Mountain rivers can transport POC eroded from the terrestrial biosphere ($POC_{non\text{-}fossil}$), recently fixed via photosynthesis from atmospheric CO_2 (e.g. *Hilton et al.* [2008b]). $POC_{non\text{-}fossil}$ transfer exports a fraction of gross primary productivity [*Malhi*, 2012] and if it escapes oxidation during transport [*Mayorga et al.*, 2005; *Cole et al.*, 2007; *Tranvik et al.*, 2009] and is buried in long-lived floodplain sediments (e.g. *Stallard* [1998]; *Aalto et al.* [2003]) or offshore (e.g. *Galy et al.* [2007b]) can be a net sink of atmospheric CO_2 [*France-Lanord and Derry*, 1997]. At the same time, physical erosion can mobilise older POC [*Galy and Eglinton*, 2011; *Pawson et al.*, 2012] which if oxidised may counter contemporary CO_2 drawdown (e.g. *Galy et al.* [2008a]; *Bouchez et al.* [2010]). In mountain rivers, fossil organic carbon from sedimentary bedrock (POC_{fossil}) can be significant [*Kao and Liu*, 1996; *Blair et al.*, 2003; *Leithold et al.*, 2006; *Hilton et al.*, 2011a], having a marked impact on the elemental and isotopic composition of particulate organic matter [*Komada et al.*, 2004; *Galy et al.*, 2007a; *Hilton et al.*, 2010]. .

The Amazon River is the world's largest fluvial system in terms of drainage area and runoff [*Meybeck and Ragu*, 1997]. It delivers 550-1500 Mt yr^{-1} of sediment to the Atlantic [*Meade et al.*, 1979; *Richey et al.*, 1986; *Dunne et al.*, 1998; *Guyot et al.*, 2005; *Martinez et al.*, 2009] and is the largest point source of POC to the oceans, at ~15 MtC yr^{-1} [*Richey et al.*, 1990; *Beusen et al.*, 2005]. The mountain headwaters in the Andes impart a strong signature on the inorganic chemistry of the particulate load [*Allegre et al.*, 1996; *Gaillardet et al.*, 1997; *Bouchez et al.*, 2011] and are thought to supply ~80-90 % of the Amazon River's sediment flux [*Gibbs*, 1967; *Meade et al.*, 1985; *Richey et al.*, 1986; *Wittmann et al.*, 2011]. In contrast, the majority of POC carried in the lowland Amazon River is thought to derive from floodplain sources [*Mayorga et al.*, 2005], which implies substantial replacement or consumption of Andean POC contributing to outgassing [*Richey et al.*, 2002].

Andean riverine POC has been sampled in the Upper Ucayali and Upper Beni rivers [*Hedges et al.*, 2000; *Mayorga et al.*, 2005; *Aufdenkampe et al.*, 2007; *Townsend-Small et al.*, 2007; *Townsend-Small et al.*, 2008], however large portions of the Andes remain un-sampled (e.g. the Madre de Dios River draining the Peruvian Andes) and the composition of Andean POC is poorly constrained in comparison to other mountain belts [*Galy et al.*, 2008b; *Hilton et al.*, 2010]. This makes it difficult to assess the fate of Andean POC during transport in the Amazon Basin. Rivers draining the Andes are known to receive significant input of clastic material from sedimentary rocks [*Allegre et al.*, 1996; *Gaillardet et al.*, 1997; *Bouchez et al.*, 2011] and it follows that POC_{fossil} should be an important component of the suspended load [*Komada et al.*, 2004; *Leithold et al.*, 2006; *Galy et al.*, 2007a; *Hilton et al.*, 2008b; 2010]. A small number of radiocarbon measurements (n = 4) from the Beni River confirm this [*Bouchez et al.*, 2010] and demonstrate that the input of POC_{fossil} and its elemental and isotopic composition in the Amazon Basin requires renewed focus.

Here, we address these knowledge gaps in headwaters of the Peruvian Andes. The study focuses on the highly productive tropical montane cloud forest of a small mountain catchment draining sedimentary bedrock representative of a wider region draining to the Ucayali and Madeira rivers, major Amazon tributaries (Figure 4.1a & 4.1b). To better constrain the compositional range of Andean POC we employed a nested catchment approach in the Kosñipata River at 2250 meters above sea level (masl) and 1360 masl and collected suspended sediments at high temporal frequency (three-hourly). This strategy was designed to capture flood events sampling at times when the composition of POC can vary widely in mountain rivers (e.g. *Hilton et al.* [2008b]; *Smith et al.*[2013]). To constrain the sources of POC we have measured a combination of element ratios (nitrogen to organic carbon ratio, N/C), stable isotopes ($\delta^{13}C_{org}$) and the radiocarbon content of POC ($\Delta^{14}C_{org}$, ‰). The approach permits a detailed investigation of POC_{fossil} input and its quantification in mountain rivers [*Kao and Liu*, 2000; *Komada et al.*, 2004; *Leithold et al.*, 2006; *Hilton et al.*, 2008b; 2010]. Following an end-member mixing analysis using N/C and $\Delta^{14}C_{org}$, the timing of $POC_{non\text{-}fossil}$ and POC_{fossil} mobilisation and the geomorphic processes responsible were assessed in the context of hydrometric measurements of suspended sediment concentration (SSC) and river stage height. Finally, the $\delta^{13}C_{org}$ and $\Delta^{14}C_{org}$ data from this Andean catchment shed new light on previous measurements of ‘old’ (^{14}C-depleted) POC downstream in the Amazon Basin [*Mayorga et al.*, 2005].

4.2. Study area

The study area is located in the Eastern Cordillera of the Central Andes (Figure 4.1a), subject to rock and surface uplift of 0.2 - 0.3 mm yr^{-1} due to the subduction of the Nasca Plate under the South American Plate [*Gregory-Wodzicki*, 2000]. Convergence has built steep topography [*Montgomery et al.*, 2001] whose juxtaposition with the South American Low

Level Jet, which carries humid winds westward over the Amazon Basin [*Marengo et al.*, 2004], drives high annual precipitation on the eastern flank of the Andes of between 1250 mm to >7000 mm [*Killeen et al.*, 2007]. The climate and tectonics combine to drive moderate denudation rates, estimated from ^{10}Be in detrital quartz, of ~0.4 mm yr^{-1} in the Central Andes [*Wittmann et al.*, 2009]. The steep slopes are prone to bedrock landslides, which contribute importantly to sediment transfer [*Blodgett and Isacks*, 2007]. In this part of the Andes, mountain rivers drain large areas of sedimentary and meta- sedimentary melanges which run parallel to the range (Figure 4.1a), known to contain POC_{fossil} [*Bouchez et al.*, 2010].

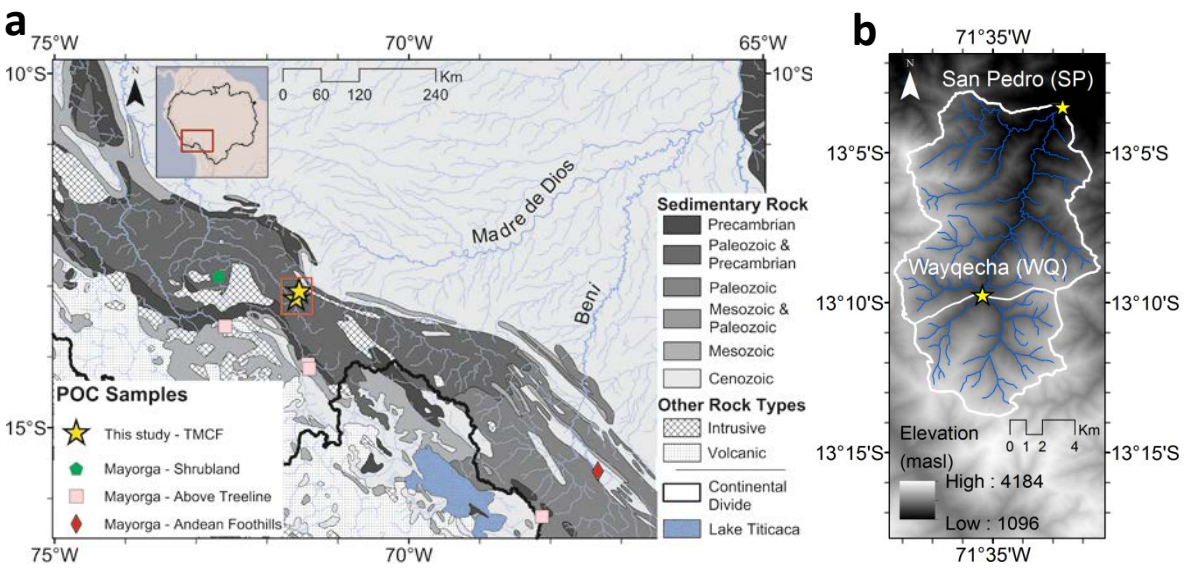


Figure 4.1: a) Geological Map of study region in Peru [*Schenk et al.*, 1999] with an inset map of the Amazon Basin with the map area indicated. The stars represent the locations of gauging stations on the Kosñipata River valley (this study) and locations of published Andean POC data are shown by other symbols [*Mayorga et al.*, 2005]. b) Kosñipata River valley, Peru with elevation (SRTM) and locations of hydrometric and sampling gauging stations.

Here we focus on the Kosñipata River in the Andes at two sites, the San Pedro catchment (gauge elevation = 1360 masl, 160 km^2) and the Wayqecha sub-basin (gauge elevation = 2250 masl, 50 km^2) (Figure 4.1b), whose bedrock geology is representative of a large Andean region (Figure 4.1a), and has not been extensively sampled by previous work [*Hedges et al.*, 2000; *Mayorga et al.*, 2005; *Aufdenkampe et al.*, 2007; *Townsend-Small et al.*, 2008]. The basins are dominantly underlain by Paleozoic (~ 450 Ma) meta-sedimentary mudstones (~80 %), with plutonic intrusions contributing ~20 % of the total San Pedro basin [*Carlotto Caillaux et al.*, 1996] (Table 4.1). Their geomorphic characteristics are typical of mountain river catchments, with the mean slope, derived from Shuttle Radar Topography Mission (SRTM) (90 x 90 m), of 28 ° in the San Pedro catchment and 26 ° in the Wayqecha sub-basin.

Table 4.1: Catchment descriptions

Gauge Station	Acronym	Latitude (°S)	Longitude (°W)	Area (km^2)	Mean Basin Elevation (masl)	Minimum Basin Elevation (masl)	Maximum Basin Elevation (masl)	Meta-Sedimentary (%)	Granite/ High Grade Mafic (%)	Mean Slope* (°)
San Pedro	SP	13°3'27"	71°32'40"	161	2805	1360	4000	79	21	28
Wayqecha	WQ	13°9'46"	71°35'21"	50	3195	2250	3910	100	0	26

* derived from SRTM (resolution 90m x 90m).

The wet climate sustains productive tropical montane cloud forest on the steep hillslopes of the San Pedro catchment [*Malhi et al.*, 2010], located in Manu National Park where logging is prohibited. The forest contains significant stores of $POC_{non\text{-}fossil}$ in biomass and soil, with total carbon stocks ranging from 114 - 151 MgC ha^{-1} [*Girardin et al.*, 2010], similar to those estimated for tropical forests worldwide [*Dixon et al.*, 1994] and representative of a wider geographical area in the Andean mountains [*Malhi et al.*, 2010]. Total carbon stocks do not vary greatly with elevation, with reduced standing biomass at high elevation offset by increased soil carbon stocks [*Gibbon et al.*, 2010; *Girardin et al.*, 2010; *Zimmermann et al.*, 2010].

4.3. Materials and methods

4.3.1. Sample collection and hydrometric measurements

At the San Pedro and Wayqecha catchment outlets, suspended sediment samples were collected in the 2010 wet season. Samples were collected at high temporal resolution (3 hourly) at both sites continuously over 2 weeks which featured several flood events. We targeted flood events: (i) because the composition of POC can vary widely on short timescales (e.g. *Hilton et al.* [2008b]; *Smith et al.* [2013]), allowing us to better constrain the composition range of Andean POC; and (ii) to ensure our samples were collected at times when water, sediment and POC transfer are thought to be volumetrically important in mountain rivers [*Hilton et al.*, 2008b; *Kao and Milliman*, 2008]. At both sample sites, large scale bed roughness, characterised as a cascade channel with turbulent flow around large boulders [*Montgomery and Buffington*, 1997] - should lead to high turbulence and mixing in the channel, meaning our samples are likely to be representative of the suspended load [*Lupker et al.*, 2011]. Collections every 3 hours were made from the surface of the turbulent flow in plastic 250 – 500 mL Nalgene™ bottles pre-rinsed with filtered river water, using a sampling pole to reach the middle of the channel. 250 mL samples were collected at peak stormflow and 500 mL samples were collected at all other sampling times. A known volume of river water was filtered through 0.7 µm glass fibre filters (Whatman GF/F, 47 mm) to recover suspended sediment. Filters were dried at ~40 °C within 1 day and stored in sterile petri-dishes.

To provide constraint on the elemental and isotopic composition of POC_{fossil}, river bed materials were collected at low flow, during the dry season in July 2009 and again at high flow during the 2010 wet season (e.g. *Galy et al.* [2007a]; [2008b]; *Hilton et al.* [2010]). Approximately 500g of sand and finer material were collected from active channel deposits.

All riverbed material (n = 7) was dried < 60 °C within one week of collection and stored in sterile sample bags until analysis.

To provide hydrodynamic context to the samples, hydrometric gauging stations were installed to monitor river stage height (m) at the San Pedro and Wayqecha catchment outlets (Figure 4.1b). At the San Pedro gauge, depth was measured 1.5 m from the river bank (total width 17 m), by a logger (WL16 Data Logger, Global Water Instrumentation, Inc), every five minutes. At the Wayqecha gauge, depth was measured with a rule from the same spot ~ 1 m from the river bank (total width 10 m) at discrete intervals upon river sample collection.

4.3.2. Geochemical analyses

Suspended sediment samples collected on the rising limb, storm peak and falling limb of two storms were selected (n = 52) for analysis from the San Pedro and Wayqecha gauging stations to evaluate the effect of storms in river POC (Figure 4.2). River suspended sediments were rinsed from the glass filter membrane using deionised water in glass beakers and the samples dried at 40°C. Pre-combusted quartz powder (with no measurable POC) was subjected to the same procedure to quantify procedural blanks. The sediment mass (mg) and known filtered volume (L) was used to calculate the suspended sediment concentration (SSC, mg L^{-1}). One large suspended sediment sample from the San Pedro outlet (04 February 2010 at 0 hr) was wet sieved into clay and silt (< 63 µm), sand (63-500 µm) and coarse sand (> 500 µm) fractions. All river bed materials (n = 7) were sieved to the 63 – 250 µm size fractions to collect a sample of lithological sources (e.g. *Galy et al.* [2008b]; *Bouchez et al.* [2010]; *Hilton et al.* [2010]). All samples were homogenised using a mortar and pestle. Inorganic carbon was removed using a 5M HCl-leach for 4 hours at 75°C to remove all detrital carbonates (including dolomite) [*Galy et al.*, 2007a; *Hilton et al.*, 2008a; 2010], thus the following analyses refer to acid-insoluble POC. The HCl-leach method has been shown to be the most robust way to return reliable organic carbon to nitrogen ratios in similar materials to

those analysed here [*Brodie et al.*, 2011]. Following deionised water rinses, samples were dried at 75 °C and decanted to clean glass vials.

An aliquot of each sediment sample (15 - 20 mg), processed following the steps outlined above, was analysed to determine their weight percent organic carbon (C_{org}, %) and nitrogen (N, %) using a Costech CHN elemental analyser (EA) by normalising to an average of standards and corrected for an internal blank and procedural blank [*Hilton et al.*, 2010; *Gröcke et al.*, 2011]. Stable isotopes of POC ($\delta^{13}C_{org}$, ‰) were determined by continuous flow from the EA coupled via CONFLO-III to a Thermo-Delta-V isotope ratio mass spectrometer in the Stable Isotope Biogeochemistry Laboratory, University of Durham. Values were normalised based on measured values of IAEA and laboratory standards, corrected for any internal blank and procedural blank and reported in $\delta^{13}C$ notation relative to VPDB. The precision (2σ) and accuracy of $\delta^{13}C_{org}$ were determined using standards measured under the same analytical conditions and were 0.1 ‰ [*Gröcke et al.*, 2011]. Replicates of suspended sediment of similar sediment matrix (n = 42) returned an average 2σ of ± 0.2 ‰ and we take this as the average precision of the analyses.

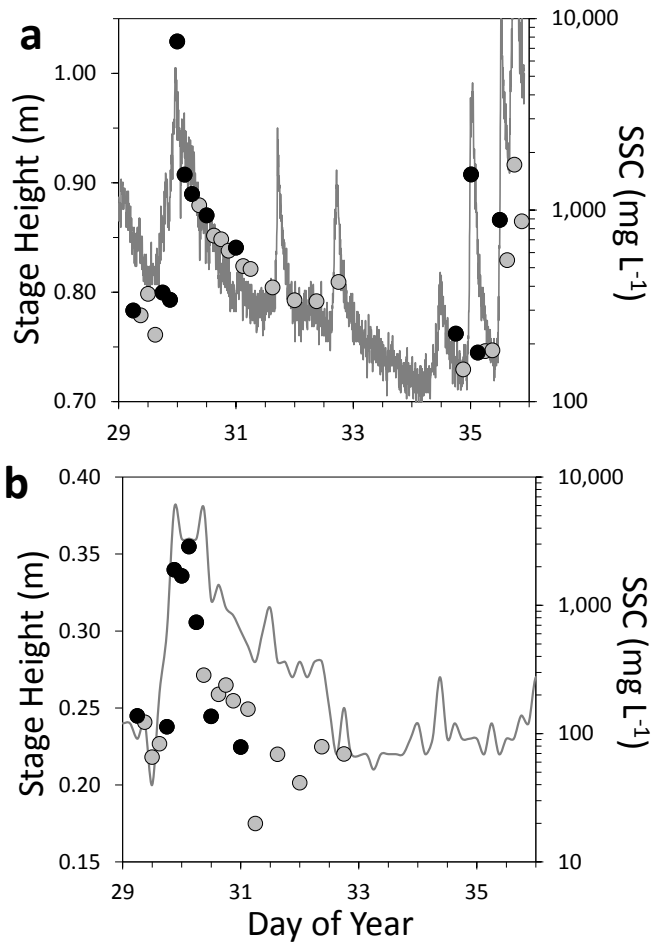


Figure 4.2: River stage height (grey line, m) over the study period for a) San Pedro (161 km^2 watershed area), and b) Wayqecha (50 km^2 watershed area) gauging stations (Figure 4.1b). Samples for geochemical analysis shown as circles with suspended sediment concentration (SSC, mg L^{-1}), where dark fill indicates the sample was also analysed for ^{14}C content.

A set of suspended sediment samples (n = 21) were prepared to graphite at the NERC Radiocarbon Facility, following inorganic carbon removal by acidification described previously, quantitative recovery of carbon in sealed quartz tubes followed by cryogenic separation of CO_2 [*Boutton et al.*, 1983]. Between 1-2 mgC was combusted for each sample and standard and CO_2 was converted to an iron/graphite mix by iron/zinc reduction [*Slota et al.*, 1987] for ^{14}C measurement by AMS in the +1 charge state at 245 keV. The ^{14}C enrichment of POC in each sample was calculated as $\Delta^{14}C_{org}$ as the relative difference between absolute international standard (relative to the year of measurement, 2011) and

sample activity corrected for age and corrected to –25 ‰ $\delta^{13}C_{VPDB}$ based on measured $\delta^{13}C_{org}$ [*Stuiver and Polach*, 1977]. The Fraction Modern (F_{mod}) is also reported where $F_{mod} = (\Delta^{14}C_{org} + 1000)/992.648$ based on the correction factor for measurement in 2011. Overall average analytical precision at 2σ was $\Delta^{14}C = 3.20 \pm 0.55$ ‰. Process standards (96H humin) and background materials (bituminous coal) were taken through all stages of sample preparation and ^{14}C analysis and were within 2σ uncertainty of expected values. The procedural quartz powder blank for the filtration stage contributed $2x10^{-4}$ mgC, which is 0.01 % of the CO_2 used for each ^{14}C analysis, meaning that contamination from GF/F filters was negligible within the uncertainty on the analysis. The inorganic carbon removal procedure did not alter the C_{org}, $\delta^{13}C$ or $\Delta^{14}C_{org}$ of standards subject to the procedure [*Hilton et al.*, 2008b].

4.4. Results

4.4.1. Suspended load and river stage height

At the San Pedro gauging station, the mean suspended sediment concentration (SSC, mg L^{-1}) ranged from 147 mg L^{-1} to 7,594 mg L^{-1}, with a mean SSC= 835 ± 476 mg L^{-1} (n = 31, ± 2 x standard error on the mean, given throughout the manuscript unless otherwise stated) (Figure 4.2a). At the Wayqecha gauging station, the mean SSC was 441 ± 330 mg L^{-1} (n = 21) and ranged from 20 mg L^{-1} to 2,869 mg L^{-1} (Figure 4.2b). SSC was generally positively correlated with stage height, a surrogate for water discharge, in both catchments. The range of SSC values and this correlation were similar to other mountain rivers worldwide [*Milliman and Syvitski*, 1992]. *Townsend-Small et al.* [2008] captured storm events with SSC < 1,800 mg L^{-1} at Chorobama River at Oxapampa, Peru and thus the new dataset represent the highest turbidity samples analysed for POC from Andean headwaters.

Over the study period stage height at the San Pedro gauge (Figure 4.2a) ranged from 0.63 m to 1.18 m, with a mean of 0.80 ± 0.003 m (n = 4405). At the Wayqecha gauge (Figure

4.2b), stage height ranged from 0.19 to 0.38 m, with a mean of 0.25 ± 0.01 m (n = 111). These values can be compared to measurements taken over an entire year at San Pedro (from November 2009 to January 2011) to examine the relative magnitude of events captured during the sampling campaign. The annual mean stage height at San Pedro was 0.50 ± 0.003 m (n = 36117), with a range from 0.08 m to 2.71 m. Exceedance probability was determined from the mean river height for the San Pedro station at 6hr intervals (n = 761) over the year record. Samples for POC were collected over a large range of flows (Figure 4.3a) and include two large events with an exceedance probability of 5.1 % and 2.2 %. The sampling period here (Figure 4.2a) therefore captured times of high turbidity (Figure 4.3b) and high stage height (Figure 4.3a) which reflect periods when most of the suspended load mass transfer is likely to occur in mountain catchments [*Hilton et al.*, 2008b; *Kao and Milliman*, 2008]. While our samples cover a representative range of flow conditions (Figure 4.3), in the absence of water discharge we have not averaged geochemical measurements by flux. Instead, we focus on discussions of the range in compositional variability as a means to better characterise Andean POC.

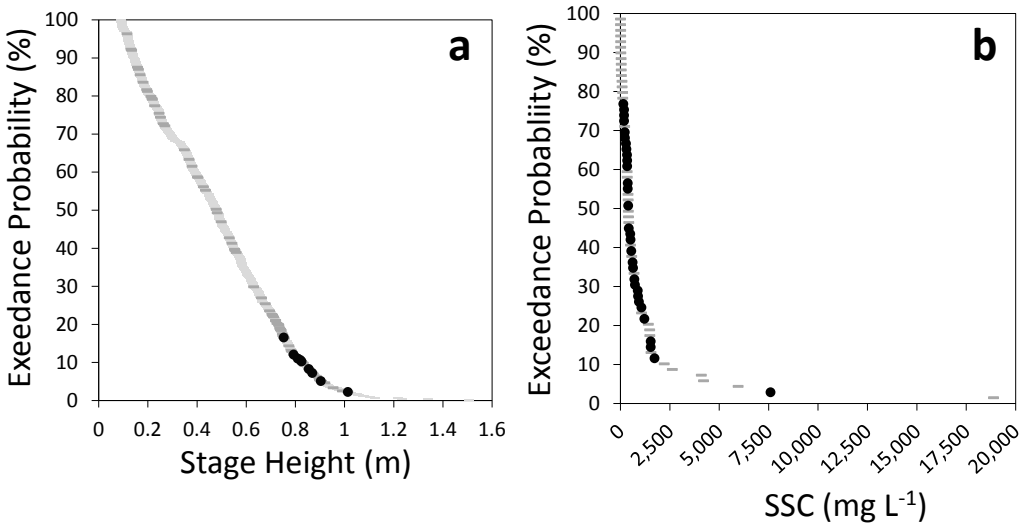


Figure 4.3: Exceedance probability (%) for hydrometric measurements from the Kosñipata River. a) Mean river height (6 hr) over the longer-term study period as light grey dashes, with suspended sediment samples from the yearlong study as dark grey dashes, and with suspended sediment samples from this study as black circles. b) Suspended sediment concentration (mg L^{-1}) of samples collected over the yearlong study as grey dashes and samples from this study as black circles.

4.4.2. Elemental geochemistry

The mean C_{org} of suspended load samples from the Kosñipata Valley over the sampling period was 0.92 ± 0.24 % (n = 54), with a slightly higher mean at San Pedro (0.96 ± 0.39 %, n = 33) than Wayqecha (0.86 ± 0.10 %, n = 21) (Table 4.2). The C_{org} were at the lower end of the range reported from other Andean sourced catchments [*Aufdenkampe et al.*, 2007; *Townsend-Small et al.*, 2008] but slightly higher than measured POC in the Beni River of between 0.47 % and 0.61 % [*Bouchez et al.*, 2010]. River bed materials had a lower mean C_{org} = 0.36 ± 0.03 % (n = 7) which was similar to the POC_{fossil} content of Andean rocks of 0.3 ± 0.1 % inferred from measurements on the Beni River [*Bouchez et al.*, 2010], thus consistent with river bed material dominated byPOC_{fossil} [*Hilton et al.*, 2010].

Table 4.2: Suspended sediment river samples

Site	Storm	Date (ddmmyyhh)	$\delta^{13}C$ (‰)[d]	C_{org} (%)	N/C	N (%)	SS (mg L^{-1})	POC (mg L^{-1})	SUERC #	$\Delta^{14}C_{org}$ (‰)[e]
SP	1	29011006	-26.3	0.86	0.17	0.14	299	2.57	34128	-492
SP	1	29011009	-24.7	0.50	0.20	0.10	282	1.42		
SP	1	29011012	-24.8	0.55	0.22	0.12	365	2.00		
SP	1	29011015	-25.7	0.70	0.19	0.13	223	1.56		
SP	1	29011018	-24.6	0.64	0.21	0.14	371	2.39	34131	-620
SP	1	29011021	-25.9	0.80	0.18	0.14	340	2.71	34132	-593
SP	1	30011000	-25.6	0.86	0.17	0.15	7594	65.30	34133	-419
SP	1	30011003	-25.5	0.81	0.20	0.16	1531	12.34	34134	-507
SP	1	30011006	-25.2	0.80	0.20	0.16	1212	9.75	34135	-477
SP	1	30011009	-24.8	0.66	0.20	0.13	1058	6.99		
SP	1	30011012	-24.5	0.57	0.25	0.14	938	5.38	34136	-712
SP	1	30011015	-24.5	0.62	0.24	0.14	736	4.53		
SP	1	30011018	-24.5	0.63	0.24	0.15	704	4.44		
SP	1	30011021	-24.5	0.59	0.23	0.14	613	3.62		
SP	1	31011000	-24.6	0.59	0.24	0.14	636	3.77	34137	-704
SP	1	31011003	-24.6	0.64	0.20	0.13	509	3.27		
SP	1	31011006	-24.9	0.71	0.19	0.13	493	3.49		
SP	1	31011015	-24.6	0.62	0.25	0.15	394	2.44		
SP	1	01021000	-25.1	0.63	0.19	0.12	338	2.12		
SP	1	01021009	-24.7	0.57	0.22	0.13	334	1.90		
SP	1	01021018	-24.9	0.64	0.21	0.13	421	2.72		
WQ	1	29011006	-25.9	0.74	0.17	0.13	137	1.02	34443	-459
WQ	1	29011009	-26.5	0.79	0.16	0.13	123	0.97		
WQ	1	29011012	-26.7	1.13	0.15	0.17	66	0.74		
WQ	1	29011015	-26.1	0.84	0.16	0.13	83	0.70		
WQ	1	29011018	-27.0	1.18	0.13	0.15	113	1.33	34444	-340
WQ	1	29011021	-26.2	1.03	0.19	0.19	1891	19.57	34144	-216
WQ	1	30011000	-26.1	1.30	0.15	0.20	1696	22.05	34145	-196
WQ	1	30011003	-26.1	0.76	0.19	0.14	2869	21.87	34146	-291
WQ	1	30011006	-25.6	0.62	0.21	0.13	737	4.56	34147	-404
WQ	1	30011009	-25.6	0.59	0.20	0.12	286	1.69		
WQ	1	30011012	-26.7	0.85	0.18	0.15	136	1.15	34445	-350
WQ	1	30011015	-25.6	0.65	0.18	0.12	202	1.33		
WQ	1	30011018	-25.2	0.59	0.20	0.12	239	1.40		
WQ	1	30011021	-25.7	0.68	0.18	0.12	180	1.22		
WQ	1	31011000	-26.2	0.94	0.15	0.14	78	0.73	34446	-334
WQ	1	31011003	-25.5	0.59	0.18	0.11	155	0.91		
WQ	1	31011006	-25.6	0.61	0.20	0.12	20	0.12		
WQ	1	31011015	-26.1	0.95	0.18	0.17	69	0.65		
WQ	1	01021000	-26.6	1.28	0.13	0.17	41	0.53		
WQ	1	01021009	-25.8	0.80	0.19	0.15	79	0.63		
WQ	1	01021018	-20.9	1.08	0.20	0.22	69	0.75		
SP	2	03021018	-25.1	0.67	0.20	0.13	226	1.52	34138	-423
SP	2	03021021	-25.3	0.63	0.18	0.11	147	0.93		
SP	2	04021000[a]	-30.3	6.83	0.03	0.20	105	7.14	34141	-15
SP	2	04021000[b]	-29.6	2.65	0.06	0.15	836	22.18	35755	-30
SP	2	04021000[c]	-29.0	1.35	0.07	0.09	592	7.98		
SP	2	04021003	-26.3	1.09	0.15	0.16	180	1.96	34442	-127
SP	2	04021006	-25.7	0.67	0.18	0.12	184	1.23		
SP	2	04021009	-26.8	0.69	0.17	0.12	185	1.28		
SP	2	04021012	-24.9	0.52	0.22	0.12	889	4.60	34143	-694
SP		04021005	-26.6	1.07	0.13	0.14	547	5.85		
SP		04021018	-25.9	0.70	0.17	0.12	1724	12.00		
SP		04021021	-25.3	0.74	0.18	0.13	873	6.46		

[a] > 500 µm, [b] 63 – 500 µm, [c] < 63 µm

[d] samples independently combusted using an elemental analyser [*Gröcke et al.*, 2011].

[e] A mathematical adjustment to account for ongoing radioactive decay of the international reference standard (oxalic acid) since AD 1950' and $\Delta^{14}C=(A_{SN}/A_{ABS}\ -1)1000‰$ (as in *Stuiver & Polach* [1977]).

C_{org} displayed a positive relationship with N (C_{org} = 6.5±0.8 × N – 0.15±0.12, n = 51, r^2 = 0.6, P < 0.0001) and the negative intercept within error of zero suggests the majority of N in the samples is associated with POC, meaning the nitrogen to organic carbon ratio (N/C) can record organic matter source (e.g. *Goñi et al.* [2008]; *Hilton et al.* [2010]). The mean N/C of the suspended load samples was 0.18 ± 0.01 (n = 54) and ranged from 0.03 to 0.25, with the same mean at San Pedro (0.18 ± 0.02, n = 33) as at Wayqecha (0.17 ± 0.01, n = 21). These values were lower than the mean of river bed materials, N/C = 0.29 ± 0.03 (n = 7), but higher than N/C measured in soil (O_H and A layers) and vegetation in the valley, with N/C values of 0.06 ± 0.01 (n = 4) and 0.05 ± 0.01 (n = 66), respectively [*Zimmermann et al.*, 2009; *Rao*, 2011].

4.4.3. Isotope geochemistry

The mean $\delta^{13}C_{org}$ of suspended POC in the Kosñipata River was -25.7 ± 0.4 ‰ (n = 54) and ranged ~9 ‰ from -20.9 ‰ to -30.3 ‰. Mean $\delta^{13}C_{org}$ values were similar at San Pedro and Wayqecha, of -25.6 ± 0.5 ‰ (n = 33) and -25.8 ± 0.5 ‰ (n = 21) respectively. The $\delta^{13}C_{org}$ values were consistent with riverine POC measured elsewhere in the Andes [*Hedges et al.*, 2000; *Mayorga et al.*, 2005; *Townsend-Small et al.*, 2005; *Aufdenkampe et al.*, 2007; *Townsend-Small et al.*, 2008], but were more enriched than those expected of C3 vegetation in mountain forests [*Körner et al.*, 1988]. Published values from tropical montane cloud forests in the Andes have C3 vegetation with $\delta^{13}C_{org}$ between -31.1 ‰ and -28.2 ‰, [*Hietz et al.*, 2002; *Townsend-Small et al.*, 2005], consistent with measurements from the Kosñipata Valley [*Rao*, 2011]. Soil profiles in the valley had more enriched $\delta^{13}C_{org}$ values compared to C3 vegetation but were still less enriched than the majority of riverine POC, with the O_H layer with a mean of -28.1 ± 2.0 ‰ (n = 2) and A layers with a mean of -26.5 ± 1.4 ‰ (n = 2) [*Zimmermann et al.*, 2009]. In contrast, the river bed materials had a more enriched $\delta^{13}C_{org}$ than the suspended load, surface vegetation and soil, with a mean -23.2 ± 0.2 ‰ (n = 7),

similar to that measured in meta-sedimentary bedrocks elsewhere [*Galy et al.*, 2008b; *Hilton et al.*, 2010].

The mean $\Delta^{14}C_{org}$ of the selected samples was -400 ± 90 ‰ (n =21) and ranged from -712 to -15 ‰ over the sampling period (Table 4.2). The mean $\Delta^{14}C_{org}$ at San Pedro was lower (-447 ± 136 ‰, n = 13) than at Wayqecha (-324 ± 63 ‰, n = 8). These values were generally lower than those measured at low SSC from other Andean catchments [*Mayorga et al.*, 2005; *Aufdenkampe et al.*, 2007; *Townsend-Small et al.*, 2007] but consistent with the range reported in the Beni River at Rurrenabaque during high flow, from -449 to -590 ‰ [*Bouchez et al.*, 2010]. The low $\Delta^{14}C_{org}$ values of POC mirror those from mountain rivers elsewhere which erode radiocarbon-dead ($\Delta^{14}C_{org}$ = -1000 ‰) POC_{fossil} from sedimentary bedrock [*Kao and Liu*, 1996; *Komada et al.*, 2004; *Leithold et al.*, 2006; *Hilton et al.*, 2008b].

4.4.4 Evidence for Mixing of POC Sources

The $\delta^{13}C_{org}$ values of the suspended load were positively correlated with the N/C ratio (r^2 = 0.73, P < 0.0001, n = 54; Figure 4.4a). A linear relationship between the stable carbon isotopic composition and the inverse of C_{org} concentration can be produced by biogeochemical processing which fractionates $\delta^{13}C_{org}$ while C_{org} varies, or it can result from a binary mixture of two end members with distinct compositions. The latter is common in river systems with rapid throughput of particulate materials (e.g. *Hilton et al.* [2008a]; [2010]), and the former mainly observed within soil profiles (e.g. *Baisden et al.* [2002]; *Zimmermann et al.* [2009]). The linear trend intercepted the measured $\delta^{13}C_{org}$ and N/C values of river bed materials, and trended toward those of C3 vegetation and soils at low N/C (Figure 4.4a), suggesting that a mixing process is setting the compositional range of the variables.

These trends were mirrored by a negative correlation between $\delta^{13}C_{org}$ and $\Delta^{14}C_{org}$ in the suspended load (r^2 = 0.67, P < 0.0001, n = 21; Figure 4.4b). A linear correlation between isotopic measurements of the same element can be indicative of mixing, and the trend ($\delta^{13}C_{org}$ = -0.006±0.001× $\Delta^{14}C_{org}$ – 28.5±0.4) intercepts the measured $\delta^{13}C_{org}$ of river bed materials at $\Delta^{14}C_{org}$ = -1000 ‰, and the $\delta^{13}C_{org}$ values of plant and soils in the valley at high $\Delta^{14}C_{org}$. Both correlations (Figure 4.4) suggest that mixing between POC_{fossil} (represented by river bed materials) and $POC_{non\text{-}fossil}$ sources plays the dominant role in controlling the N/C, $\delta^{13}C_{org}$ and $\Delta^{14}C_{org}$ values of the suspended load, analogous to the binary mixing of POC sources observed in small mountain rivers draining sedimentary bedrock throughout the world [*Kao and Liu*, 2000; *Komada et al.*, 2004; *Leithold et al.*, 2006; *Hilton et al.*, 2008b; 2010].

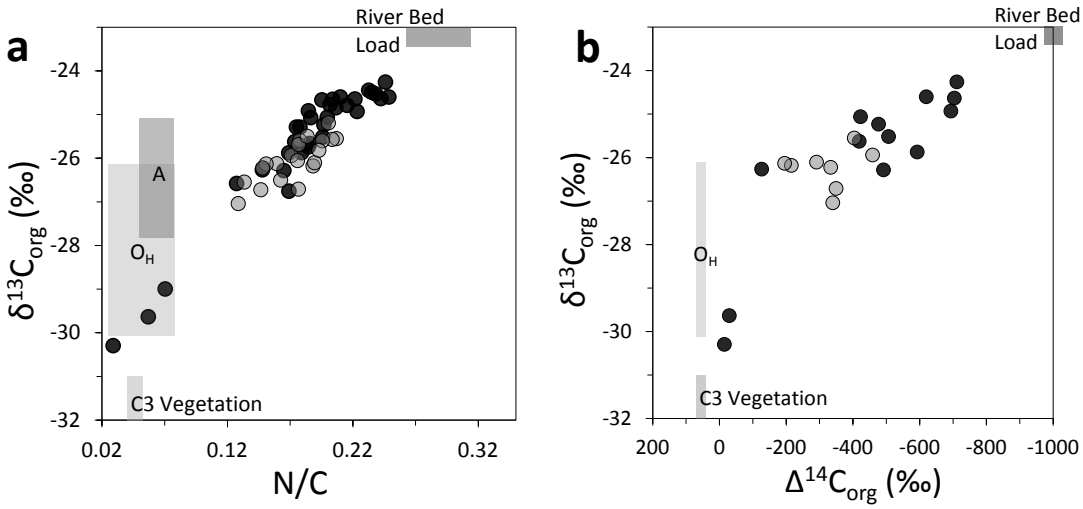


Figure 4.4: Elemental and isotopic composition of POC in suspended load (circles) from the Kosñipata River. Samples collected from San Pedro as black circles and from Wayqecha as grey circles,, with analytical uncertainties smaller than the point size. a) The stable isotopes of POC ($\delta^{13}C_{org}$, ‰) versus the nitrogen to organic ratio (N/C) , b) $\delta^{13}C_{org}$ (‰) versus the radiocarbon content ($\Delta^{14}C_{org}$, ‰). For display, river materials plotted at the radiocarbon depleted end member ($\Delta^{14}C_{org}$ = -1000 ‰ see main text for discussion). Boxes show ranges from published sources [Zimmermann et al., 2009; Rao, 2011], where O_H and A are soil horizons.

4.5. Discussion

4.5.1 Source of Andean POC

Constraining the source of POC carried by rivers is fundamental to understanding how the erosion, transfer, processing and/or deposition of POC impacts the carbon cycle and how these carbon transfers might be moderated by changing climate. The erosion and transfer of $POC_{non\text{-}fossil}$ represents an export of primary productivity [*Hilton et al.*, 2008b; 2012] which if escapes oxidation during transport [*Mayorga et al.*, 2005; *Cole et al.*, 2007; *Tranvik et al.*, 2009] and is buried in long-term sedimentary deposits, would result in a sink of atmospheric CO_2 [*Galy et al.*, 2007a]. In contrast, erosion in mountain belts underlain by sedimentary bedrock can mobilise POC_{fossil} [*Blair et al.*, 2003; *Hilton et al.*, 2011a; *Graz et al.*, 2012]. POC_{fossil} input can play an important role in setting the elemental and isotopic composition of riverine POC [*Komada et al.*, 2004; *Hilton et al.*, 2010], while its oxidation counters the CO_2 drawdown caused by $POC_{non\text{-}fossil}$ burial [*Copard et al.*, 2007; *Bouchez et al.*, 2010; *Hilton et al.*, 2011a]. Here we examine the composition of POC in this Andean river to better constrain the input of these components.

Various approaches have been used to quantify the POC_{fossil} contribution to river suspended load. Radiocarbon presents an ideal tracer if there is organic carbon input from relatively young sources (e.g. $\Delta^{14}C_{org}$ > -100 ‰) and aged soils are not prevalent [*Gomez et al.*, 2010], which is often the case in mountain catchments [*Hilton et al.*, 2008b]. Due to the 5730 year half-life of ^{14}C [*Godwin*, 1962] one can assume that the carbon derived from bedrock, termed POC_{fossil}, is indistinguishable from background (i.e. radiocarbon dead) [*Galy et al.*, 2007b; *Hilton et al.*, 2008b] and with knowledge of the $\Delta^{14}C_{org}$ content of soils and vegetation, the fraction of POC_{fossil} (F_f) and assuming that these are the predominant two carbon sources can be determined following two component mixing theory:

$$\Delta^{14}C_x = F_{nf} \times \Delta^{14}C_{nf} + F_f \times \Delta^{14}C_f \quad (1)$$

where $\Delta^{14}C_x$ is the $\Delta^{14}C_{org}$ of the measured POC sample, $\Delta^{14}C_{nf}$ and $\Delta^{14}C_f$ are the $\Delta^{14}C_{org}$ values of the $POC_{non\text{-}fossil}$ end member, and POC_{fossil} end member, respectively. The mass fraction of $POC_{non\text{-}fossil}$ and POC_{fossil} to the total POC content are F_{nf} and F_f, respectively. Thus, by definition, $F_{nf} + F_f = 1$ for a binary mixture, and so:

$$F_f = \frac{\Delta^{14}C_x - \Delta^{14}C_{nf}}{\Delta^{14}C_f - \Delta^{14}C_{nf}} \quad (2)$$

To constrain the $\Delta^{14}C_{nf}$ (Equation 2) eroded from the catchment, we can apply the technique of Galy et al., [2008a] assuming the rivers carry a well-mixed sample of POC sources (Figure 4.4) and plotting C_{org} versus the C_{org} multiplied by the fraction modern (F_{mod}) from radiocarbon (Figure 4.5). This approach is analogous to the 'standard addition' method, if we start with a sample with only POC_{fossil} (i.e. $C_{org} \times F_{mod} = 0$) adding $POC_{non\text{-}fossil}$ in increments, this will increase C_{org} and F_{mod}. If the system is mixed, the intercept of the linear trend informs us of the average C_{org} of POC_{fossil} [*Galy et al.*, 2008a; *Bouchez et al.*, 2010], while the gradient reflects the average F_{mod} of $POC_{non\text{-}fossil}$, i.e. average age of carbon sources from recently photosynthesised material [*Galy and Eglinton*, 2011]. For the samples from the first storm in the Kosñipata River, (n = 16; Figure 4.2) the linear trend (Figure 4.5) suggests an average POC_{fossil} content of 0.37 ± 0.03 %, consistent with the measured C_{org} from river bed materials (mean C_{org} = 0.36 ± 0.03 %) thought to be dominated by POC_{fossil}. The average F_{mod} of the eroded biosphere of 1.056 ± 0.015 is consistent with extrapolated atmospheric ^{14}C values around the time of sampling [*Hua and Barbetti*, 2004] and measurements from Andean soils [*Townsend-Small et al.*, 2007]. The data suggest a young age of $POC_{non\text{-}fossil}$, which is to be expected given the high rates of physical erosion and surface turnover in mountain catchments [*Hilton et al.*, 2012].

To determine the F_f (and F_{nf}) for each sample with ^{14}C analyses, we set $\Delta^{14}C_f$ = -1000 ‰ (radiocarbon dead) and $\Delta^{14}C_{nf}$ to the linear gradient of the 'standard addition' method

(Figure 4.5) of F_{mod} = 1.056 ± 0.015, equivalent to $\Delta^{14}C_{org}$ = 48 ± 15 ‰. The propagated uncertainty of the end members suggests F_f (and F_{nf}) can be quantified to within 0.02 on average using $\Delta^{14}C_{org}$. The linear trend between N/C and $\delta^{13}C_{org}$ (Figure 4.4) suggests these variables can also be used to quantify F_{nf} in the absence of $\Delta^{14}C_{org}$. This is beneficial, since it extends the assessment to the larger sample set (e.g. *Hilton et al.* [2010]). Here we use the N/C, since the N/C of $POC_{non\text{-}fossil}$ sources appears relatively constant in comparison to $\delta^{13}C_{org}$ (Figure 4.4a) [*Zimmermann et al.*, 2009; *Rao*, 2011]. Using the measured N/C of river bed materials as the POC_{fossil} composition (N/C = 0.29 ± 0.03) and the published N/C of vegetation and soil (N/C = 0.05 ± 0.02) [*Zimmermann et al.*, 2009; *Rao*, 2011], we adapt equation (2) to quantify F_{nf} using N/C ($F_{nf\text{-}N/C}$). The absolute uncertainty on $F_{nf\text{-}N/C}$ based on the end-member values ranges from 0.08 to 0.14, with an average of 0.1, which is 6-10 times lower than the range of F_{nf} values. A plot of F_{nf} from $\Delta^{14}C_{org}$ versus $F_{nf\text{-}N/C}$ has a significant linear relationship ($P < 0.0001$) with a gradient of 1.0 ± 0.1 and intercept within error of zero (-0.05 ± 0.09). Therefore, $F_{nf\text{-}N/C}$ provides a robust quantification of POC_{fossil} input.

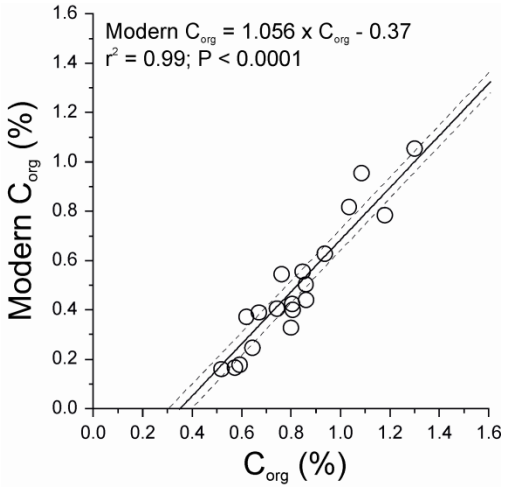


Figure 4.5: Organic carbon concentration (C_{org} %) versus modern C_{org} % (C_{org}% × Fraction Modern, F_{mod}) for San Pedro and Wayqecha river POC samples for a single hydrological event. Linear fit is the solid line and 95 % confidence intervals as dashed lines, (r^2 = 0.99, P < 0.0001, n =16). At modern C_{org} = 0 % the fossil contribution can be determined.

The results of this mixing analysis demonstrate the significant input of POC_{fossil} to the river load of these catchments, with an average F_{nf} of 0.49 ± 0.05 (n = 54), ranging between 0.17 ± 0.05 to 0.94 ± 0.09. These values indicate that up to ~80 % of the POC carried by this river throughout this period was derived from sedimentary bedrock, with a range between 6 % and 80 %. Even when F_f is low, POC_{fossil} contributes the same fraction of mass to the suspended sediment, demonstrated by the constant weight % of POC_{fossil} (0.37 ± 0.03 %) observed in the suspended load (Figure 4.5. These values of F_{nf} are within the range measured in small mountain rivers elsewhere [*Kao and Liu*, 2000; *Komada et al.*, 2004; *Hilton et al.*, 2008b; *Hilton et al.*, 2010]. However, they are the first which suggest that POC_{fossil} input to Andean headwaters is quantitatively important across a range of hydrometric conditions important for sediment export (Figure 4.3 and see chapter 6). Given the prevalence of sedimentary bedrocks in Andean catchments of this region (Figure 4.1), it is likely that POC_{fossil} input is more widespread and may impact the composition of POC in the lowland Amazon Basin (see Section 5.3).

4.5.2 Hydrologic and geomorphic controls on POC source

In the study of POC transfer in mountain rivers it has been challenging to constrain both the source of POC and the hydrological conditions under which POC is transported, with one or the other not measured (e.g. *Lyons et al.* [2002]; *Leithold et al.* [2006]; *Hilton et al.* [2008a]). Only with this combination can the processes by which POC is mobilised be better constrained [*Kao and Liu*, 2000; *Hatten et al.*, 2012; *Hilton et al.*, 2012], allowing us assess how and why POC delivery varies in space and time. Here, we benefit from high frequency sampling of river loads during the rising limb, peak and falling limb of flood events (Figure 4.2) and geochemical quantification of POC_{fossil} and $POC_{non\text{-}fossil}$ inputs (Figure 4.4).

The available data suggest that the source of POC is variable over the course of flood events in both catchments (Figure 4.6). The highest values of F_{nf} generally occur at the flood peak (Figure 4.6a), in accordance with findings from mountain rivers in Taiwan [*Hilton et al.*, 2008b; 2012]. Additional constraint comes from examining different hydrological regimes, afforded by the high temporal resolution of our sampling method (Figure 4.2 & 4.3). During rising river stage, F_{nf} is generally higher than during the falling stage (Figure 4.6b). This observation is consistent with the erosion processes known to operate in mountain catchments. In these turbid rivers, aquatic productivity is minimal and is not a dominant source of POC (Figure 4.4a). Therefore $POC_{non\text{-}fossil}$ must be mostly supplied from the steep forested hillslopes which are tightly coupled to incising river channels [*Fuller et al.*, 2003]. Erosion by overland flow [*Gomi et al.*, 2008] and in the absence of soil saturation fast lateral flow through soil horizons, can mobilise $POC_{non\text{-}fossil}$ from soil and plant debris [*Crespo et al.*, 2011].

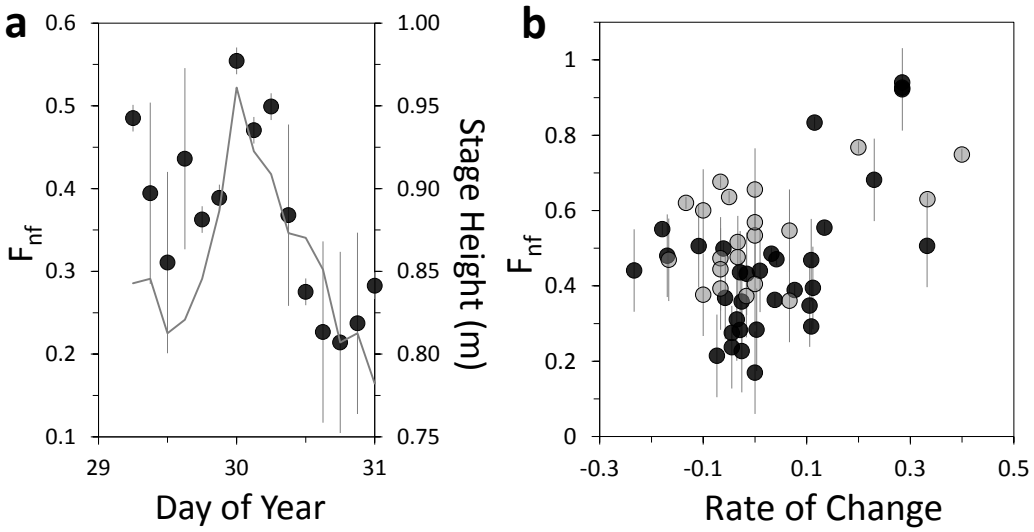


Figure 4.6: a) The fraction non-fossil POC (F_{nf}) during flood events plotted as circles, with river stage height (m) shown as grey line. The first storm sampled over the study period is shown for San Pedro and other sampled events (Figure 4.2) show a similar pattern. F_{nf} increases as stage height increases. b) F_{nf} versus rate of change of river height over the 6 hours preceding sample collection, with samples from San Pedro as black circles and Wayqecha as grey circles. Positive rate of change indicate the rising limb of flood hydrographs and negative rate of change show the falling limb. In all parts, whiskers show errors on F_{nf} values.

Another source of $POC_{non\text{-}fossil}$ during heavy rainfall is from mass wasting processes which supply soil and coarse woody debris [*Hilton et al.*, 2011b; *West et al.*, 2011] along with clastic sediment and POC_{fossil} to the river [*Hovius et al.*, 2000; *Hilton et al.*, 2011a]. Mechanical attrition of this coarse woody debris can add $POC_{non\text{-}fossil}$ (cf. [*Attal and Lavé*, 2009]). Both processes act to increase the supply of $POC_{non\text{-}fossil}$ during heavy rainfall and thus the rising limb and peak of flood events (Figure 4.6) [*Hilton et al.*, 2012].

To corroborate the inferred erosion processes responsible for $POC_{non\text{-}fossil}$ delivery to the river channel, the origin of $POC_{non\text{-}fossil}$ can be assessed using the $\delta^{13}C_{org}$ which varies between standing biomass and partially degraded soil organic matter in the valley [*Zimmermann et al.*, 2009; *Rao*, 2011]. If we project the suspended load compositions at low N/C and high $\Delta^{14}C_{org}$ (i.e. the $POC_{non\text{-}fossil}$ end member) we find that most of the samples suggest supply from the upper soil (O_H) with $\delta^{13}C_{org}$ ~-26 ‰ to -28 ‰ (Figure 4.4). We also find that plant debris can be important at the peak of floods, with the second storm having $\delta^{13}C_{org}$ values <-29.5 ‰ at low N/C and high $\Delta^{14}C_{org}$ (Figure 4.4). These observations confirm the dual role of overland flow and mass wasting processes in supplying $POC_{non\text{-}fossil}$ to mountain rivers.

The hydrological controls on POC source are superimposed upon a difference in the proportion of $POC_{non\text{-}fossil}$ and POC_{fossil} between the San Pedro and Wayqecha catchments (Figure 4.4). During the first sampled storm (Figure 4.2), mean F_{nf} was 0.49 ± 0.05 (n = 21) at San Pedro and ranged from 0.17 to 0.55. In the Wayqecha sub-catchment, F_{nf} was higher (mean = 0.54 ± 0.05, n = 21), with higher values at the extremes of the range from 0.36 to 0.77. These differences cannot be explained by an increased relative contribution of $POC_{non\text{-}fossil}$ at Wayqecha, because the carbon stock in standing biomass and soil is approximately constant with elevation in this forest [*Zimmermann et al.*, 2009; *Girardin et al.*, 2010].

Instead, they are likely to reflect an increased relative contribution from POC_{fossil} at San Pedro. POC_{fossil} can be supplied to river channels by bedrock landslides [*Hilton et al.*, 2011b], debris flows and gully erosion [*Leithold et al.*, 2006]. In the San Pedro catchment, the mean slope is higher than the upstream area at Wayqecha by 2 °. Due to the important control on mass wasting processes by slope angle [*Dietrich et al.*, 2003; *Clarke and Burbank*, 2010], one would expect a higher frequency of mass wasting events which can supply POC_{fossil} to channels across the San Pedro catchment area. This is consistent with the higher measured SSC in San Pedro (mean 835 mg L^{-1}) downstream compared to Wayqecha (mean 441 mg L^{-1}) upstream, demonstrating enhanced input of clastic material which contains POC_{fossil} in this catchment.

4.5.3. Implications for Supply of Andean POC to the Amazon River

In the major tributaries of the Amazon Basin, radiocarbon depleted POC has been observed during high flow and at high SSC [*Aufdenkampe et al.*, 2007], with a number of $\Delta^{14}C_{org}$ values <-300 ‰ [*Mayorga et al.*, 2005; *Bouchez et al.*, 2010]. This 'old' POC is not present in samples collected from lowland rivers with no direct Andean inputs, whose $\Delta^{14}C_{org}$ values are generally > 0 ‰ [*Hedges et al.*, 1986b; *Mayorga et al.*, 2005], leading to the hypothesis that the signature is derived from the Andes. However, while published measurements of Andean POC from the Upper Beni River and Upper Ucayali River show some radiocarbon depletion [*Mayorga et al.*, 2005; *Townsend-Small et al.*, 2007], the majority have $\Delta^{14}C_{org}$ values >-200 ‰ and have much higher $\delta^{13}C_{org}$ values than observed in the lowland rivers. Therefore, the reasons behind the observed ^{14}C-depletion in the Amazon Basin remain uncertain. It may derive from an aging of POC [*Mayorga et al.*, 2005], implying that old soil POC exists in the tributaries sourced from the Andes, or from the input of POC_{fossil} eroded from sedimentary rocks (e.g. *Galy el al.*[2008a]; *Hilton et al.* [2010]).

These scenarios cannot be assessed without improved constraint on the isotopic composition of Andean POC.

Existing Andean POC measurements are from samples collected toward the end of the dry season when river discharge and SSC were low. Low water stage samples may reflect compositions not prevalent during high runoff and SSC [*Hilton et al.*, 2008b; *Hatten et al.*, 2012], such as those influenced by aquatic productivity [*Townsend-Small et al.*, 2007]. In addition, some of the sampled Andean POC come from glacial catchments above the tree line draining plutonic bedrocks (Figure 4.1a) [*Mayorga et al.*, 2005] which are not representative of the humid slopes of much of the Andes where tropical forest thrives [*Gentry and Ortiz*, 1993; *Still et al.*, 1999; *Malhi et al.*, 2010] and sedimentary bedrock is widespread (Figure 4.1a). The new constraint on Andean POC composition from the Kosñipata River, whose underlying bedrock geology and productive forest are representative of a larger area (Figure 4.1a), allow us to re-examine the existing measurements of $\Delta^{14}C_{org}$ and $\delta^{13}C_{org}$ from the Amazon basin (Figure 4.4).

When the published POC data from Andean-fed tributaries of the lowland Amazon River are examined alongside the new $\Delta^{14}C_{org}$ and $\delta^{13}C_{org}$ measurements from the Andes , the vast majority describe a general linear trend which intersects the $\delta^{13}C_{org}$ of Andean river bed materials (-23.2 ± 0.2 ‰) at low $\Delta^{14}C_{org}$, and soil and vegetation values at high $\Delta^{14}C_{org}$ (Figure 4.7). In stark contrast, lowland rivers with no Andean river inputs (presumed to source POC from the floodplain) have a much higher $\Delta^{14}C_{org}$ and a larger range in $\delta^{13}C_{org}$. We therefore propose that the observed ‘old’ POC in the lowland Amazon Basin is derived from mixing of radiocarbon-dead POC_{fossil} from the Andes (similar to the Kosñipata River) with young $POC_{non\text{-}fossil}$ (Figure 4.7). Given that sedimentary rocks are prevalent in the Peruvian Andes draining to the Amazon, consisting of ~70 % of the total area (Figure 4.1a), the findings are consistent with other large basins fed by tectonically active mountain belts

where POC_{fossil} is not completely oxidised [*Galy et al.*, 2007b; 2008a]. The explanation for the paired evolution of $\delta^{13}C_{org}$ and $\Delta^{14}C_{org}$ values in the lowland Amazon challenges an interpretation that the vast majority of Andean POC is mineralised within a short distance from the Andes during transport [*Mayorga et al.*, 2005]. Instead, the mixing hypothesis described here (Figure 4.7) suggests that POC_{fossil} may contribute between ~10 % and ~50 % of the POC carried in lowland rivers of the Amazon Basin (based on $\Delta^{14}C_{org}$), but has not previously been considered as quantitatively important. In addition, the new data show that Andean $POC_{non\text{-}fossil}$ eroded from tropical montane cloud forests can have similar isotopic composition as lowland forests, with a very low $\delta^{13}C_{org}$ (~-30 ‰) and high $\Delta^{14}C_{org}$ (Figure 4.7). In light of the new data, the compositional range of the published POC data suggests less loss of Andean $POC_{non\text{-}fossil}$ than is commonly asserted [*Mayorga et al.*, 2005]. Our data thus provide impetus to further investigate the role of Andean POC in the Amazon River. Here we have focused on characterisation of POC source in turbid waters of small mountain catchments in the Kosñipata River. However, it would be beneficial to obtain further measurements from catchments draining POC_{fossil} (e.g. *Bouchez et al.* [2010]) to ascertain whether the isotopic and elemental compositions measured here are fully representative. While outside the scope of the current study, quantification of the fluxes of $POC_{non\text{-}fossil}$ and POC_{fossil} (in t km^{-2} yr^{-1}) exported from Andean catchments (e.g. *Hilton et al.* [2011a]; [2012]) would also help re-assess the net contribution of POC from the mountainous headwaters (e.g. Figure 4.7). See chapter 6 for $POC_{non\text{-}fossil}$ and POC_{fossil} fluxes from the Kosñipata River.

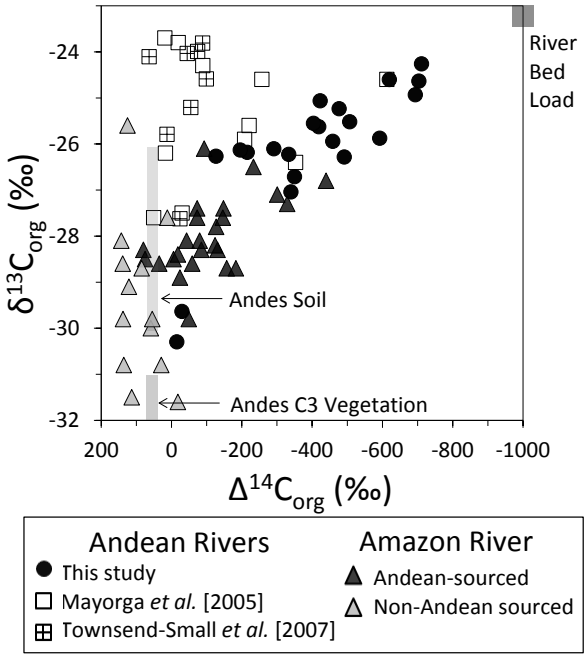


Figure 4.7: Stable isotopic composition ($\delta^{13}C_{org}$, ‰) and radiocarbon content ($\Delta^{14}C_{org}$, ‰) of POC for published data and those collected in this study. Andean headwater samples from high altitude sites collected at low turbidity from *Mayorga et al.* [2005] are shown as squares, and from *Townsend-Small et al.* [2007] are shown as squares with crosses. All other samples were collected during the wet season, with Andean samples from the Kosñipata River in this study (black circles), Andean sourced Amazon River samples (dark grey triangles), Amazon River tributaries with no Andean source (light grey triangles), with samples re-classified from *Mayorga et al.* [2005] based on their upstream contributing area.

4.6. Conclusions

We measured the elemental (N/C) and stable carbon isotopic composition ($\delta^{13}C_{org}$) and radiocarbon content ($\Delta^{14}C_{org}$) of POC in an Andean mountain river draining sedimentary bedrock representative of a larger region. The data from turbid flood events (SSC up to 7,600 mg L^{-1}) provide new insight on the composition and source of Andean POC at times when the majority of particulate materials are exported. N/C, $\delta^{13}C_{org}$ and $\Delta^{14}C_{org}$ distinguish between very young ($\Delta^{14}C_{org}$ ~50 ‰) $POC_{non\text{-}fossil}$ from the terrestrial biosphere from radiocarbon-dead POC_{fossil} from sedimentary bedrock. Using an end member mixing model, we quantify the proportion of these POC sources and we find a significant presence of POC_{fossil} in Andean river POC, contributing a constant 0.37 % to the solid suspended load mass and up to

80 % of the total POC. By examining POC source during rising, peak and falling stages of floods we show that an enrichment of $POC_{non\text{-}fossil}$ occurs during rainfall events, when erosion processes supply $POC_{non\text{-}fossil}$ to the mountain river. Finally, the new data suggest that input of Andean POC_{fossil} can explain the presence of 'old' POC (^{14}C-depleted) reported in the suspended load of the lower Amazon Basin, implying a greater persistence of Andean POC during fluvial transport than previously recognised.

4.7. Acknowledgements

Funding for radiocarbon analyses was awarded by the National Environmental Research Council (NERC) on Allocation # 1516.0910. KEC was funded by the Natural Sciences and Engineering Research Council of Canada (NSERC) and Clarendon Fund PhD scholarships. This paper is a product of the Andes Biodiversity and Ecosystems Research Group (ABERG). We thank: ACCA Peru (Wayqecha) and Incaterra (San Pedro) for field support; J.A. Gibaja Lopez, J. Huamán Ovalle, R.J. Abarca Martínez, I. Cuba Torres, A. Alfaro-Tapia, D. Oviedo Licona, and J. Farfan Flores for field assistance; J. Peterkin and F. Davies for laboratory and analytical support; Y. Rao for some plant and soil data; A. Galy, R. Aalto, S. Dadson and J. Bouchez for discussion and comments prior to submission and L. Derry, M. Evans and an anonymous referee for their constructive comments which significantly improved the manuscript.

4.8. References

Aalto, R., Maurice-Bourgoin, L., Dunne, T., Montgomery, D. R., Nittrouer, C. A., and Guyot, J. L. (2003), Episodic sediment accumulation on Amazonian flood plains influenced by El Nino/Southern Oscillation, *Nature*, *425*(6957), 493-497, doi: http://dx.doi.org/10.1038/nature02002.

Allegre, C. J., Dupre, B., Negrel, P., and Gaillardet, J. (1996), Sr-Nd-Pb isotope systematics in Amazon and Congo River systems: Constraints about erosion processes, *Chemical Geology*, *131*(1-4), 93-112, doi: http://dx.doi.org/10.1016/0009-2541(96)00028-9.

Attal, M., and Lavé, J. (2009), Pebble abrasion during fluvial transport: Experimental results and implications for the evolution of the sediment load along rivers, *Journal of Geophysical Research*, *114*(F4), F04023, doi: http://dx.doi.org/10.1029/2009jf001328.

Aufdenkampe, A. K., Mayorga, E., Hedges, J. I., Llerena, C., Quay, P. D., Gudeman, J., Krusche, A. V., and Richey, J. E. (2007), Organic matter in the Peruvian headwaters of the Amazon: Compositional evolution from the Andes to the lowland Amazon mainstem, *Organic Geochemistry*, *38*(3), 337-364, doi: http://dx.doi.org/10.1016/j.orggeochem.2006.06.003.

Baisden, W. T., Amundson, R., Cook, A. C., and Brenner, D. L. (2002), Turnover and storage of C and N in five density fractions from California annual grassland surface soils, *Global Biogeochemical Cycles*, *16*(4), 1117, doi: http://dx.doi.org/10.1029/2001GB001822.

Beusen, A. H. W., Dekkers, A. L. M., Bouwman, A. F., Ludwig, W., and Harrison, J. (2005), Estimation of global river transport of sediments and associated particulate C, N, and P, *Global Biogeochemical Cycles*, *19*(4), doi: http://dx.doi.org/10.1029/2005gb002453.

Blair, N. E., Leithold, E. L., Ford, S. T., Peeler, K. A., Holmes, J. C., and Perkey, D. W. (2003), The persistence of memory: The fate of ancient sedimentary organic carbon in a modern sedimentary system, *Geochimica et Cosmochimica Acta*, *67*(1), 63-73, doi: http://dx.doi.org/10.1016/s0016-7037(02)01043-8.

Blodgett, T. A., and Isacks, B. L. (2007), Landslide erosion rate in the eastern cordillera of northern Bolivia, *Earth Interactions*, *11*, 1-30, doi: http://dx.doi.org/10.1175/2007EI222.1.

Bouchez, J., Beyssac, O., Galy, V., Gaillardet, J., France-Lanord, C., Maurice, L., and Moreira-Turcq, P. (2010), Oxidation of petrogenic organic carbon in the Amazon floodplain as a source of atmospheric CO_2, *Geology*, *38*(3), 255-258, doi: http://dx.doi.org/10.1130/g30608.1.

Bouchez, J., Gaillardet, J., France-Lanord, C., Maurice, L., and Dutra-Maia, P. (2011), Grain size control of river suspended sediment geochemistry: Clues from Amazon River depth profiles, *Geochemistry Geophysics Geosystems*, *12*, doi: http://dx.doi.org/10.1029/2010gc003380.

Boutton, T. W., Wong, W. W., Hachey, D. L., Lee, L. S., Cabrera, M. P., and Klein, P. D. (1983), Comparison of quartz and pyrex tubes for combustion of organic samples for stable carbon isotope analysis, *Analytical Chemistry*, *55*(11), 1832-1833.

Brodie, C. R., Leng, M. J., Casford, J. S. L., Kendrick, C. P., Lloyd, J. M., Yongqiang, Z., and Bird, M. I. (2011), Evidence for bias in C and N concentrations and $\delta^{13}C$ composition of terrestrial and aquatic organic materials due to pre-analysis acid preparation methods, *Chemical Geology*, *282*(3), 67-83, doi: http://dx.doi.org/10.1016/j.chemgeo.2011.01.007.

Canfield, D. E. (1994), Factors Influencing organic-carbon preservation in marine-sediments, *Chemical Geology*, *114*(3-4), 315-329.

Carlotto Caillaux, V. S., Rodriguez, G., Fernando, W., Roque, C., Dionicio, J., and Chávez, R. (1996), Geología de los cuadrángulos de Urubamba y Calca, Instituto Geológica Nacional, Lima, Peru.

Clarke, B. A., and Burbank, D. W. (2010), Bedrock fracturing, threshold hillslopes, and limits to the magnitude of bedrock landslides, *Earth and Planetary Science Letters*, *297*(3), 577-586, doi: http://dx.doi.org/10.1016/j.epsl.2010.07.011.

Cole, J. J., Prairie, Y. T., Caraco, N. F., McDowell, W. H., Tranvik, L. J., Striegl, R. G., Duarte, C. M., Kortelainen, P., Downing, J. A., and Middelburg, J. J. (2007), Plumbing the global carbon cycle: integrating inland waters into the terrestrial carbon budget, *Ecosystems*, *10*(1), 172-185, doi: http://dx.doi.org/10.1007/s10021-006-9013-8.

Copard, Y., Amiotte-Suchet, P., and Di-Giovanni, C. (2007), Storage and release of fossil organic carbon related to weathering of sedimentary rocks, *Earth and Planetary Science Letters*, *258*(1), 345-357, doi: http://dx.doi.org/10.1016/j.epsl.2007.03.048.

Crespo, P. J., Feyen, J., Buytaert, W., Bücker, A., Breuer, L., Frede, H. G., and Ramírez, M. (2011), Identifying controls of the rainfall–runoff response of small catchments in the tropical Andes (Ecuador), *Journal of Hydrology*, *407*(1), 164-174, doi: http://dx.doi.org/10.1016/j.jhydrol.2011.07.021.

Dietrich, W. E., Bellugi, D. G., Sklar, L. S., Stock, J. D., Heimsath, A. M., and Roering, J. J. (2003), Geomorphic transport laws for predicting landscape form and dynamics, *Geophysical Monograph-American Geophysical Union*, *135*, 103-132, doi: http://dx.doi.org/10.1029/135GM09.

Dixon, R. K., Brown, S., Houghton, R., Solomon, A., Trexler, M., and Wisniewski, J. (1994), Carbon pools and flux of global forest ecosystems, *Science*, *263*(5144), 185-189.

Dunne, T., Mertes, L. A. K., Meade, R. H., Richey, J. E., and Forsberg, B. R. (1998), Exchanges of sediment between the flood plain and channel of the Amazon River in Brazil, *Geological Society of America Bulletin*, *110*(4), 450-467.

France-Lanord, C., and Derry, L. A. (1997), Organic carbon burial forcing of the carbon cycle from Himalayan erosion, *Nature*, *390*(6655), 65-67.

Fuller, C. W., Willett, S. D., Hovius, N., and Slingerland, R. (2003), Erosion rates for Taiwan mountain basins: New determinations from suspended sediment records and a stochastic model of their temporal variation, *The Journal of Geology*, *111*(1), 71-87, doi: http://dx.doi.org/10.1086/344665.

Gaillardet, J., Dupre, B., Allegre, C. J., and Negrel, P. (1997), Chemical and physical denudation in the Amazon River basin, *Chemical Geology*, *142*(3-4), 141-173.

Galy, V., Bouchez, J., and France-Lanord, C. (2007a), Determination of total organic carbon content and delta C-13 in carbonate-rich detrital sediments, *Geostandards and Geoanalytical Research*, *31*(3), 199-207, doi: http://dx.doi.org/10.1111/j.1751-908X.2007.00864.x.

Galy, V., France-Lanord, C., Beyssac, O., Faure, P., Kudrass, H., and Palhol, F. (2007b), Efficient organic carbon burial in the Bengal fan sustained by the Himalayan erosional system, *Nature*, *450*(7168), 407-U406, doi: http://dx.doi.org/10.1038/nature06273.

Galy, V., Beyssac, O., France-Lanord, C., and Eglinton, T. (2008a), Recycling of graphite during Himalayan erosion: A geological stabilization of carbon in the crust, *Science, 322*(5903), 943-945, doi: http://dx.doi.org/10.1126/science.1161408.

Galy, V., France-Lanord, C., and Lartiges, B. (2008b), Loading and fate of particulate organic carbon from the Himalaya to the Ganga-Brahmaputra delta, *Geochimica et Cosmochimica Acta, 72*(7), 1767-1787, doi: http://dx.doi.org/10.1016/j.gca.2008.01.027.

Galy, V., and Eglinton, T. (2011), Protracted storage of biospheric carbon in the Ganges-Brahmaputra basin, *Nature Geoscience, 4*(12), 843-847, doi: http://dx.doi.org/10.1038/ngeo1293.

Gentry, S., and Ortiz, S. R. (1993), Patrones de composición florística en la Amazonia Peruana, in *Amazona Peruana Vegetación humeda tropical en la llano subandino*, edited by R. Kalliola, M. Puhakka and W. Danjoy, pp. 155-166, PAUT and ONERN, Jyvaskyla, Finland.

Gibbon, A., Silman, M. R., Malhi, Y., Fisher, J. B., Meir, P., Zimmermann, M., Dargie, G. C., Farfan, W. R., and Garcia, K. C. (2010), Ecosystem carbon storage across the grassland-forest transition in the high Andes of Manu National Park, Peru, *Ecosystems, 13*(7), 1097-1111, doi: http://dx.doi.org/10.1007/s10021-010-9376-8.

Gibbs, R. J. (1967), Amazon River - Environmental factors that control its dissolved and suspended load, *Science, 156*(3783), 1734-1737.

Girardin, C. A. J., Malhi, Y., Aragao, L. E. O. C., Mamani, M., Huasco, W. H., Durand, L., Feeley, K. J., Rapp, J., Silva-Espejo, J. E., Silman, M., Salinas, N., and Whittaker, R. J. (2010), Net primary productivity allocation and cycling of carbon along a tropical forest elevational transect in the Peruvian Andes, *Global Change Biology, 16*(12), 3176-3192, doi: http://dx.doi.org/10.1111/j.1365-2486.2010.02235.x.

Godwin, H. (1962), Half-life of radiocarbon, *Nature, 195*, 984.

Gomez, B., Baisden, W. T., and Rogers, K. M. (2010), Variable composition of particle-bound organic carbon in steepland river systems, *Journal of Geophysical Research, 115*(F4), F04006, doi: http://dx.doi.org/10.1029/2010jf001713.

Gomi, T., Sidle, R. C., Ueno, M., Miyata, S., and Kosugi, K. (2008), Characteristics of overland flow generation on steep forested hillslopes of central Japan, *Journal of Hydrology, 361*(3), 275-290, doi: http://dx.doi.org/10.1029/2007WR005894.

Goñi, M. A., Monacci, N., Gisewhite, R., Crockett, J., Nittrouer, C., Ogston, A., Alin, S. R., and Aalto, R. (2008), Terrigenous organic matter in sediments from the Fly River delta-clinoform system (Papua New Guinea), *Journal of geophysical research, 113*(F1), F01S10, doi: http://dx.doi.org/10.1029/2006JF000653.

Graz, Y., Di-Giovanni, C., Copard, Y., Mathys, N., Cras, A., and Marc, V. (2012), Annual fossil organic carbon delivery due to mechanical and chemical weathering of marly badlands areas, *Earth Surface Processes and Landforms, 37*(12), 1263-1271, doi: http://dx.doi.org/10.1002/esp.3232.

Gregory-Wodzicki, K. M. (2000), Uplift history of the Central and Northern Andes: a review, *Geological Society of America Bulletin, 112*(7), 1091-1105, doi: http://dx.doi.org/10.1130/0016-7606(2000)112<1091:UHOTCA>2.0.CO;2

Gröcke, D. R., Hori, R. S., Trabucho-Alexandre, J., Kemp, D. B., and Schwark, L. (2011), An open ocean record of the Toarcian oceanic anoxic event, *Solid Earth*, *2*, 245-257, doi: http://dx.doi.org/10.5194/se-2-245-2011.

Guyot, J. L., Filizola, N., and Laraque, A. (2005), The suspended sediment flux of the River Amazon at Obidos, Brazil, 1995-2003, in *Sediment Budgets 1*, edited by D. E. Walling and A. J. Horowitz, pp. 347-354, International Association of Hydrological Sciences, Wallingford, UK.

Hatten, J. A., Goñi, M. A., and Wheatcroft, R. A. (2012), Chemical characteristics of particulate organic matter from a small, mountainous river system in the Oregon Coast Range, USA, *Biogeochemistry*, 1-24, doi: http://dx.doi.org/10.1007/s10533-010-9529-z.

Hedges, J. I., Clark, W. A., Quay, P. D., Richey, J. E., Devol, A. H., and Santos, U. d. M. (1986a), Compositions and Fluxes of Particulate Organic Material in the Amazon River, *Limnology and Oceanography*, *31*(4), 717-738.

Hedges, J. I., Ertel, J. R., Quay, P. D., Grootes, P. M., Richey, J. E., Devol, A. H., Farwell, G. W., Schmidt, F. W., and Salati, E. (1986b), Organic carbon-14 in the Amazon River system, *Science*, *231*(4742), 1129-1131.

Hedges, J. I., and Keil, R. G. (1995), Sedimentary organic-matter preservation - an assessment and speculative systhesis, *Marine Chemistry*, *49*(2-3), 81-115.

Hedges, J. I., Mayorga, E., Tsamakis, E., McClain, M. E., Aufdenkampe, A., Quay, P., Richey, J. E., Benner, R., Opsahl, S., Black, B., Pimentel, T., Quintanilla, J., and Maurice, L. (2000), Organic matter in Bolivian tributaries of the Amazon River: A comparison to the lower mainstream, *Limnology and Oceanography*, *45*(7), 1449-1466.

Hietz, P., Wanek, W., Wania, R., and Nadkarni, N. M. (2002), Nitrogen-15 natural abundance in a montane cloud forest canopy as an indicator of nitrogen cycling and epiphyte nutrition, *Oecologia*, *131*(3), 350-355, doi: http://dx.doi.org/10.1007/S00442-002-0896-6.

Hilton, R. G., Galy, A., and Hovius, N. (2008a), Riverine particulate organic carbon from an active mountain belt: Importance of landslides, *Global Biogeochemical Cycles*, *22*, BG1017, doi: http://dx.doi.org/10.1029/2006GB002905.

Hilton, R. G., Galy, A., Hovius, N., Chen, M.-C., Horng, M.-J., and Chen, H. (2008b), Tropical-cyclone-driven erosion of the terrestrial biosphere from mountains, *Nature Geoscience*, *1*(11), 759-762, doi: http://dx.doi.org/10.1038/ngeo333.

Hilton, R. G., Galy, A., Hovius, N., Horng, M.-J., and Chen, H. (2010), The isotopic composition of particulate organic carbon in mountain rivers of Taiwan, *Geochimica et Cosmochimica Acta*, *74*(11), 3164-3181, doi: http://dx.doi.org/10.1016/j.gca.2010.03.004.

Hilton, R. G., Galy, A., Hovius, N., Horng, M.-J., and Chen, H. (2011a), Efficient transport of fossil organic carbon to the ocean by steep mountain rivers: An orogenic carbon sequestration mechanism, *Geology*, *39*(1), 71-74, doi: http://dx.doi.org/10.1130/g31352.1.

Hilton, R. G., Meunier, P., Hovius, N., Bellingham, P. J., and Galy, A. (2011b), Landslide impact on organic carbon cycling in a temperate montane forest, *Earth Surface Processes and Landforms*, *36*(12), 1670-1679, doi: http://dx.doi.org/10.1002/esp.2191.

Hilton, R. G., Galy, A., Hovius, N., Kao, S.-J., Horng, M.-J., and Chen, H. (2012), Climatic and geomorphic controls on the erosion of terrestrial biomass from subtropical mountain forest,

Global Biogeochemical Cycles, *26*(3), GB3014, doi: http://dx.doi.org/10.1029/2012gb004314.

Hovius, N., Stark, C. P., Chu, H. T., and Lin, J. C. (2000), Supply and removal of sediment in a landslide-dominated mountain belt: Central Range, Taiwan, *Journal of Geology*, *108*(1), 73-89, doi: http://dx.doi.org/10.1086/314387.

Hua, Q., and Barbetti, M. (2004), Review of tropospheric bomb 14C data for carbon cycle modeling and age calibration purposes, *Radiocarbon*, *46*(3), 1273-1298.

Kao, S. J., and Liu, K.-K. (1996), Particulate organic carbon export from a subtropical mountainous river (Lanyang Hsi) in Taiwan, *Limnology and Oceanography*, *41*(8), 1749-1757.

Kao, S. J., and Liu, K. K. (2000), Stable carbon and nitrogen isotope systematics in a human-disturbed watershed (Lanyang-Hsi) in Taiwan and the estimation of biogenic particulate organic carbon and nitrogen fluxes, *Global Biogeochem. Cycles*, *14*(1), 189-198, doi: http://dx.doi.org/10.1029/1999gb900079.

Kao, S. J., and Milliman, J. D. (2008), Water and sediment discharge from small mountainous rivers, Taiwan: The roles of lithology, episodic events, and human activities, *The Journal of Geology*, *116*(5), 431-448, doi: http://dx.doi.org/10.1086/590921.

Killeen, T. J., Douglas, M., Consiglio, T., Jørgensen, P. M., and Mejia, J. (2007), Dry spots and wet spots in the Andean hotspot, *Journal of Biogeography*, *34*(8), 1357-1373, doi: http://dx.doi.org/10.1111/j.1365-2699.2006.01682.x.

Komada, T., Druffel, E. R. M., and Trumbore, S. E. (2004), Oceanic export of relict carbon by small mountainous rivers, *Geophysical Research Letters*, *31*(7), L07504, doi: http://dx.doi.org/10.1029/2004gl019512.

Körner, C., Farquhar, G., and Roksandic, Z. (1988), A global survey of carbon isotope discrimination in plants from high altitude, *Oecologia*, *74*(4), 623-632.

Leithold, E. L., Blair, N. E., and Perkey, D. W. (2006), Geomorphologic controls on the age of particulate organic carbon from small mountainous and upland rivers, *Global Biogeochemical Cycles*, *20*(3), doi: http://dx.doi.org/10.1029/2005gb002677.

Lupker, M., France-Lanord, C., Lavé, J., Bouchez, J., Galy, V., Métivier, F., Gaillardet, J., Lartiges, B., and Mugnier, J.-L. (2011), A Rouse-based method to integrate the chemical composition of river sediments: Application to the Ganga basin, *Journal of Geophysical Research*, *116*(F4), F04012, doi: http://dx.doi.org/10.1029/2010jf001947.

Lyons, W. B., Nezat, C. A., Carey, A. E., and Hicks, D. M. (2002), Organic carbon fluxes to the ocean from high-standing islands, *Geology*, *30*(5), 443-446, doi: http://dx.doi.org/10.1130/0091-7613(2002)030<0443:ocftto>2.0.co;2.

Malhi, Y., Silman, M., Salinas, N., Bush, M., Meir, P., and Saatchi, S. (2010), Introduction: Elevation gradients in the tropics: laboratories for ecosystem ecology and global change research, *Global Change Biology*, *16*(12), 3171-3175, doi: http://dx.doi.org/10.1111/j.1365-2486.2010.02323.x.

Malhi, Y. (2012), The productivity, metabolism and carbon cycle of tropical forest vegetation, *Journal of Ecology*, *100*(1), 65-75, doi: http://dx.doi.org/10.1111/j.1365-2745.2011.01916.x.

Marengo, J. A., Soares, W. R., Saulo, C., and Nicolini, M. (2004), Climatology of the low-level jet east of the Andes as derived from the NCEP-NCAR reanalyses: Characteristics and temporal variability, *Journal of climate*, *17*(12), 2261-2280.

Martinez, J. M., Guyot, J. L., Filizola, N., and Sondag, F. (2009), Increase in suspended sediment discharge of the Amazon River assessed by monitoring network and satellite data, *Catena*, *79*(3), 257-264, doi: http://dx.doi.org/10.1016/j.catena.2009.05.011.

Mayorga, E., Aufdenkampe, A. K., Masiello, C. A., Krusche, A. V., Hedges, J. I., Quay, P. D., Richey, J. E., and Brown, T. A. (2005), Young organic matter as a source of carbon dioxide outgassing from Amazonian rivers, *Nature*, *436*(7050), 538-541, doi: http://dx.doi.org/10.1038/nature03880.

McClain, M. E., and Naiman, R. J. (2008), Andean influences on the biogeochemistry and ecology of the Amazon River, *Bioscience*, *58*(4), 325-338, doi: http://dx.doi.org/10.1641/b580408.

Meade, R. H., Nordin, C. F., Curtis, W. F., Costarodrigues, F. M., Dovale, C. M., and Edmond, J. M. (1979), Sediment loads in the Amazon River, *Nature*, *278*(5700), 161-163.

Meade, R. H., Dunne, T., Richey, J. E., Santos, U. D., and Salati, E. (1985), Storage and remobilisation of suspended sediment in the lower Amazon River of Brazil, *Science*, *228*(4698), 488-490.

Meybeck, M., and Ragu, A. (1997), River discharges to the oceans: An assessment of suspended solids, major ions and nutrients *Rep.*, 245 pp, United Nations Environmental Programme, World Health Organization, Nairobi, Kenya.

Milliman, J. D., and Syvitski, J. P. M. (1992), Geomorphic tectonic control of sediment discharge to the ocean - the importance of small mountain rivers, *Journal of Geology*, *100*(5), 525-544.

Montgomery, D. R., and Buffington, J. M. (1997), Channel-reach morphology in mountain drainage basins, *Geological Society of America Bulletin*, *109*(5), 596-611, doi: http://dx.doi.org/10.1130/0016-7606(1997)109<0596:CRMIMD>2.3.CO;2.

Montgomery, D. R., Balco, G., and Willett, S. D. (2001), Climate, tectonics, and the morphology of the Andes, *Geology*, *29*(7), 579-582, doi: http://dx.doi.org/10.1130/0091-7613(2001)029<0579:CTATMO>2.0.CO;2.

Pawson, R. R., Evans, M. G., and Allott, T. E. H. A. (2012), Fluvial carbon flux from headwater peatland streams: significance of particulate carbon flux, *Earth Surface Processes and Landforms*, doi: http://dx.doi.org/10.10002/esp.3257.

Rao, Y. (2011), Variation in plant carbon and nitrogen isotopes along an altitudinal gradient in the Peruvian Andes, B.Sc. thesis, 60 pp, Department of Earth Sciences, Durham University, Durham.

Richey, J. E., Meade, R. H., Salati, E., Devol, A. H., Nordin, C. F., and Dossantos, U. (1986), Water discharge and suspended sediment concentrations in the Amazon River 1982-1984, *Water Resources Research*, *22*(5), 756-764.

Richey, J. E., Valarezo, C., Valarezo, C., and Valarezo, C. (1990), Biogeochemistry of carbon in the Amazon River, *Limnology and Oceanography*, *35*, 352-371.

Richey, J. E., Melack, J. M., Aufdenkampe, A. K., Ballester, V. M., and Hess, L. L. (2002), Outgassing from Amazonian rivers and wetlands as a large tropical source of atmospheric CO_2, *Nature, 416*(617-620), doi: http://dx.doi.org/10.1038/416617a.

Schenk, C. J., Viger, R. J., and Anderson, C. P. (1999), South America Geologic Map (geo6ag), U.S. Geological Survey, Centrel Energy Resources Team, Denver, Colorado, USA.

Slota, P. J., Jull, A. J. T., Linick, T. W., and Toolin, L. J. (1987), Preparation of small samples for ^{14}C accelerator targets by catalytic reduction of CO, *Radiocarbon, 29*, 303-306.

Smith, J. C., Galy, A., Hovius, N., Tye, A. M., Turowski, J. M., and Schleppi, P. (2013), Runoff-driven export of particulate organic carbon from soil in temperate forested uplands, *Earth and Planetary Science Letters, 365*, 198-208, doi: http://dx.doi.org/10.1016/j.epsl.2013.01.027.

Stallard, R. F. (1998), Terrestrial sedimentation and the carbon cycle: Coupling weathering and erosion to carbon burial, *Global Biogeochemical Cycles*, *12*(2), 231-257.

Still, C. J., Foster, P. N., and Schneider, S. H. (1999), Simulating the effects of climate change on tropical montane cloud forests, *Nature, 398*(6728), 608-610, doi: http://dx.doi.org/10.1038/19293.

Stuiver, M., and Polach, H. A. (1977), Discussion: Reporting of ^{14}C data, *Radiocarbon*, *19*(3), 355-363.

Townsend-Small, A., McClain, M. E., and Brandes, J. A. (2005), Contributions of carbon and nitrogen from the Andes Mountains to the Amazon River: Evidence from an elevational gradient of soils, plants, and river material, *Limnology and Oceanography*, *50*(2), 672-685.

Townsend-Small, A., Noguera, J. L., McClain, M. E., and Brandes, J. A. (2007), Radiocarbon and stable isotope geochemistry of organic matter in the Amazon headwaters, Peruvian Andes, *Global Biogeochemical Cycles, 21*(2), doi: http://dx.doi.org/10.1029/2006gb002835.

Townsend-Small, A., McClain, M. E., Hall, B., Noguera, J. L., Llerena, C. A., and Brandes, J. A. (2008), Suspended sediments and organic matter in mountain headwaters of the Amazon River: Results from a 1-year time series study in the central Peruvian Andes, *Geochimica et Cosmochimica Acta, 72*(3), 732-740, doi: http://dx.doi.org/10.1016/j.gca.2007.11.020.

Tranvik, L. J., Downing, J. A., Cotner, J. B., Loiselle, S. A., Striegl, R. G., Ballatore, T. J., Dillon, P., Finlay, K., Fortino, K., and Knoll, L. B. (2009), Lakes and reservoirs as regulators of carbon cycling and climate, *Limnology and Oceanography*, *54*(6), 2298-2314.

West, A. J., Lin, C. W., Lin, T. C., Hilton, R. G., Liu, S. H., Chang, C. T., Lin, K. C., Galy, A., Sparkes, R. B., and Hovius, N. (2011), Mobilization and transport of coarse woody debris to the oceans triggered by an extreme tropical storm, *Limnology and Oceanography*, *56*(1), 77-85, doi: http://dx.doi.org/10.4319/lo.2011.56.1.0077.

Wittmann, H., von Blanckenburg, F., Guyot, J. L., Maurice, L., and Kubik, P. (2009), From source to sink: Preserving the cosmogenic ^{10}Be-derived denudation rate signal of the Bolivian Andes in sediment of the Beni and Mamoré foreland basins, *Earth and Planetary Science Letters, 288*(3), 463-474, doi: http://dx.doi.org/10.1016/j.epsl.2009.10.008.

Wittmann, H., von Blanckenburg, F., Maurice, L., Guyot, J.-L., Filizola, N., and Kubik, P. W. (2011), Sediment production and delivery in the Amazon River basin quantified by in situ-produced cosmogenic nuclides and recent river loads, *Geological Society of America Bulletin*, *123*(5-6), 934-950, doi: http://dx.doi.org/10.1130/b30317.1.

Zimmermann, M., Meir, P., Bird, M. I., Malhi, Y., and Ccahuana, A. J. Q. (2009), Climate dependence of heterotrophic soil respiration from a soil-translocation experiment along a 3000 m tropical forest altitudinal gradient, *European Journal of Soil Science, 60*(6), 895-906, doi: http://dx.doi.org/10.1111/j.1365-2389.2009.01175.x.

Zimmermann, M., Meir, P., Silman, M., Fedders, A., Gibbon, A., Malhi, Y., Urrego, D. H., Bush, M. B., Feeley, K. J., Garcia, K., Farfan, W., Goetz, B. P., Johnson, W. T., Kline, K. M., Modi, A. T., Rurau, Q. N. M., Staudt, B. T., and Zamora, F. (2010), No differences in soil carbon stocks across the tree line in the Peruvian Andes, *Ecosystems*, (13), 62-74, doi: http://dx.doi.org/10.1007/s10021-009-9300-2.

Linking statement: Chapter 4 to 5

The previous chapters examined streamflow (chapter 3) and river POC during storm activity (chapter 4). In chapter (4) an examination of POC source behaviour throughout storm activity revealed information about erosional processes at play in the catchment. Now, in this chapter (5), I examine landslide activity to gain insight into the largest erosional process in the valley.

This chapter addresses the third research aim: **to examine landslide rates and slope turnover times for the Kosñipata Valley using remote sensing, and to estimate the amount of soil and vegetation mobilised by landslides**. It determines a mean annual landslide rate (1988 to 2012) covering the time period of the river study (2010). This, in addition to valley-wide carbon stock data, allows for the amount of carbon mobilised by landslides to be estimated. Knowledge of landslide mobilised soil and vegetation (non-fossil carbon sources) will be valuable when the importance of landslide derived $POC_{non\text{-}fossil}$ is examined in chapter 6.

I was the main author, designed, and wrote the paper. As well, I conducted all of the remote sensing analysis and the data analysis (except running the reverse-gamma probability analysis). Josh West, who was the main supervisor and main editor of this paper, provided advice, and helped design the research. He also ran the reverse-gamma probability analysis. Bob Hilton helped with the research design and provided guidance so that the work would link into the river POC papers. Greg Asner and Robin Martin provided the high resolution Carnegie Airborne Observatory (CAO) LiDAR derived DEM (3 x 3 m). Miles Silman and Sassan Saatchi provided guidance throughout and provided satellite images that were used. Beto Quesada provided unpublished soil carbon stock data. William Farfan provided unpublished above ground biomass data. Mark New provided support in the early stages of this study and initiated the project. Yadvinder Malhi provided general guidance throughout,

providing suggestions for analysis and editing the text. Bob, Greg, Miles also provided comments on the manuscript before submission.

This chapter was submitted in 2013 to *Proceedings of the National Academy of Sciences* (PNAS). The paper was rejected after review. It will be reworked according to the comments from the PNAS reviewers and the editor, and submitted to Journal of Geophysical Research-Earth Surface or Earth Surface Dynamics by late 2014.

Chapter 5 : Fluvial incision links landslides, carbon transfer and plant diversity in an Andean Valley

Kathryn E. Clark[1*], A. Joshua West[2], Robert G. Hilton[3], Gregory P. Asner[4], Miles R. Silman[5], Sassan S. Saatchi[6], Carlos A. Quesada[7], William Farfan Rios[5], Roberta E. Martin[4], Mark New[1,8] and Yadvinder Malhi[1]

[1] School of Geography and the Environment, University of Oxford, UK. (*correspondence: kathryn.clark23@gmail.com)

[2] Department of Earth Sciences, University of Southern California, Los Angeles, USA. (joshwest@usc.edu)

[3] Department of Geography, Durham University, UK. (r.g.hilton@durham.ac.uk)

[4] Department of Global Ecology, Carnegie Institution for Science, Stanford, CA, USA. (gpa@carnegiescience.edu)

[5] Department of Biology and Center for Energy, Environment, and Sustainability, Wake Forest University, Winston-Salem, NC, USA. (silmanmr@wfu.edu)

[6] Jet Propulsion Laboratory, California Institute of Technology, Pasadena, CA, USA. (saatchi@jpl.nasa.gov)

[7] Instituto Nacional de Pesquisas da Amazônia, Manaus, Brazil. (quesada.beto@gmail.com)

[8] African Climate and Development Initiative, University of Cape Town, South Africa. (mark.new@acdi.uct.ac.za)

Abstract

Landslides are a dominant feature of montane landscapes, but it has remained difficult to assemble direct evidence for their role in evolution of topography, shaping of the structure and services of forest ecosystems, and cycling and transport of carbon. The importance of landslides in linking physical processes with the biosphere is particularly relevant in tropical montane landscapes, which are not well understood despite high productivity and diversity, and which may act as a long term carbon sink through removal and burial of organic material. Here, we present a novel analysis of landslide occurrence and recovery in a forested valley in the eastern Andes of Peru. We combine this information with elevation and biomass data to (i) understand threshold conditions for landslide frequency, and how these relate to drivers of landscape evolution, (ii) estimate net carbon mobilized by landslides, and how this varies spatially as a result of heterogeneity in landslide distribution, and (iii) consider possible implications for diversity in the forest ecosystem. We determine landslide occurrence at an annual resolution over 25-years using satellite images from 1988 to 2012. Valley wide landslide frequency is high, at 0.09 % yr^{-1} by area, indicating forest turnover times through landslides of ~1200 years. Using high-resolution airborne LiDAR data (3 m x 3 m resolution), we demonstrate that landslide activity increases substantially (up to 0.16 % yr^{-1}) once the threshold slope angle is reached (>~38 °). Enhanced river incision downstream of a geomorphological knickpoint at ~1700 m steepens hillslopes, leading to higher landslide frequencies, preferentially increasing carbon mobilisation, and potentially influencing diversity.

5.1. Introduction

Mountain topography is generated by the interaction of rock uplift and erosion. In the basic conceptual model for topographic evolution, fluvial incision into uplifted rock mass steepens slopes, while landslides, triggered once slopes reach a critical failure angle [*Burbank et al.*, 1996; *Montgomery*, 2001], reduce slope angle and lower the terrain [*Carson and Petley*, 1970; *Hovius et al.*, 2000; *Korup*, 2005; *Korup et al.*, 2010; *Larsen and Montgomery*, 2012]. Over time, these processes reach a steady state both topographically and in the balance between rates of uplift and erosion [*Willett and Brandon*, 2002]. When topographic boundary conditions change, for example when base level drops, landscapes adjust through propagation of incision into uplifted rock [*Whipple*, 2004]. Knickpoints or knickzones in river profiles, i.e., discrete changes in the topographic profile of the river channel, are characteristic of the change in river incision in such landscapes and are prevalent in tectonically active mountains around the world [*Lavé and Avouac*, 2001; *Clark et al.*, 2005; *Whittaker et al.*, 2007; *Giaconia et al.*, 2012]. With topographic evolution towards steady state, landslide activity is predicted to increase in areas of the catchment where incision steepens slopes downstream of knickzones [*Whipple and Tucker*, 1999; *Korup*, 2006; *Larsen and Montgomery*, 2012]. The resulting catchment-scale variability in the rate of landslide activity has been modelled numerically [*Howard*, 1994], observed in analogue experiments [*Bigi et al.*, 2006], and inferred from topographic metrics [*Korup and Schlunegger*, 2007; *Gallen et al.*, 2011]. However, there are only limited empirical datasets that report the spatial link between fluvial incision and landslide dynamics [*Korup*, 2006; *Larsen and Montgomery*, 2012], and it has remained difficult to directly demonstrate the coupling between channel incision and hillslope failure within tectonically active river basins. Moreover, the wider implications of the spatially heterogeneous landslide activity that is predicted to result from transient incision are largely unexplored.

These implications include important effects on the montane biosphere. Landslides in mountain topography are known to remove standing biomass and soil, clearing whole sections of the forest and transporting materials downslope [*Restrepo and Alvarez*, 2006; *Hilton et al.*, 2011; *West et al.*, 2011]. Conceptual models of montane forest dynamics suggest that geomorphic disturbance could influence the structure of ecosystems [*Kessler*, 1999; *Restrepo et al.*, 2009; *Walker et al.*, 2013]. These structural changes in the ecosystem should be present at the same scale as the spatial patterns of landslide dynamics, acting over tens to thousands of km^2 [*Hovius et al.*, 2000; *Larsen and Montgomery*, 2012]. Moreover, spatial variability in geomorphic processes persists on timescales of 10^5-10^6 years, while forest turnover occurs over 10^2-10^3 years [*Restrepo and Alvarez*, 2006; *Restrepo et al.*, 2009; *Hilton et al.*, 2011; *Ramos Scharrón et al.*, 2012], such that geomorphic heterogeneity is likely to be maintained over repeated cycles of forest turnover, long enough to influence ecosystem development. Landslides may consequently link fluvial incision and the steepening of hillslopes, and their ultimate tectonic drivers, with key features of montane ecosystems. However, it has been difficult to clearly identify these connections because previous studies of landsliding and assessment of ecosystem structure and dynamics have considered disparate spatial and temporal scales (e.g. *Restrepo et al.* [2009]).

While landslides and consequent ecosystem modification occur at local scales, they may also have critical effects on the carbon cycle at regional and even global scales. A portion of the vegetation and soil mobilised by landslides is delivered to the river system and eventually transported downstream. Understanding the source of this material within catchments is important for assessing its potential entrainment into rivers, and the resulting preservation efficiency of the eroded organic carbon, which ultimately determines the carbon balance of erosional processes (e.g., *Hilton et al.* [2008]; *Galy and Eglinton* [2011]; *West et al.* [2011]). It is also important for understanding what factors set the composition of

sedimentary biomarkers that are transported by rivers, because molecular characteristics and isotopic composition vary with elevation [*Feakins et al.*, 2007; *Sheldon and Tabor*, 2009]. Spatially heterogeneous landslide patterns, which may selectively sample portions of the landscape for organic material, may thus be expected to have an important influence both on the carbon budget and on biomarker records.

In this study, we assemble a 25-year duration landslide inventory for an Andean river basin in Peru with a prominent knickzone that we attribute to transient incision. We used this inventory to assess the spatial relationship between incision and landslide probability, providing direct evidence to test the basic hypothesis that landslide activity should be enhanced on hillslopes steepened by incision in the downstream reaches of the river. To then assess the wider implications of the resulting heterogeneity in landslide activity for the biosphere, we (i) use data on standing biomass and soil carbon stocks in order to quantify the spatial variability in landslide mobilized carbon, (ii) estimate rates of landslide revegetation, and (iii) compare the observed landslide distribution to species diversity in the valley. Overall, we seek to better understand how transient geomorphic processes introduce spatial heterogeneity which can influence the evolution of the physical landscape while impacting the ecological structure and biogeochemical cycles operating in a mountain forest.

5.2. Study area

The Kosñipata Valley is situated in the Eastern Andes of Peru (13°3’27”S 71°32’40”W). Elevation in the catchment ranges from 1200 metres above sea level (masl) to 4000 masl with a mean elevation of 2700 ± 600 masl and a catchment area of 185 km^2. The study area focuses on landslides in the forested portion of the valley, covering 150 km^2. The remaining 35 km^2 of the catchment at the mountain tops is mostly puna grassland (Figure 5.1a) with some shrubland above the timberline at 3300 ± 250 masl. In the forested area, vegetation consists of sub-alpine cloud forest at high elevations (3400 to 3600 masl), upper

montane cloud forest between 2000 to 3400 masl, and lower montane cloud forest and sub-montane tropical rainforest between 1200 to 2000 masl (Figure 5.1a) [*Horwath,* 2011]. The valley is partially contained in Manu National Park, where logging is prohibited. The Kosñipata River, which flows through the study area, is ~ 17 km long and at the foothills flows into the Alto Madre de Dios River which feeds the Madre de Dios River, a tributary of the Amazon River. The ecological and environmental characteristics of the valley are closely monitored, and there are extensive datasets on plants, soil, productivity, carbon and nutrient cycling and climate [*Malhi et al.*, 2010]. Tree species richness ranges from 40-180 spp ha^{-1} ≥ 10 cm diameter at breast height (dbh) and total forest C-stocks [*Gibbon et al.*, 2010; *Horwath,* 2011; *Girardin et al.*, 2013a; *Gurdak et al.*, 2013] are representative of the wider Andean region [*Saatchi et al.*, 2011].

The South American Low Level Jet carries humid winds westward over the Amazon Basin and then south along the flank of the Andes, driving orographic rainfall in the Eastern Cordillera of the Central Andes [*Marengo et al.*, 2004]. Precipitation ranges from 2000 to 5000 mm yr^{-1}; highest precipitation is in the lowest part of the valley and this decreases with the increase in elevation [*Girardin et al.*, 2013b; *Huaraca Huasco et al.*, 2013]. The valley has > 74 % cloud cover throughout the year in a band of persistent cloud that spans much of the Eastern Andes [*Halladay et al.*, 2012] (Figure 5.1a).

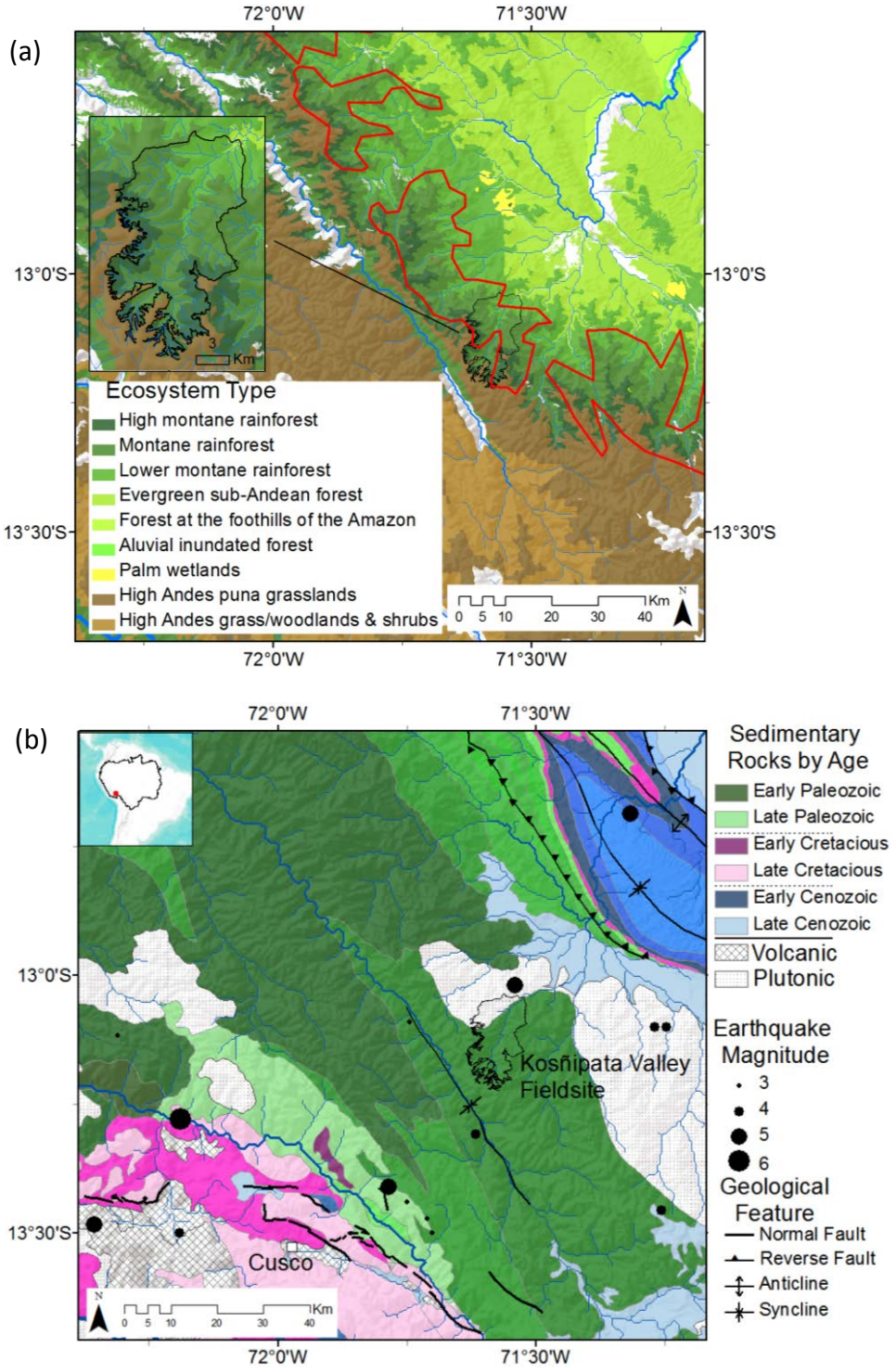


Figure 5.1: a) Ecosystem types in the eastern Andes of Peru [*Consbio*, 2011]. Bare areas are cities, agriculture, glaciers and riverbed, with the Kosñipata Valley field site magnified in the inset. Areas delimited by red polygons are regions of high annual cloud cover > 74 % [*Halladay et al.*, 2012]. b) Georectified geological map [*Mendívil Echevarría and Dávila Manrique*, 1994; *Carlotto Caillaux et al.*, 1996; *Vargas Vilchez and Hipolito Romero*, 1998; *INGEMMET*, 2013], where the sedimentary rocks are on a scale ranging from dark to light colour within each era. Active faults [*Sébrier et al.*, 1985; *Cabrera et al.*, 1991] and documented earthquakes since 1975 [*USGS*, 2013].

The Kosñipata Valley is in an active tectonic setting. The Eastern Cordillera of the Central Andes is subject to rock and surface uplift of 0.2-0.3 mm yr^{-1} due to the subduction of the Nazca Plate under the South American Plate [*Gregory-Wodzicki*, 2000]. Since 1978, there have been ~ 4 registered earthquakes larger than magnitude M_L=5 within a distance of 65 km from the Kosñipata Valley (Figure 5.1b) [*Gregory-Wodzicki*, 2000; *USGS*, 2013]. The Cusco fault zone is the nearest most active region, ~ 50 km southwest of the study site, consisting of normal faults stretching for 200 km long and 15 km wide parallel to the Andean plateau [*Cabrera et al.*, 1991] where deep earthquakes are common [*Tavera and Buforn*, 2001; *USGS*, 2013]. In the Andean foothills, ~ 20 km northeast of the study site, there is an active fold and thrust belt [*Sébrier et al.*, 1985; *Vargas Vilchez and Hipolito Romero*, 1998]. The bedrock geology in the Kosñipata Valley is representative of the wider Eastern Andes [*Clark et al.*, 2013]. The valley is dominated by metamorphosed sedimentary rocks in the high elevations (mostly mudstone protoliths of ~ 450 Ma) and a plutonic region in the lower elevations (Figure 5.1b) [*Carlotto Caillaux et al.*, 1996].

Landslides are a common geomorphic process in the Andes, covering 1-6 % of mountain catchments [*Stoyan*, 2000; *Blodgett and Isacks*, 2007], but rates in the Kosñipata Valley have not been measured. While physical erosion rates in the Kosñipata section of the Andes are not well constrained, detrital cosmogenic nuclide concentrations in river sediments downstream from the Madre de Dios River suggest denudation rates higher than those in the Bolivian Andes [*Wittmann et al.*, 2011], where landslides are estimated to denude the landscape at a rate of 9 ± 5 mm yr^{-1} [*Blodgett and Isacks*, 2007].

5.3. Materials and methods

5.3.1. Landslide mapping

Forest landslides were manually mapped over a 25-year period from 1988 to 2012 from Landsat 5 and Landsat 7 satellite images (Figure 5.2a). Landslide boundaries were delineated using a number of pan-sharpened, high resolution QuickBird-2 and WorldView-2 satellite images with resolutions of 2.4 m x 2.4 m and 2 m x 2 m, respectively. These high resolution images were collected in 2005, 2009, 2010 and 2011. Geospatial analysis was carried out in ArcGIS. There were 38 usable images over the 25-year period, with 1-3 available for each year (Table S1). Unusable images were covered in clouds (n > 100). Two aerial photographs were used to identify and remove pre-1988 landslides from this study. Landslides with an area smaller than ~ 2 x 2 pixels (area < 0.004 km^2) may not be fully accounted for [*Stark and Hovius*, 2001] due to the Landsat grid-resolution of 30 m x 30 m. There is a difference in resolution between Landsat and the high resolution images. Landsat was used although at a lower resolution in order to evaluate annual landslide occurrence. The Kosñipata landslide dataset broadly follows a frequency-area distribution that is generally characteristic of landslides from other regions (*Malamud et al.* [2004] and references therein), and this distribution indicates that landslide area was underestimated by at most < 5 % due to missing small-area landslides (Figure S5.1). Thus, it is reasonable to use medium resolution imagery to monitor annual change in landslide activity. The Landsat images had a mean visibility of 59 % (Table S1) due to topographic shadow, cloud shadow, and no-data strips (on Landsat 7 images post 2002). Landsat imagery produced a distinct topographic shadow – a shadow produced by hillslopes – which covered ~ 23 % of the study area consistently (35 km^2 out of 150 km^2), and landslides that fell within these shadow areas were not visible. Topographic shadow affected southwest facing slopes (223 ± 52 °). Further details are described in the supplementary section.

5.3.2. Landslide frequency, turnover and probability

We calculated landslide frequency (L_f, % yr^{-1}) and slope turnover (τ_{ls}, yr) by $1km^2$ grid cells (Figure 5.2b & c). We corrected for landslides obscured by topographic shadow by assuming landslide occurrence in the visible portion of each cell was representative of the entire cell. Cells with > 50 % topographic shadow were removed from analysis. Landslide frequencies over the 25 year length of the study (L_f, % yr^{-1}) were calculated based on the corrected landslide area divided by the total forested area. The average rate of slope turnover due to landslides (τ_{ls}, yr) was calculated as the inverse of landslide frequency. This metric reflects the time required for landslides to impact all of the landscape based on their frequency of occurrence [*Restrepo et al.*, 2009; *Hilton et al.*, 2011]. To determine landslide probability (P_{ls}), each landslide was subdivided into 3 m x 3 m cells using a Carnegie Airborne Observatory (CAO) DEM [*Asner et al.*, 2012]. Probability was determined as a function of elevation (by 300 masl intervals, Figure 5.3a) and of slope (by 1 ° intervals, Figure 5.3b) for the visible portion of the study area, following published approaches [*Meunier et al.*, 2008]. Slopes <20 ° were removed because of artefacts due to landslide deposits on low slope surfaces. Further details are described in the supplementary section.

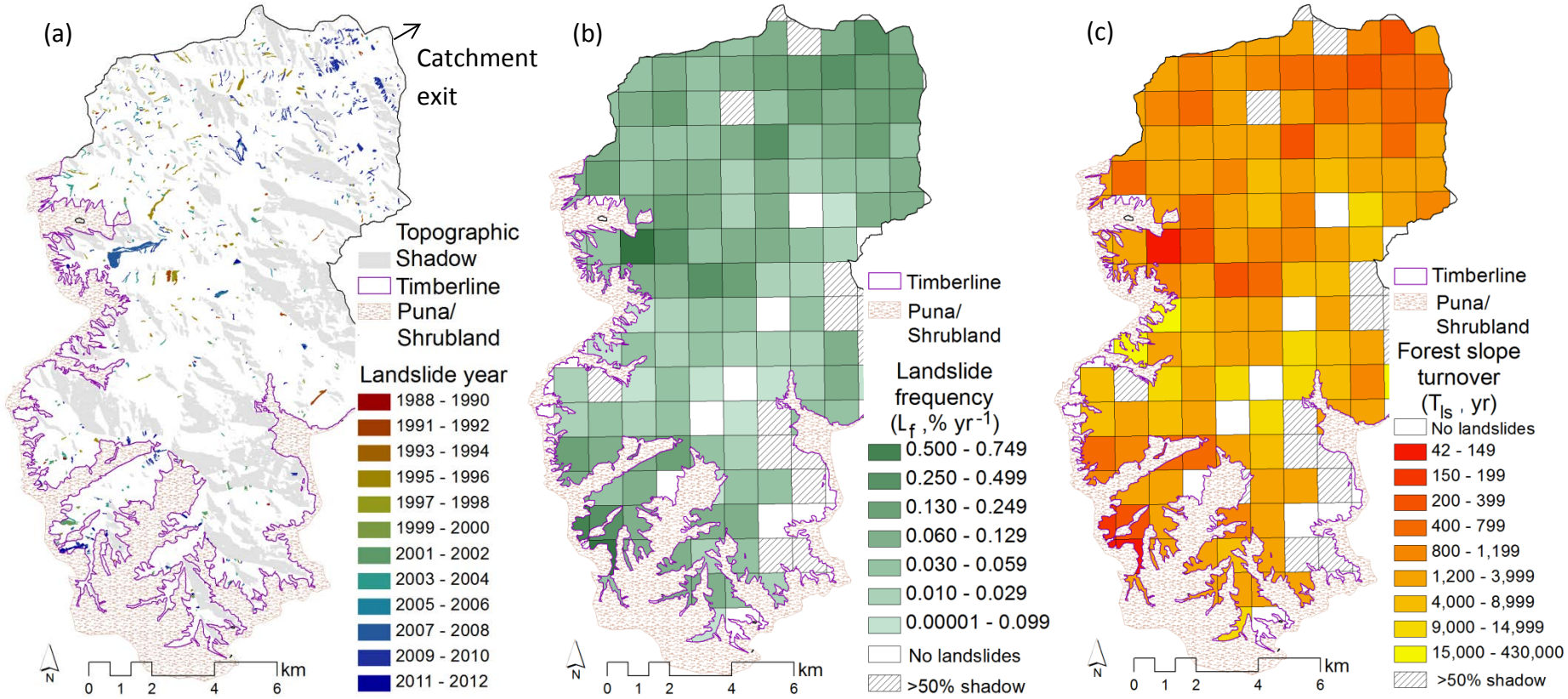


Figure 5.2: a) Landslide distribution in the Kosñipata Valley over the 25-year study period mapped from Landsat satellite images with annual resolution, with Landsat topographic shadow regions in light grey. b) Landslide frequency (L_f, % yr^{-1}), and c) forest slope turnover (τ_{ls}, yr) by year on a 1km^2 grid. Grid cells with > 50 % Landsat topographic shadow were removed from the analysis in (b) and (c).

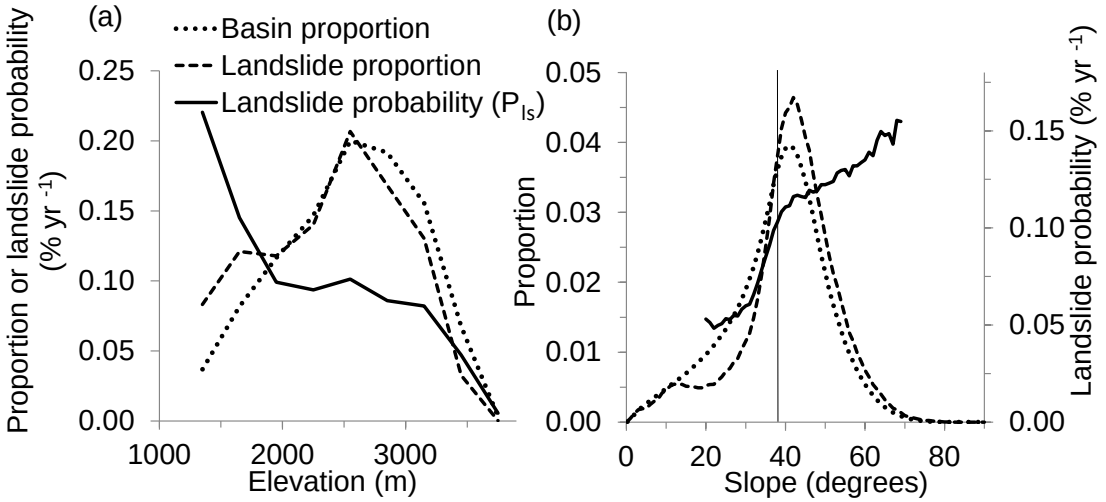


Figure 5.3: The proportion of catchment area as a function of elevation for the basin (dotted line) and mapped landslides (dashed line) with the resultant landslide probability (P_{ls}, % yr^{-1}) (solid line). a) Landslide occurrence by pixel, calculated over 300m elevation bin sizes from the 3 m x 3 m DEM, is elevated at low elevations (dashed line is higher than dotted line) and reduced at higher elevations (dashed line lower than dotted line). The non-uniform spatial distribution is reflected in landslide probability (solid line). b) Landslide probability by pixel (at one degree bin size from the slope map created from the same DEM) is greatest at high slopes. Vertical line at 38 ° delineates threshold slope angle where slopes have significantly higher landslide probability.

5.3.3. Landslide revegetation

The high resolution imagery also made it possible to estimate when landslides were "revegetated," i.e. dominated by a closed forest canopy to an extent that we could no longer visually distinguish the landslide scar or bare ground in the high resolution imagery [*Blodgett and Isacks*, 2007]. For each year in the inventory we determined the fraction of area of the landslides that were fully recovered as of 2011 (Figure 5.4). For landslide years prior to 2008, i.e. all landslide years with observable recovery, we ran a linear regression between landslide area recovered (area of fully recovered landslides from a given year as a % of total landslide

area from that year) and the number of years that had passed since landslide occurrence (the difference between the given year and 2011). This analysis used a total of 18 data points, one for each year between 1988 and 2007 except for 2 years that had no measured landslides (Figure 5.4; Table S2).

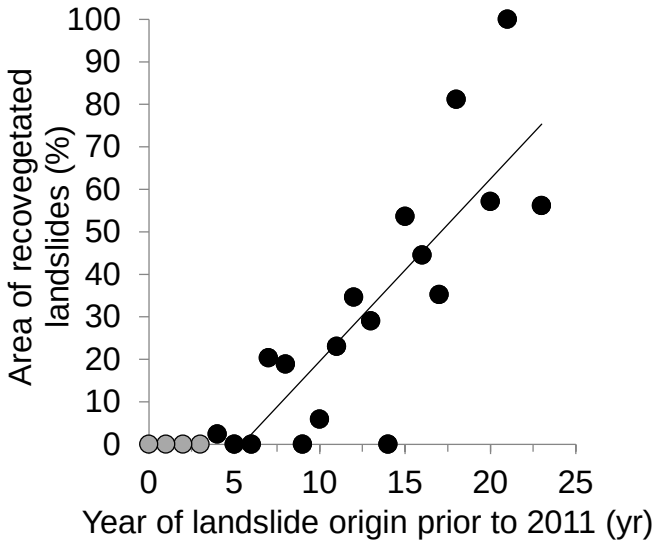


Figure 5.4: Landslide recovery time as percent area recovered by 2011, evaluated from a WorldView-2 pan-sharpened satellite image at 2m x 2m resolution. Each data point represents the landslides from a single year during the study period (black and grey circles; n = 23). Landslides occurring at least 4 years prior to 2011 (black circles) were used to determine equation 1 (area of recovered landslides (%) = 4.394±0.735 × year of landslide origin prior to 2011 – 23.406±10.196), where the mean estimated time for 100 % recovery of all the landslides of a given year is ~28 yrs (r^2 = 0.7, n = 18).

5.4. Results and discussion

5.4.1. Landslide frequencies and patterns

Approximately 2 % (3 km^2) of the Kosñipata Valley study area experienced landslides over the last 25 years. This is similar to landslide coverage in the Ecuadorian and Bolivian Andes [*Stoyan*, 2000; *Blodgett and Isacks*, 2007]. On average, over the 25 year study period, valley-wide landslide frequency was 0.09 % yr^{-1}, and ranged from no landslides detected to 2.5 % yr^{-1} for individual 1 x 1 km grid cells (Figure 5.2b). The inverse of landslide frequency gives a valley wide forest slope turnover time of ~1200 yrs, ranging from ~40 yrs to < 400

000 yrs for individual grid cells (Figure 5.2c). These forest slope turnover times are rapid, with the average over ~10 times faster than those estimated in the western Southern Alps of New Zealand [*Hilton et al.*, 2011] and in Guatemala [*Restrepo and Alvarez*, 2006] and ~25 times faster than in Mexico and in Central America [*Restrepo and Alvarez*, 2006]. The short turnover times in the Kosñipata are comparable to the shortest times observed in New Zealand, in the Waitangitaona Basin [*Hilton et al.*, 2011].

Over the altitudinal gradient in the Kosñipata Valley, there is a spatial trend in landslide frequencies, with low frequencies at high elevations, a plateau at mid-elevations and then a sharp increase at the lowest elevations (Figure 5.3a). The spatial and temporal patterns of landslides in mountain landscapes depend on variability of proximal landslide triggers such as rainfall and seismic activity [*Densmore and Hovius*, 2000; *Lin et al.*, 2008; *Meunier et al.*, 2008], as well as geomorphic parameters, most notably slope angle [*Bussmann et al.*, 2008; *Lin et al.*, 2008; *Larsen and Montgomery*, 2012]. All of these may vary with elevation. Herein these factors will be considered in the context of river incision-driven slope steepening, climatic and earthquake triggering, with the implications for carbon mobilisation and forest structure explored.

5.4.2. Link between landslide frequency and river incision and implications for the threshold hillslope model of topographic evolution

In the Kosñipata valley, for slope angles >~38 ° the proportion of landslide cells is greater than basin proportion, and the probability of landsliding increases significantly (Figure 5.3b). This is strong indication that this 38 ° angle, which is also the mean slope of the forested areas of the Kosñipata, represents the threshold slope angle for the system. This threshold angle is typical of active mountain ranges around the world, with values determined elsewhere ranging from 30 ° to 40 ° [*Blodgett and Isacks*, 2007; *Lin et al.*, 2008]. Of the total Kosñipata basin area, 60 % of the basin had slopes >38 °, with a mean slope of 37.8 ± 12.4 °

using the CAO DEM with a 3 x 3 m resolution (mean slope of 27.4 ± 8.9 ° using SRTM with a 90 x 90 m resolution). Above the threshold angle, landslide frequencies varied from 0.10 to 0.16 % yr^{-1} (Fig 3b), all higher than the basin mean rate of 0.09 % yr^{-1}. See the supplementary section for further details.

Across the whole catchment, landslide probability varied significantly with elevation, with the highest probability (> 0.2 % yr^{-1}) at elevations lower than 1500 masl (Figure 5.3a). The significant increase in the landslide frequency at lower elevations in the Kosñipata Valley (Figure 5.3a) spatially coincides with a knickpoint in the river channel profile at ~1700 m elevation (Figure 5.5a & b). Below this point, the river channel becomes significant steeper, and the frequency of landslide activity increases significantly. We attribute this coincidence to fluvial incision downstream of the knickpoint, which steepens the river channel as well as the surrounding hillslopes, leading to greater landslide frequency as slopes are oversteepened beyond the threshold angle. Thus the Kosñipata dataset illustrates the effect predicted by the threshold slope model, that landslide activity should result from fluvial downcutting.

Knickpoints are common features in mountain rivers globally [*Burbank et al.*, 1996; *Clark et al.*, 2005; *Korup et al.*, 2010]. They can generally be explained either by tectonic effects associated with uplift, or lithological effects associated with variable rock strength [*Korup et al.*, 2005; *Cook et al.*, 2009], or changes in climate regime that result in increased stream power [*Whipple*, 2001; *Crosby and Whipple*, 2006]. In the case of the Kosñipata, there is a contrast within the catchment between meta-sedimentary bedrock in the headwaters, versus plutonic granite at lower elevations.

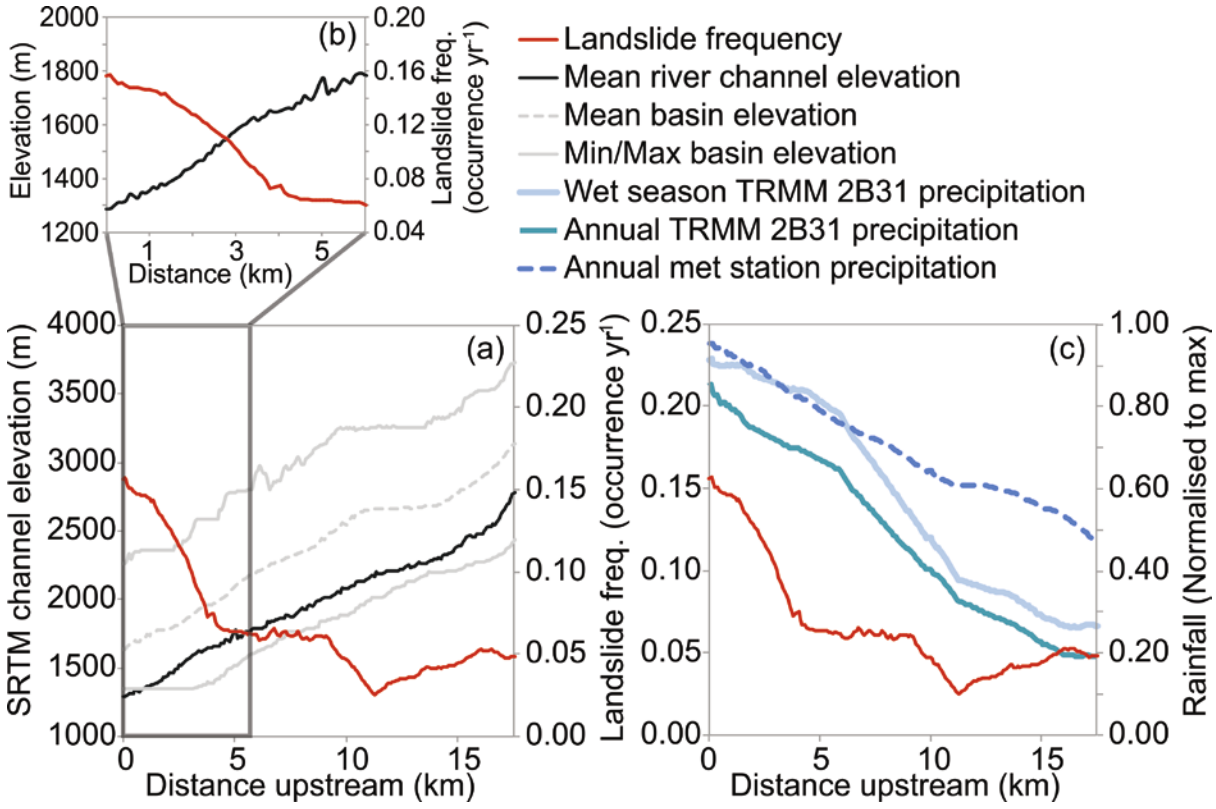


Figure 5.5: Downstream profiles over 0.44 km^2 swath along the Kosñipata River. a) Stream channel (blue) and min., max., and mean catchment topography (black and grey dashed lines), along with landslide frequencies (red line). Grey box indicates region of incision downstream of prominent knickzone in the river channel at ~1700 m elevation which coincides with significant increase in landslide frequency. b) Inset of the knickzone shown in (a). c) Landslide frequency (red line) with mean normalised precipitation from meteorological station data (dashed light blue), wet season 2B31 TRMM precipitation (dark blue line), and annual 2B31 TRMM precipitation (grey line). 2B31 TRMM is at 4 x 4 km resolution from *Bookhagen* [in review].

These lithologies will have contrasting rock strength, and so may be able to maintain differences in landscape steepness that could explain the observed knickpoint. The contact between these units is not well defined throughout the basin but is generally in the region of 1650 m to 2250 m in elevation. Although this estimated contact zone is similar to the location of the knickpoint in the river profile, there is not a clear distinction of higher landslides frequency between the two lithological groups. Moreover, the very observation that landslide frequency is higher in the downstream reaches suggests that differences in rock strength are not a likely explanation for the transition in channel steepness, because a lithologically-

controlled knickpoint, associated with distinct changes in rock competence, would not be expected to result in landscape-wide increases in the hillslope failure. Instead a more likely explanation is that the Kosñipata Valley is responding to a pulse of uplift, and that the knickpoint is progressively working upstream through headward incision, with the hillslopes downstream responding through landslide activity. Such a tectonic explanation is consistent with the presence of major reverse faults, active on Holocene timescales [*USGS*, 2013], running orthogonal to the flow direction of the Kosñipata about ~20km NW from the outlet (Figure 5.1b). Uplift associated with slip on these faults could generate the kind of knickpoints seen in the Kosñipata (as in *Giaconia et al.* [2012]), with high landslide activity at elevations below this point as a response. We thus view the Kosñipata as a non-equilibrium landscape, with a transient knickzone that reflects increased incision in the lower reaches of the river. The observed landslide distribution demonstrates that the erosive processes that are driving the system towards topographic steady state involve a coupling of this incision to hillslope failure.

5.4.3. Role of rainfall and earthquakes for spatial landslide patterns?

Rainfall-triggered landslides occur through an increase in pore pressure and seepage forces during periods of heavy rainfall [*Terzaghi*, 1951]. The increased pore pressure decreases the effective stress in the soil and as a result reduces the soil shear strength, ultimately resulting in slope failure [*Wang and Sassa*, 2003]. Variability in rainfall has been linked to landslide activity in various mountainous regions of the world [*Densmore and Hovius*, 2000; *Restrepo et al.*, 2003; *Lin et al.*, 2008; *Meunier et al.*, 2008]. We have evaluated whether rainfall patterns in the Kosñipata Valley can account for the spatial distribution of landsliding using both meteorological station data from nine stations in the valley along the altitudinal gradient (900 m to 3500 m) [*Rapp*, 2010; *SENAMHI*, 2012; *Girardin et al.*, 2013b; *Huaraca Huasco et al.*, 2013] (Figure 5.5c & S5.3a) and rainfall data

from the NASA Tropical Rainfall Measuring Mission (TRMM) 2B31 data (4 x 4 km) [*Bookhagen*, in review] (Figure 5.5c & S5.3b). For both the met station and the TRMM data, rainfall totals follow an approximately linear trend downstream, without the distinct, non-linear increase that is seen in landslide frequency at low elevations (Figure 5.5c). The number of "extreme events" identified in TRMM 2B31 data also shows a generally linear increase downstream, without a kink around 1700 m that would be coincident with the landslide dataset. These interpretations should be treated with some caution since there is limited meteorology station data, and the TRMM products underestimate rainfall in the Andes and thus may also underestimate extreme events [*Scheel et al.*, 2011]. Higher rainfall at lower elevations may be an important trigger for landslide failure, and it is difficult to rule out a coincident change in rainfall and/or extreme storm events with landslide occurrence, but overall, based on the available data, rainfall patterns do not seem sufficient to explain the observed variability in landslide frequency (Figure S5.3).

A major storm occurred on March 4th 2010, during which rainfall measured at a meteorological station at 1400m elevation in the valley was 45 mm hr^{-1}, with 200 mm falling in 4.5 hr. This storm in 2010 triggered ~185 landslides with ~0.7 km^2 cumulative area at elevations from 1250m to 2600m, clearly an extreme event within the 25-year dataset (Figure S5.2 & S5.4; Table S2). The landslides resulting from this storm, together with field observation of frequent hillslope failure during and immediately after other smaller storms, indicate that precipitation is indeed a proximal trigger for landslide failure in the Kosñipata Valley, confirming other work in mountain forests (Figure S5.4) [*Densmore and Hovius*, 2000; *Restrepo et al.*, 2003; *Meunier et al.*, 2008]. However, such immediate climatic triggers do not contradict the observation that the basin-scale slope characteristics are the underlying controls on the spatial distribution of landslides throughout the valley, in the case of the Kosñipata driven by slope-steepening through incision.

Seismic waves [*Harp and Keefer*, 1990] and the ground acceleration associated with earthquakes [*Densmore and Hovius*, 2000] have been observed to trigger landslides in mountainous regions around the world [*Hovius et al.*, 2000; *Keefer*, 2002], and in the Andes [*Tibaldi et al.*, 1995; *Rodrıguez et al.*, 1999]. Earthquake events may also be important in priming the landscape for landslides, due to rock deformation from shaking, and this effect can last for some time, from several decades to even longer [*Hovius et al.*, 2011]. The Kosñipata Valley lies in a seismically active region (Figure 5.1b) [*Silgado*, 1978; *USGS*, 2013]. However, there were no major earthquakes causing significant ground motion in the study region during the 25-year period of observations. In principle, the higher landslide frequency at lower elevations might be related to landscape priming associated with previous events along frontal faults in the Andean foothills (Figure 5.1b). However we see no evidence that earthquake-priming is a dominant effect in determining spatial variability in landslide frequency in the Kosñipata. In particular there is no *a priori* reason why such priming should lead to a discontinuous variation in landslide frequency with elevation, i.e. there is no clear reason why it would result in a kink in the frequency of landslides at ~ 1700 m elevation rather than a continuous decrease with distance away from the fault ~ 50 km away northeast in the foothills of the Andes (Figure 5.1) [*Meunier et al.*, 2008]. Thus, while earthquake activity may have some relevance in this system, over the 25-year period considered here, it appears to be the long-term geomorphic effects associated with uplift, river incision, and steepening of valley-side slopes that are the major determinants of where most landslides occur.

5.4.4. Landslides and the mobilization of organic material

The association between uplift, river incision, and landslide activity that we observe means that the mobilisation of forest biomass from hillslopes by landslides is not spatially uniform. This is important because the location of the source area for organic material affects

whether and where material is input into the river system. This in turn affects whether organic matter is eventually deposited and preserved in downstream sedimentary archives, rather than being remineralized within the forest system. Thus the location of landslide disturbance within river catchments can influence the overall carbon balance of montane forest systems [*Restrepo et al.*, 2009; *Hilton et al.*, 2011; *Walker et al.*, 2013]. The spatial distribution of landslides also determines which organic biomarkers eventually make their way from the forest vegetation into sedimentary archives. Important features of these biomarkers that are used in paleoenvironmental reconstruction, such as their molecular characteristics and isotopic compositions, depend on the elevation at which the organic compounds are formed [*Feakins et al.*, 2007]. If the observed heterogeneous spatial distribution of landslides selectively mobilizes some portions of the landscape for organic material, it may introduce an important 'sampling' bias.

To consider these implications, we have assessed the distribution of organic material mobilized by Kosñipata landslides. In order to estimate the organic carbon stock, we collated soil and vegetation datasets from the Kosñipata Valley. The datasets consist of soil carbon stocks, above ground living biomass (trees), root carbon stocks [*Girardin et al.*, 2013a], wood debris carbon stocks [*Gurdak et al.*, 2013], and epiphyte carbon stocks [*Horwath*, 2011]. In order to estimate the carbon stocks of the above ground living biomass we assumed a wood carbon concentration of 46 % measured in stems and leaves (n = 130) throughout the Kosñipata Valley [*Rao*, 2011]. Each dataset consisted of data from 4 to 12 plots along the altitudinal gradient. Linear regressions were determined for each dataset (e.g. soil, stems, roots, woody debris) separately, where the carbon stock (MgC ha^{-1}) was on the y-axis and elevation (masl) was on the x-axis, following previous work [*Hilton et al.*, 2011]. In the case of the epiphytes, two separate regressions (one for elevations of 1100 m to 1522 m and another for elevations of 2040 m to 3600 m) were determined since there was a significant

decrease in epiphyte density below the cloud immersion zone [*Horwath*, 2011] (Figure S5.5; Table S3). Carbon stocks at each elevation were estimated for each dataset using the regressions and summed to determine total carbon stocks by elevation band (300 m). The resulting estimated mean carbon stock for the forested valley is ~42,100 tC km^{-2}, with ~31,600 tC km^{-2} in soil and ~10,500 tC km^{-2} in vegetation (Figure S5.5). This is consistent with broad trends in the tropics in which soil carbon stocks increase with elevation and are frequently greater than vegetation carbon stocks [*Raich et al.*, 1997; *Raich et al.*, 2006; *Gibbon et al.*, 2010].

The landslide mobilization of carbon was determined by multiplying landslide frequency (SI Materials and Methods) by the carbon stock (tC km^{-2}) for each elevation band. Based on our field observations that landslides in the Kosñipata effectively remove the entire soil layer, we assume that all landslides are bedrock landslides and remove the entire soil carbon stock. In the Kosñipata Valley, landslides mobilise ~40 tC km^{-2} yr^{-1}, with ~30 tC km^{-2} yr^{-1} derived from soil and 10 tC km^{-2} yr^{-1} from vegetation (Fig 6a). This area-normalized landslide carbon flux in the Kosñipata is ~ 5 times greater than the mean landslide flux measured in New Zealand, but similar to fluxes in the New Zealand basins with the highest landslide rates [*Hilton et al.*, 2011]. Kosñipata landslide fluxes are similar to those seen in Guatemala when hurricane return time is most frequent [*Ramos Scharrón et al.*, 2012].

Over the total study area of ~150 km^2 the estimated total flux of carbon mobilized by landslides was ~ 6000 tC yr^{-1}, ~ 4450 tC yr^{-1} from soil and ~1550 tC yr^{-1} from vegetation (Figure 5.6b). In terms of carbon stocks, the contribution of soil (70 %) in the Kosñipata Valley is more important than that of vegetation (30 %). This can partially explain the observation that soil organic carbon (from upper horizons) is the dominant source of particulate organic carbon (POC) carried in the Kosñipata River [*Clark et al.*, 2013]. A more detailed assessment of the coupling of landslide mobilisation and onward fluvial transport

requires quantification of river POC flux in the catchment, which lies outside the scope of this chapter is evaluated in chapter 6.

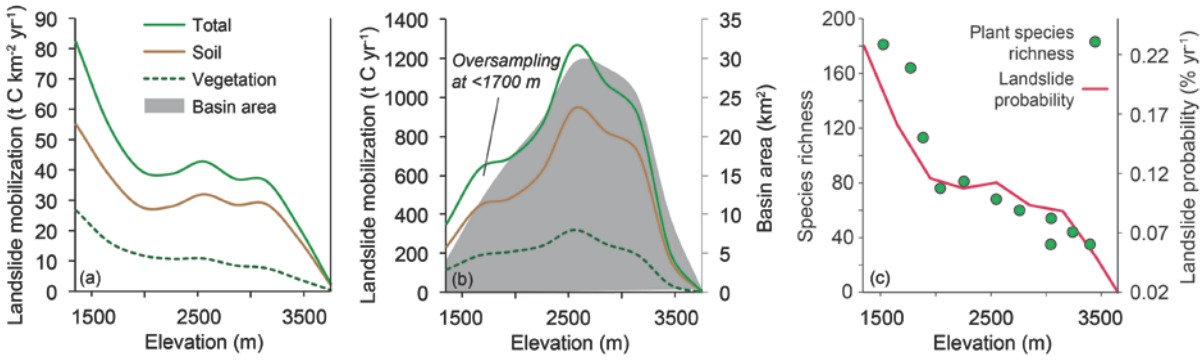


Figure 5.6: a) Area-normalised mobilisation of organic carbon (tC km^{-2} yr^{-1}) and b) total mobilisation of carbon by landslides (tC yr^{-1}) over the altitudinal gradient contributed by the soil organic carbon stock (brown line), vegetation carbon stock (dashed line) and sum of soil + vegetation (total, green line). Landslide probability is highest at low elevations so the yield is highest there (a), but the total flux due to landslides is dominated by mid-elevations that comprise the majority of basin area (b). These estimates are for the forested portion of the valley only. See Figure S5.6 for estimates that include puna grasslands. c) Plant species richness (circles) from the Kosñipata forest plots as a function of elevation compared to landslide probability (red line).

The altitudinal trends demonstrate that landslide mobilization (t km^{-2} yr^{-1}) is most frequent at lower elevations (Figure 5.6a); while the area in the Kosñipata <1700 m comprises 10 % of the total catchment area, these elevations supply 16 % of the organic material mobilised by landslides. This is due to the high landslide frequencies at lower elevations (Figure 5.3a), and because total carbon stocks only increase slightly with an increase in elevation (Figure S5.5). The mid-elevations (2100 m to 3000 m) mobilise the majority (~54 %) of the organic material from valley hillslopes because these elevations cover the greatest proportion of total basin area (Figure 5.6b), consistent with findings elsewhere [*Hilton et al.*, 2011]. Thus, the heterogeneity of landslides means that mass-wasting processes preferentially over-sample the lower elevations in the Kosñipata, but the

total supply of organic material is still dominated by the elevation ranges that make up most of the catchment area.

5.4.5. Revegetation of landslide scars

The biomass and soil removed by landslides is replaced on hillslopes over time. The duration and dynamics of vegetation recovery are important because they influence vegetation structure and soil structure, provide habitat for various species, and play an integral role in nutrient cycling [*Bussmann et al.*, 2008; *Restrepo et al.*, 2009]. Revegetation was determined through an evaluation of complete canopy closure on landslide scars in a high resolution WorldView-2 image from 2011. There were signs of landslide recovery as soon as four years after landslide occurrence (Figure 5.4). From the linear regression in Figure 5.4, we estimated that 100 % of the landslide area of a given year recovered ~28 yrs after landslide occurrence. A very large landslide visible in an air photo from 1963 is still visible in 2011, indicating that very large landslides may take longer (> 48 years) to recover and repeat landsliding may complicate this analysis. In addition, revegetation time is considerably less than complete carbon stock recovery time. Thus vegetation recovery time of individual landslides can range from 4 to > 48 years (n = 145). In the Bolivian Andes the time required for complete revegetation of individual landslides has been estimated at 10 to 35 yrs based on dating trees on landslide scars and evaluating canopy closure in three aerial photographs spanning several decades [*Blodgett and Isacks*, 2007]. The revegetation time we have calculated in the Kosñipata Valley is consistent with the Bolivian sites, located in a similar montane forest of the same elevation range [*Blodgett and Isacks*, 2007].

Post-landslide vegetation modelling in the Ecuadorian Andes (1900-2100 masl) revealed that initial revegetation occurs within 80 years after a landslide, but it takes at least 200 years for the post-landslide forest to develop the biomass of a mature tropical montane forest [*Dislich and Huth*, 2012]. Thus, although most landslide scars in the Kosñipata Valley

recover quickly, it takes much longer, perhaps hundreds of years, to reach the full maturity of a tropical montane cloud forest. The timescale of this maturation process may be important when considering the impact of landslides on ecosystem dynamics and species diversity.

5.4.6. Influence of incision-driven hillslope steepening and failure on plant composition:

The repeated cycles of landslide activity followed by revegetation, which we have shown take place over timescales of ~10^1-10^2 yrs, generate a regular disturbance to the forest ecosystem. Rates of erosion (on the order of mm yr^{-1}) mean that the spatial variability in river incision and hillslope failure are expected to persist for a much longer duration (10^3 yr or more). Therefore, geomorphically-imposed gradients in forest disturbance are engrained for long periods of time. Previous work has suggested that landslide disturbance may play an important role in determining ecosystem function and diversity [*Restrepo et al.*, 2009]. Bedrock landslides can remove the entire standing biomass and soil from sections of forest [*Hilton et al.*, 2011] producing patches of bare rock that undergo 'quasi-primary' succession [*Restrepo et al.*, 2009]. This promotes movement of organisms and ecosystem reorganisation [*Hupp*, 1983; *Walker et al.*, 2013], while inhibiting ecosystem retrogression and nutrient depletion [*Peltzer et al.*, 2010]. On landslide surfaces in the Bolivian Andes, plant species richness increased from early to late succession and then could show a decline in very mature or senescent forests [*Kessler*, 1999].

A dense network of forest plots in the Kosñipata Valley [*Malhi et al.*, 2010] enables us to evaluate how landslide activity (Figure 5.3a) corresponds with trends in plant species richness over the scale at which we see strong gradients in forest disturbance by landsliding. To the first order, the spatial patterns in species richness – the number of plant species per 1 ha plot – is similar to changes in the frequency of landsliding (Figure 5.6c). Species richness is lowest at high elevations in the valley and increases slightly with decreasing elevation to 2000 m. There is then a large increase in species richness (from 80 to 180 species ha^{-1}) on

forested hillslopes between 2000 m and ~1700 m, coincident with the significant increase in landslide frequency in this zone (Figure 5.6c). At face value, this hints that landslide rates of landslide frequency might play a role in shaping forest ecosystem biodiversity, at least in terms of the range of habitats available at any elevation. A link between landslides and ecosystem structure has been proposed by *Restrepo et al.* [2009] among others [*Hupp*, 1983; *Kessler*, 1999; *Walker et al.*, 2013], but empirical evidence has thus far been lacking. One possibility is that our observations of coincident changes in landslide frequencies and species richness may be a manifestation of intermediate disturbance theory [*Connell*, 1978]. Landslides in the lower Kosñipata Valley can cause turnover of the entire biomass and soil structure within hundreds of years (Figure 5.2c), perhaps generating a level of disturbance that allows diversity at mid-elevations to be enhanced to values comparable to the famously diverse lowland Amazonian forests.

However, it is important to recognize that the Amazonian lowlands are highly diverse yet generally landslide-free, so landslide disturbance alone cannot explain overall patterns of diversity along the gradient from the Andes to the Amazon. Moreover, although the strong spatial coincidence in elevation trends of species richness and landslide frequency (Figure 5.6c) points to a possible link between erosional processes and biodiversity, there are other important climatic and ecological controls which play important roles in guiding diversity patterns within the Kosñipata Valley. Systematic changes in temperature or precipitation with elevation are expected to influence biodiversity [*Gaston*, 2000]. Though likely to play some role in the Kosñipata, these climatic parameters change continuously with elevation (Figure 5.5c) while the variation in species richness changes discontinuously, with a notable non-linear “kink” to higher species richness below 1700m elevation, mirroring the kink in landslide occurrence. There may be explanations for such a discontinuous trend in diversity other than landslide disturbance. The highly diverse zone at 1500-1700m coincides with a

transition between lowland/submontane species and montane cloud forest species, and one possibility is that the co-habitation of two biomes may be expected to significantly increase local diversity. However, such an increase would be expected to peak at the 1500-1700 m ecotone with declines on either side. A second possibility is that species diversity would be raised in central regions, as a result of the mid-domain hypothesis suggests, but this would not predict an abrupt change in diversity as observed by *Colwell and Lees* [2000]; *Kessler* [2009]. A third possibility is that the location of the cloud base or the end of the cloud immersion zone may suppress biodiversity in plant species at high elevations. The cloud immersion zone ends between 1600 masl and 1900 masl [*Horwath*, 2011; *Huaraca Huasco et al.*, 2013]. It is possible that cloud immersion supresses diversity at elevations >1700m. In other words, in the absence of the cloud base there might be a decline in species diversity with elevation, associated for example with changes in temperature. Hence, cloud immersion could in principle contribute to the observed 'kink' in the elevational trend in species diversity observed in the Kosñipata Valley.

It is difficult to conclusively distinguish the role of cloud immersion from that of landslide disturbance in guiding the observed diversity trends. The patterns we observe with elevation (Figure 5.6c) may reflect a combination of a complex mix of geomorphic, climatic and ecological factors. In any case, the indication within our data of links between tectonic uplift, fluvial incision, hillslope failure, and biological diversity should provide impetus for future studies of species diversity along geomorphically-imposed gradients of disturbance.

Heterogeneity would be expected in vegetation distribution in areas subject to landsliding because landslides occur on steep slopes, on a range of elevations and variation in climate, and these would naturally produce variation in habitats, known as environmental heterogeneity [*Dufour et al.*, 2006]. To test the importance of landslides in plant species richness and rule out other environmental factors, a further study would need to be carried out

on a landscape scale, possibly throughout the entire Eastern Andes, evaluating landslide frequency and plant diversity on and off of landslide scars. On site plant inventories, and hyperspectral imaging data and high resolution satellite imagery [*Broadbent et al.*, 2008] in regions of low and high landslide frequency may help identify the role that landslides play in plant species diversity at the landscape scale.

5.5. Conclusions

The spatial variability of landslides identified on the forested slopes of the Kosñipata Valley confirms that landslide activity increases substantially above a threshold slope angle at slopes >38 ° (up to 0.16 % yr^{-1}), and that high landslide frequencies track zones of high rates of bedrock river incision, characterised by a knickzone <1700 m in the river channel. Other factors including rainfall and seismic activity may be proximal triggers of landslides but do not appear to determine the decadal-scale landslide distribution in the Kosñipata Valley. The observed distribution of landslides illustrates that the propagation of erosion in a mountainous landscape takes place through channel incision that leads to hillslope failure.

This coupling has important ramifications not just for physical landscape evolution but also for linking the tectonic drivers of uplift and erosion with the biosphere. Observed co-variation of landslide activity and species richness in the Kosñipata raises the intriguing possibility that incision in response to tectonic uplift, and the landscape heterogeneity that it introduces, may guide species distributions and enhance biodiversity by providing a mosaic of niches for different species to thrive.

The spatial heterogeneity produced by erosional processes, which persists over timescales $>10^3$ years, imposes variability in the cycles of organic material mobilization and vegetation recovery on hillslopes, which occur over timescales of 10^1-10^2 years. The result is a pattern of spatially non-uniform sourcing of the organic material that is supplied to rivers.

In the Kosñipata Valley, high landslide activity at low elevations (<1700 m) means an oversampling of the hillslopes at these elevations (~16 % contribution to total organic matter mobilised from Kosñipata hillslopes) relative to their areal extent within the basin (<10 % total basin area). Such non-uniform sourcing has implications both for the preservation of organic carbon, and thus for the carbon budget of the montane forest, and for defining biomarker characteristics, many of which depend on elevation.

5.6. Acknowledgements

This paper is a product of the Andes Biodiversity and Ecosystems Research Group (ABERG). KEC was funded by the Natural Sciences and Engineering Research Council of Canada (NSERC) and Clarendon Fund PhD scholarships. AJW was supported to work in the Kosñipata by NSF-EAR 1227192 and RGH was supported by a NERC New Investigator Grant (NE/I001719/1). YM is supported by the Jackson Foundation and a European Research Council Advanced Investigator Grant. The Carnegie Airborne Observatory is made possible by the Avatar Alliance Foundation, Grantham Foundation for the Protection of the Environment, John D. and Catherine T. MacArthur Foundation, Gordon and Betty Moore Foundation, W. M. Keck Foundation, Margaret A. Cargill Foundation, Mary Anne Nyburg Baker and G. Leonard Baker Jr., and William R. Hearst III. We thank D. Knapp, T. Kennedy-Bowdoin, C. Anderson, and R. Tupayachi for CAO data collection and analysis; M. Palace for the QuickBird-2 satellite images; S. Abele for GIS advice; S. Feakins for comments prior to submission.

5.7. References

Asner, G. P., Knapp, D. E., Boardman, J., Green, R. O., Kennedy-Bowdoin, T., Eastwood, M., Martin, R. E., Anderson, C., and Field, C. B. (2012), Carnegie Airborne Observatory-2: Increasing science data dimensionality via high-fidelity multi-sensor fusion, *Remote Sensing of Environment, 124*(0), 454-465, doi: http://dx.doi.org/10.1016/j.rse.2012.06.012.

Bigi, A., Hasbargen, L. E., Montanari, A., and Paola, C. (2006), Knickpoints and hillslope failures: Interactions in a steady-state experimental landscape, in *Tectonics, Climate, and Landscape Evolution*, edited by S. D. Willett, N. Hovius, M. T. Brandon and D. M. Fisher, pp. 295-307, Geological Society of America, Boulder, Colorado, USA.

Blodgett, T. A., and Isacks, B. L. (2007), Landslide erosion rate in the eastern cordillera of northern Bolivia, *Earth Interactions, 11*, 1-30, doi: http://dx.doi.org/10.1175/2007EI222.1.

Bookhagen, B. (in review), High resolution spatiotemporal distribution of rainfall seasonality and extreme events based on a 12-year TRMM time series.

Broadbent, E. N., Asner, G. P., Peña-Claros, M., Palace, M., and Soriano, M. (2008), Spatial partitioning of biomass and diversity in a lowland Bolivian forest: Linking field and remote sensing measurements, *Forest Ecology and Management, 255*(7), 2602-2616, doi: http://dx.doi.org/10.1016/j.foreco.2008.01.044.

Burbank, D. W., Leland, J., Fielding, E., Anderson, R. S., Brozovic, N., Reid, M. R., and Duncan, C. (1996), Bedrock incision, rock uplift and threshold hillslopes in the northwestern Himalayas, *Nature, 379*(6565), 505-510.

Bussmann, R. W., Wilcke, W., and Richter, M. (2008), Landslides as important disturbance regimes - Causes and regeneration, in *Gradients in a tropical mountain ecosystem of Ecuador*, edited by E. Beck, J. Bendix, I. Kottke, F. Makeschin and R. Mosandl, pp. 321-330, Springer-Verlag, Berlin Heildelburg.

Cabrera, J., Sébrier, M., and Mercier, J. L. (1991), Plio-Quaternary geodynamic evolution of a segment of the Peruvian Andean Cordillera located above the change in the subduction geometry: The Cuzco region, *Tectonophysics, 190*(2), 331-362.

Carlotto Caillaux, V. S., Rodriguez, G., Fernando, W., Roque, C., Dionicio, J., and Chávez, R. (1996), Geología de los cuadrángulos de Urubamba y Calca, Instituto Geológica Nacional, Lima, Peru.

Carson, M. A., and Petley, D. J. (1970), The existence of threshold hillslopes in the denudation of the landscape, *Transactions of the Institute of British Geographers, 49*, 71-95.

Clark, K. E., Hilton, R. G., West, A. J., Malhi, Y., Gröcke, D. R., Bryant, C. L., Ascough, P. L., Robles Caceres, A., and New, M. (2013), New views on "old" carbon in the Amazon River: Insight from the source of organic carbon eroded from the Peruvian Andes, *Geochemistry, Geophysics, Geosystems, 14*(5), 1644-1659, doi: http://dx.doi.org/10.1002/ggge.20122.

Clark, M. K., Maheo, G., Saleeby, J., and Farley, K. A. (2005), The non-equilibrium landscape of the southern Sierra Nevada, California, *GSA TODAY, 15*(9), 4, doi: http://dx.doi.org/10:1130/1052-5173(2005)015<4:TNELOT>2.0.CO.

Colwell, R. K., and Lees, D. C. (2000), The mid-domain effect: geometric constraints on the geography of species richness, *Trends in Ecology & Evolution, 15*(2), 70-76, doi: http://dx.doi.org/10.1016/S0169-5347(99)01767-X.

Connell, J. H. (1978), Diversity in tropical rain forests and coral reefs, *Science*, *199*(4335), 1302-1310.

Consbio (2011), Ecosistemas Terrestres de Peru (Data Basin Dataset) for ArcGIS, edited by The Nature Conservancy/NatureServe.

Cook, K. L., Whipple, K. X., Heimsath, A. M., and Hanks, T. C. (2009), Rapid incision of the Colorado River in Glen Canyon–insights from channel profiles, local incision rates, and modeling of lithologic controls, *Earth Surface Processes and Landforms, 34*(7), 994-1010, doi: http://dx.doi.org/10.1002/esp.1790.

Crosby, B. T., and Whipple, K. X. (2006), Knickpoint initiation and distribution within fluvial networks: 236 waterfalls in the Waipaoa River, North Island, New Zealand, *Geomorphology, 82*(1–2), 16-38, doi: http://dx.doi.org/10.1016/j.geomorph.2005.08.023.

Densmore, A. L., and Hovius, N. (2000), Topographic fingerprints of bedrock landslides, *Geology, 28*(4), 371-374, doi: http://dx.doi.org/10.1130/0091-7613(2000)28<371:TFOBL>2.0.CO;2

Dislich, C., and Huth, A. (2012), Modelling the impact of shallow landslides on forest structure in tropical montane forests, *Ecological Modelling, 239*, 40-53, doi: http://dx.doi.org/10.1016/j.ecolmodel.2012.04.016.

Dufour, A., Gadallah, F., Wagner, H. H., Guisan, A., and Buttler, A. (2006), Plant species richness and environmental heterogeneity in a mountain landscape: effects of variability and spatial configuration, *Ecography, 29*(4), 573-584, doi: http://dx.doi.org/10.1111/j.0906-7590.2006.04605.x.

Feakins, S. J., Eglinton, T. I., and deMenocal, P. B. (2007), A comparison of biomarker records of northeast African vegetation from lacustrine and marine sediments (ca. 3.40 Ma), *Organic Geochemistry, 38*(10), 1607-1624, doi: http://dx.doi.org/10.1016/j.orggeochem.2007.06.008.

Gallen, S. F., Wegmann, K. W., Frankel, K. L., Hughes, S., Lewis, R. Q., Lyons, N., Paris, P., Ross, K., Bauer, J. B., and Witt, A. C. (2011), Hillslope response to knickpoint migration in the Southern Appalachians: implications for the evolution of post-orogenic landscapes, *Earth Surface Processes and Landforms, 36*(9), 1254-1267, doi: http://dx.doi.org/10.1002/esp.215.

Galy, V., and Eglinton, T. (2011), Protracted storage of biospheric carbon in the Ganges-Brahmaputra basin, *Nature Geoscience, 4*(12), 843-847, doi: http://dx.doi.org/10.1038/ngeo1293.

Gaston, K. J. (2000), Global patterns in biodiversity, *Nature, 405*(6783), 220-227, doi: http://dx.doi.org/10.1038/35012228.

Giaconia, F., Booth-Rea, G., Martínez-Martínez, J., Azañón, J., and Pérez-Peña, J. (2012), Geomorphic analysis of the Sierra Cabrera, an active pop-up in the constrictional domain of conjugate strike-slip faults: The Palomares and Polopos fault zones (eastern Betics, SE Spain), *Tectonophysics*, doi: http://dx.doi.org/10.1016/j.tecto.2012.08.028.

Gibbon, A., Silman, M. R., Malhi, Y., Fisher, J. B., Meir, P., Zimmermann, M., Dargie, G. C., Farfan, W. R., and Garcia, K. C. (2010), Ecosystem carbon storage across the grassland-forest

transition in the high Andes of Manu National Park, Peru, *Ecosystems, 13*(7), 1097-1111, doi: http://dx.doi.org/10.1007/s10021-010-9376-8.

Girardin, C. A. J., Aragão, L. E. O. C., Malhi, Y., Huaraca Huasco, W., Metcalfe, D. B., Durand, L., Mamani, M., Silva-Espejo, J. E., and Whittaker, R. J. (2013a), Fine root dynamics along an elevational gradient in tropical Amazonian and Andean forests, *Global Biogeochemical Cycles*, doi: http://dx.doi.org/10.1029/2011GB004082.

Girardin, C. A. J., Silva-Espejo, J. E., Doughty, C. E., Huaraca Huasco, W., Metcalfe, D. B., Durand-Baca, L., Marthews, T. R., Aragao, L. E. O. C., Farfan Rios, W., García Cabrera, K., Halladay, K., Fisher, J. B., Galiano-Cabrera, D. F., Huaraca-Quispe, L. P., Alzamora-Taype, I., Equiluz-Mora, L., Salinas-Revilla, N., Silman, M., Meir, P., and Malhi, Y. (2013b), Productivity and carbon allocation in a tropical montane cloud forest of the Peruvian Andes, *Plant Ecology and Diversity, 7*(1-2), 107-123, doi: http://dx.doi.org/10/1080/17550874.2013.820222.

Gregory-Wodzicki, K. M. (2000), Uplift history of the Central and Northern Andes: a review, *Geological Society of America Bulletin, 112*(7), 1091-1105, doi: http://dx.doi.org/10.1130/0016-7606(2000)112<1091:UHOTCA>2.0.CO;2

Gurdak, D. J., Aragao, L. E. O. C., Rozas-Dávila, A., Huaraca Huasco, W., García Cabrera, K., Doughty, C. E., Farfan-Rios, W., Silva-Espejo, J. E., Metcalfe, D. B., Silman, M. R., and Malhi, Y. (2013), Assessing above-ground woody debris dynamics along a gradient of elevation in Amazonian cloud forests in Peru: balancing above-ground inputs and respriation outputs, *Plant Ecology and Diversity, 7*(1-2), 143-160, doi: http://dx.doi.org/10.1080/17550874.2013.818073.

Halladay, K., Malhi, Y., and New, M. (2012), Cloud frequency climatology at the Andes/Amazon transition: 1. Seasonal and diurnal cycles, *Journal of geophysical research, 117*, D23102, doi: http://dx.doi.org/10.1029/2012JD017770.

Harp, E. L., and Keefer, D. K. (1990), Landslides triggered by the earthquake, *United States Geological Survey, Professional Paper;(USA), 1487*.

Hilton, R. G., Galy, A., Hovius, N., Chen, M.-C., Horng, M.-J., and Chen, H. (2008), Tropical-cyclone-driven erosion of the terrestrial biosphere from mountains, *Nature Geoscience, 1*(11), 759-762, doi: http://dx.doi.org/10.1038/ngeo333.

Hilton, R. G., Meunier, P., Hovius, N., Bellingham, P. J., and Galy, A. (2011), Landslide impact on organic carbon cycling in a temperate montane forest, *Earth Surface Processes and Landforms, 36*(12), 1670-1679, doi: http://dx.doi.org/10.1002/esp.2191.

Horwath, A. (2011), Epiphytic bryophytes as cloud forest indicators: Stable isotopes, biomass and diversity along an altitudinal gradient in Peru, 260 pp, Plant Sciences, University of Cambridge, Cambridge.

Hovius, N., Stark, C. P., Chu, H. T., and Lin, J. C. (2000), Supply and removal of sediment in a landslide-dominated mountain belt: Central Range, Taiwan, *Journal of Geology, 108*(1), 73-89, doi: http://dx.doi.org/10.1086/314387.

Hovius, N., Meunier, P., Lin, C.-W., Chen, H., Chen, Y.-G., Dadson, S., Horng, M.-J., and Lines, M. (2011), Prolonged seismically induced erosion and the mass balance of a large earthquake, *Earth and Planetary Science Letters, 304*(3), 347-355, doi: http://dx.doi.org/10.1016/j.epsl.2011.02.005.

Howard, A. D. (1994), A detachment-limited model of drainage basin evolution, *Water Resources Research*, *30*(7), 2261-2285.

Huaraca Huasco, W., Girardin, C. A. J., Doughty, C. E., Metcalfe, D. B., Baca, L. D., Silva-Espejo, J. E., Cabrera, D. G., Aragão, L. E. O., Davila, A. R., Marthews, T. R., Huaraca-Quispe, L. P., Alzamora-Taype, I., Eguiluz-Mora, L., Farfan-Rios, W., Cabrera, K. G., Halladay, K., Salinas-Revilla, N., Silman, M., Meir, P., and Malhi, Y. (2013), Seasonal production, allocation and cycling of carbon in two mid-elevation tropical montane forest plots in the Peruvian Andes, *Plant Ecology and Diversity*, *7*(1-2), doi: http://dx.doi.org/10.1080/17550874.2013.819042.

Hupp, C. R. (1983), Seedling establishment on a landslide site, *Castanea*, *48*(2), 89-98.

INGEMMET (2013), GEOCATMIN - Geologia integrada por proyectos regionales, edited by Instituto Geológico Minero Metalúrgico.

Keefer, D. K. (2002), Investigating landslides caused by earthquakes–a historical review, *Surveys in Geophysics*, *23*(6), 473-510.

Kessler, M. (1999), Plant species richness and endemism during natural landslide succession in a perhumid montane forest in the Bolivian Andes, *Ecotropica*, *5*, 123-136.

Kessler, M. (2009), The impact of population processes on patterns of species richness: lessons from elevational gradients, *Basic and applied Ecology*, *10*(4), 295-299, doi: http://dx.doi.org/10.1016/j.baae.2008.10.006.

Korup, O. (2005), Distribution of landslides in southwest New Zealand, *Landslides*, *2*(1), 43-51, doi: http://dx.doi.org/10.1007/s10346-004-0042-0.

Korup, O., Schmidt, J., and McSaveney, M. J. (2005), Regional relief characteristics and denudation pattern of the western Southern Alps, New Zealand, *Geomorphology*, *71*(3), 402-423, doi: http://dx.doi.org/10.1016/j.geomorph.2005.04.013.

Korup, O. (2006), Rock-slope failure and the river long profile, *Geology*, *34*(1), 45-48, doi: http://dx.doi.org/10.1130/G21959.1.

Korup, O., and Schlunegger, F. (2007), Bedrock landsliding, river incision, and transience of geomorphic hillslope-channel coupling: Evidence from inner gorges in the Swiss Alps, *Journal of Geophysical Research: Earth Surface (2003–2012)*, *112*(F3), doi: http://dx.doi.org/10.1029/2006JF000710.

Korup, O., Densmore, A. L., and Schlunegger, F. (2010), The role of landslides in mountain range evolution, *Geomorphology*, *120*(1), 77-90, doi: http://dx.doi.org/10.1016/j.geomorph.2009.09.017.

Larsen, I. J., and Montgomery, D. R. (2012), Landslide erosion coupled to tectonics and river incision, *Nature Geoscience*, *5*(7), 468-473, doi: http://dx.doi.org/10.1038/ngeo1479.

Lavé, J., and Avouac, J. (2001), Fluvial incision and tectonic uplift across the Himalayas of central Nepal, *Journal of Geophysical Research: Solid Earth (1978–2012)*, *106*(B11), 26561-26591, doi: http://dx.doi.org/10.1029/2001JB000359.

Lin, G.-W., Chen, H., Hovius, N., Horng, M.-J., Dadson, S., Meunier, P., and Lines, M. (2008), Effects of earthquake and cyclone sequencing on landsliding and fluvial sediment transfer in a mountain catchment, *Earth Surface Processes and Landforms*, *33*(9), 1354-1373, doi: http://dx.doi.org/10.1002/esp.1716.

Malamud, B. D., Turcotte, D. L., Guzzetti, F., and Reichenbach, P. (2004), Landslide inventories and their statistical properties, *Earth Surface Processes and Landforms*, *29*(6), 687-711, doi: http://dx.doi.org/10.1002/esp.1064.

Malhi, Y., Silman, M., Salinas, N., Bush, M., Meir, P., and Saatchi, S. (2010), Introduction: Elevation gradients in the tropics: laboratories for ecosystem ecology and global change research, *Global Change Biology*, *16*(12), 3171-3175, doi: http://dx.doi.org/10.1111/j.1365-2486.2010.02323.x.

Marengo, J. A., Soares, W. R., Saulo, C., and Nicolini, M. (2004), Climatology of the low-level jet east of the Andes as derived from the NCEP-NCAR reanalyses: Characteristics and temporal variability, *Journal of climate*, *17*(12), 2261-2280.

Mendívil Echevarría, S., and Dávila Manrique, D. (1994), Geología de los cuadrángulos de Cuzco y Livitaca, Instituto Geológica Nacional, Lima, Peru.

Meunier, P., Hovius, N., and Haines, J. A. (2008), Topographic site effects and the location of earthquake induced landslides, *Earth and Planetary Science Letters*, *275*(3), 221-232, doi: http://dx.doi.org/10.1016/j.epsl.2008.07.020.

Montgomery, D. R. (2001), Slope distributions, threshold hillslopes, and steady-state topography, *American Journal of Science*, *301*(4-5), 432-454, doi: http://dx.doi.org/10.2475/ajs.301.4-5.432.

Peltzer, D. A., Wardle, D. A., Allison, V. J., Baisden, W. T., Bardgett, R. D., Chadwick, O. A., Condron, L. M., Parfitt, R. L., Porder, S., and Richardson, S. J. (2010), Understanding ecosystem retrogression, *Ecological Monographs*, *80*(4), 509-529, doi: http://dx.doi.org/10.1890/09-1552.1.

Raich, J. W., Russell, A. E., and Vitousek, P. M. (1997), Primary productivity and ecosystem development along an elevational gradient on Mauna Loa, Hawai'i, *Ecology*, *78*(3), 707-721.

Raich, J. W., Russell, A. E., Kitayama, K., Parton, W. J., and Vitousek, P. M. (2006), Temperature influences carbon accumulation in moist tropical forests, *Ecology*, *87*(1), 76-87, doi: http://dx.doi.org/10.1890/05-0023.

Ramos Scharrón, C. E., Castellanos, E. J., and Restrepo, C. (2012), The transfer of modern organic carbon by landslide activity in tropical montane ecosystems, *Journal of Geophysical Research: Biogeosciences (2005–2012)*, *117*(G3), doi: http://dx.doi.org/10.1029/2011JG001838.

Rao, Y. (2011), Variation in plant carbon and nitrogen isotopes along an altitudinal gradient in the Peruvian Andes, B.Sc. thesis, 60 pp, Department of Earth Sciences, Durham University, Durham.

Rapp, J. M. (2010), Climate control on plant performance across an Andean altitudinal gradient, pp, Deptartment of Biology, Wake Forest University, Winston-Salem, North Carolina.

Restrepo, C., Vitousek, P., and Neville, P. (2003), Landslides significantly alter land cover and the distribution of biomass: an example from the Ninole ridges of Hawai'i, *Plant Ecology, 166*(1), 131-143, doi: http://dx.doi.org/10.1023/A:1023225419111.

Restrepo, C., and Alvarez, N. (2006), Landslides and their contribution to land-cover change in the mountains of Mexico and Central America, *Biotropica, 38*(4), 446-457, doi: http://dx.doi.org/10.1111/j.1744-7429.2006.00178.x.

Restrepo, C., Walker, L. R., Shiels, A. B., Bussmann, R., Claessens, L., Fisch, S., Lozano, P., Negi, G., Paolini, L., and Poveda, G. (2009), Landsliding and its multiscale influence on mountainscapes, *Bioscience, 59*(8), 685-698, doi: http://dx.doi.org/10.1525/bio.2009.59.8.10.

Rodrıguez, C., Bommer, J., and Chandler, R. (1999), Earthquake-induced landslides: 1980–1997, *Soil Dynamics and Earthquake Engineering, 18*(5), 325-346, doi: http://dx.doi.org/10.1016/S0267-7261(99)00012-3.

Saatchi, S. S., Harris, N. L., Brown, S., Lefsky, M., Mitchard, E. T., Salas, W., Zutta, B. R., Buermann, W., Lewis, S. L., and Hagen, S. (2011), Benchmark map of forest carbon stocks in tropical regions across three continents, *Proceedings of the National Academy of Sciences, 108*(24), 9899-9904, doi: http://dx.doi.org/10.1073/pnas.1019576108.

Scheel, M. L. M., Rohrer, M., Huggel, C., Santos Villar, D., Silvestre, E., and Huffman, G. J. (2011), Evaluation of TRMM Multi-satellite Precipitation Analysis (TMPA) performance in the Central Andes region and its dependency on spatial and temporal resolution, *Hydrology and Earth System Sciences, 15*(8), 2649-2663, doi: http://dx.doi.org/10.5194/hess-15-2649-2011.

Sébrier, M., Mercier, J. L., Mégard, F., Laubacher, G., and Carey-Gailhardis, E. (1985), Quaternary normal and reverse faulting and the state of stress in the central Andes of south Peru, *Tectonics, 4*(7), 739-780.

SENAMHI (2012), Clima: Datos históricos Peru, edited, Servicio Nacional de Meteorologia e Hidrologia del Peru, Lima, Peru.

Sheldon, N. D., and Tabor, N. J. (2009), Quantitative paleoenvironmental and paleoclimatic reconstruction using paleosols, *Earth-Science Reviews, 95*(1), 1-52, doi: http://dx.doi.org/10.1016/j.earscirev.2009.03.004.

Silgado, E. (1978), Historia de los sismos más notables ocurridos en el Perú (1513-1974)*Rep.*, Sector Engería y Minas, Instituto de Geología y Minería, Lima, Republica del Perú.

Stark, C. P., and Hovius, N. (2001), The characterization of landslide size distributions, *Geophysical Research Letters, 28*(6), 1091-1094, doi: http://dx.doi.org/10.1029/2000GL008527.

Stoyan, R. (2000), Aktivität, Ursachen und Klassifikation der Rutschungen in San Francisco/Süd Ecuador, pp, University of Erlangen-Nuremberg, Germany.

Tavera, H., and Buforn, E. (2001), Source mechanism of earthquakes in Perú, in *Journal of Seismology*, edited, pp. 519-540.

Terzaghi, K. (1951), *Mechanism of landslides*, Harvard University, Department of Engineering, Cambridge, Massachusetts.

Tibaldi, A., Ferrari, L., and Pasquarè, G. (1995), Landslides triggered by earthquakes and their relations with faults and mountain slope geometry: an example from Ecuador, *Geomorphology*, *11*(3), 215-226.

USGS (2013), Earthquakes v3.6, 2013-07-02, in *USGS Earthquake Hazards Program*, edited by United States Geological Survey, USGS.

Vargas Vilchez, L., and Hipolito Romero, A. (1998), Geología de los cuadrángulos de Río Pinquén, Pilcopata y Chontachaca. Hojas: 25-t, 26-t y 27-t, Instituto Geológica Nacional, Lima, Peru.

Walker, L. R., Shiels, A. B., Bellingham, P. J., Sparrow, A. D., Fetcher, N., Landau, F. H., and Lodge, D. J. (2013), Changes in abiotic influences on seed plants and ferns during 18 years of primary succession on Puerto Rican landslides, *Journal of Ecology*, *101*(3), 650-661, doi: http://dx.doi.org/10.1111/1365-2745.12071.

Wang, G., and Sassa, K. (2003), Pore-pressure generation and movement of rainfall-induced landslides: effects of grain size and fine-particle content, *Engineering geology*, *69*(1), 109-125, doi: http://dx.doi.org/10.1016/S0013-7952(02)00268-5.

West, A. J., Lin, C. W., Lin, T. C., Hilton, R. G., Liu, S. H., Chang, C. T., Lin, K. C., Galy, A., Sparkes, R. B., and Hovius, N. (2011), Mobilization and transport of coarse woody debris to the oceans triggered by an extreme tropical storm, *Limnology and Oceanography*, *56*(1), 77-85, doi: http://dx.doi.org/10.4319/lo.2011.56.1.0077.

Whipple, K. X., and Tucker, G. E. (1999), Dynamics of the stream-power river incision model: Implications for height limits of mountain ranges, landscape response timescales, and research needs, *Journal of Geophysical Research: Solid Earth (1978–2012)*, *104*(B8), 17661-17674, doi: http://dx.doi.org/10.1029/1999JB900120.

Whipple, K. X. (2001), Fluvial landscape response time: How plausible is steady-state denudation?, *American Journal of Science*, *301*(4-5), 313-325, doi: http://dx.doi.org/10.2475/ajs.301.4-5.313.

Whipple, K. X. (2004), Bedrock rivers and the geomorphology of active orogens, *Annual Review of Earth Planetary Science*, *32*, 151-185, doi: http://dx.doi.org/10.1146/annurev.earth.32.101802.120356.

Whittaker, A. C., Cowie, P. A., Attal, M., Tucker, G. E., and Roberts, G. P. (2007), Bedrock channel adjustment to tectonic forcing: Implications for predicting river incision rates, *Geology*, *35*(2), 103-106, doi: http://dx.doi.org/10.1130/G23106A.1.

Willett, S. D., and Brandon, M. T. (2002), On steady states in mountain belts, *Geology*, *30*(2), 175-178, doi: http://dx.doi.org/10.1130/0091-7613(2002)030<0175:OSSIMB>2.0.CO;2.

Wittmann, H., von Blanckenburg, F., Maurice, L., Guyot, J.-L., Filizola, N., and Kubik, P. W. (2011), Sediment production and delivery in the Amazon River basin quantified by in situ-produced cosmogenic nuclides and recent river loads, *Geological Society of America Bulletin*, *123*(5-6), 934-950, doi: http://dx.doi.org/10.1130/b30317.1.

Chapter 5: Supplementary information:
Fluvial incision links landslides, carbon transfer and plant diversity in an Andean Valley

Kathryn E. Clark[1*], A. Joshua West[2], Robert G. Hilton[3], Gregory P. Asner[4], Miles R. Silman[5], Sassan S. Saatchi[6], Carlos A. Quesada[7], William Farfan Rios[5], Roberta E. Martin[4], Mark New[1,8] and Yadvinder Malhi[1]

S5.1. Materials and methods

S5.1.1. Landslide mapping

In this study we focus on the forested regions of the valley in order to understand the impact that landslides have on the mobilization of organic material and on plant composition of the tropical montane forest. The timberline (highest elevation of continual forest) was mapped using orthorectified pan-sharpened Quickbird-2 imagery from 2009, with resolution of 2.4 m x 2.4 m, to exclude regions above the timberline (Figures 5.1a & 5.2). Forest landslides were mapped over a 25-year period from 1988 to 2012 using Landsat 5 (Landsat Thematic Mapper) and Landsat 7 (Landsat Enhanced Thematic Mapper Plus) satellite images in ArcGIS (Figure 5.2a). All of the images were acquired in the dry season from May to October (Table S5.1). Landsat images were processed with a Standard Terrain Correction (Level 1T) which consists of systematic radiometric and geometric processing using ground control points and a digital elevation model (DEM) for ortho-georectification [*USGS*, 2013]. Ground control points are from the Global Land Survey 2010 (GLS2010) with Shuttle Radar Topography Mission (SRTM) as a digital surface model (DSM) source [*USGS*, 2013]. Landslide boundaries were delineated using a number of pan-sharpened, high resolution Quickbird-2 and WorldView-2 satellite images with resolutions of 2.4 m x 2.4 m and 2 m x 2 m, respectively with images from 2005, 2009, 2010 and 2011. The landslide inventory was produced by manually mapping landslide scars and their deposits by visually comparing

images from one year to the next evaluating contrasting colour changes suggesting a landslide had occurred. The Landsat landslides were verified in the high resolution Quickbird-2 and WorldView-2 images. A composite image of Landsat bands 5 (near-infrared, 1.55-1.75 μm), 3 (visible red, 0.63-0.69 μm) and 7 (mid-infrared, 2.08-2.35 μm) was used as recommended by Blodgett and Isacks [2007] in order to identify landslide scars with the greatest spectral difference to cloud forest. Bedrock outcrops are minimal in the valley and thus not subject to mislabelling as landslides. There were 38 usable images over the 25-year period, with 1-3 available per year (Table S5.1). To determine whether landslides mapped from the first years of the catalogue occurred before 1988 we used aerial photographs which covered the study area from 1963 and 1988. These images revealed several landslides identified in the early images which occurred before 1988 so these were categorised in the inventory as being pre-1988 events. Because of their uncertain dates, these pre-1988 events were not considered in the analysis.

S5.1.2. Landsat imagery limitations

The major benefit of Landsat imagery is the availability of at least one image per year throughout the 25-year period of study (Table S5.1), such that we were able to date landslides and determine landslide rates and turnover time for the Kosñipata Valley over a multi-decade time window. However there are several disadvantages of using Landsat imagery, including relatively low resolution and thus exclusion of small landslides, and visibility interference (e.g. topographic shadow, cloud shadow, and no-data gaps).

Table S5.1: Landsat images used and their visibility of the study area

#	Year	day/month	Landsat satellite	% Visibility
1	1988	22/06	5	61
2	1988	25/06	5	74
3	1989	27/07	5	72
4	1990	02/10	5	72
5	1991	01/07	5	74
6	1991	17/07	5	71
7	1992	30/04	5	35
8	1993	04/06	5	72
9	1994	25/07	5	54
10	1995	09/05	5	66
11	1996	12/06	5	70
12	1996	17/07	5	70
13	1997	18/08	5	46
14	1998	04/07	5	55
15	1999	21/06	5	69
16	1999	07/07	5	72
17	2000	23/06	5	68
18	2001	09/05	5	49
19	2002	20/05	7	42
20	2003	19/05	5	59
21	2004	18/06	7	49
22	2004	13/08	7	50
23	2004	05/08	5	59
24	2005	15/07	7	50
25	2006	15/05	7	65
26	2007	22/08	7	58
27	2007	26/05	5	59
28	2007	06/08	7	51
29	2008	06/06	7	62
30	2009	19/08	5	56
31	2010	06/08	5	68
32	2011	06/06	5	40
33	2011	02/09	7	32
24	2012	02/07	7	36

(i) Low resolution. The resolution of the Landsat imagery is 30 m x 30 m, which is too low to delineate individual landslides accurately in this small catchment. To address this problem, we used higher resolution satellite images to help delineate the landslide areas. Quickbird-2 and WorldView-2 satellite images covering the whole study area ranging within 2005 to 2011 were used for this purpose. We used pan-sharpened images with resolutions of 2.4 m x 2.4 m for Quickbird-2 and 2 m x 2 m for the WorldView-2. There were several benefits to using high resolution images to map out the landslide area. The main reason is

because landslides on a Landsat image would suggest a larger area than on higher resolution imagery. This is because the dominant reflectance of bare ground dominates the grid cell even if the landslide did not cover the entire cell. Another benefit is that when there were small or clumped landslides the high resolution imagery allowed us to accurately separate and identify each landslide.

(ii) Small landslides. The relative importance of small, unmapped landslides was can be accessed using the difference between the frequency-area distribution between the Landsat-derived landslides and higher resolution satellite images. Small landslides ~2 x 2 pixels (area < 400m^2) were too small to be picked up by the low resolution Landsat imagery and may not be fully accounted for [*Stark and Hovius*, 2001]. Small landslides are visible in the high resolution imagery, but since they were not evident on the Landsat images and therefore their ages could not be determined, they were left out of this analysis. Mapping all of the landslides in the high resolution (Quickbird-2 and WorldView-2) images could circumvent this problem, but only a few of these images are currently available, and they do not cover the extended period of the Landsat imagery that is important for our analysis. The relative importance of the small landslides that have not been included in our mapping can be estimated from the frequency-area distribution. The Kosñipata landslide dataset broadly follows a frequency-area distribution that is generally characteristic of landslides from other regions (*Malamud et al.* [2004] and references therein), with a long tail described by a power law (Figure S5.1). However there is a slight tendency towards underestimating smaller landslide abundance relative to other landslide inventories [*Malamud et al.*, 2004]. Some of this may reflect real differences in the Kosñipata landslide distribution, perhaps due to lithology, climate, or other factors [*Stark and Hovius*, 2001]. If we assume that all of the observed difference is due to missing small landslides because of the low resolution of the Landsat imagery, we can place an estimated upper bound on how much missing landslide

area this represents. This would imply that the total catchment-wide landslide area was underestimated by at most <5 % due to missing small landslides.

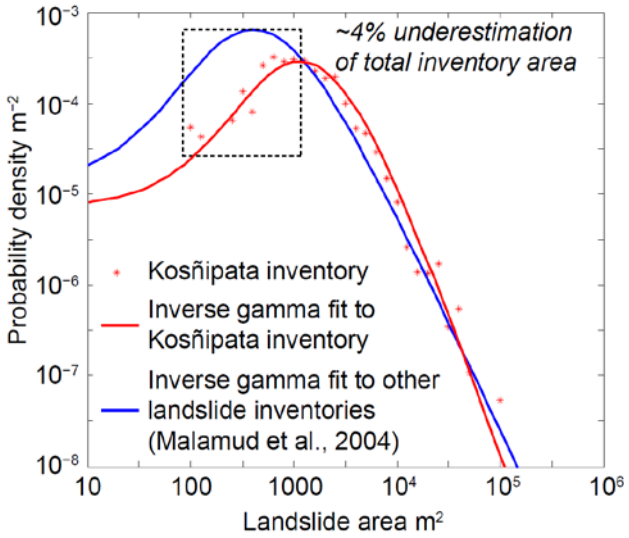


Figure S5.1: Frequency-magnitude curve for landslide areas from the Kosñipata landslide inventory (stars) with an inverse gamma function fit by maximum likelihood estimation (red line). The best fit parameters for the Kosñipata Valley following the three-parameter inverse-gamma probability distribution in equation 3 in *Malamud et al.* [2004] are p = 2.18, a = 5.18 x 10^3 m^2, s = -478 m^2. The total area of "missing" small-area landslides in the Kosñipata inventory was determined based on the difference between the gamma fit from *Malamud et al.* [2004] (blue line), and the Kosñipata fit, converted to a total area (red line). Based on this comparison, underestimation of the total landslide inventory area for the Kosñipata was calculated as 4 % of the total area (0.125 km^2). The use of the inverse gamma distribution is empirical, and there is no *a priori* reason why the fit to the Kosñipata inventory should have the same parameters as other landslide datasets [*Malamud et al.*, 2004]. Nonetheless, this comparison gives a reasonable estimate of the scale of uncertainty introduced by the use of Landsat imagery, and indicates that for the purposes of this study our methods are justified, with high resolution landslide mapping not being necessary.

(iii) Visibility interference. The areal proportion of visibility of the images had a mean of 59 % and varied between 35 % and 74 % (Table S5.1) with the remaining part of the image obscured by topographic shadow, clouds, cloud shadows, or no-data gaps associated with the damage to the Landsat 7 satellite Scan-Line-Corrector in 2003. Topographic shadow, composed of consistent shadow cast on the mountain-side, due to the angle of the sun at the time of image acquisition, affected a minimum of ~23 % of the study site in each Landsat

image. Topographic shadow affected southwest facing slopes (223 ± 52 °). We determined that the Landsat topographic shadow covered 35 km^2 (out of 150 km^2) by calculating the minimal overlapping topographic shadow coverage in cloudless images (n = 4). Any landslide area that fell within this area was not visible in the Landsat imagery. Since we could not accurately map the regions which fell under the Landsat topographic shadow we took the following approaches: (i) to determine landslide rates and slope turnover we corrected for the topographic shadowed area, and (ii) to determine landslide probability and proportion we considered only the visible (non-topographic shadow) area for this analysis. The remaining part of the image obscured by cloud shadow (clouds and cloud shadow) or no-data gaps accounted for ~18 % reduction in visibility ranging from ~3 % to 42 %. In addition, to account for cloud shadow and no-data strips we took a minimal approach and assumed that landslides that occurred in one year, but were obscured, would have been mapped in a subsequent year when visibility was improved. This has some impact in our inter-annual landslide results where clearer images may result in more landslides mapped (Figure S5.2). However, reduced visibility due to cloud shadow and no-data Landsat 7 striping since 2003 which affected ~10 images of which >25 % of the image was obscured (25-45 %; with topographic shadow totalling ~50-70 %; Table S5.1). Because of the high temporal resolution of images in this study (cf. *Hovius et al.* [1997]), with duplicate or triplicate images in some years, it is likely that landslides were spotted within a year of their occurrence if obscured by cloud shadow or no-data strips.

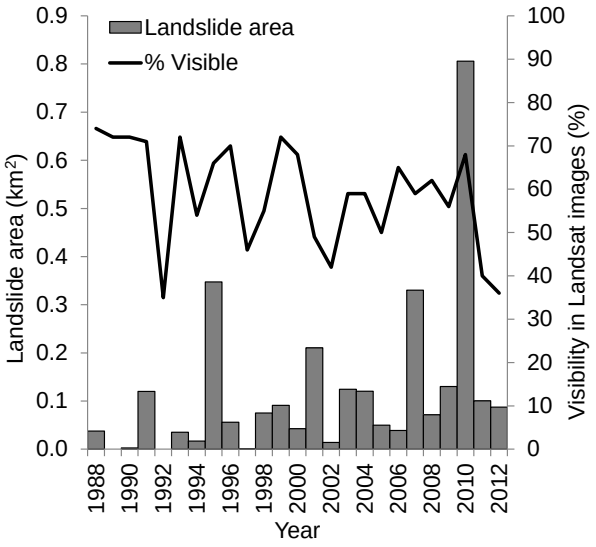


Figure S5.2: Landslide area (km^2) per year and variability in visible coverage for the 36 Landsat images used, where the maximum visibility was determined for years with multiple images. 2010 had most landslide activity due to a large storm March 4th 2010.

S5.1.3. Landslide frequencies and turnover

We calculated landslide frequency (L_f, % yr^{-1}) and slope turnover (τ_{ls}, yr) by 1km^2 grid cells (Figure 5.2b & c). First, we accounted for portions of cells obscured by topographic shadow. To do this we assumed that in each grid cell the visible area ('forested area') was representative of the area that was under topographic shadow ('topographic shadow area'). Thus, for each cell we determined the fraction under topographic shadow ($F_{topographic\ shadow}$) and fraction covered by landslide ($F_{landslide}$) in order to determine the corrected fraction of landslide ($F_{landslide\ corrected}$) and corrected landslide area (Equations S1 to S4). Thus the fraction of landslide area in each cell did not change, and the landslide area was corrected using the quantification of the fraction of the cell covered by topographic shadow. This approach should lead to no systematic under or over-estimation of landslide activity. Grid cells where >50 % of the area was covered by topographic shadow ($F_{topographic\ shadow}$) were excluded from this calculation to avoid unnecessary extrapolation and those cells were discounted from the analysis.

$$F_{landslide} = \frac{landslide\ area}{forest\ area} \quad (S1)$$

$$F_{topographic\ shadow} = \frac{topographic\ shadow\ area}{forest\ area} \quad (S2)$$

$$F_{landslide\ corrected} = \frac{F_{landslide}}{\left(1 - F_{topotraphic\ shadow}\right)^2} \quad (S3)$$

$$corrected\ landslide\ area = landslide\ area \times F_{landslide\ corrected} + landslide\ area \quad (S4)$$

Landslide frequency as a fraction (L_f, occurrence yr^{-1}) were calculated based on the total corrected landslide area divided by the total forested area and divided by 25 years (the length of the study) and then multiplied by 100 to get a landslide frequency as a percentage (L_f, % yr^{-1}; Equations S5 & S6).

$$\frac{landslide\ freq.}{year} = \frac{corrected\ landslide\ area}{forest\ area} \times \frac{1}{25\ years} \quad (S5)$$

$$landslide\ freq.\left(L_f\ \frac{\%}{yr}\right) = 100 \times \left(\frac{landslide\ freq.}{year}\right) \quad (S6)$$

Slope turnover due to landsliding (τ_{ls}, yr) was calculated as the inverse of landslide frequency (Equation S7). This reflects the time required for landslides to impact all of the landscape based on their rate of occurrence, in analogy with other studies [*Restrepo et al.*, 2009; *Hilton et al.*, 2011]. We calculated landslide frequency and turnover with this method rather than on an annual basis due to the reduction of visibility in several of the images due to cloud shadow and no-data stripes (as discussed in section S1.2).

$$Slope\ turnover\ (\tau_{ls}, \mathrm{yr}) = \frac{year}{landslide\ freq.} \quad (S7)$$

S5.1.4. Landslide probability

To determine landslide probability (P_{ls}) and landslide proportion each landslide was subdivided into 3 m x 3 m cells (the resolution the DEM [*Asner et al.*, 2012], see the following section), and proportion (Equations S8 & S9) and probability (Equation S10) were determined as a function of elevation (by 300 masl intervals, Figure 5.3a) and of slope (by 1 ° intervals, Figure 5.3b). ArcGIS was used following published approaches [*Meunier et al.*, 2008]. Slopes <20 ° were removed because of artefacts due to landslide deposits on low slope surfaces.

$$Basin\ proportion = \frac{basin\ pixel\ count}{total\ basin\ pixel\ count} \quad (S8)$$

$$Landslide\ proportion\ = \frac{landslide\ pixel\ count}{total\ landslide\ pixel\ count} \quad (S9)$$

$$Landslide\ probability\ \%\ (P_{ls}) = \frac{Landslide\ proportion}{Basin\ proportion} \times 100 \quad (S10)$$

S5.1.5. High resolution DEM

The DEM used in the landslide probability analysis was generated from the Carnegie Airborne Observatory 2 (CAO-2) next generation Airborne Taxonomic Mapping System (AToMS) with an Airborne Light Detection and Ranging (LiDAR) [*Asner et al.*, 2012]. The CAO data was processed to 1.12 m spot spacing using a modelling technique. Laser ranges from the LiDAR were combined with the embedded high resolution Global Positioning System-Inertial Measurement Unit (GPS-IMU) data to determine the 3-D locations of laser returns, producing a ‘cloud’ of LiDAR data. The LiDAR data cloud consists of a very large

number of georeferenced point elevation estimates (cm), where elevation is relative to a reference ellipsoid (WGS 1984). To estimate canopy height above ground, LiDAR data points were processed to identify which laser pulses penetrated the canopy volume and reached the ground surface. We used these points to interpolate a raster digital terrain model (DTM) for the ground surface. This was achieved using a 10 m x 10 m kernel passed over each flight block; the lowest elevation estimate in each kernel was assumed to be ground. Subsequent points were evaluated by fitting a horizontal plane to each of the ground seed points. If the closest unclassified point was < 5.5 ^{o} and < 1.5 m higher in elevation, it was classified as ground. This process was repeated until all points within the block were evaluated. The cell resolution was derived from the DEM resampled in ArcGIS to a 3 m x 3 m DEM to smooth the topography from a 1.12 m x 1.12 m DEM. Cells in the topographic shadow area and the area of the catchment with a gap in the data (~3 km^2 centralised in the upper elevations) were removed from this analysis.

S5.1.6. STRM DEM

Additionally, we tried to evaluate landslide probability, landslide proportion, and threshold angle using SRTM DEM data (resolution 90 m x 90 m) but the resolution was not sufficient to distinguish the trends that we observe when using the high resolution Carnegie Airborne Observatory DEM (resolution 3 m x 3 m) (Figure 5.3b). It is possible that at a larger spatial scale trends in landslide distribution would immerge.

S5.2. Tables for supplementary information

Table S5.2: Inter-annual landslide variability in the Kosñipata Valley

Rank	Year	Area affected by landslides (km^2)	% of valley affected by landslides
1	2010	0.809	0.64
2	1995	0.347	0.27
3	2007	0.331	0.26
4	2001	0.210	0.17
5	2009	0.131	0.10
6	2003	0.124	0.10
7	2004	0.120	0.10
8	1991	0.120	0.09
9	2011	0.101	0.08
10	1999	0.091	0.07
11	2012	0.087	0.07
12	1998	0.075	0.06
13	2008	0.071	0.06
14	1996	0.056	0.04
15	2005	0.050	0.04
16	2000	0.042	0.03
17	2006	0.039	0.03
18	1988	0.036	0.03
19	1993	0.035	0.03
20	1994	0.017	0.01
21	2002	0.014	0.01
22	1990	0.003	0.00
23	1997	0.001	0.00
24	1992	0.000	0.00
25	1989	0.000	0.00

Table S5.3: Regression lines for carbon stocks (MgC ha^{-1}) of the Kosñipata Valley

Equation	R^2	Number of plots	Source of data
AGLB = -0.0211 x Elevation + 118.66	0.5	12	This study
BGLB = -0.0022 x Elevation + 22.371	0.4	5	[*Girardin et al.*, 2013]
WD = -0.0004 x Elevation + 9.536	0.02	4	[*Gurdak et al.*, 2013]
Epiphytes >2000m = -0.01 x Elevation +18.999	0.02	4	[*Horwath*, 2011]
Epiphytes <2000m = -0.0023 x Elevation + 5.598	1	2	[*Horwath*, 2011]
Soil = 0.0546 x Elevation + 176.62	0.1	11	This study

ABLB = Above ground living biomass (includes trees)

BGLB = Below ground living biomass (includes fine and coarse roots)

WD = Woody debris

Table S5.4: Valley-wide (forest area + puna area) landslide carbon mobilisation (tC km^{-2} yr^{-1}).

	San Pedro catchment	WQ catchment
Total	28.2	21.6
Soil	21.3	16.9
Vegetation	6.9	4.7

S5.3. Figures for supplementary information

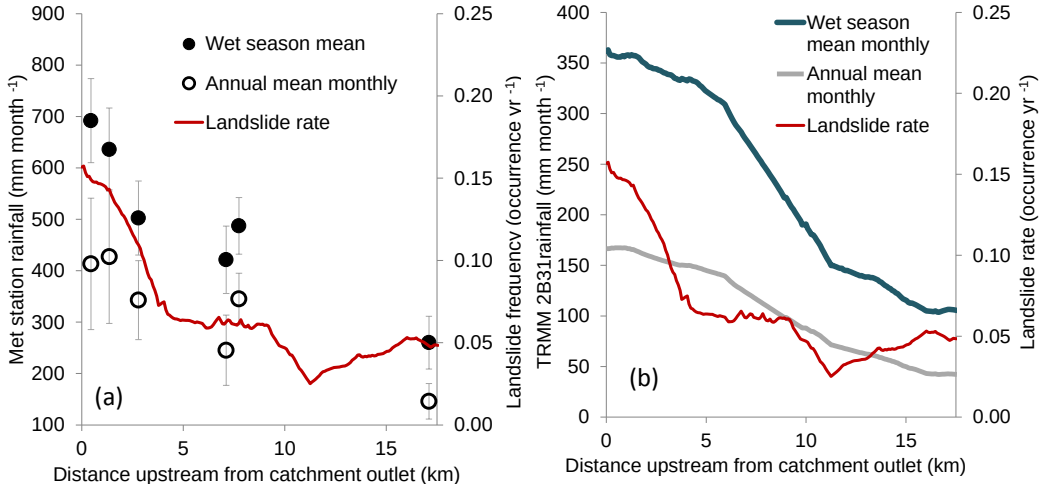


Figure S5.3: Downstream profiles over 0.44 km^2 swath along the Kosñipata River. a) Landslide frequency (red line) with meteorological station rainfall data for the wet season (mm month^{-1}; filled circles) and annual (mm month^{-1}; open circles) with error bars 2 x standard error. Rainfall data originates from 6 meteological stations in the study area [*Rapp*, 2010; *Rapp and Silman*, 2012; *SENAMHI*, 2012]. b) Landslide rate (red line) with TRMM 2B31 monthly rainfall data for the wet season (dark blue line) and annual (grey line) 2B31 TRMM is at 4 x 4 km resolution from *Bookhagen* [in review].

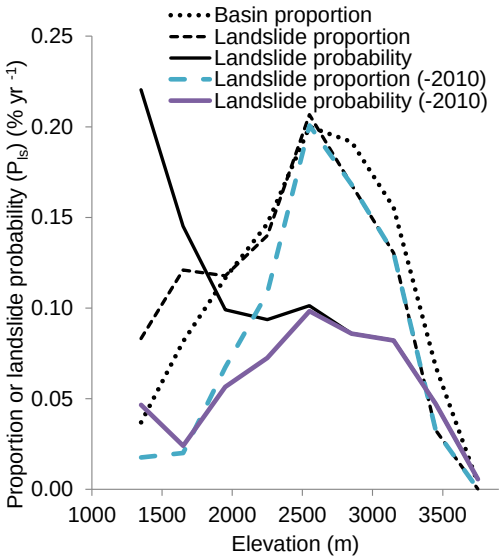


Figure S5.4: A modified version of Figure 5.3b, where the 2010 landslides are removed to determine landslide proportion (thick blue dashed line) and landslide probability (thick purple line), showing that landslide activity was very low when 2010 landslides were removed. This suggests the importance of storms in landslide frequencies in the lower elevations of the valley as a large storm March 4th 2010 only occurred in the lower region of the valley.

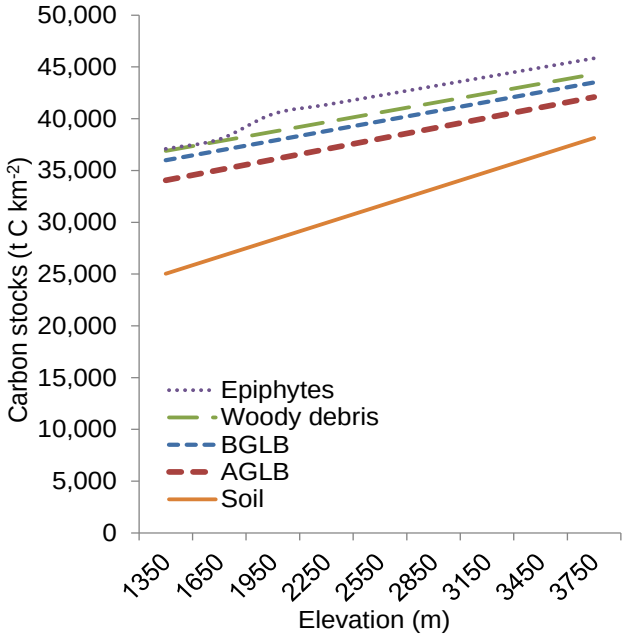


Figure S5.5: Cumulative valley-wide carbon stock estimates for soil and vegetation (tC km^{-2}) for the tropical montane forest of Kosñipata Valley, in the eastern Andes of Peru. Estimates were made by determining linear trends of stocks with elevation from established data sets [*Horwath*, 2011; *Girardin et al.*, 2013; *Gurdak et al.*, 2013] (Table S3). The basin wide carbon stocks are a total of soil (yellow solid line), above ground living biomass (AGLB = stems, thick red dashed line), below ground living biomass (BGLB = fine and course roots, blue dashed line), woody debris (WD, green long-dashed line), and epiphytes (purple dotted line). In the case of epiphytes two trends were used one in the cloud immersion zone (>2000 m) and in the intermediate cloud zone (<1500 m) to capture the change in carbon stocks [*Horwath*, 2011].

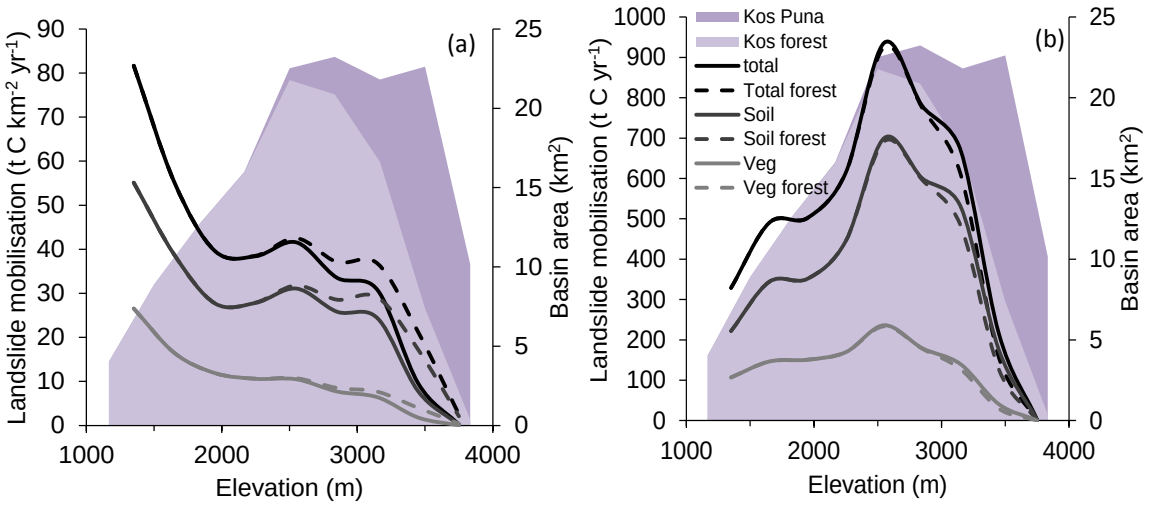


Figure S5.6: a) Area-normalisation of organic carbon (tC km^{-2} yr^{-1}) and b) total mobilisation of carbon by landslides (tC yr^{-1}) over the altitudinal gradient. The total represents the contribution for the entire valley (puna and forest) for soil organic carbon stock (dark grey line), vegetation carbon stock (light grey line) and sum of soil + vegetation (total, black line; Table S4). Mobilisation of landslide carbon over forested regions dominates valley-wide yields (Figure 5.6a and 5.6b) (dashed lines). The forested portion of the basin is represented by the light purple shaded region and the puna grassland portion of the basin is represented by the dark purple shaded region. There is a small addition in carbon that is mobilised by landslides when the puna grasslands regions (dashed lines) are considered. The additional area (dark purple) lowers the valley wide carbon mobilised by landslides (Table S5.4).

S5.4. References for supplementary information

Asner, G. P., Knapp, D. E., Boardman, J., Green, R. O., Kennedy-Bowdoin, T., Eastwood, M., Martin, R. E., Anderson, C., and Field, C. B. (2012), Carnegie Airborne Observatory-2: Increasing science data dimensionality via high-fidelity multi-sensor fusion, *Remote Sensing of Environment, 124*(0), 454-465, doi: http://dx.doi.org/10.1016/j.rse.2012.06.012.

Blodgett, T. A., and Isacks, B. L. (2007), Landslide erosion rate in the eastern cordillera of northern Bolivia, *Earth Interactions, 11*, 1-30, doi: http://dx.doi.org/10.1175/2007EI222.1.

Bookhagen, B. (in review), High resolution spatiotemporal distribution of rainfall seasonality and extreme events based on a 12-year TRMM time series.

Girardin, C. A. J., Aragão, L. E. O. C., Malhi, Y., Huaraca Huasco, W., Metcalfe, D. B., Durand, L., Mamani, M., Silva-Espejo, J. E., and Whittaker, R. J. (2013), Fine root dynamics along an elevational gradient in tropical Amazonian and Andean forests, *Global Biogeochemical Cycles*, doi: http://dx.doi.org/10.1029/2011GB004082.

Gurdak, D. J., Aragao, L. E. O. C., Rozas-Dávila, A., Huaraca Huasco, W., García Cabrera, K., Doughty, C. E., Farfan-Rios, W., Silva-Espejo, J. E., Metcalfe, D. B., Silman, M. R., and Malhi, Y. (2013), Assessing above-ground woody debris dynamics along a gradient of elevation in Amazonian cloud forests in Peru: balancing above-ground inputs and respriation outputs, *Plant Ecology and Diversity, 7*(1-2), 143-160, doi: http://dx.doi.org/10.1080/17550874.2013.818073.

Hilton, R. G., Meunier, P., Hovius, N., Bellingham, P. J., and Galy, A. (2011), Landslide impact on organic carbon cycling in a temperate montane forest, *Earth Surface Processes and Landforms, 36*(12), 1670-1679, doi: http://dx.doi.org/10.1002/esp.2191.

Horwath, A. (2011), Epiphytic bryophytes as cloud forest indicators: Stable isotopes, biomass and diversity along an altitudinal gradient in Peru, 260 pp, Plant Sciences, University of Cambridge, Cambridge.

Hovius, N., Stark, C. P., and Allen, P. A. (1997), Sediment flux from a mountain belt derived by landslide mapping, *Geology, 25*(3), 231-234.

Malamud, B. D., Turcotte, D. L., Guzzetti, F., and Reichenbach, P. (2004), Landslide inventories and their statistical properties, *Earth Surface Processes and Landforms, 29*(6), 687-711, doi: http://dx.doi.org/10.1002/esp.1064.

Meunier, P., Hovius, N., and Haines, J. A. (2008), Topographic site effects and the location of earthquake induced landslides, *Earth and Planetary Science Letters, 275*(3), 221-232, doi: http://dx.doi.org/10.1016/j.epsl.2008.07.020.

Rapp, J. M. (2010), Climate control on plant performance across an Andean altitudinal gradient, pp, Deptartment of Biology, Wake Forest University, Winston-Salem, North Carolina.

Rapp, J. M., and Silman, M. R. (2012), Diurnal, seasonal, and altitudinal trends in microclimate across a tropical montane cloud forest, *Climate research, 55*(1), 17-32, doi: http://dx.doi.org/10.3354/cr01127.

Restrepo, C., Walker, L. R., Shiels, A. B., Bussmann, R., Claessens, L., Fisch, S., Lozano, P., Negi, G., Paolini, L., and Poveda, G. (2009), Landsliding and its multiscale influence on mountainscapes, *Bioscience, 59*(8), 685-698, doi: http://dx.doi.org/10.1525/bio.2009.59.8.10.

SENAMHI (2012), Clima: Datos históricos Peru, edited, Servicio Nacional de Meteorologia e Hidrologia del Peru, Lima, Peru.

Stark, C. P., and Hovius, N. (2001), The characterization of landslide size distributions, *Geophysical Research Letters, 28*(6), 1091-1094, doi: http://dx.doi.org/10.1029/2000GL008527.

USGS (2013), Landsat Processing Details, edited, United States Geological Survey, U.S. Deptarment of the Interior.

Linking statement: Chapter 5 to 6

The previous chapters examined streamflow (chapter 3), river POC during storm activity (chapter 4) and landslide rates and carbon mobilised by landslides (chapter 5). Now in this chapter (6) I bring all of the previous chapters together, along with a new year-long POC and suspended sediment dataset to evaluate river POC and suspended sediment fluxes and assess the importance of landslides in the river $POC_{non\text{-}fossil}$ yield.

Specifically, this chapter addresses the two final research aims of the thesis: 1) **to quantify annual fluxes of suspended sediment, and non-fossil and fossil POC in the river**; and 2) **to compare the contribution of landslide derived soil and vegetation carbon to river $POC_{non\text{-}fossil}$ fluxes**. It evaluates POC (non-fossil and fossil) fluxes for the one-year streamflow study (chapter 3), utilising an isotope mixing model developed in chapter 4. The $POC_{non\text{-}fossil}$ yield is then compared to the non-fossil mobilisation due to landslide activity (chapter 5) assessing the role of landslide debris in river $POC_{non\text{-}fossil}$.

I was the main author and wrote the paper, and also designed the structure, conducted and organised the field work with the help of research assistants, and carried out the data analysis with the exception of running samples for the stable isotope and elemental concentration analysis. Bob Hilton, who was the main supervisor on this paper, helped to design the field experiment, provided the protocol for sediment sample preparation, ran the isotope and elemental concentration samples, and gave guidance and instruction on data analysis. As well, he was the main editor of the paper. Josh West provided direction in the field and sampling design, and also edited the paper. Arturo Robles was the main field assistant. Darren Gröcke ran the samples for stable isotopes and elemental concentrations. Toby Marthews provided insight into Andean and Amazon forest carbon cycling. Greg Asner provided the high resolution Carnegie Airborne Observatory (CAO) LiDAR derived DEM (3 x 3 m) used to derived upslope area. Yadvinder Malhi and Mark New provided guidance.

This chapter will be submitted in 2015 to either Geology or Geophysical Research Letters after chapter 5 has been submitted.

Chapter 6 : Export of particulate organic carbon by an Andean river and implications of its delivery to the lowland Amazon River

K. E. Clark[1*], R. G. Hilton[2], A. J. West[3], A. Robles Caceres[4], D. R. Gröcke[5], T. R. Marthews[1], G. P. Asner[6], M. New[1,7], and Y. Malhi[1]

[1] School of Geography and the Environment, University of Oxford, UK. (*correspondence: kathryn.clark23@gmail.com)

[2] Department of Geography, Durham University, UK. (r.g.hilton@durham.ac.uk)

[3] Department of Earth Sciences, University of Southern California, Los Angeles, USA. (joshwest@usc.edu)

[4] Facultad de Ciencias Biológicas, Universidad Nacional de San Antonio Abad del Cusco, Cusco, Peru.

[5] Department of Earth Sciences, Durham University, UK. (d.r.grocke@durham.ac.uk)

[6] Department of Global Ecology, Carnegie Institution for Science, Stanford, CA, USA. (gpa@carnegiescience.edu)

[7] African Climate and Development Initiative, University of Cape Town, South Africa. (mark.new@acdi.uct.ac.za)

Abstract

Physical erosion in mountain river catchments can mobilise significant amounts of clastic sediment, while exporting organic carbon and nutrients from forest ecosystems. In the Andes mountain range, there is a vast expanse of highly productive forest that is subject to high erosion rates which supplies sediment, carbon and nutrients to the lowland Amazon River. Despite this recognition, the rates of particulate organic carbon (POC) export remain poorly constrained in the Andes, as do the controls on this flux. Here, we focus on the Kosñipata River, Peru, an Andean tributary of the Madre de Dios River, where water discharge measurements and suspended sediment samples were collected over one year at two gauging stations. Using rating curves to relate solid load constituents to water discharge, the suspended sediment yield over the sampling period was estimated to be 970 - 1200 tC km^{-2} yr^{-1}, similar to longer-term estimates over the larger catchment area, and suggests the Madre de Dios basin has erosion rates ~10 times greater than the Amazon Basin average. We use stable isotopes of POC and organic carbon to nitrogen ratios to distinguish the export of POC from sedimentary rocks (POC_{fossil}) from POC from soil and vegetation ($POC_{non\text{-}fossil}$). The total POC yield (fossil + non-fossil) over the sampling period was 9.1 – 12.2 tC km^{-2} yr^{-1}, approximately three to five times the total POC yield in the lowland Amazon Basin (2.3 tC km^{-2} yr^{-1}), with most POC (70-80 %) exported between December and March in the wet season. Rating curve estimates of $POC_{non\text{-}fossil}$ yield were 5.2 – 6.9 tC km^{-2} yr^{-1}, with $POC_{non\text{-}fossil}$ transport significantly enhanced during flood events. At the forest plot scale, the net carbon budget of Andean forest (net productivity minus heterotrophic respiration) has been shown to be close to zero, but the contribution of $POC_{non\text{-}fossil}$ to carbon export was not accounted for. Our results suggest that fate of the fluvially exported $POC_{non\text{-}fossil}$ may determine whether the Andean forest is a carbon sink or source. Indeed, in the Madre de Dios basin, the Andean river $POC_{non\text{-}fossil}$ transfer equates to ~3 % of the biomass C sink in the

lowland forests. The POC_{fossil} yield was significant, at 3.9 – 5.3 tC km^{-2} yr^{-1}. Given the extent of sedimentary bedrock in the Peruvian Andes and high erosion rates sustained in the Andes over the Madre de Dios catchment (Andean area = 35,600 km^2), the POC_{fossil} flux may be ~0.17 MtC yr^{-1}. Only ~0.02 MtC yr^{-1} is estimated to be exported by the Madeira River downstream, implying selective deposition and storage of POC_{fossil} in the Amazon floodplain, or a significant oxidation of POC_{fossil} and release of carbon dioxide. The results suggest a significant contribution of $POC_{non\text{-}fossil}$ and POC_{fossil} to the lowland Amazon Basin and the fate of this material needs to be better constrained to fully understand the organic carbon budget on the Amazon River Basin.

6.1. Introduction

Tropical forests and soils contain ~430 PgC stored within organic matter [*Dixon et al.*, 1994] representing >70 % of the carbon dioxide (CO_2) stock of the pre-industrial atmospheric reservoir [*Sundquist and Visser*, 2004]. Physical erosion acts to export some of this terrestrial organic carbon, supplying it to river systems who together deliver 0.1 to 0.4 PgC yr^{-1} of particulate organic carbon (POC) to the oceans [*Seitzinger et al.*, 2005; *Mayorga et al.*, 2010; *IPCC*, 2013]. It is important to understand the rates of erosional carbon export and the controls on the C flux, because this lateral C transfer may contribute to long-lived CO_2 sequestration if the POC is buried in continental or marine deposits [*Berner*, 1982; *France-Lanord and Derry*, 1997; *Stallard*, 1998; *Galy et al.*, 2007b; *Kao et al.*, 2014]. Alternatively, oxidation of this POC during fluvial transport or continental transit can fuel ecosystems [*Mayorga et al.*, 2005] and if the carbon is old, in the extreme case derived from sedimentary rock [*Galy and Eglinton*, 2011; *Hilton et al.*, 2011a], its oxidation on transit to the oceans represent a source of geological CO_2 to the atmosphere [*Bouchez et al.*, 2010; *Vihermaa et al.*, 2014].

High rates of physical erosion occur in mountains [*Larsen et al.*, 2014], and because of the close association between POC and clastic sediment, these locations also experience very highest rates of POC erosion [*Milliman*, 1995; *Kao and Liu*, 1997; *Hicks et al.*, 2000; *Lyons et al.*, 2002; *Hilton et al.*, 2008a; *Wheatcroft et al.*, 2010; *Milliman and Farnsworth*, 2011; *Hilton et al.*, 2012; *Goñi et al.*, 2013]. In some cases, rivers draining mountain belts export this POC efficiently to ocean basins (e.g. *Hilton et al.* [2008a]; *Wheatcroft et al.* [2010]; *Kao et al.* [2014]). However, many mountain rivers drain into larger river systems and their POC and sediment are transported for thousands of kilometres before reaching long-lived sedimentary deposits (e.g. *Galy et al.* [2008b]; *Blair and Aller* [2012]; *Bouchez et al.* [2014]; *Moreira-Turcq et al.* [in press]). The Amazon Basin (~$6x10^6$ km^2) is such a case, with its headwaters in the Andes thought to dominate the budget of clastic sediment, supplying a significant component of the 550-1550 Mt yr^{-1} exported to the Atlantic Ocean (e.g. *Gibbs* [1967]; *Meade et al.* [1979]; *Richey et al.* [1986]; *Allegre et al.* [1996]; *Dunne et al.* [1998]; *Guyot et al.* [2005]; *Filizola and Guyot* [2009]; *Martinez et al.* [2009]). Despite this recognition, the rates of POC transfer from the Andes remain poorly constrained [*Richey et al.*, 1990a; *Moreira-Turcq et al.*, 2003; *Bouchez et al.*, 2014]. In particular, it is clear that there is a growing need to constrain the source of POC, with recent work highlighting the importance of rock-derived POC input to Andean rivers [*Bouchez et al.*, 2010; *Clark et al.*, 2013; *Bouchez et al.*, 2014].

Here we use a detailed set of suspended sediment samples and hydrometric river gauging measurements to quantify total POC yields in an Andean river catchment over a water year. We use stable isotopes of POC and the organic carbon to nitrogen ratio of the suspended load to isolate the POC derived from sedimentary rocks (POC_{fossil}) from that eroded from vegetation and soil ($POC_{non\text{-}fossil}$). POC yields are considered in the context of

suspended sediment yields from mountain catchments. Additionally, we evaluate what controls the export and the role they play in regional C dynamics

6.2. Study Area

The study area is located in the Central Andes in the Eastern Cordillera (Figure 6.1). The region experiences moderate rates of rock and surface uplift of 0.2 - 0.3 mm yr^{-1} due to plate convergence and the subduction of the Nasca Plate under the South American Plate [*Gregory-Wodzicki*, 2000]. This convergence zone has built steep topography [*Montgomery et al.*, 2001]. The South American Low Level Jet, which carries humid winds westward over the Amazon Basin [*Marengo et al.*, 2004] is redirected by this steep convergence zone. This drives the high annual precipitation up to 7000 mm yr^{-1} in certain parts of the Eastern Andes [*Killeen et al.*, 2007]. The climate and tectonic setting combine to result in moderate-to-high denudation rates compared to other mountain belts [*Milliman and Farnsworth*, 2011] of ~0.4 mm yr^{-1} in the Central Andes estimated from cosmogenic radionuclide concentrations in detrital quartz [*Wittmann et al.*, 2009] and decadal river gauging [*Guyot et al.*, 1996]. The slopes are steep and prone to bedrock landslides, which contribute to sediment and carbon transfer [*Blodgett and Isacks*, 2007; *Clark et al.*, in prep]. In this part of the Andes, mountain rivers drain large areas of sedimentary and meta-sedimentary melanges that comprise of ~70 % of the drainage area [*Clark et al.*, 2013].

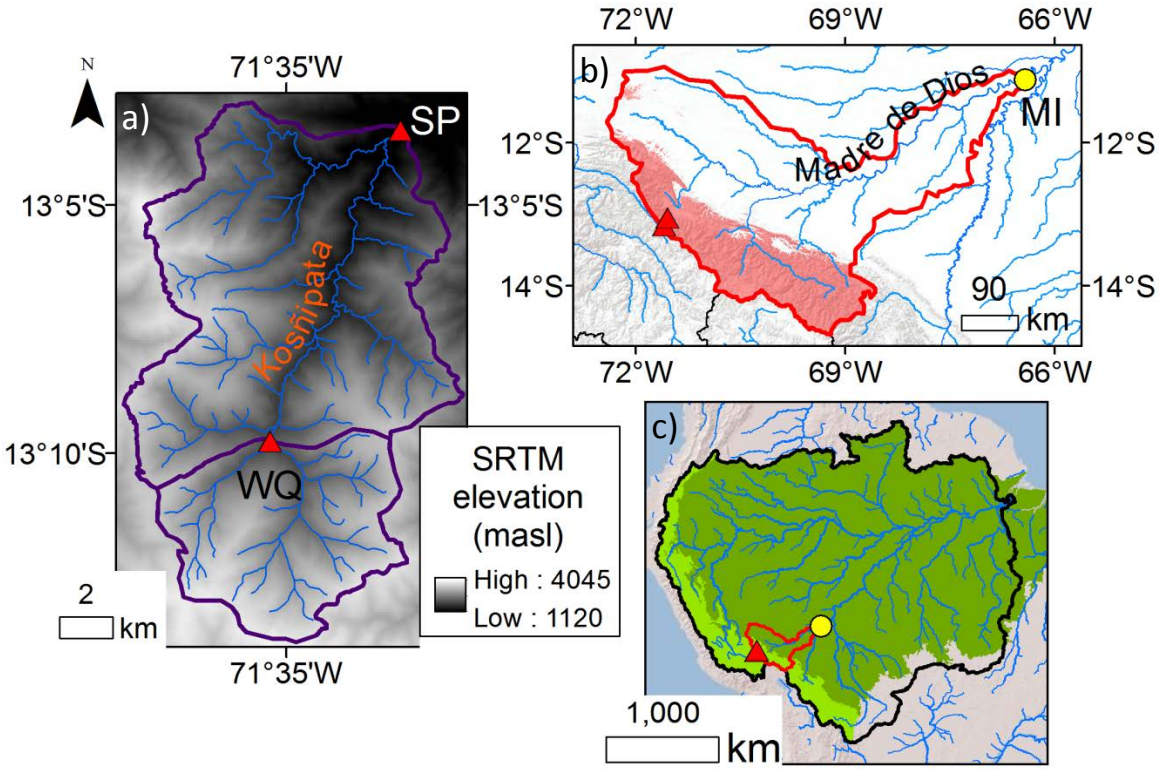


Figure 6.1: a) An altitudinal map, using shuttle radar topographic mission (SRTM) digital elevation model at 90 x 90 m resolution, showing the Wayqecha and San Pedro gauging stations (red triangles) along the Kosñipata River. b) The Kosñipata River feeds the Madre de Dios River a tributary of the Amazon. The Madre de Dios Basin (red outline) at the Miraflores river gauging station (MI, yellow circle) is 124,000 km^2 and the Andean portion of the Madre de Dios Basin (red region) > 550 masl is 35,600 km^2. The river network was produced from HydroSHEDS (hydrological data and maps based on shuttle elevation derivatives at multiple scales) [*Lehner et al.*, 2008]. c) The Amazon River network with the two river gauging stations in the Andes (red triangle) and the Miraflores river gauging station (yellow dot) in Amazonia. The Andean portion of Amazonia (light green) and Amazonia *sensu stricto* (dark green) from [*Eva et al.*, 2005] fall mostly within the Amazon Basin (within black outline) [*Lehner et al.*, 2008].

Here we focus on the Kosñipata River in the Peruvian Andes, a tributary of the Madre de Dios River which feeds the Amazon River (Figure 6.1c). Due to high erosion rates combined with pristine montane forest, this valley is an ideal location to understand erosion and export of POC. The wet climate, of the Kosñipata Valley, sustains productive tropical montane cloud forest [*Malhi et al.*, 2010] and is located in Manu National Park where logging is prohibited. 80 % of the valley is comprised of tropical forest with the remainder comprised of high elevation grasslands (Table 6.1). The forest contains significant stores of

organic carbon with (42,100 tC km^{-2}), with 31,600 tC km^{-2} in soils and 10,500 tC km^{-2} in biomass [*Clark et al.*, in prep]. Total carbon stocks are consistent throughout the valley, with a slight increase with elevation, due to an increase of soil stocks with elevation accompanied by a reduction in biomass [*Zimmermann et al.*, 2010; *Clark et al.*, in prep]. These values are similar to those estimated in other tropical forests [*Raich et al.*, 1997; *Raich et al.*, 2006] and representative of a wider geographical area in the Andean mountains [*Saatchi et al.*, 2007; *Gibbon et al.*, 2010; *Mitchard et al.*, 2014].

The geology of the Kosñipata Valley is ~80 % Paleozoic (~ 450 Ma) meta-sedimentary mudstones which contain POC_{fossil}, with plutonic intrusions contributing the remaining ~20 % [*Carlotto Caillaux et al.*, 1996] (Table 6.1). The geological characteristics are representative of the Madre de Dios Basin, containing a large part of the eastern Andes in southern Peru and in northern Bolivia [*Carlotto Caillaux et al.*, 1996; *INGEMMET*, 2013], covering approximately ~35,600 km^2, and may be similar to a wider region draining to the Beni River and feeding the Madeira River Basin [*Bouchez et al.*, 2014].

Table 6.1: Descriptions of the Wayqecha and San Pedro catchments on the Kosñipata River.

Catchment	Area (km^2)	Mean slope* (°)	Mean elevation* (masl)	Elevation range (masl)	Landcover type¤ (~ %)	Geology^ (~ %)	Gauge lat/long (S, W)	Gauge elevation (masl)
Wayqecha	48.5	26	3195	2262 to 3927	TMCF (50), puna /transition (50)	mudstones (100)	13°9'46", 71°35'21"	2250
San Pedro	164.4	28	2805	1354 to 4003	TMCF (80), puna /transition (20)	mudstones (80), pluton intrusions (20)	13°3'37", 71°32'40"	1360

* Based on Shuttle Radar Topography Mission (SRTM) data with a 90 m x 90 m resolution.
^ Basin geology derived from [*Carlotto Caillaux et al.*, 1996].
¤ Landcover types were determined using 2009 Quickbird 2 imagery.

Suspended sediment samples were collected between 11/2009 and 02/2011 from two gauging stations, the San Pedro catchment (1360 masl, 164.4 km^2) and the Wayqecha sub-basin (2250 masl, 48.5 km^2) (Table 6.1, Figure 6.1a). These are the locations of previous work and here we greatly expand the sample set which focused on a set of 2 storm events in

January and February 2010 to better constrain the source of POC carried by Andean rivers as described in *Clark et al.* [2013]. The existing data demonstrates that POC_{fossil} can contribute between ~10 % and 80 % of the total POC [*Clark et al.*, 2013]. Rainfall in the valley ranges from 5300 mm yr^{-1} around the San Pedro gauging station to 1560 mm yr^{-1} in the high elevations of the Wayqecha catchment [*Girardin et al.*, 2013; *Huaraca Huasco et al.*, 2013]. Basin-wide rainfall is ~3000 mm yr^{-1} [*Clark et al.*, in review]. The wet season is from December to March, the wet-dry transition season is April, the dry season is May to September, and the dry-wet transition season is October and November [*Clark et al.*, in review]. Stream runoff at the San Pedro gauging station is 2721 mm yr^{-1} (Table 6.1) [*Clark et al.*, in review].

6.3. Materials and Methods

6.3.1. Sample collection and hydrometric measurements

At the San Pedro and Wayqecha catchment outlets, suspended sediment samples were collected from November 2009 to February 2011 (Figure 6.1a) which covers 2 periods of the wet season. Throughout the campaign, samples were collected at a weekly to monthly interval at both sites. Previous work has focused on a two week sub-experiment in the 2010 wet season, when were collected every 3 hours, described in *Clark et al.* [2013]. The sampling strategy was designed to provide suspended sediments from a range of water discharges (Q_w, m^3 s^{-1}) and during flood events in order to quantify sediment and POC fluxes [*Hilton et al.*, 2008b; *Kao and Milliman*, 2008; *Townsend-Small et al.*, 2008]. Collections of volumes from 250 – 6400 mL were made from the surface of the flow at the middle of the channel, in plastic bottles pre-rinsed with filtered river water. Smaller volumes were collected at high flow and larger volumes were collected during the dry season. At both sample sites, our samples are likely to be representative of the suspended load due to large scale bed roughness which produce highly turbulent and mixed suspended sediment in the channel

[*Lupker et al.*, 2011]. The known volume of river water was filtered through 0.7 µm glass fibre filters (Whatman GF/F, 47 mm) to recover suspended sediment. Filters were dried at ~40 °C within two days and stored in sterile petri-dishes.

At the San Pedro gauging station, the width of the river varied from ~11 m to 17 m and the Q_w varied from 21 m^3 s^{-1} to 8.5 m^3 s^{-1} in the wet and dry seasons [*Clark et al.*, in review]. Q_w was determined over this study period using an empirical relationship between stage height and Q_w from the measurements, and applied to the continuous stage height record and then applied to instantaneous river height measures (5 to 15 min; *Clark et al.* [in review]).

At the Wayqecha gauging station, the total river width varied from 6 to 9 m and discharge varied from 8 m^3 s^{-1} to 2.3 m^3 s^{-1} in the wet and dry seasons [*Clark et al.*, in review]. In contrast, at the Wayqecha gauging station all available instantaneous discharge (m^3 s^{-1}) measurements (n = 59) over the study year were used to determine mean monthly discharge in the absence of a reliable continuous measurement of stream height. It is worth noting that the Wayqecha Q_w record is therefore of lower precision and introduces more uncertainty into flux calculations than at San Pedro [*Clark et al.*, in review].

6.3.2. Geochemical analyses

Suspended sediment samples collected throughout the year and during storm events (on the rising limb, storm peak and falling limb of two storms) were selected for analysis from the San Pedro (n = 68) and Wayqecha (n = 45) gauging stations (Figure 6.2). River suspended sediments were rinsed from the glass filter membrane using deionised water in glass beakers and the samples dried at 40 °C [*Hilton et al.*, 2010; *Clark et al.*, 2013]. The same procedure was carried out on pre-combusted quartz powder which contained no measurable POC to quantify procedural blanks. The sediment mass (mg) and known filtered

volume (L) was used to calculate the suspended sediment concentration (SSC, mg L^{-1}). Samples were homogenised using a mortar and pestle. Inorganic carbon, such as detrital carbonates including dolomite, was removed using a 5M HCl-leach for 4 hours at 75 °C [*Galy et al.*, 2007a; *Hilton et al.*, 2008a; 2010]. Thus, this analysis refers to acid-insoluble POC. The HCl-leach method has been shown by *Brodie et al.* [2011] to be the most robust way to return reliable organic carbon to nitrogen ratios measured in similar materials to those analysed here. Following several deionised water rinses to remove acid salts, the suspended load samples were dried at 75 °C and transferred to clean glass vials.

An aliquot of each sediment sample (~2 mg to ~26 mg) was analysed to determine their weight percent organic carbon (C_{org}, %) and nitrogen (N, %; used to determine the N/C % ratio), using a Costech CHN elemental analyser (EA). The results normalised by standards and corrected for an internal and procedural blank [*Hilton et al.*, 2010; *Gröcke et al.*, 2011; *Clark et al.*, 2013]. Stable isotopes of POC ($\delta^{13}C_{org}$, ‰) were determined by continuous flow from the EA coupled via CONFLO-III to a Thermo-Delta-V isotope ratio mass spectrometer in the Stable Isotope Biogeochemistry Laboratory, University of Durham. Values were normalised based on measured values of IAEA and laboratory standards, corrected for any internal blank and procedural blank and reported in $\delta^{13}C$ notation relative to VPDB. The precision (2σ) and accuracy of $\delta^{13}C_{org}$ were determined using standards measured under the same analytical conditions and were 0.1 ‰ [Gröcke et al., 2011]. Replicates of the river suspended sediment samples (n = 21) returned an average 2σ of ± 0.1 ‰ and we take this as the average precision of the analyses. Quartz sand blanks were subjected to the decarbonisation process and revealed no $\delta^{13}C$ signal (n = 3) suggesting that the decarbonisation did not add $\delta^{13}C$ to the river suspended sediment samples.

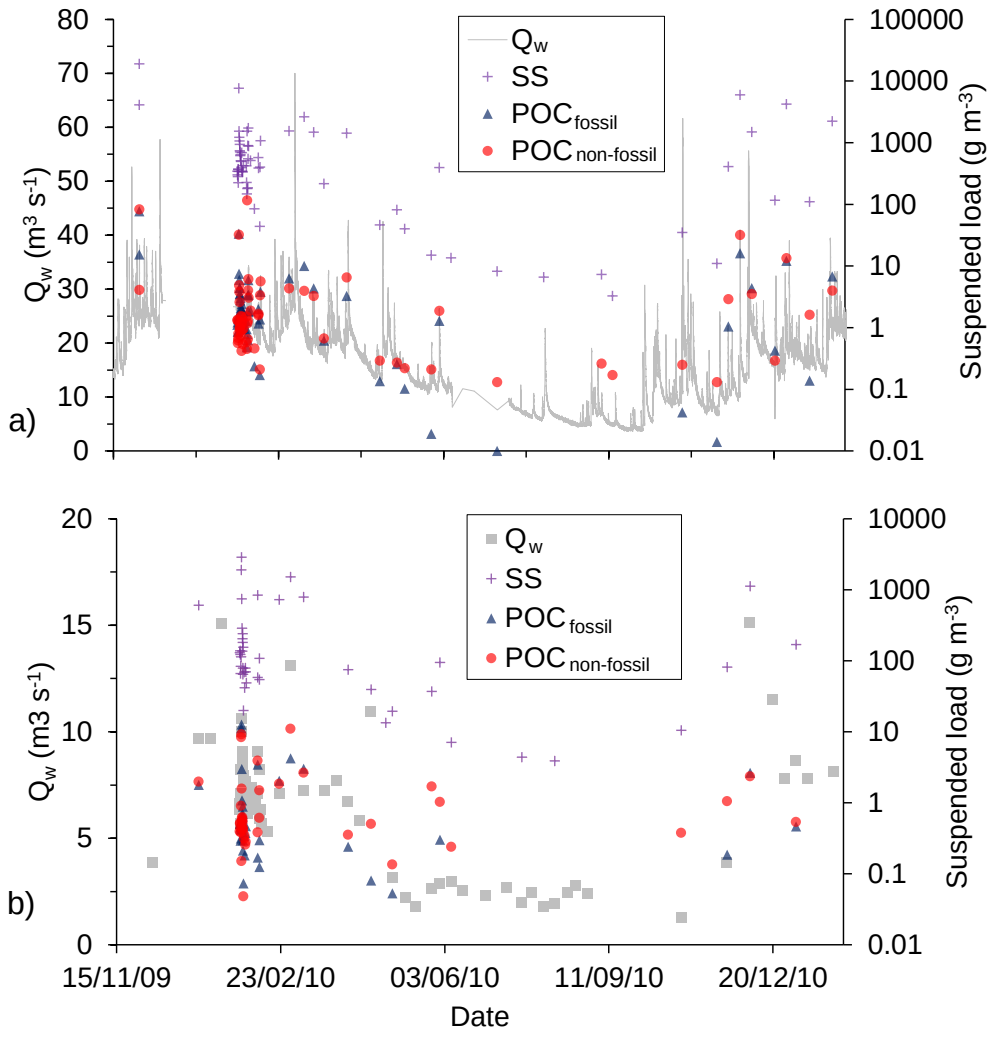


Figure 6.2: River discharge (Q_w, m^3 s^{-1}) over the study period for a) San Pedro (164.4 km^2 watershed area), and b) Wayqecha (48.5 km^2 watershed area) gauging stations (Figure 6.1a), with suspended sediment samples (SS), POC_{fossil} and $POC_{non\text{-}fossil}$ concentrations (g m^{-3}) on the secondary axis.

6.3.3. Rating curves

Suspended sediment concentrations (SSC, g m^{-3}) were used along with the measured C_{org} and $F_{non\text{-}fossil}$ to calculate the concentrations of $POC_{non\text{-}fossil}$ (g m^{-3}) and POC_{fossil} (g m^{-3}) (Table S6.1) [*Hilton et al.*, 2011a; *Hilton et al.*, 2012]. These particulate constituent concentrations were compared to Q_w measurements to examine whether power-law rating curves describe patterns in the dataset [*Cohn*, 1995; *Vogel et al.*, 2003; *Hilton et al.*, 2008b; *Wheatcroft et al.*, 2010; *Hatten et al.*, 2012] (Figure S6.1). Power law rating curves can be

used to quantify solid load fluxes using continuous water discharge datasets [*Hilton et al.*, 2011a; *Hatten et al.*, 2012; *Goñi et al.*, 2013; *Smith et al.*, 2013]. However, previous work has described a threshold behaviour of $POC_{non\text{-}fossil}$ transport in mountain rivers [*Hilton et al.*, 2012; *Clark et al.*, 2013; *Smith et al.*, 2013] which mean that power law rating curves may not describe relationships between Q_w and $POC_{non\text{-}fossil}$. Alternatives include using non-linear threshold rating curves [*Hilton et al.*, 2008b], linear models [*Townsend-Small et al.*, 2008; *Hilton et al.*, 2012] or an alternative approach to quantifying flux using flux-weighted averaging [*Walling and Webb*, 1981; *Ferguson*, 1987; *Hilton et al.*, 2012]. Here, rating curves were used in the first instance because of the known 'flashy' nature of river hydrographs in the Peruvian Andes, with storm-induced floods an important feature [*Townsend-Small et al.*, 2008; *Clark et al.*, 2013; *Clark et al.*, in review]. The flux-weighed methods tend to underestimate fluxes during large floods [*Ferguson*, 1987; *Dadson et al.*, 2005; *Hilton et al.*, 2008b; *Hilton et al.*, 2012].

6.3.4. Annual sediment yields

At San Pedro, the annual sediment fluxes were determined by summing up the instant flux for each month. Yield was determined by dividing the flux by the basin area (164.4 km^2) (Table 6.2, Figure 6.5). For the Wayqecha basin, the mean monthly sediment and POC concentrations (n = 11) were multiplied by the mean monthly discharge to determine monthly sediment flux. The monthly fluxes were summed to determine the annual fluxes (Table 6.2). In August there were no river measurements at the Wayqecha gauging station and linear extrapolation was carried out to determine runoff and sediment flux [*Clark et al.*, 2013]. The fluxes were very low in the dry season and would not affect the annual yield. This method was chosen for the Wayqecha gauging station because the rating curves did a poor job of predicting sediment and POC concentrations (Figure S6.2 b, d & f). Fluxes may be overestimated at Wayqecha. This is likely due to the method used to determine annual fluxes

at Wayqecha and is discussed further in the results. The paired sampling suggests that the Wayqecha sub-catchment may have a lower flux than San Pedro catchment (Table S6.2, Figure S6.3a).

6.4. Results

6.4.1. Elemental and isotope geochemistry

The stable isotope composition of POC ($\delta^{13}C_{org}$) and elemental composition (N/C ratio) of the 113 suspended sediments collected 11/2009-02/2011 in the Kosñipata River are consistent with a smaller (n= 54) dataset collected over 2 storm events in 01/2010 to 02/2010 [*Clark et al.*, 2013]. The $\delta^{13}C_{org}$ ranged from -23 ‰ to -30 ‰ and the N/C ranged from 0.03 to 0.25 (Table S6.1). $\delta^{13}C_{org}$ values were positively, linearly correlated with N/C ($r = 0.92$, $P < 0.0001$, $n = 67$) (Figure 6.3). Such a trend can be explained by a mixture of POC from fossil organic carbon in sedimentary rocks (POC_{fossil}), ^{13}C-enriched and high N/C ratios, and POC from vegetation and soil ($POC_{non\text{-}fossil}$) ^{13}C-depleted and low N/C ratios. To constrain the fossil component, river bedload was sampled throughout the year (n = 7), as it contains a mixure of bedrock sources from throughout the valley [*Clark et al.*, 2013]. The linear trend described by the samples suggests that the majority of $POC_{non\text{-}fossil}$ has a composition most similar to O_h layer soil (Figure 6.3). The findings concur with other small mountain river catchments where POC_{fossil} and $POC_{non\text{-}fossil}$ are mixed during erosion and fluvial transport [*Komada et al.*, 2004; *Hilton et al.*, 2010; *Kao et al.*, 2014] and previous work in the catchment [*Clark et al.*, 2013]. The C_{org} % at the San Pedro gauging station ranged from 0.48 % to 6.8 % with a mean of 0.99 %, and at the Wayqecha gauging station ranged from 0.44 to 4.5 % with a mean of 1.1 % (Table S6.1).

There were seasonal differences in $\delta^{13}C_{org}$ (‰) evident at both stations (Figure 6.4). The wet season had a range in $\delta^{13}C_{org}$ values ranging from -27 to -24 ‰, confirming a linear

two end-member mixing between a fossil source (~ -23 ‰) and non-fossil source (-27 to -30 ‰) (Figure 6.3), as established by *Clark et al.* [2013]. The dry season had an enriched $\delta^{13}C_{org}$ signal with values mostly between -28 and -29 ‰. The transitional seasons formed a link between the wet season and the dry season with $\delta^{13}C_{org}$ from -26 to -28 ‰ (Figure 6.4).

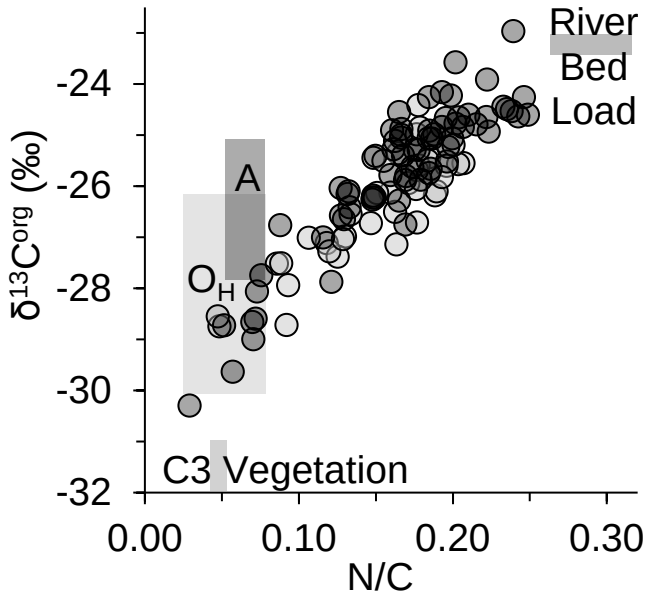


Figure 6.3: Elemental and isotopic composition of POC in suspended load (circles) from the Kosñipata River. Samples collected from San Pedro as black circles and from Wayqecha as grey circles, with analytical uncertainties small than the point size. a) The stable isotopes of POC ($\delta^{13}C_{org}$, ‰) versus the nitrogen to organic carbon ratio (N/C). Boxes show ranges from published sources [*Zimmermann et al.*, 2009; *Rao*, 2011], where O_H and A are soil horizons.

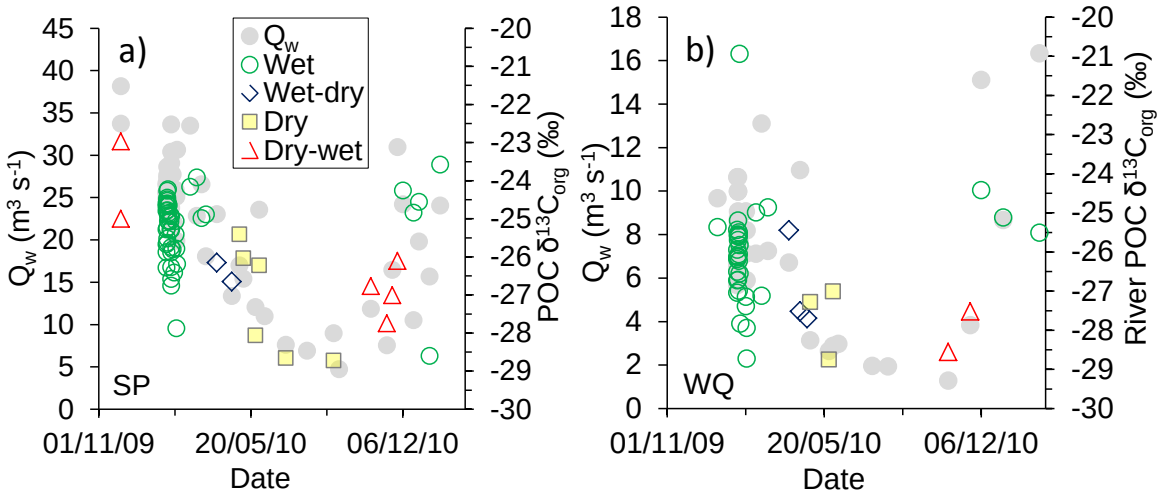


Figure 6.4: Seasonal variation of POC $\delta^{13}C_{org}$ (‰) and measured Q_w (m^3 s^{-1}) over the sampling period for the a) San Pedro gauging station (n = 67) and for the b) Wayqecha gauging station (n = 42). Several suspended sediment samples at low flow in the dry season did not yield a $\delta^{13}C_{org}$ result (SP n = 3 and WQ n = 3; Table S6.1). ^{13}C-depleted POC dominates the dry season POC.

6.4.2. End member mixing analysis

The determination of POC source was evaluated in *Clark et al.* [2013], showed that the isotopic ($\delta^{13}C_{org}$) and elemental composition (N/C) of suspended load POC can be modelled as a mixture of POC_{fossil} from sedimentary rocks, and $POC_{non\text{-}fossil}$ from and soil and vegetation. The river POC samples analysed here followed the same linear trend described in *Clark et al.* [2013] in which $\delta^{13}C_{org}$ (‰) was positively correlated with the N/C ratio (Figure 6.3), which is consistent with the mixing hypothesis. Full details can be found in *Clark et al.* [2013], but in summary here an end-member mixing analysis (Equation 2) was developed which used $\Delta^{14}C_{org}$ (radiocarbon) from a sub-set of river suspended sediment samples to determine the fraction of POC derived from POC_{fossil} (F_f), with an estimated uncertainty of 0.02. We further found that the N/C ratio of the POC samples could also be used reliably to quantify F_f in the absence of $\Delta^{14}C_{org}$ measurements [*Clark et al.*, 2013], in analogy with other mountain rivers (Hilton et al. 2010). A comparison of F_f from $\Delta^{14}C_{org}$ and $F_{nf_N/C}$ from N/C revealed a significant linear relationship ($p < 0.0001$), indicating that N/C

provides a robust quantification of POC_{fossil} input for the Kosñipata River, with an uncertainty on F_f of 0.08 to 0.14 [*Clark et al.*, 2013].

Here we use the mixing model from *Clark et al.* [2013] and the N/C of the river POC and the composition of end-members (fossil and soil/vegetation) to quantify the fraction of fossil organic carbon (F_f) in each sample (Table S6.2). The $POC_{non\text{-}fossil}$ measured samples comprised 0.64 % and 0.76 % of the suspended sediment at the San Pedro and Wayqecha gauging stations respectively (Table 6.2). The POC_{fossil} contribution was a smaller but similar component with a mean of 0.33 % and 0.32 % of the suspended sediment at the San Pedro and Wayqecha gauging stations respectively (Table 6.2).

Table 6.2: Suspended sediment and POC fluxes for the Kosñipata Valley

Annual	San Pedro*	San Pedro* estimated range	Wayqecha^
SS (t km^{-2} yr^{-1})	966+270	966 to 1236	1267±634
SS (t yr^{-1})	158,674+44,429	158,674 to 203,103	61,407±30,704
POC_f (tC km^{-2} yr^{-1})	3.9+1.4	3.9 to 5.3	3.5±1.8
POC_f (t yr^{-1})	640+237	640 to 877	170±85
POC_{nf} (tC km^{-2} yr^{-1})	5.2+1.7	5.2 to 6.9	5.3±2.7
POC_{nf} (t yr^{-1})	857+274	857 to 1131	268±134
POC total (tC km^{-2} yr^{-1})	9.1+3.1	9.1 to 12.2	8.8±4.5
POC total (t yr^{-1})	1497+522	1497 to 2049	438±219
Stream runoff (mm d^{-1})	7.5		8.5
% POC_f of SS (measured)	0.33		0.32
% POC_{nf} of SS (measured)	0.64		0.76
% POC of SS (measured)	0.97		1.08
% POC_f of SS (annual)	0.40		0.28
% POC_{nf} of SS (annual)	0.54		0.44
% POC of SS (annual)	0.94		0.72

*Errors on the rating curves are -28 %, -37 % and -32 % for SS, POC_{fossil} and $POC_{non\text{-}fossil}$ respectively (Table S6.2). Rating curve errors are greater than those on the error on the mixing model. Positive errors are only given because the rating curves underestimate fluxes.
^ Errors for straight averages of discrete samples have errors that reach 50% [*Ferguson*, 1987].

6.4.3. Sediment and POC rating curves

At the San Pedro gauging station power-law rating curves were used to describe the solid load concentrations with Q_w (Figure S6.1a, c & e, Table S6.3). The power-law curves were applied to continual Q_w [*Clark et al.*, in review] to determine instantaneous fluxes over the sampling period. Suspended sediment load and POC_{fossil} demonstrated a power-law

relationship with Q_w (Figure S6.1a & c). $POC_{non\text{-}fossil}$ demonstrated a threshold behaviour [*Clark et al.*, 2013] and two power-law rating curves were necessary to describe $POC_{non\text{-}fossil}$ concentration with Q_w (Figure S6.1e, Table S6.3).

At the Wayqecha gauging, due to limited Q_w measures throughout the study period (n = 59) [*Clark et al.*, in review] available samples (n = 45) were used to determine mean monthly solid load concentrations and then multiplied by monthly stream runoff flux to determine monthly sediment load fluxes.

6.4.4. Suspended load behaviour

6.4.4.1. San Pedro gauging station

The concentration of suspended sediment was strongly related to the Q_w and well described by a power law rating curve (Figure S6.1a). Suspended sediment concentrations ranged from a minimum of < 5 g m^{-3} to a maximum of ~19,000 g m^{-3} (Table S6.1). To prevent an overestimation of suspended sediment during stormflow, suspended sediment was capped at 19,000 g m^{-3}. Instantaneous fluxes generated using the rating curve reached the cap for < 1 hour throughout the year (0.01 %). The rating curve predicted the measured suspended sediment samples well, following the one-to-one line, however, the rating curve underestimated the highest measured suspended sediment concentrations (Figure S6.2a).

Measured samples covered a wide range of $POC_{non\text{-}fossil}$ concentrations with a minimum of ~0.1 g m^{-3} to a maximum of 116 g m^{-3} (Table S6.1). To best characterise the relationship between $POC_{non\text{-}fossil}$ and Q_w throughout the year, the rating curve was split at a Q_w of 22 m^3 s^{-1}, forming two power-law rating curves (Figure S6.1e). This is in line with the threshold behaviour of $POC_{non\text{-}fossil}$ export reported in other mountain rivers [*Hilton et al.*, 2012; *Smith et al.*, 2013], in which supply of $POC_{non\text{-}fossil}$ is greatly enhanced once steep forested slopes are effectively coupled to the channel during high rainfall. The high exponent

on the threshold $POC_{non\text{-}fossil}$ rating curve (Figure S6.1e) would have led to very high $POC_{non\text{-}fossil}$ at the highest Q_w in the record (e.g. *Hilton et al.* [2008b]). To prevent an overestimation at the highest Q_w, $POC_{non\text{-}fossil}$ concentration was capped at 116 g m^{-3} (our maximum measured $POC_{non\text{-}fossil}$; Table S6.1). The cap limited $POC_{non\text{-}fossil}$ concentration for an equivalent of 1.5 days (0.4 %) over the year. The measured $POC_{non\text{-}fossil}$ and the rating curve $POC_{non\text{-}fossil}$ concentration were in agreement, except with samples > 10 g m^{-3} which tended to be underestimated by the rating curve (Figure S6.2e). Along with a cap of 116 g m^{-3}, our $POC_{non\text{-}fossil}$ flux estimates would be conservative as the rating curve under-predicts $POC_{non\text{-}fossil}$ at high Q_w.

Measured POC_{fossil} samples had a wide range of concentrations with a minimum of < 0.01 g m^{-3} up to a maximum of 77 g m^{-3} (Table S6.1). The concentration of particulate organic carbon from fossil sources (POC_{fossil}) had a strong relationship with Q_w (Figure S6.1c). POC_{fossil} concentration was closely linked with the suspended sediment concentration (Figure S6.1a) and is well documented in river suspended load [*Blair et al.*, 2003; *Hilton et al.*, 2011a]. POC_{fossil} concentrations determined using the rating curve equalled the measured POC_{fossil} concentrations, with some underestimation of POC_{fossil} at high concentrations (Figure S6.2c). POC_{fossil} was capped at 77 g m^{-3} (the maximum measured concentration) and limited POC_{fossil} concentrations for a total period of 6 hrs 45 min (0.08 %) over the year.

6.4.4.2. Wayqecha gauging station

The minimum suspended sediment concentration was 3 g m^{-3} and the maximum was 2,869 g m^{-3} (Table S6.1). Overall, the positive relationship of suspended sediment load with Q_w was not well described by a power law rating curve (Figures S6.1b & S6.2b). This is likely to primarily reflect the larger uncertainty on Q_w at the Wayqecha gauging station [*Clark et al.*, in review]. The measured POC_{fossil} samples had a minimum sample concentration of 0.05 g m^{-3} and a maximum concentration of 12.6 g m^{-3} (Table S6.1). The

measured $POC_{non\text{-}fossil}$ samples had a minimum concentration of 0.05 g m^{-3} and a maximum concentration of 13 g m^{-3} (Table S6.1). To evaluate the rating curve for $POC_{non\text{-}fossil}$, samples were separated into wet season (n = 36) and dry season (n = 6; Figure S6.1f). Based on measured samples, the $POC_{non\text{-}fossil}$ concentration did not appear to change with an increase in Q_w throughout the dry season, and in the wet season showed a similar threshold behaviour as at San Pedro.

The rating curves proved to be poor indicators of suspended load concentrations at the Wayqecha gauging station (Figure S6.1b, d, f). As a result, the measured samples were used to determine an annual average sediment load yields for suspended sediment, POC_{fossil} and $POC_{non\text{-}fossil}$ (Table 6.2), as suggested by *Ferguson* [1987]. The estimated uncertainty on the average annual yields is estimated at ~50 % [*Ferguson*, 1987] (Table 6.2), which is less than the estimated error that would be expected using the rating curve method (Table S6.2).

6.4.4.3. Rating curve accuracy

During the two week wet season sampling campaign, there were 24 paired suspended sediment samples and Q_w measurements collected, measured at a high temporal resolution (3 hrs) so that instantaneous measured flux could be determined and be compared to the fluxes from the rating curves. At the San Pedro gauging station, the rating curve underestimated the suspended sediment yield by 28 % on average (Table S6.2). This suggests that the suspended sediment flux values for the San Pedro gauging station are conservative (Table 6.2). At the San Pedro gauging station, during the 2-week wet season campaign, the rating curve underestimated $POC_{non\text{-}fossil}$ and POC_{fossil} yields by 32 % and 37 % respectively, indicating that annual fluxes would also be conservative (Table S6.2). However, at the Wayqecha gauging station, the flux measures showed a significant amount of imprecision, with the rating curve over-estimating suspended sediment flux by 59 % on average when compared to

the measured samples (Table S6.2). This indicates that a rating curve derived annual sediment yield would be erroneous.

These uncertainties are much larger than those returned by the end member mixing model. As such, we consider that the uncertainty on $POC_{non\text{-}fossil}$ and POC_{fossil} flux is dominated by the rating curve method. For the San Pedro gauging station, the rating curve under-estimates the instantaneous flux for all solid load constituents. Therefore, flux values are reported as a range between the rating curve estimate, and the estimate plus the accuracy on the rating curve method (e.g. 5.2 – 6.9 tC km^{-2} yr^{-1}). For Wayqecha, where rating curves were not well constrained, we report the uncertainty as ± 50 % of the estimated annual yield [*Ferguson*, 1987].

6.4.4.4. Inter-basin comparisons

Over the 2 week period of high frequency sampling February 2010 [*Clark et al.*, 2013], there were 24 paired samples collected at both the San Pedro gauging station and Wayqecha gauging station (Table S6.2). During this time the instantaneous suspended sediment yield from measured samples at the Wayqecha station was 44 % lower than the yield from measured samples at the San Pedro gauging station (Table S6.2). Over this 2 week study period there was an increase in suspended sediment sourcing downstream of the Wayqecha sub-catchment (Table S6.2). This was most likely due to rainfall occurring more frequently at the San Pedro gauging station (36 % of the time), than at the Wayqecha gauging station (18 % of the time) over the 2 week 3 hourly collection period. Additionally, paired measured samples over the course of the year (n = 11) showed that the suspended sediment flux was 31 % greater at the San Pedro gauging station (Table S6.2). This suggests that although the measured Wayqecha runoff may be higher than at San Pedro, the measured suspended sediment yield was generally greater at San Pedro (Figure S6.3a).

6.4.5. Annual transfer

The annual suspended sediment yield for the San Pedro catchment (164.4 km^2) was 996 – 1236 t km^{-2} yr^{-1} (159,000 – 302,000 t yr^{-1} flux). The yield for the Wayqecha catchment (48.5 km^2) was 1267 ± 634 t km^{-2} yr^{-1} (61,000 ± 30,700 t yr^{-1} flux; Table 6.2). Given the uncertainty in the fluxes measurements, the sediment yields are similar for the two basins (Table 6.2). The yield is 100 % greater than that estimated in the Chorobamba River Valley of the Eastern Andes of Peru at ~120 to 620 t km^{-2} yr^{-1} (c.f. *Townsend-Small et al.* [2008]) where the slopes are less steep and annual rainfall totals are lower.

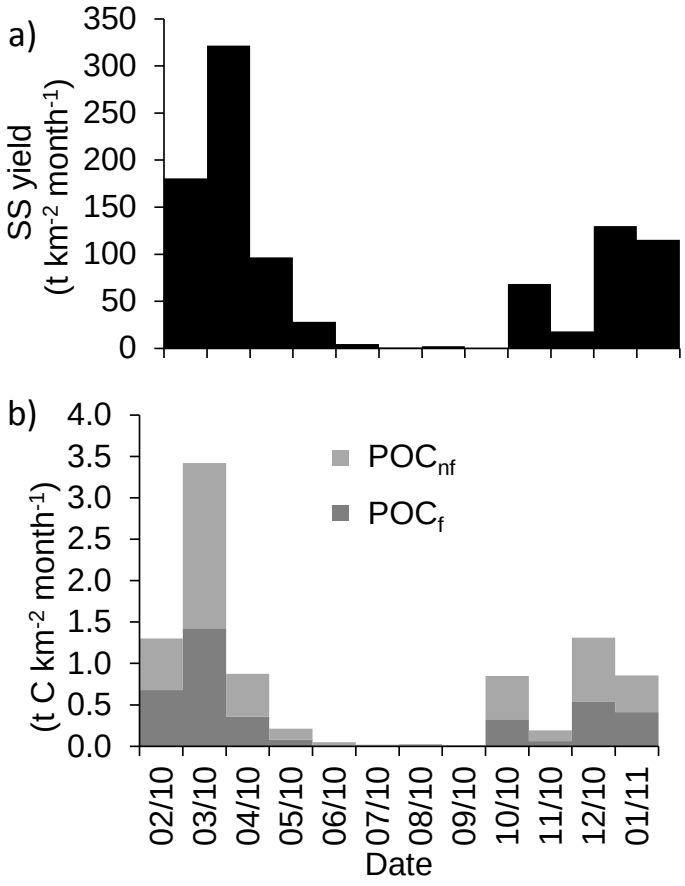


Figure 6.5: Annual breakdown by month of a) suspended sediment flux, and b) $POC_{non\text{-}fossil}$ and POC_{fossil} fluxes for the San Pedro catchment.

The annual $POC_{non\text{-}fossil}$ yield was 5.2 to 6.9 and 5.3 ± 2.7 tC km^{-2} yr^{-1} for the San Pedro and Wayqecha catchments respectively (Table 6.2). The annual POC_{fossil} yields were similar with 3.9 to 5.3 and 3.5 ± 1.8 tC km^{-2} yr^{-1} for the San Pedro and Wayqecha catchments

respectively (Table 6.2). These yields are relatively low compared to several other mountain rivers, but considering the lower suspended sediment flux of the Kosñipata Valley (Figure 6.6), they fit well in with the global trend for mountain catchments[*Korup et al.*, 2004; *Hilton et al.*, 2008b; *Hatten et al.*, 2012; *Hilton et al.*, 2012; *Smith et al.*, 2013]. A compilation of $POC_{non\text{-}fossil}$ yields versus suspended sediment yields indicates that the Taiwanese samples are not distinct from other mountain rivers on a global scale [*Galy*, in prep].

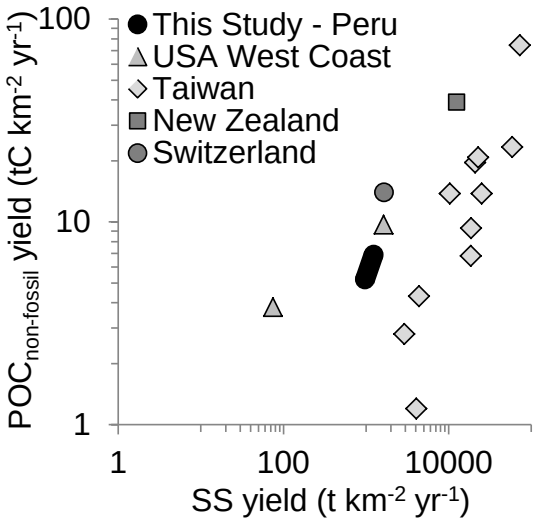


Figure 6.6: Suspended sediment yield versus the $POC_{non\text{-}fossil}$ yield for this study, 11 catchments in Taiwan [*Hilton et al.*, 2012], the western Southern Alps of New Zealand [*Korup et al.*, 2004; *Hilton et al.*, 2008a], the Santa Clara and Alsea Rivers in the West Coast of the USA [*Hatten et al.*, 2012], and a headwater catchment in the Swiss Alps [*Smith et al.*, 2013].

The $POC_{non\text{-}fossil}$ of the annual suspended sediment contribution was 0.54 % and 0.46 % to suspended sediment at the San Pedro and Wayqecha gauging stations respectively. The contribution of Kosñipata River $POC_{non\text{-}fossil}$ as C_{org} % is in the middle of the range, when compared to other catchments. The $POC_{non\text{-}fossil}$ yield in the Kosñipata Valley was lower than in the Swiss Alps and the Californian mountain rivers [*Hatten et al.*, 2012; *Smith et al.*, 2013] but higher than in several catchments in Taiwan (Figure 6.6) [*Hilton et al.*, 2008a; *Hilton et*

al., 2012]. The POC_{fossil} annual contribution was a smaller a mean contribution of 0.40 % and 0.28 % to suspended sediment at the San Pedro and Wayqecha gauging stations respectively (Table 6.2).

6.5. Discussion

6.5.1. Fluvial transport of $POC_{non\text{-}fossil}$

At the San Pedro gauging station, the behaviour of the $POC_{non\text{-}fossil}$ with an increase in Q_w is fundamentally different from that of suspended sediment and POC_{fossil} (Figure S6.1a, c, e). At low $Q_w < 15\ m^{-3}\ s^{-1}$ the $POC_{non\text{-}fossil}$ concentration remained low and relatively invariant. Above these Q_w values, increased Q_w resulted in a marked increase in $POC_{non\text{-}fossil}$ concentration, suggesting a form of threshold behaviour (Figure S6.1e). Thresholds in river $POC_{non\text{-}fossil}$ concentration have been demonstrated in this river previously [*Clark et al.*, 2013], in another Andean catchment [*Townsend-Small et al.*, 2008] and in other mountain rivers [*Hilton et al.*, 2012; *Smith et al.*, 2013]. Reasons for this threshold depend on the fact 1) that C_{org} (%) and F_{nf} do not decrease at high Q_w (Figure S6.5) [*Clark et al.*, 2013] and 2) that fraction non-fossil (F_{nf}) can be enriched at peak flow (Figure S6.5a) [*Clark et al.*, 2013]. The river channel is largely free from live vegetation [*Clark et al.*, 2013] which is common in mountain rivers where river incision and flood events dominate [*Hartshorn et al.*, 2002; *Townsend-Small et al.*, 2008; *Hilton et al.*, 2012]. Therefore, river $POC_{non\text{-}fossil}$ is supply limited and so has a tendency to display thresholds of mobilisation.

The supply of soil and vegetation material comes from two main geomorphic processes. First, bedrock landslides can clear entire tracks of mountain forest and deliver this material to the river channel network [*Hilton et al.*, 2008a; *West et al.*, 2011; *Clark et al.*, in prep]. This process mobilises $POC_{non\text{-}fossil}$ ranging from fine-grained, mineral-associated $POC_{non\text{-}fossil}$, to entire tree trunks [*Hilton et al.*, 2011b; *West et al.*, 2011]. Second, overland

surface flow and shallow landsliding can mobilise loose material and $POC_{non\text{-}fossil}$ from surface soils [*Gomi et al.*, 2008] and the rate of transport depends on hillslope steepness [*Roering et al.*, 2001]. Rainfall can drive both landslide activity and overland surface flow, resulting in efficient hillslope-channel coupling and delivery of $POC_{non\text{-}fossil}$ to river channels [*Hilton et al.*, 2012]. The dependence of $POC_{non\text{-}fossil}$ on supply is evident in stormflow hysteresis, as $POC_{non\text{-}fossil}$ concentrations fall after rainfall ceases [*Hilton et al.*, 2008b; *Clark et al.*, 2013]. The variable supply of OC at high Q_w demonstrates the importance of high frequency river sampling to capture variance in $POC_{non\text{-}fossil}$.

As a result of this supply-limited behaviour, two power-law rating curves were used to describe the trend between $POC_{non\text{-}fossil}$ and Q_w at the San Pedro gauging station. $POC_{non\text{-}fossil}$ concentrations remained low and relatively invariant with $Q_w < 22$ m^3 s^{-1} (Figure S6.1e). They then increased rapidly > 22 m^3 s^{-1} and so this Q_w value was chosen to describe the threshold behaviour in this instance. The Q_w value equates to an area normalised runoff of ~0.5 mm hr^{-1}.

In addition to Q_w, $POC_{non\text{-}fossil}$ transport has been shown to be sensitive to the rate of change of Q_w, i.e. intense rainfall events play an important role [*Clark et al.*, 2013]. When the dataset is sub-divided based on the rate of change of Q_w, there was also a good fit for the pattern seen in the $POC_{non\text{-}fossil}$ (Figure S6.6b). The rate of change was determined as the difference of the river height as a mean ± 15 min at the time of sample collection was made, minus the river stage height as a mean ± 15 min 3 hrs previous to sample collection. A rate of change > 0.02 was defined as rising and a rate of change < 0.02 was defined as no change/falling. The rising limb had a very steep exponent and did not include any low Q_w or low $POC_{non\text{-}fossil}$ samples (Figure S6.6b). The no-change/falling limb samples were mostly during low flow. At this time baseflow dominates Q_w, therefore providing little $POC_{non\text{-}fossil}$ supply.

6.5.2. Controls on sediment and POC export

6.5.2.1. Climate

Seasonality played a significant role in the erosion and export of suspended sediment and POC at the San Pedro gauging station. The wet season, covering 4 months from December to March, was responsible for most of the solid constituent export, with 77 %, 78 % and 73 % of the suspended sediment, POC_{fossil} and $POC_{non\text{-}fossil}$ flux occurring, respectively (Table 6. 4; Figures 6.5 & 6. 7). In contrast, during the dry season (5 months from May to September) the river exported < 5 % of the annual yields (Table S6.4; Figure 6.5). The dry season contributed only a small fraction of the solid load export, first because the capacity of a river to entrain fine sediment (and POC) increases with water flow velocity and turbulence, and so low Q_w allows fine suspended sediment and POC to settle [*Garcia and Parker*, 1991; *Hamm et al.*, 2011] and be deposited in transient bars in the channel. Second, the hydrological budget of this catchment shows that the majority of the river water during the dry season is sourced from delayed runoff via deep groundwater [*Clark et al.*, in review]. When combined with the very low rainfall, this results in minimal overland flow and surface erosion processes, thought to play a major role in the delivery of $POC_{non\text{-}fossil}$ to river channels [*Hilton et al.*, 2012; *Clark et al.*, 2013; *Smith et al.*, 2013].

Seasonality was also evident in the $\delta^{13}C$ values of the POC (Figure 6.4) and the N/C values which were positively correlated to $\delta^{13}C$ (Figure 6.3). In general, in the wet season the POC $\delta^{13}C$ values were more depleted at ~ -28 ‰, while displaying a much larger seasonal variability (-26 to -30 ‰) (Table S6.1, Figure 6.4). The variability in the isotopic composition of POC in this catchment is mostly controlled by the addition of POC_{fossil} (with $\delta^{13}C$ ~ -23 ‰) and $POC_{non\text{-}fossil}$ (with $\delta^{13}C$ ~ -26 to -30 ‰) (Figure 6.3) [*Clark et al.*, 2013] and therefore the observed seasonal changes can be interpreted in terms of temporal variability in POC source in the river catchment. Following the wet season, as Q_w and rainfall decrease, the suspended sediment loads are greatly reduced (Figure 6.4) indicating that minimal POC_{fossil},

which is intimately associated with clastic sediment [*Blair et al.*, 2003; *Hilton et al.*, 2011a] is transported by the river. As a result, the influence of the POC_{fossil} on $\delta^{13}C$ is decreased in the dry season and the river POC $\delta^{13}C$ suggests a dominant source from vegetation and soil (Figure 6.4).

This contrasts somewhat with previous work in the Peruvian Andes in a less steep, less erosive catchment in the Chorobamba River [*Townsend-Small et al.*, 2007; *Townsend-Small et al.*, 2008]. There, in-stream photosynthesis by aquatic autotrophs is thought to be responsible for depleted $\delta^{13}C$ values during the dry season. While POC from this source could be present in the Kosñipata River during low turbidity in the dry season, we note that the dry season N/C values are 0.04-0.07, more consistent with a source from vegetation and soil (Figure 6.2) rather than aquatic biomass (N/C >0.1) [*Townsend-Small et al.*, 2007]. Nevertheless, the important distinction between POC_{fossil} and recently photosynthesised organic carbon ($POC_{non\text{-}fossil}$) is accounted for by the mixing analysis (Figure 6.3). In addition, it is worth remembering that the POC transport during the dry season is minimal (<5 %).

In addition to seasonal patterns, individual storm events and the associated rainfall-driven changes in suspended load and POC transport (e.g. *Hilton et al.* [2012]) suggest a strong climate control on the mobilisation and transport of material in this catchment. Storms played a significant role in the erosion and transfer of soil and standing biomass to the river (Figure 6. 7b). $POC_{non\text{-}fossil}$ was the most sensitive to storm events in the valley, with 50 % of the annual yield transferred in only 8 days of the year. The largest storm event had a stream runoff of 1.3 mm hr^{-1} over the peak when $Q_w > 50$ m^{-3} s^{-1}. The storm event which lasted 3 days contributed a ~25 % of the annual $POC_{non\text{-}fossil}$ yield (Table S6.5), but only ~2 % of the Q_w yield.

6.5.2.2. Landslides

In the Kosñipata Valley, landslides are a significant mass wasting process and play a pivotal role in mobilising $POC_{non\text{-}fossil}$ from hillslopes [*Clark et al.*, in prep]. Previous studies have suggested that bedrock and shallow-soil landslides can supply a large portion of the soil and vegetation found in river $POC_{non\text{-}fossil}$ [*Hilton et al.*, 2008b; *Hilton et al.*, 2011b; *Hovius et al.*, 2011; *Smith et al.*, 2013; *Stallard*, 2013]. In the San Pedro catchment, landslide activity mobilised ~28 tC km^{-2} yr^{-1} of soil and vegetation [*Clark et al.*, in prep], which is significantly larger yield than previous estimates in mountain forests [*Hilton et al.*, 2011b]. This annual yield is much higher than the estimated rate of $POC_{non\text{-}fossil}$ export from the valley, 5.2 – 6.9 tC km^{-2} yr^{-1} (Table 6.2). We must acknowledge that the length of the sampling window was different, with landslide activity quantified over 25 years from satellite imagery, whereas and the river study represents samples collected over 1.25 yr and may be an underestimate (Section 4.2.3). However, the suspended sediment yield over the sampling period was similar to longer term estimates [*Guyot et al.*, 1996], suggesting the $POC_{non\text{-}fossil}$ yields are representative of longer periods of time. Therefore, the difference between landslide mobilised $POC_{non\text{-}fossil}$ and fluvial export of $POC_{non\text{-}fossil}$ is still significant even after accounting for uncertainties on these fluxes.

Landslides mobilise a large range of grain sizes of $POC_{non\text{-}fossil}$, including coarse material which is not sampled by river POC. Therefore, the differences between the yields can be accounted for if only ~20 – 25 % of the landslide mobilised $POC_{non\text{-}fossil}$ was fine grained (i.e. finer than sand) and contributed to POC suspended load. In addition, some of the material which landslides mobilise may be stored within landslide deposits over decades [*Korup et al.*, 2004; *Hovius et al.*, 2011]. This has important implications for the carbon balance of the Andean forest ecosystem. The net primary productivity (NPP) of the Kosñipata Valley ranges from 115,080 to 197,280 tC yr^{-1} [*Girardin et al.*, 2013; *Huaraca Huasco et al.*, 2013; *Oliveras*, in prep]. Landslides mobilise 28 tC km^{-2} yr^{-1} (4,600 tC yr^{-1}) [*Clark et al.*, in

prep]. We estimate that fluvial export of $POC_{non\text{-}fossil}$ was 860 – 1130 tC yr^{-1} (Table 6.2). Whilst landslides mobilise 2 to 4 % yr^{-1} of the NPP [*Clark et al.*, in prep], rivers transfer only 0.4 to 1.0 % yr^{-1} of the NPP out of the valley (See section 5.5). Thus, it appears that 3470 – 3740 tC yr^{-1}, equating to 2 to 3 % yr^{-1} of the NPP was mobilised by landslides but did not leave the valley as fine grained, suspended load $POC_{non\text{-}fossil}$. This carbon may be transferred as course woody debris [*West et al.*, 2011], may be buried onsite in the valley (Figure S6.4), may contribute to DOC after partial degradation, or may be degassed from landslide debris deposits releasing recently sequestered CO_2 back to the atmosphere.

The mean accumulated upslope area is ~130 000 m^2 before hillslopes join the river channel. As well, almost all of the landslides are connected to a river channel (96 % of the total area manual and 86 % automatic; Table S6.6) using standard definitions [*Meunier et al.*, 2008; *Hilton et al.*, 2011b]. However, not all of this material was immediately transported out of the catchment by the river (Figure S6.4a & b). In many regions of high to mid-elevations, landslide deposits reached small streams where the carrying capacity is low. This meant that the eroded material could remain onsite and subsequently be transferred out of the valley over an extended period of time (Figure S6.4a & b) [*Ramos Scharrón et al.*, 2012]. Additionally, in the lower elevations of the San Pedro catchment, alluvial sediment deposits are evident along the river. Landslide derived material can be buried onsite and transiently stored (Figure S6.4c & d). Thus, although landslides provide a large amount of material with the potential to be transferred into streamflow as $POC_{non\text{-}fossil}$, the connectivity of those landslides to the river channel is not the most important factor at play. More research needs to be done to evaluate the fate of landslide mobilised carbon in landslide deposits, evaluating debris C stocks, CO_2 respiration and C residence time.

Finally, there were ~ 185 landslides triggered by the largest storm event of the year (Table S6.5) mobilising high amounts of sediment and soil and vegetation carbon stocks.

Over this period, it is likely that $POC_{non\text{-}fossil}$ transported by the river would have had a significant component derived from landsliding. Physical forcing driven by a large localised storm event was an important contributor to river $POC_{non\text{-}fossil}$ in the valley.

6.5.3. Global controls on $POC_{non\text{-}fossil}$ yields in mountain river catchments

Previous work from the mountain belt of Taiwan has suggested that sediment yield is a dominant control on the yields of $POC_{non\text{-}fossil}$ in mountain river catchments [*Hilton et al.*, 2012]. A growing body of literature has since quantified POC yields and accounted for POC_{fossil} in mountain catchments [*Hatten et al.*, 2012; *Goñi et al.*, 2013; *Smith et al.*, 2013]. This new data allows us to question whether or not sediment yield is the master variable controlling $POC_{non\text{-}fossil}$ export across these mountain forest sites. The suspended sediment yield at San Pedro was 960 – 1200 t km^{-2} yr^{-1} over the sampling period (Table 6.2) which is moderate to high when compared to global sediment yields [*Milliman and Farnsworth*, 2011; *Larsen et al.*, 2014]. These erosion rates are roughly ten times the average sediment yield in the Amazon Basin of ~100 t km^{-2} yr^{-1} [*Guyot et al.*, 1996]. The sediment yield of the Kosñipata Valley is greater than the sediment yield in several other mountain catchments outside of the tropics where yields range from 75 to 150 t km^{-2} yr^{-1} and tectonic uplift rates are lower than in Peru [*Hatten et al.*, 2012; *Goñi et al.*, 2013]. However, the sediment yield of the Kosñipata Valley is lower than mountain islands where there is heavy rainfall and high tectonic uplift rates, with suspended sediment yields of ~2100 to 30,000 t km^{-2} yr^{-1} in Taiwan [*Kao and Liu*, 1996; *Dadson et al.*, 2003; *Hilton et al.*, 2011a], New Zealand [*Hicks et al.*, 2000; *Lyons et al.*, 2002], and New Guinea [*Milliman*, 1995].

The $POC_{non\text{-}fossil}$ yield for the Kosñipata Valley was 5.2 – 6.9 tC km^{-2} yr^{-1} (Table 6.2). This yield is higher than in three catchments in Taiwan which have yields ranging from 1.2 to 4.6 tC km^{-2} yr^{-1} [*Kao and Liu*, 1997; *Hilton et al.*, 2012], and in the Alsea river in Oregon with a yield of 3.8 tC km^{-2} yr^{-1} [*Hatten et al.*, 2012]. Outside of the tropics there are a couple

mountain catchments with higher $POC_{non\text{-}fossil}$ than found in this study, such as in the Santa Clara River in Southern California (10 tC km^{-2} yr^{-1}) [*Hatten et al.*, 2012] and in a 1st order tributary of the Alp River in Switzerland (14 tC km^{-2} yr^{-1}) [*Smith et al.*, 2013]. The mountain islands of Taiwan and New Zealand have the highest $POC_{non\text{-}fossil}$ yields in the world ranging from 7 to 85 tC km^{-2} yr^{-1} [*Hilton et al.*, 2008a; *Hilton et al.*, 2008b; *Hilton et al.*, 2012]. When considered together, there is a global trend between suspended sediment and $POC_{non\text{-}fossil}$ yield; that is, the higher the suspended sediment, the higher the $POC_{non\text{-}fossil}$ yield (Figure 6.6).

While the $POC_{non\text{-}fossil}$ yields from the Peruvian Andes are broadly consistent with other mountain river catchments once suspended sediment yield has been accounted for (Figure 6.6), it is clear that there are significant differences beyond the uncertainties on these fluxes. For example, the $POC_{non\text{-}fossil}$ yield at San Pedro is roughly 2-3 times higher than catchments in Taiwan where suspended sediment yield is similar (Figure 6.6). This may reflect the difference in $POC_{non\text{-}fossil}$ stocks in soil and vegetation on hillslopes, which are ~19,000 tC km^{-2} in Taiwan [*West et al.*, 2011; *Hilton et al.*, 2012] while are over double that value in the Kosñipata valley, at ~42,000 tC km^{-2} [*Clark et al.*, in prep].

However, it is worth noting that [*Hilton et al.*, 2012] comment that the $POC_{non\text{-}fossil}$ yields from Taiwan are likely to be precise, but may be an underestimation due to the flux-weighted averaging method used to estimate flux. However, the role of the biomass C stock can also explain higher $POC_{non\text{-}fossil}$ yields in the temperate catchments. Temperate forest ecosystems tend to store more $POC_{non\text{-}fossil}$ in soil relative to biomass [*Dixon et al.*, 1994], and given how important soil horizons are for the source of $POC_{non\text{-}fossil}$ [*Clark et al.*, 2013; *Smith et al.*, 2013], this may explain why the Andean yields are lower for a given suspended sediment yield than other temperate mountain catchments (Figure 6.6).

There may be other contributing factors to the high rates of river suspended sediment and $POC_{non\text{-}fossil}$ transfer in other mountainous regions such as in southern California and in the Swiss Alps. The site in the Swiss Alps is < 1 km^2, a small mountain headwater stream with much lower Q_w than some of the other study locations with drainage areas >100 km^2 [*Smith et al.*, 2013]. This may impact the processes of $POC_{non\text{-}fossil}$ supply and transport and it is possible that the region may have variable physical and climatological forcing different to the small study area. In the high sediment yielding catchments of California, the ecosystems contain anthropogenic sediment fluxes generated from cities, agriculture, and forestry [*Hatten et al.*, 2012].

6.5.4. $POC_{non\text{-}fossil}$ export and the carbon budget of Andean forest

Erosion and fluvial transport of $POC_{non\text{-}fossil}$ represents an export of organic matter from the forest ecosystem [*Hilton et al.*, 2012; *Ciais et al.*, 2013]. Importantly, organic carbon laterally transferred from one ecosystem to another via rivers or air, influences the carbon budget of the ecosystem, but is largely ignored or discounted from C budget analyses [*Iwata et al.*, 2005; *Ciais et al.*, 2013]. In the Kosñipata River Valley, the net primary production of forest (NPP – the carbon equivalent of above and below ground biomass production) is ~1000 tC km^{-2} yr^{-1} [*Girardin et al.*, 2013; *Huaraca Huasco et al.*, 2013; *Oliveras*, in prep]. The fluvial $POC_{non\text{-}fossil}$ transfer of 5.2 – 6.9 tC km^{-2} yr^{-1} represents ~0.4 – 1.0 % of the NPP of the forest, a similar proportion as reported elsewhere [*Hilton et al.*, 2008a; *Hilton et al.*, 2008b] and the carbon export appears to be sustained by ecosystem productivity.

However, when we examine the net carbon balance of the ecosystem, it is clear that the fluvial export of $POC_{non\text{-}fossil}$ has a crucial role to play. Net ecosystem productivity (NEP) quantifies the medium-term net carbon uptake/storage [*Marthews et al.*, 2012] by accounting for heterotrophic respiration, R_h, (respiration not derived from plants) where NEP = NPP –

R_h [*Marthews et al.*, 2012]. In the Kosñipata Valley, NEP is close to ~0 tC km^{-2} yr^{-1} [*Marthews et al.*, 2012], with heterotrophic respiration balancing the annual net production of live biomass. Therefore, the export of 5.2 – 6.9 tC km^{-2} yr^{-1} of $POC_{non\text{-}fossil}$ has the potential to govern the net carbon balance of the Andean montane forest. The role of erosion and lateral transfers of carbon is made more significant if we also consider the erosion of $POC_{non\text{-}fossil}$ by landslides, which suggest significant amounts of biomass and soil are transported as coarse debris [*Clark et al.*, in prep] not collected by river suspended load samples (e.g. *West et al.* [2011]).

If Andean $POC_{non\text{-}fossil}$ avoids respiration as it is transported downstream, because NEP is approximately zero, this would suggest that the Andes ecosystem is a net sink of CO_2 on intermediate timescales. River suspended load samples collected over depth profiles in the major tributaries and main-stem of the Amazon River shed new light on the fate of Andean POC [*Bouchez et al.*, 2014]. They suggest that previous observations of a downstream evolution of $\delta^{13}C_{org}$ values, interpreted as significant re-working of Andean POC [*Quay et al.*, 1992; *Hedges et al.*, 2000], may need to be reconsidered [*Bouchez et al.*, 2014]. The early pioneering studies did not account for POC_{fossil} input, which varies through the basin downstream of the Andes [*Bouchez et al.*, 2010] and modifies the $\delta^{13}C_{org}$ values [*Clark et al.*, 2013]. In addition, $POC_{non\text{-}fossil}$ from this Andean catchment has $\delta^{13}C_{org}$ and N/C values which are similar to forests and soils growing in the lowland ecosystems [*Clark et al.*, 2013]. This makes it hard to track and distinguish Andean $POC_{non\text{-}fossil}$ using bulk elemental and isotopic analyses of POC. Compound-specific stable hydrogen isotopes, $\delta^{13}C$ and radiocarbon measurements provide new insights [*Clark et al.*, 2013; *Ponton et al.*, in review], but it is clear we need a better constraint on the fate of Andean $POC_{non\text{-}fossil}$ to assess how lateral transfer of carbon impacts the CO_2 balance of Andean mountain forest.

6.5.5. Andean POC export and contribution to the Amazon Basin carbon budget

The Kosñipata River drains to the Madre de Dios River (124,000 km^2), a tributary of the Amazon (Figure 6.1c). The study catchments have similar bedrock geology (meta-sedimentary bedrock with some volcanic and granitic portions), vegetation cover, and above ground biomass and soil stocks of larger swaths of the Peruvian Andes draining to the Madre de Dios (MdD) River [*Saatchi et al.*, 2007; *Consbio*, 2011; *Clark et al.*, 2013; *Asner*, in prep]. At the Miraflores gauge on the Madre de Dios River (Figure 6.1c), the suspended sediment flux measured from 1983 to 1990 was 71 Mt yr^{-1} [*Guyot et al.*, 1996]. The inorganic geochemistry of sediments and mass-budget suggests the Andes are the dominant source of this sediment [*Gibbs*, 1967; *Stallard and Edmond*, 1983; *Meade et al.*, 1985; *Richey and Victoria*, 1993; *Berner and Rao*, 1994; *Allegre et al.*, 1996; *Gaillardet et al.*, 1997]. As such, the Andean portion of the Madre de Dios Basin which covers 35,600 km^2, (area > 550 masl; Figure 6.1b) has a suspended sediment yield of ~2000 t km^{-2} yr^{-1} [*Guyot et al.*, 1996]. This value is higher, but in the same order of magnitude as the suspended sediment yield measured in this study at the San Pedro gauging station (960 – 1200 t km^{-2} yr^{-1}) and Wayqecha gauging station (1260 ± 360 t km^{-2} yr^{-1}; Table 6.2). The short-term Kosñipata River measurements made here therefore can be representative of the surrounding Andes of the Madre de Dios basin, although somewhat lower. The Madre de Dios contributes to the Madeira River [*Guyot et al.*, 1996], a major Amazon tributary which carries a disproportionately large suspended sediment yield compared to other Andean-fed Amazon tributaries [*McClain and Naiman*, 2008].

If the $POC_{non\text{-}fossil}$ yield measured in the San Pedro watershed is representative of a wider Andean area in the Madre de Dios basin, where steep slopes, high rainfall and productive forests coincide [*Killeen et al.*, 2007; *Marthews et al.*, 2012; *Asner et al.*, 2014; *Mitchard et al.*, 2014], then this net C transfer may reach 0.19 – 0.25 MtC yr^{-1} over 35,600

km^2. According to this C flux, the biomass C sink over the Amazonian lowland portion of the MdD catchment (88,400 km^2) was 6.87 ± 0.94 MtC yr^{-1} (77.7 ± 11 tC km^{-2} yr^{-1}) [*Malhi*, 2010].. Thus, our data suggests that the lateral transfer of Andean $POC_{non\text{-}fossil}$ may contribute an additional ~3 % (2 – 4 %) of C when compared to the C stored in biomass in the MdD lowland basin. Although there is uncertainty in these results, this suggests, that for this period, that Andean $POC_{non\text{-}fossil}$ represents a substantial addition of C to the lowland Amazon. Moreover, the Andean $POC_{non\text{-}fossil}$ export is important to consider over longer-timescales, because erosion and burial of $POC_{non\text{-}fossil}$ can contribute to CO_2 sequestration [*Stallard*, 1998; *Galy et al.*, 2007b; *Kao et al.*, 2014] (see Section 6.5.5).

Physical erosion in the Andes also mobilises POC_{fossil} [*Bouchez et al.*, 2010; *Clark et al.*, 2013]. In the Kosñipata Valley, the POC_{fossil} comprised 0.4 % of the annual suspended sediment load. Assuming that the POC_{fossil} component remains coupled with the suspended sediment load [*Hilton et al.*, 2011a] throughout the Andes draining to the Madre de Dios River, this would equate to a POC_{fossil} flux of 0.28 MtC yr^{-1}. Using the POC_{fossil} yield (3.9 – 5.3 tC km^{-2} yr^{-1}) and the Andean source area, the POC_{fossil} flux would be 0.14 – 0.19 MtC yr^{-1}. This is a significant flux of POC_{fossil}, although smaller than the estimate of POC_{fossil} export in the neighbouring Beni River (Andean source area of 68,000 km^2) of ~0.26 MtC yr^{-1} [*Bouchez et al.*, 2010] and alone represents over half of the POC_{fossil} flux estimated in the lowland Amazon Basin [*Bouchez et al.*, 2014]. The flux is also similar to the POC_{fossil} flux exported to the Bay of Bengal by the Ganges-Brahmaputra Rivers [*Galy et al.*, 2007b; *Galy et al.*, 2008a].

Our estimates of total POC flux (fossil and non-fossil) over the Andean portion of the Madre de Dios basin equate to 0.33 – 0.44 MtC yr^{-1}, equivalent to ~2 – 4 % of the total Amazon River total POC yield to the Atlantic Ocean of ~11-14 MtC yr^{-1} [*Richey et al.*, 1990b; *Moreira-Turcq et al.*, 2003] from ~0.6 % of the total drainage area. The fate of

Andean $POC_{non\text{-}fossil}$ and POC_{fossil} once it leaves the Andes is not well constrained because their geochemical composition is partly masked by mixing with lowland-derived $POC_{non\text{-}fossil}$ added to the river as it travels in the Amazon [*Quay et al.*, 1992; *Hedges et al.*, 2000; *Clark et al.*, 2013; *Bouchez et al.*, 2014]. However, the average age of biospheric POC carried by the Madeira River has been quantified as 2850 years [*Bouchez et al.*, 2014], much older than Andean $POC_{non\text{-}fossil}$, which on average is very young (mean river $\Delta^{14}C_{org}$ ~50 ‰) [*Clark et al.*, 2013]. This finding suggests that if Andean $POC_{non\text{-}fossil}$ makes a significant contribution to lowland POC flux, it is likely to have resided in floodplain deposits for a period of time prior to remobilisation. The exchange of POC and sediment with the lowland floodplain is likely to be very important [*Aalto et al.*, 2003; *Moreira-Turcq et al.*, 2013], but is not well quantified at the large scale.

Finally, if we consider POC_{fossil}, *Bouchez et al.* [2010]'s estimate that 0.02 % of the suspended sediment at the outlet of the Madeira River is sourced from POC_{fossil}, corresponding to a POC_{fossil} flux of ~0.02 MtC yr^{-1} downstream of the confluence of the Beni and Madre de Dios Rivers. Adding the estimates of the Andean-derived POC_{fossil} flux for both these basins gives 0.40 – 0.45 MtC yr^{-1}. The marked discrepancy (>0.35 MtC yr^{-1}) suggests that either POC_{fossil} is efficiently buried in the lowland floodplain during overbank deposition [*Dunne et al.*, 1998; *Aalto et al.*, 2003], which is possible if the majority of POC_{fossil} is delivered at high stage (Figure 6.7). Alternatively, POC_{fossil} has been oxidised during floodplain transit as suggested by *Bouchez et al.* [2010], releasing ancient CO_2 to the atmosphere [*Bouchez et al.*, 2010]. In the lowlands of the Madre de Dios in the Tambopata River, which drains the Andes, CO_2 degassing from fossil sources has been recognised [*Vihermaa et al.*, 2014]. Given the magnitude of this carbon flux, which is more than half of the silicate weathering CO_2 drawdown in the Madeira Basin of ~0.8 MtC yr^{-1} [*Gaillardet et*

al., 1999], it is extremely important to better constrain the fate of POC_{fossil} in the Amazon basin.

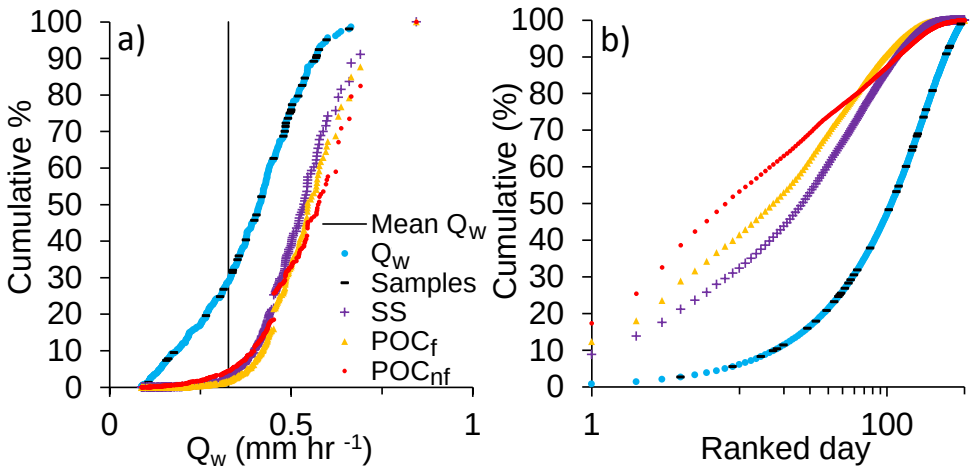


Figure 6.7: a) Cumulative flux of river discharge (Q_w) and the associated $POC_{non\text{-}fossil}$, POC_{fossil}, and suspended sediment (SS) against total daily Q_w (mm hr^{-1}) over the course of the year study period at the San Pedro river gauging station. Mean Q_w was 0.32 mm hr^{-1} (black vertical line). Samples are well distributed over the different hydrologic conditions (black dashes). b) Cumulative flux as in a) ranked by day (n = 335) where 1 is the largest Q_w day and 335 is the lowest Q_w day, demonstrating the important role of flood events in the flux of $POC_{non\text{-}fossil}$, POC_{fossil} and suspended sediment in the Kosñipata Valley.

6.6. Conclusions

We determined the suspended sediment, $POC_{non\text{-}fossil}$, POC_{fossil} yields for the Kosñipata River, in the Andes of Peru, for a one year study period. This data confirms the importance of fossil bedrock in Andean river POC. $POC_{non\text{-}fossil}$ contribution (0.54 %) to suspended sediment was greater than POC_{fossil} (0.4 %) over the year. At the San Pedro gauging station, the rating curve confirmed that $POC_{non\text{-}fossil}$ increased rapidly at high Q_w. Storms created episodic streamflow and transported 50 % of the $POC_{non\text{-}fossil}$ yield within 8 days of the year. Seasonality was important for annual fluxes as most of the sediment and POC was transported in the river in the wet season. The Andean River laterally transfers 5.2 – 6.9 tC km^{-2} yr^{-1} of $POC_{non\text{-}fossil}$ to Amazonia, which represents 0.4 – 1.0 % of the Andean

forest NPP. Since the Andean NEP is ~0 tC km^{-2} yr^{-1}, our findings suggest that the fate of $POC_{non\text{-}fossil}$ exported by Andean rivers plays a major role in determining whether the Andean montane forest is a carbon source or sink. Andean river $POC_{non\text{-}fossil}$ transferred laterally to Amazonia equates to ~3 % of the biomass C sink in the Madre de Dios lowland forests. Over the wider Madre de Dios basin, which drains ~6 % of the Amazonian Andes (35 600 km^2), we estimated the fluxes of $POC_{non\text{-}fossil}$ (0.19 – 0.25 MtC yr^{-1}) and POC_{fossil} (0.14 – 0.19 MtC yr^{-1}) to the lowland Amazon River Basin. Together these POC fluxes equate to 2 – 4 % of the total POC export to the Atlantic Ocean by the Amazon River, from only 0.6 % of the drainage area. However, the fate of Andean $POC_{non\text{-}fossil}$ and POC_{fossil} in the lowland rivers needs to be better constrained in order to fully quantify the impact of erosion and lateral carbon fluxes on the CO_2 budget of the Amazon ecosystem. Net oxidation of Andean POC_{fossil} has the potential to release significant amounts of geological CO_2 to the atmosphere on geological timescales, but transient storage of $POC_{non\text{-}fossil}$ and contribution to oceanic POC export may represent an important CO_2 sink.

6.7. Acknowledgements

This paper is a product of the Andes Biodiversity and Ecosystems Research Group (ABERG). KEC was funded by the Natural Sciences and Engineering Research Council of Canada (NSERC) and Clarendon Fund PhD scholarships. RGH was supported by a NERC New Investigator Grant (NE/I001719/1) and AJW was supported to work in the Kosñipata by NSF-EAR 1227192. YM is supported by the Jackson Foundation and a European Research Council Advanced Investigator Grant. We thank ACCA Peru (Wayqecha) and Incaterra (San Pedro) for field support; L.V. Morales, R.J. Abarca Martínez, M.H. Yucra Hurtado, R. Paja Yurca, J. A. Gibaja Lopez, I. Cuba Torres, J. Huamán Ovalle, A. Alfaro-Tapia, R. Butrón Loayza, J. Farfan Flores, D. Oviedo Licona, D. Ocampo for field assistance. The Carnegie Airborne Observatory is made possible by the Avatar Alliance Foundation, Grantham

Foundation for the Protection of the Environment, John D. and Catherine T. MacArthur Foundation, Gordon and Betty Moore Foundation, W. M. Keck Foundation, Margaret A. Cargill Foundation, Mary Anne Nyburg Baker and G. Leonard Baker Jr., and William R. Hearst III. We thank D. Knapp, T. Kennedy-Bowdoin, C. Anderson, and R. Tupayachi for CAO data collection and analysis.

6.8. References

Aalto, R., Maurice-Bourgoin, L., Dunne, T., Montgomery, D. R., Nittrouer, C. A., and Guyot, J. L. (2003), Episodic sediment accumulation on Amazonian flood plains influenced by El Nino/Southern Oscillation, *Nature, 425*(6957), 493-497, doi: http://dx.doi.org/10.1038/nature02002.

Allegre, C. J., Dupre, B., Negrel, P., and Gaillardet, J. (1996), Sr-Nd-Pb isotope systematics in Amazon and Congo River systems: Constraints about erosion processes, *Chemical Geology, 131*(1-4), 93-112, doi: http://dx.doi.org/10.1016/0009-2541(96)00028-9.

Asner, G. P., Anderson, C. B., Martin, R. E., Knapp, D. E., Tupayachi, R., Sinca, F., and Malhi, Y. (2014), Landscape-scale changes in forest structure and functional traits along an Andes-to-Amazon elevation gradient, *Biogeosciences, 11*(3), 843-856, doi: http://dx.doi.org/10.5194/bg-11-843-2014.

Asner, G. P. (in prep), Above ground biomass and carbon stocks of the Peruvian Andes.

Berner, R. A. (1982), Burial of organic carbon and pyrite sulfur in the modern ocean: its geochemical and environmental significance, *American Journal of Science, 282*(4), 451-473.

Berner, R. A., and Rao, J.-L. (1994), Phosphorus in sediments of the Amazon River and estuary: Implications for the global flux of phosphorus to the sea, *Geochimica et Cosmochimica Acta, 58*(10), 2333-2339.

Blair, N. E., Leithold, E. L., Ford, S. T., Peeler, K. A., Holmes, J. C., and Perkey, D. W. (2003), The persistence of memory: The fate of ancient sedimentary organic carbon in a modern sedimentary system, *Geochimica et Cosmochimica Acta, 67*(1), 63-73, doi: http://dx.doi.org/10.1016/s0016-7037(02)01043-8.

Blair, N. E., and Aller, R. C. (2012), The fate of terrestrial organic carbon in the marine environment, *Annual review of marine science, 4*, 401-423, doi: http://dx.doi.org/10.1146/annurev-marine-120709-142717.

Blodgett, T. A., and Isacks, B. L. (2007), Landslide erosion rate in the eastern cordillera of northern Bolivia, *Earth Interactions, 11*, 1-30, doi: http://dx.doi.org/10.1175/2007EI222.1.

Bouchez, J., Beyssac, O., Galy, V., Gaillardet, J., France-Lanord, C., Maurice, L., and Moreira-Turcq, P. (2010), Oxidation of petrogenic organic carbon in the Amazon floodplain as a source of atmospheric CO_2, *Geology, 38*(3), 255-258, doi: http://dx.doi.org/10.1130/g30608.1.

Bouchez, J., Galy, V., Hilton, R. G., Gaillardet, J., Moreira-Turcq, P., Pérez, M. A., France-Lanord, C., and Maurice, L. (2014), Source, transport and fluxes of Amazon River particulate organic carbon: insights from river sediment depth-profiles, *Geochimica et Cosmochimica Acta,* (133), 280-298, doi: http://dx.doi.org/10.1016/j.gca.2014.02.032.

Brodie, C. R., Leng, M. J., Casford, J. S. L., Kendrick, C. P., Lloyd, J. M., Yongqiang, Z., and Bird, M. I. (2011), Evidence for bias in C and N concentrations and $\delta^{13}C$ composition of terrestrial and aquatic organic materials due to pre-analysis acid preparation methods, *Chemical Geology, 282*(3), 67-83, doi: http://dx.doi.org/10.1016/j.chemgeo.2011.01.007.

Carlotto Caillaux, V. S., Rodriguez, G., Fernando, W., Roque, C., Dionicio, J., and Chávez, R. (1996), Geología de los cuadrángulos de Urubamba y Calca, Instituto Geológica Nacional, Lima, Peru.

Ciais, P., Dolman, A. J., Bombelli, A., Duren, R., Peregon, A., Rayner, P. J., Miller, C., Gobron, N., Kinderman, G., and Marland, G. (2013), Current systematic carbon cycle observations and needs for implementing a policy-relevant carbon observing system, *Biogeosciences Discussions, 10*(7), doi: http://dx.doi.org/10.5194/bgd-10-11447-2013.

Clark, K. E., Hilton, R. G., West, A. J., Malhi, Y., Gröcke, D. R., Bryant, C. L., Ascough, P. L., Robles Caceres, A., and New, M. (2013), New views on "old" carbon in the Amazon River: Insight from the source of organic carbon eroded from the Peruvian Andes, *Geochemistry, Geophysics, Geosystems, 14*(5), 1644-1659, doi: http://dx.doi.org/10.1002/ggge.20122.

Clark, K. E., West, A. J., Hilton, R. G., Asner, G. P., Silman, M. R., Saatchi, S. S., Quesada, C. A., Farfan Rios, W., Horwath, A. B., Martin, R. E., New, M., and Malhi, Y. (in prep), Storm-triggered landslides in an Andean Valley: Links to topography, organic carbon, and biodiversity?

Clark, K. E., Torres, M. A., West, A. J., Hilton, R. G., New, M., Horwath, A. B., Fisher, J. B., Rapp, J. M., Robles Caceres, A., and Malhi, Y. (in review), The hydrological regime of a forested tropical Andean valley.

Cohn, T. A. (1995), Recent advances in statistical methods for the estimation of sediment and nutrient transport in rivers, *Reviews of Geophysics, 33*(S2), 1117-1123, doi: http://dx.doi.org/10.1029/95RG00292.

Consbio (2011), Ecosistemas Terrestres de Peru (Data Basin Dataset) for ArcGIS, edited by The Nature Conservancy/NatureServe.

Dadson, S., Hovius, N., Pegg, S., Dade, W. B., Horng, M., and Chen, H. (2005), Hyperpycnal river flows from an active mountain belt, *Journal of Geophysical Research: Earth Surface (2003–2012), 110*(F4), doi: http://dx.doi.org/10.1029/2004JF000244.

Dadson, S. J., Hovius, N., Chen, H., Dade, W. B., Hsieh, M.-L., Willett, S. D., Hu, J.-C., Horng, M.-J., Chen, M.-C., Stark, C. P., Lague, D., and Lin, J.-C. (2003), Links between erosion, runoff variability and seismicity in the Taiwan orogen, *Nature, 426*(6967), 648-651, doi: http://www.nature.com/nature/journal/v426/n6967/suppinfo/nature02150_S1.html.

Dixon, R. K., Brown, S., Houghton, R., Solomon, A., Trexler, M., and Wisniewski, J. (1994), Carbon pools and flux of global forest ecosystems, *Science*, *263*(5144), 185-189.

Dunne, T., Mertes, L. A. K., Meade, R. H., Richey, J. E., and Forsberg, B. R. (1998), Exchanges of sediment between the flood plain and channel of the Amazon River in Brazil, *Geological Society of America Bulletin*, *110*(4), 450-467.

Eva, H. D., Huber, O., Achard, F., Balslev, H., Beck, S., Behling, H., Belward, A. S., Beuchle, R., Cleef, A., Colchester, M., Duivenvoorden, J., Hoogmoed, M., Junk, W., Kabat, P., Kruijt, B., Malhi, Y., Müller, J. M., Pereira, J. M., Peres, C., Prance, G. T., Roberts, J., and Salo, J. (2005), A proposal for defining the geographical boundaries of Amazonia*Rep.*, European Communities, Luxembourg.

Ferguson, R. I. (1987), Accuracy and precision of methods for estimating river loads, *Earth Surface Processes and Landforms, 12*(1), 95-104, doi: http://dx.doi.org/10.1002/esp.3290120111.

Filizola, N., and Guyot, J. L. (2009), Suspended sediment yields in the Amazon basin: an assessment using the Brazilian national data set, *Hydrological Processes*, *23*(22), 3207-3215, doi: http://dx.doi.org/10.1002/hyp.7394.

France-Lanord, C., and Derry, L. A. (1997), Organic carbon burial forcing of the carbon cycle from Himalayan erosion, *Nature*, *390*(6655), 65-67.

Gaillardet, J., Dupre, B., Allegre, C. J., and Negrel, P. (1997), Chemical and physical denudation in the Amazon River basin, *Chemical Geology*, *142*(3-4), 141-173.

Gaillardet, J., Dupré, B., Louvat, P., and Allègre, C. J. (1999), Global silicate weathering and CO_2 consumption rates deduced from the chemistry of large rivers, *Chemical Geology*, *159*(1–4), 3-30, doi: http://dx.doi.org/10.1016/S0009-2541(99)00031-5.

Galy, V., Bouchez, J., and France-Lanord, C. (2007a), Determination of total organic carbon content and delta C-13 in carbonate-rich detrital sediments, *Geostandards and Geoanalytical Research*, *31*(3), 199-207, doi: http://dx.doi.org/10.1111/j.1751-908X.2007.00864.x.

Galy, V., France-Lanord, C., Beyssac, O., Faure, P., Kudrass, H., and Palhol, F. (2007b), Efficient organic carbon burial in the Bengal fan sustained by the Himalayan erosional system, *Nature*, *450*(7168), 407-U406, doi: http://dx.doi.org/10.1038/nature06273.

Galy, V., Beyssac, O., France-Lanord, C., and Eglinton, T. (2008a), Recycling of graphite during Himalayan erosion: A geological stabilization of carbon in the crust, *Science*, *322*(5903), 943-945, doi: http://dx.doi.org/10.1126/science.1161408.

Galy, V., France-Lanord, C., and Lartiges, B. (2008b), Loading and fate of particulate organic carbon from the Himalaya to the Ganga-Brahmaputra delta, *Geochimica et Cosmochimica Acta*, *72*(7), 1767-1787, doi: http://dx.doi.org/10.1016/j.gca.2008.01.027.

Galy, V., and Eglinton, T. (2011), Protracted storage of biospheric carbon in the Ganges-Brahmaputra basin, *Nature Geoscience*, *4*(12), 843-847, doi: http://dx.doi.org/10.1038/ngeo1293.

Galy, V. (in prep).

Garcia, M., and Parker, G. (1991), Entrainment of Bed Sediment into Suspension, *Journal of Hydraulic Engineering*, *117*(4), 414-435, doi: http://dx.doi.org/10.1061/(ASCE)0733-9429(1991)117:4(414).

Gibbon, A., Silman, M. R., Malhi, Y., Fisher, J. B., Meir, P., Zimmermann, M., Dargie, G. C., Farfan, W. R., and Garcia, K. C. (2010), Ecosystem carbon storage across the grassland-forest transition in the high Andes of Manu National Park, Peru, *Ecosystems*, *13*(7), 1097-1111, doi: http://dx.doi.org/10.1007/s10021-010-9376-8.

Gibbs, R. J. (1967), Amazon River - Environmental factors that control its dissolved and suspended load, *Science*, *156*(3783), 1734-1737.

Girardin, C. A. J., Silva-Espejo, J. E., Doughty, C. E., Huaraca Huasco, W., Metcalfe, D. B., Durand-Baca, L., Marthews, T. R., Aragao, L. E. O. C., Farfan Rios, W., García Cabrera, K., Halladay, K., Fisher, J. B., Galiano-Cabrera, D. F., Huaraca-Quispe, L. P., Alzamora-Taype, I., Equiluz-Mora, L., Salinas-Revilla, N., Silman, M., Meir, P., and Malhi, Y. (2013), Productivity and carbon allocation in a tropical montane cloud forest of the Peruvian Andes,

Plant Ecology and Diversity, *7*(1-2), 107-123, doi: http://dx.doi.org/10/1080/17550874.2013.820222.

Gomi, T., Sidle, R. C., Ueno, M., Miyata, S., and Kosugi, K. (2008), Characteristics of overland flow generation on steep forested hillslopes of central Japan, *Journal of Hydrology*, *361*(3), 275-290, doi: http://dx.doi.org/10.1029/2007WR005894.

Goñi, M. A., Hatten, J. A., Wheatcroft, R. A., and Borgeld, J. C. (2013), Particulate organic matter export by two contrasting small mountainous rivers from the Pacific Northwest, U.S.A, *Journal of Geophysical Research: Biogeosciences*, *118*(1), 112-134, doi: http://dx.doi.org/10.1002/jgrg.20024.

Gregory-Wodzicki, K. M. (2000), Uplift history of the Central and Northern Andes: a review, *Geological Society of America Bulletin*, *112*(7), 1091-1105, doi: http://dx.doi.org/10.1130/0016-7606(2000)112<1091:UHOTCA>2.0.CO;2

Gröcke, D. R., Hori, R. S., Trabucho-Alexandre, J., Kemp, D. B., and Schwark, L. (2011), An open ocean record of the Toarcian oceanic anoxic event, *Solid Earth*, *2*, 245-257, doi: http://dx.doi.org/10.5194/se-2-245-2011.

Guyot, J. L., Fillzola, N., Quintanilla, J., and Cortez, J. (1996), Dissolved solids and suspended sediment yields in the Rio Madeira basin, from the Bolivian Andes to the Amazon, *IAHS Publication*, 55-64.

Guyot, J. L., Filizola, N., and Laraque, A. (2005), The suspended sediment flux of the River Amazon at Obidos, Brazil, 1995-2003, in *Sediment Budgets 1*, edited by D. E. Walling and A. J. Horowitz, pp. 347-354, International Association of Hydrological Sciences, Wallingford, UK.

Hamm, N. T., Dade, W. B., and Renshaw, C. E. (2011), Fine particle deposition to porous beds, *Water Resources Research*, *47*(11), W11508, doi: http://dx.doi.org/10.1029/2010WR010295.

Hartshorn, K., Hovius, N., Dade, W. B., and Slingerland, R. L. (2002), Climate-Driven Bedrock Incision in an Active Mountain Belt, *Science*, *297*(5589), 2036-2038, doi: http://dx.doi.org/10.1126/science.1075078.

Hatten, J. A., Goñi, M. A., and Wheatcroft, R. A. (2012), Chemical characteristics of particulate organic matter from a small, mountainous river system in the Oregon Coast Range, USA, *Biogeochemistry*, 1-24, doi: http://dx.doi.org/10.1007/s10533-010-9529-z.

Hedges, J. I., Mayorga, E., Tsamakis, E., McClain, M. E., Aufdenkampe, A., Quay, P., Richey, J. E., Benner, R., Opsahl, S., Black, B., Pimentel, T., Quintanilla, J., and Maurice, L. (2000), Organic matter in Bolivian tributaries of the Amazon River: A comparison to the lower mainstream, *Limnology and Oceanography*, *45*(7), 1449-1466.

Hicks, D. M., Gomez, B., and Trustrum, N. A. (2000), Erosion thresholds and suspended sediment yields, Waipaoa River Basin, New Zealand, *Water Resources Research*, *36*(4), 1129-1142, doi: http://dx.doi.org/10.1029/1999WR900340.

Hilton, R. G., Galy, A., and Hovius, N. (2008a), Riverine particulate organic carbon from an active mountain belt: Importance of landslides, *Global Biogeochemical Cycles*, *22*, BG1017, doi: http://dx.doi.org/10.1029/2006GB002905.

Hilton, R. G., Galy, A., Hovius, N., Chen, M.-C., Horng, M.-J., and Chen, H. (2008b), Tropical-cyclone-driven erosion of the terrestrial biosphere from mountains, *Nature Geoscience, 1*(11), 759-762, doi: http://dx.doi.org/10.1038/ngeo333.

Hilton, R. G., Galy, A., Hovius, N., Horng, M.-J., and Chen, H. (2010), The isotopic composition of particulate organic carbon in mountain rivers of Taiwan, *Geochimica et Cosmochimica Acta, 74*(11), 3164-3181, doi: http://dx.doi.org/10.1016/j.gca.2010.03.004.

Hilton, R. G., Galy, A., Hovius, N., Horng, M.-J., and Chen, H. (2011a), Efficient transport of fossil organic carbon to the ocean by steep mountain rivers: An orogenic carbon sequestration mechanism, *Geology, 39*(1), 71-74, doi: http://dx.doi.org/10.1130/g31352.1.

Hilton, R. G., Meunier, P., Hovius, N., Bellingham, P. J., and Galy, A. (2011b), Landslide impact on organic carbon cycling in a temperate montane forest, *Earth Surface Processes and Landforms, 36*(12), 1670-1679, doi: http://dx.doi.org/10.1002/esp.2191.

Hilton, R. G., Galy, A., Hovius, N., Kao, S.-J., Horng, M.-J., and Chen, H. (2012), Climatic and geomorphic controls on the erosion of terrestrial biomass from subtropical mountain forest, *Global Biogeochemical Cycles, 26*(3), GB3014, doi: http://dx.doi.org/10.1029/2012gb004314.

Hovius, N., Galy, A., Hilton, R. G., Sparkes, R., Smith, J., Shuh-Ji, K., Hongey, C., In-Tian, L., and West, A. J. (2011), Erosion-driven drawdown of atmospheric carbon dioxide: The organic pathway, *Applied Geochemistry, 26*, S285-S287, doi: http://dx.doi.org/10.1016/j.apgeochem.2011.03.082.

Huaraca Huasco, W., Girardin, C. A. J., Doughty, C. E., Metcalfe, D. B., Baca, L. D., Silva-Espejo, J. E., Cabrera, D. G., Aragão, L. E. O., Davila, A. R., Marthews, T. R., Huaraca-Quispe, L. P., Alzamora-Taype, I., Eguiluz-Mora, L., Farfan-Rios, W., Cabrera, K. G., Halladay, K., Salinas-Revilla, N., Silman, M., Meir, P., and Malhi, Y. (2013), Seasonal production, allocation and cycling of carbon in two mid-elevation tropical montane forest plots in the Peruvian Andes, *Plant Ecology and Diversity, 7*(1-2), doi: http://dx.doi.org/10.1080/17550874.2013.819042.

INGEMMET (2013), GEOCATMIN - Geologia integrada por proyectos regionales, edited by Instituto Geológico Minero Metalúrgico.

IPCC (2013), Climate change 2013: The physical science basis. Contribution of Working Group I to the fifth Assessment Report of the Intergovernmental Panel on Climage Change *Rep.*, 1535 pp, Cambridge, UK and New York, NY, USA.

Iwata, H., Malhi, Y., and von Randow, C. (2005), Gap-filling measurements of carbon dioxide storage in tropical rainforest canopy airspace, *Agricultural and Forest Meteorology, 132*(3–4), 305-314, doi: http://dx.doi.org/10.1016/j.agrformet.2005.08.005.

Kao, S. J., and Liu, K.-K. (1996), Particulate organic carbon export from a subtropical mountainous river (Lanyang Hsi) in Taiwan, *Limnology and Oceanography, 41*(8), 1749-1757.

Kao, S. J., and Liu, K. K. (1997), Fluxes of dissolved and nonfossil particulate organic carbon from an Oceania small river (Lanyang Hsi) in Taiwan, *Biogeochemistry, 39*(3), 255-269.

Kao, S. J., and Milliman, J. D. (2008), Water and sediment discharge from small mountainous rivers, Taiwan: The roles of lithology, episodic events, and human activities, *The Journal of Geology, 116*(5), 431-448, doi: http://dx.doi.org/10.1086/590921.

Kao, S. J., Hilton, R. G., Selvaraj, K., Dai, M., Zehetner, F., Huang, J. C., Hsu, S. C., Sparkes, R., Liu, J. T., Lee, T. Y., Yang, J. Y. T., Galy, A., Xu, X., and Hovius, N. (2014), Preservation of terrestrial organic carbon in marine sediments offshore Taiwan: mountain building and atmospheric carbon dioxide sequestration, *Earth Surface Dynamics, 2*(1), 127-139, doi: http://dx.doi.org/10.5194/esurf-2-127-2014.

Killeen, T. J., Douglas, M., Consiglio, T., Jørgensen, P. M., and Mejia, J. (2007), Dry spots and wet spots in the Andean hotspot, *Journal of Biogeography, 34*(8), 1357-1373, doi: http://dx.doi.org/10.1111/j.1365-2699.2006.01682.x.

Komada, T., Druffel, E. R. M., and Trumbore, S. E. (2004), Oceanic export of relict carbon by small mountainous rivers, *Geophysical Research Letters, 31*(7), L07504, doi: http://dx.doi.org/10.1029/2004gl019512.

Korup, O., McSaveney, M. J., and Davies, T. R. H. (2004), Sediment generation and delivery from large historic landslides in the Southern Alps, New Zealand, *Geomorphology, 61*(1–2), 189-207, doi: http://dx.doi.org/10.1016/j.geomorph.2004.01.001.

Larsen, I. J., Montgomery, D. R., and Greenberg, H. M. (2014), The contribution of mountains to global denudation, *Geology*, G35136. 35131, doi: http://dx.doi.org/10.1130/G35136.1

Lehner, B., Verdin, K., and Jarvis, A. (2008), New Global Hydrography Derived From Spaceborne Elevation Data, *Eos, Transactions American Geophysical Union, 89*(10), 93-94, doi: http://dx.doi.org/10.1029/2008EO100001.

Lupker, M., France-Lanord, C., Lavé, J., Bouchez, J., Galy, V., Métivier, F., Gaillardet, J., Lartiges, B., and Mugnier, J.-L. (2011), A Rouse-based method to integrate the chemical composition of river sediments: Application to the Ganga basin, *Journal of Geophysical Research, 116*(F4), F04012, doi: http://dx.doi.org/10.1029/2010jf001947.

Lyons, W. B., Nezat, C. A., Carey, A. E., and Hicks, D. M. (2002), Organic carbon fluxes to the ocean from high-standing islands, *Geology, 30*(5), 443-446, doi: http://dx.doi.org/10.1130/0091-7613(2002)030<0443:ocftto>2.0.co;2.

Malhi, Y. (2010), The carbon balance of tropical forest regions, 1990–2005, *Current Opinion in Environmental Sustainability, 2*(4), 237-244, doi: http://dx.doi.org/10.1016/j.cosust.2010.08.002.

Malhi, Y., Silman, M., Salinas, N., Bush, M., Meir, P., and Saatchi, S. (2010), Introduction: Elevation gradients in the tropics: laboratories for ecosystem ecology and global change research, *Global Change Biology, 16*(12), 3171-3175, doi: http://dx.doi.org/10.1111/j.1365-2486.2010.02323.x.

Marengo, J. A., Soares, W. R., Saulo, C., and Nicolini, M. (2004), Climatology of the low-level jet east of the Andes as derived from the NCEP-NCAR reanalyses: Characteristics and temporal variability, *Journal of climate, 17*(12), 2261-2280.

Marthews, T. R., Malhi, Y., Girardin, C. A. J., Silva Espejo, J. E., Aragão, L. E. O. C., Metcalfe, D. B., Rapp, J. M., Mercado, L. M., Fisher, R. A., Galbraith, D. R., Fisher, J. B., Salinas-Revilla, N., Friend, A. D., Restrepo-Coupe, N., and Williams, R. J. (2012), Simulating forest productivity along a neotropical elevational transect: temperature variation and carbon use efficiency, *Global Change Biology, 18*(9), 2882-2898, doi: http://dx.doi.org/10.1111/j.1365-2486.2012.02728.x.

Martinez, J. M., Guyot, J. L., Filizola, N., and Sondag, F. (2009), Increase in suspended sediment discharge of the Amazon River assessed by monitoring network and satellite data, *Catena, 79*(3), 257-264, doi: http://dx.doi.org/10.1016/j.catena.2009.05.011.

Mayorga, E., Aufdenkampe, A. K., Masiello, C. A., Krusche, A. V., Hedges, J. I., Quay, P. D., Richey, J. E., and Brown, T. A. (2005), Young organic matter as a source of carbon dioxide outgassing from Amazonian rivers, *Nature, 436*(7050), 538-541, doi: http://dx.doi.org/10.1038/nature03880.

Mayorga, E., Seitzinger, S. P., Harrison, J. A., Dumont, E., Beusen, A. H. W., Bouwman, A. F., Fekete, B. M., Kroeze, C., and Van Drecht, G. (2010), Global Nutrient Export from WaterSheds 2 (NEWS 2): Model development and implementation, *Environmental Modelling & Software, 25*(7), 837-853, doi: http://dx.doi.org/10.1016/j.envsoft.2010.01.007.

McClain, M. E., and Naiman, R. J. (2008), Andean influences on the biogeochemistry and ecology of the Amazon River, *Bioscience, 58*(4), 325-338, doi: http://dx.doi.org/10.1641/b580408.

Meade, R. H., Nordin, C. F., Curtis, W. F., Costarodrigues, F. M., Dovale, C. M., and Edmond, J. M. (1979), Sediment loads in the Amazon River, *Nature, 278*(5700), 161-163.

Meade, R. H., Dunne, T., Richey, J. E., Santos, U. D., and Salati, E. (1985), Storage and remobilisation of suspended sediment in the lower Amazon River of Brazil, *Science, 228*(4698), 488-490.

Meunier, P., Hovius, N., and Haines, J. A. (2008), Topographic site effects and the location of earthquake induced landslides, *Earth and Planetary Science Letters, 275*(3), 221-232, doi: http://dx.doi.org/10.1016/j.epsl.2008.07.020.

Milliman, J. D. (1995), Sediment discharge to the ocean from small mountainous rivers: The New Guinea example, *Geo-Marine Letters, 15*(3-4), 127-133.

Milliman, J. D., and Farnsworth, K. L. (2011), Runoff, erosion, and delivery to the coastal ocean, in *River discharge to the coastal ocean: a global synthesis*, edited, pp. 13-69, Cambridge University Press, Cambridge, UK.

Mitchard, E. T. A., Feldpausch, T. R., Brienen, R. J. W., Lopez-Gonzalez, G., Monteagudo, A., Baker, T. R., Lewis, S. L., Lloyd, J., Quesada, C. A., Gloor, M., ter Steege, H., Meir, P., Alvarez, E., Araujo-Murakami, A., Aragão, L. E. O. C., Arroyo, L., Aymard, G., Banki, O., Bonal, D., Brown, S., Brown, F. I., Cerón, C. E., Chama Moscoso, V., Chave, J., Comiskey, J. A., Cornejo, F., Corrales Medina, M., Da Costa, L., Costa, F. R. C., Di Fiore, A., Domingues, T. F., Erwin, T. L., Frederickson, T., Higuchi, N., Honorio Coronado, E. N., Killeen, T. J., Laurance, W. F., Levis, C., Magnusson, W. E., Marimon, B. S., Marimon Junior, B. H., Mendoza Polo, I., Mishra, P., Nascimento, M. T., Neill, D., Núñez Vargas, M. P., Palacios, W. A., Parada, A., Pardo Molina, G., Peña-Claros, M., Pitman, N., Peres, C. A., Poorter, L., Prieto, A., Ramirez-Angulo, H., Restrepo Correa, Z., Roopsind, A., Roucoux, K. H., Rudas, A., Salomão, R. P., Schietti, J., Silveira, M., de Souza, P. F., Steininger, M. K., Stropp, J., Terborgh, J., Thomas, R., Toledo, M., Torres-Lezama, A., van Andel, T. R., van der Heijden, G. M. F., Vieira, I. C. G., Vieira, S., Vilanova-Torre, E., Vos, V. A., Wang, O., Zartman, C. E., Malhi, Y., and Phillips, O. L. (2014), Markedly divergent estimates of Amazon forest carbon density from ground plots and satellites, *Global Ecology and Biogeography*, n/a-n/a, doi: http://dx.doi.org/10.1111/geb.12168.

Montgomery, D. R., Balco, G., and Willett, S. D. (2001), Climate, tectonics, and the morphology of the Andes, *Geology*, *29*(7), 579-582, doi: http://dx.doi.org/10.1130/0091-7613(2001)029<0579:CTATMO>2.0.CO;2.

Moreira-Turcq, L. S., Moreira Turcq, P., Kim, J. H., Turcq, B., Cordeiro, R. C., Caquineau, S., Mandengo-Yogo, M., and Sinninghe Damsté, J. S. (in press), A mineralogical and organic geochemical overview of the effects of Holocene changes in Amazon River flow on three floodplain lakes, *Palaeogeography, Palaeoclimatology, Palaeoecology*, doi: http://dx.doi.org/10.1016/j.palaeo.2014.03.017.

Moreira-Turcq, P., Seyler, P., Guyot, J. L., and Etcheber, H. (2003), Exportation of organic carbon from the Amazon River and its main tributaries, *Hydrological Processes*, *17*(7), 1329-1344, doi: http://dx.doi.org/10.1002/hyp.1287.

Moreira-Turcq, P., Bonnet, M.-P., Amorim, M., Bernardes, M., Lagane, C., Maurice, L., Perez, M., and Seyler, P. (2013), Seasonal variability in concentration, composition, age, and fluxes of particulate organic carbon exchanged between the floodplain and Amazon River, *Global Biogeochemical Cycles*, *27*(1), 119-130, doi: http://dx.doi.org/10.1002/gbc.20022.

Oliveras, I. (in prep), Puna NPP in the Peruvian Andes.

Ponton, C., West, A. J., Feakins, S. J., and Galy, V. (in review), Biomarkers in transit reveal the nature of fluvial integration.

Quay, P. D., Wilbur, D. O., Richey, J. E., Hedges, J. I., and Devol, A. H. (1992), Carbon Cycling in the Amazon River: Implications from the 13 C Compositions of Particles and Solutes, *Limnology and Oceanography*, *37*(4), 857-871, doi: http://dx.doi.org/10.2307/2837944.

Raich, J. W., Russell, A. E., and Vitousek, P. M. (1997), Primary productivity and ecosystem development along an elevational gradient on Mauna Loa, Hawai'i, *Ecology*, *78*(3), 707-721.

Raich, J. W., Russell, A. E., Kitayama, K., Parton, W. J., and Vitousek, P. M. (2006), Temperature influences carbon accumulation in moist tropical forests, *Ecology*, *87*(1), 76-87, doi: http://dx.doi.org/10.1890/05-0023.

Ramos Scharrón, C. E., Castellanos, E. J., and Restrepo, C. (2012), The transfer of modern organic carbon by landslide activity in tropical montane ecosystems, *Journal of Geophysical Research: Biogeosciences (2005–2012)*, *117*(G3), doi: http://dx.doi.org/10.1029/2011JG001838.

Rao, Y. (2011), Variation in plant carbon and nitrogen isotopes along an altitudinal gradient in the Peruvian Andes, B.Sc. thesis, 60 pp, Department of Earth Sciences, Durham University, Durham.

Richey, J. E., Meade, R. H., Salati, E., Devol, A. H., Nordin, C. F., and Dossantos, U. (1986), Water discharge and suspended sediment concentrations in the Amazon River 1982-1984, *Water Resources Research*, *22*(5), 756-764.

Richey, J. E., Hedges, J. I., Devol, A. H., Quay, P. D., Victoria, R., Martinelli, L., and Forsberg, B. R. (1990a), Biogeochemistry of carbon in the Amazon River, *Limnol. Oceanogr*, *35*(2), 352-371.

Richey, J. E., Valarezo, C., Valarezo, C., and Valarezo, C. (1990b), Biogeochemistry of carbon in the Amazon River, *Limnology and Oceanography*, *35*, 352-371.

Richey, J. E., and Victoria, R. L. (1993), C, N, and P Export Dynamics in the Amazon River, in *Interactions of C, N, P and S Biogeochemical Cycles and Global Change*, edited by R. Wollast, F. T. Mackenzie and L. Chou, pp. 123-139, Springer Berlin Heidelberg.

Roering, J. J., Kirchner, J. W., and Dietrich, W. E. (2001), Hillslope evolution by nonlinear, slope-dependent transport: Steady state morphology and equilibrium adjustment timescales, *Journal of Geophysical Research, 106*(B8), 16499-16513, doi: http://dx.doi.org/10.1029/2001jb000323.

Saatchi, S. S., Houghton, R. A., Dos Santos AlvalÁ, R. C., Soares, J. V., and Yu, Y. (2007), Distribution of aboveground live biomass in the Amazon basin, *Global Change Biology, 13*(4), 816-837, doi: http://dx.doi.org/10.1111/j.1365-2486.2007.01323.x.

Seitzinger, S. P., Harrison, J. A., Dumont, E., Beusen, A. H. W., and Bouwman, A. F. (2005), Sources and delivery of carbon, nitrogen, and phosphorus to the coastal zone: An overview of Global Nutrient Export from Watersheds (NEWS) models and their application, *Global Biogeochemical Cycles, 19*(4), GB4S01, doi: http://dx.doi.org/10.1029/2005GB002606.

Smith, J. C., Galy, A., Hovius, N., Tye, A. M., Turowski, J. M., and Schleppi, P. (2013), Runoff-driven export of particulate organic carbon from soil in temperate forested uplands, *Earth and Planetary Science Letters, 365*, 198-208, doi: http://dx.doi.org/10.1016/j.epsl.2013.01.027.

Stallard, R. F., and Edmond, J. M. (1983), Geochemistry of the Amazon: 2. The influence of geology and weathering environment on the dissolved load, *Journal of Geophysical Research: Oceans, 88*(C14), 9671-9688.

Stallard, R. F. (1998), Terrestrial sedimentation and the carbon cycle: Coupling weathering and erosion to carbon burial, *Global Biogeochemical Cycles, 12*(2), 231-257.

Stallard, R. F. (2013), Considerations of erosion and storage of carbon, focusing on tropical landscapes in Puerto Rico and Panama, paper presented at AGU Fall Meeting Abstracts.

Sundquist, E., and Visser, K. (2004), *The geologic history of the carbon cycle*, 425-472 pp., Oxford, UK.

Townsend-Small, A., Noguera, J. L., McClain, M. E., and Brandes, J. A. (2007), Radiocarbon and stable isotope geochemistry of organic matter in the Amazon headwaters, Peruvian Andes, *Global Biogeochemical Cycles, 21*(2), doi: http://dx.doi.org/10.1029/2006gb002835.

Townsend-Small, A., McClain, M. E., Hall, B., Noguera, J. L., Llerena, C. A., and Brandes, J. A. (2008), Suspended sediments and organic matter in mountain headwaters of the Amazon River: Results from a 1-year time series study in the central Peruvian Andes, *Geochimica et Cosmochimica Acta, 72*(3), 732-740, doi: http://dx.doi.org/10.1016/j.gca.2007.11.020.

Vihermaa, L. E., Waldron, S., Garnett, M. H., and Newton, J. (2014), Old carbon contributes to aquatic emissions of carbon dioxide in the Amazon, *Biogeosciences Discussions, 11*, 1773-1800, doi: http://dx.doi.org/10.5194/bgd-11-1773-2014.

Vogel, R. M., Stedinger, J. R., and Hooper, R. P. (2003), Discharge indices for water quality loads, *Water Resources Research, 39*(10), 1273, doi: http://dx.doi.org/10.1029/2002WR001872.

Walling, D. E., and Webb, B. W. (1981), Reliability of suspended sediment load data, paper presented at Erosion and Sediment Transport Measurement: Symposium IAHS Publication.

West, A. J., Lin, C. W., Lin, T. C., Hilton, R. G., Liu, S. H., Chang, C. T., Lin, K. C., Galy, A., Sparkes, R. B., and Hovius, N. (2011), Mobilization and transport of coarse woody debris to the oceans triggered by an extreme tropical storm, *Limnology and Oceanography, 56*(1), 77-85, doi: http://dx.doi.org/10.4319/lo.2011.56.1.0077.

Wheatcroft, R. A., Goni, M. A., Hatten, J. A., Pasternack, G. B., and Warrick, J. A. (2010), The role of effective discharge in the ocean delivery of particulate organic carbon by small, mountainous river systems, *Limnology and Oceanography*, *55*(1), 161.

Wittmann, H., von Blanckenburg, F., Guyot, J. L., Maurice, L., and Kubik, P. (2009), From source to sink: Preserving the cosmogenic ^{10}Be-derived denudation rate signal of the Bolivian Andes in sediment of the Beni and Mamoré foreland basins, *Earth and Planetary Science Letters, 288*(3), 463-474, doi: http://dx.doi.org/10.1016/j.epsl.2009.10.008.

Zimmermann, M., Meir, P., Bird, M. I., Malhi, Y., and Ccahuana, A. J. Q. (2009), Climate dependence of heterotrophic soil respiration from a soil-translocation experiment along a 3000 m tropical forest altitudinal gradient, *European Journal of Soil Science, 60*(6), 895-906, doi: http://dx.doi.org/10.1111/j.1365-2389.2009.01175.x.

Zimmermann, M., Meir, P., Silman, M., Fedders, A., Gibbon, A., Malhi, Y., Urrego, D. H., Bush, M. B., Feeley, K. J., Garcia, K., Farfan, W., Goetz, B. P., Johnson, W. T., Kline, K. M., Modi, A. T., Rurau, Q. N. M., Staudt, B. T., and Zamora, F. (2010), No differences in soil carbon stocks across the tree line in the Peruvian Andes, *Ecosystems*, (13), 62-74, doi: http://dx.doi.org/10.1007/s10021-009-9300-2.

Chapter 6: Supplementary information:

Export of particulate organic carbon by an Andean river and implications of its delivery to the lowland Amazon River

K. E. Clark[1*], R. G. Hilton[2], A. J. West[3], A. Robles Caceres[4], D. R. Gröcke[5], T. R. Marthews[1], G. P. Asner[6], M. New[1,7], and Y. Malhi[1]

S6.1. Tables for supplementary information

Table S6.1a: Suspended sediment samples measured at the San Pedro river gauging station

Date	hr	SSC (g m^{-3})	C_{org} (%)	$\delta^{13}C_{org}$ (‰)[d]	N/C	$F_{f\ n/c}$	$F_{nf\ n/c}$	POC_f (g m^{-3})	POC_{nf} (g m^{-3})
30/11/2009	16	4090	0.48	-23.0	0.24	0.79	0.21	15.33	4.10
30/11/2009	17	18880	0.85	-25.0	0.17	0.48	0.52	76.89	83.09
29/01/2010	3	342	0.71	-25.3	0.16	0.46	0.54	1.11	1.31
31/01/2010	18	686	0.57	-24.2	0.20	0.62	0.38	2.40	1.49
31/01/2010	21	343	0.68	-25.1	0.17	0.48	0.52	1.12	1.21
03/02/2010	12	420	0.66	-24.9	0.16	0.45	0.55	1.26	1.51
06/02/2010	3	514	0.72	-25.8	0.17	0.49	0.51	1.83	1.88
08/02/2010	9	84	0.83	-26.4	0.13	0.34	0.66	0.24	0.46
10/02/2010	18	570	0.63	-25.1	0.18	0.56	0.44	1.99	1.59
10/02/2010	21	385	0.74	-25.4	0.15	0.41	0.59	1.16	1.67
11/02/2010	18	44	0.87	-25.8	0.16	0.45	0.55	0.17	0.21
11/02/2010	21	401	1.18	-27.9	0.12	0.29	0.71	1.35	3.36
12/02/2010	2	1068	0.88	-26.2	0.15	0.40	0.60	3.79	5.62
01/03/2010	11	1549	0.68	-24.2	0.19	0.59	0.41	6.27	4.31
10/03/2010	12	2624	0.53	-23.9	0.22	0.72	0.28	9.95	3.94
16/03/2010	9	1480	0.51	-25.0	0.19	0.57	0.43	4.33	3.25
22/03/2010	12	216	0.60	-24.9	0.17	0.48	0.52	0.62	0.67
05/04/2010	7	1414	0.69	-26.2	0.13	0.33	0.67	3.25	6.51
25/04/2010	8	46	0.91	-26.7	0.13	0.32	0.68	0.14	0.29
05/05/2010	17	82	0.65	-25.4	0.17	0.48	0.52	0.26	0.27
10/05/2010	11	40	0.82	-26.0	0.13	0.31	0.69	0.10	0.22
26/05/2010	11	15	1.56	-28.1	0.07	0.08	0.92	0.02	0.21
31/05/2010	11	391	0.80	-26.2	0.15	0.41	0.59	1.28	1.86
07/06/2010	12	13	-	-	-	-	-	-	-
05/07/2010	14	8	1.74	-28.7	0.07	0.07	0.93	0.01	0.13
02/08/2010	15	7	-	-	-	-	-	-	-
06/09/2010	15	7	3.55	-28.7	0.05	-0.01	1.01		0.26
13/09/2010	9	3	5.02	-	0.04	-0.04	1.04		0.17
25/10/2010	13	35	0.83	-26.8	0.09	0.15	0.85	0.04	0.25
15/11/2010	13	11	1.34	-27.7	0.08	0.09	0.91	0.01	0.13
22/11/2010	13	408	0.96	-27.0	0.12	0.27	0.73	1.04	2.88
29/11/2010	15	5955	0.80	-26.1	0.13	0.34	0.66	16.03	31.77
06/12/2010	17	1484	0.53	-24.3	0.18	0.56	0.44	4.38	3.49
20/12/2010	18	116	0.62	-24.8	0.19	0.59	0.41	0.42	0.29
27/12/2010	17	4201	0.61	-24.6	0.16	0.47	0.53	12.08	13.40
10/01/2011	17	110	1.59	-28.6	0.07	0.08	0.92	0.14	1.61

24/01/2011	12	2215	0.49	-23.6	0.20	0.63	0.37	6.78	3.98
29/01/2010	6	299	0.86	-26.3	0.16	0.47	0.53	1.22	1.35
29/01/2010	9	282	0.50	-24.7	0.20	0.60	0.40	0.86	0.56
29/01/2010	12	365	0.55	-24.8	0.22	0.69	0.31	1.37	0.62
29/01/2010	15	223	0.70	-25.7	0.19	0.56	0.44	0.87	0.68
29/01/2010	18	371	0.64	-24.6	0.21	0.67	0.33	1.59	0.80
29/01/2010	21	340	0.80	-25.9	0.18	0.53	0.47	1.45	1.26
30/01/2010	0	7594	0.86	-25.6	0.17	0.51	0.49	33.36	31.93
30/01/2010	3	1531	0.81	-25.5	0.20	0.61	0.39	7.47	4.86
30/01/2010	6	1212	0.80	-25.2	0.20	0.61	0.39	5.95	3.81
30/01/2010	9	1058	0.66	-24.8	0.20	0.63	0.37	4.40	2.59
30/01/2010	12	938	0.57	-24.3	0.25	0.82	0.18	4.40	0.98
30/01/2010	15	736	0.62	-24.5	0.24	0.77	0.23	3.50	1.03
30/01/2010	18	704	0.63	-24.5	0.24	0.78	0.22	3.48	0.96
30/01/2010	21	613	0.59	-24.4	0.23	0.76	0.24	2.75	0.86
31/01/2010	0	636	0.59	-24.6	0.24	0.80	0.20	3.03	0.74
31/01/2010	3	509	0.64	-24.7	0.20	0.64	0.36	2.09	1.18
31/01/2010	6	493	0.71	-24.9	0.18	0.56	0.44	1.94	1.54
31/01/2010	15	394	0.62	-24.6	0.25	0.83	0.17	2.02	0.42
01/02/2010	0	338	0.63	-25.1	0.19	0.57	0.43	1.20	0.92
01/02/2010	9	334	0.57	-24.6	0.22	0.71	0.29	1.36	0.54
01/02/2010	18	421	0.64	-24.8	0.21	0.65	0.35	1.77	0.95
03/02/2010	18	226	0.67	-25.1	0.20	0.62	0.38	0.94	0.58
03/02/2010	21	147	0.63	-25.3	0.18	0.52	0.48	0.48	0.45
04/02/2010	0[a]		6.83	-30.3	0.03	-0.10	1.10		
04/02/2010	0[b]	1533	2.65	-29.6	0.06	0.02	0.98		115.58
04/02/2010	0[c]		1.35	-29.0	0.07	0.07	0.93		
04/02/2010	3	180	1.09	-26.3	0.15	0.40	0.60	0.78	1.17
04/02/2010	6	183	0.67	-25.7	0.18	0.56	0.44	0.69	0.55
04/02/2010	9	185	0.69	-26.8	0.17	0.49	0.51	0.63	0.65
04/02/2010	12	889	0.52	-24.9	0.22	0.72	0.28	3.32	1.28
04/02/2010	15	547	1.07	-26.6	0.13	0.31	0.69	1.84	4.01
04/02/2010	18	1724	0.70	-25.9	0.17	0.49	0.51	5.89	6.11
04/02/2010	21	873	0.74	-25.3	0.18	0.53	0.47	3.42	3.05

[a] > 500 µm, [b] 63 – 500 µm, [c] < 63 µm [*Clark et al.*, 2013].
[d]samples independently combusted using an elemental analyser [*Gröcke et al.*, 2011].
– Small samples that did not yield a result.

Table S6.1b: Suspended sediment samples measured at the Wayqecha river gauging station.

Date	hr	SS ($g\ m^{-3}$)	C_{org} (%)	$\delta^{13}C_{org}$ (‰)[a]	N/C	$F_{f_n/c}$	$F_{nf_n/c}$	POC_f ($g\ m^{-3}$)	POC_{nf} ($g\ m^{-3}$)
04/01/2010	15	601	0.63	-25.4	0.16	0.47	0.53	1.78	1.99
29/01/2010	3	128	0.70	-25.4	0.18	0.56	0.44	0.50	0.40
31/01/2010	12	64	1.02	-27.0	0.13	0.32	0.68	0.21	0.44
02/02/2010	9	48	1.10	-27.8	-	-	-	-	-
09/02/2010	9	837	0.88	-27.1	0.16	0.47	0.53	3.43	3.91
09/02/2010	12	58	0.95	-27.4	0.13	0.30	0.70	0.17	0.38
10/02/2010	18	108	1.67	-28.7	0.09	0.16	0.84	0.30	1.50
10/02/2010	21	54	1.36	-27.9	0.09	0.17	0.83	0.12	0.61
22/02/2010	9	723	0.54	-25.0	0.18	0.52	0.48	2.03	1.85
01/03/2010	14	1504	1.01	-27.1	0.12	0.28	0.72	4.19	11.05
09/03/2010	12	784	0.72	-24.9	0.18	0.53	0.47	3.01	2.64
05/04/2010	10	74	0.80	-25.4	0.15	0.40	0.60	0.24	0.35
19/04/2010	9	39	1.49	-27.5	0.09	0.14	0.86	0.08	0.51
28/04/2010	12	13	1.44	-27.7	-	-	-	-	-
02/05/2010	14	19	0.97	-27.3	0.12	0.28	0.72	0.05	0.14
26/05/2010	14	37	4.50	-28.7	0.05	-0.02	1.02		1.70
31/05/2010	14	95	1.41	-27.0	0.11	0.23	0.77	0.30	1.03
07/06/2010	10	7	3.21	-	0.04	-0.06	1.06		0.24
20/07/2010	7	4	-	-	-	-	-	-	-
09/08/2010	12	4	-	-	-	-	-	-	-
25/10/2010	14	10	3.53	-28.6	0.05	-0.03	1.03		0.38
22/11/2010	14	81	1.53	-27.5	0.09	0.15	0.85	0.18	1.05
06/12/2010	14	1121	0.44	-24.4	0.18	0.53	0.47	2.63	2.35
03/01/2011	9	168	0.60	-25.1	0.16	0.46	0.54	0.46	0.54
18/02/2011	14	164	0.66	-25.5	0.15	0.43	0.57	0.47	0.62
29/01/2010	6	137	0.74	-25.9	0.17	0.50	0.50	0.51	0.51
29/01/2010	9	123	0.79	-26.5	0.16	0.46	0.54	0.45	0.52
29/01/2010	12	66	1.13	-26.7	0.15	0.40	0.60	0.29	0.45
29/01/2010	15	83	0.84	-26.1	0.16	0.45	0.55	0.31	0.38
29/01/2010	18	113	1.18	-27.0	0.13	0.32	0.68	0.43	0.91
29/01/2010	21	1891	1.03	-26.2	0.19	0.57	0.43	11.22	8.35
30/01/2010	0	1696	1.30	-26.1	0.15	0.41	0.59	9.14	12.92
30/01/2010	3	2869	0.76	-26.1	0.19	0.58	0.42	12.64	9.23
30/01/2010	6	737	0.62	-25.6	0.21	0.65	0.35	2.97	1.59
30/01/2010	9	286	0.59	-25.6	0.20	0.64	0.36	1.08	0.61
30/01/2010	12	136	0.85	-26.7	0.18	0.52	0.48	0.60	0.55
30/01/2010	15	202	0.65	-25.6	0.18	0.53	0.47	0.70	0.63
30/01/2010	18	239	0.59	-25.2	0.20	0.62	0.38	0.88	0.53
30/01/2010	21	180	0.68	-25.7	0.18	0.52	0.48	0.64	0.58
31/01/2010	0	78	0.94	-26.2	0.15	0.40	0.60	0.30	0.44
31/01/2010	3	155	0.59	-25.5	0.18	0.55	0.45	0.50	0.41
31/01/2010	6	20	0.61	-25.6	0.20	0.60	0.40	0.07	0.05
31/01/2010	15	69	0.95	-26.1	0.18	0.52	0.48	0.34	0.31
01/02/2010	0	41	1.28	-26.5	0.13	0.34	0.66	0.18	0.35
01/02/2010	9	79	0.80	-25.8	0.19	0.59	0.41	0.37	0.26
01/02/2010	18	69	1.08	-20.9	0.20	0.62	0.38	0.46	0.28

[a]samples independently combusted using an elemental analyser [*Gröcke et al.*, 2011].
– Small samples that did not yield a result.

Table S6.2: Fluxes and yields of paired suspended load samples from the San Pedro and Wayqecha gauging stations.

			San Pedro Catchment			Wayqecha Catchment			
Sample group	n		Measured flux and yield	Rating curve flux	Error in rating curve* (%)	Measured flux	Rating curve flux	Error in rating curve* (%)	SP-WQ / SP measured flux (%)
2-week paired°	24	SS (t hr^{-1})	83	60	-28	13.9	5.6	-59	-
2-week paired°	24	SS (t km^{-2} hr^{-1})	0.51	0.37	-28	0.29	0.12	-59	+44
2-week paired°	24	POC_f (tC hr^{-1})	0.37	0.23	-37	0.07	0.19	+183	-
2-week paired°	24	POC_f (tC km^{-2} hr^{-1})	0.0022	0.0014	-37	0.0014	0.0039	+183	+39
2-week paired°	24	POC_{nf} (tC hr^{-1})	0.26	0.18	-32	0.06	0.03	-57	-
2-week paired°	24	POC_{nf} (tC km^{-2} hr^{-1})	0.0016	0.0011	-32	0.0013	0.0005	-57	+20
2-week paired°	24	Runoff (mm hr^{-1})	0.56	0.56	-	0.60	0.60	-	-7.5
All paired	11	SS (t hr^{-1})	73	47	-35	15	7	-55	-
All paired	11	SS (t km^{-2} hr^{-1})	0.44	0.29	-35	0.31	0.14	-55	+31
All paired	11	POC_f (tC hr^{-1})	0.25	0.19	-23	0.04	0.14	+248	-
All paired	11	POC_f (tC km^{-2} hr^{-1})	0.0015	0.0012	-23	0.0009	0.0030	+248	+43
All paired	11	POC_{nf} (tC hr^{-1})	0.21	0.22	+1.5	0.08	0.03	-59	-
All paired	11	POC_{nf} (t C km^{-2} hr^{-1})	0.0013	0.0013	+1.5	0.0016	0.0006	-59	-20
All paired	11	Runoff (mm hr^{-1})	0.47	0.47	-	0.48	0.48	-	-1.4

* Error in rating curve determined by (rating flux- measured flux) /measured flux × 100
°The 2-week paired samples were from 29/01/2010 to 1/02/2010, and 10/02/2010. Hourly fluxes were determined by summing measurements (n = 24 per gauging station) and assuming the measurements were representative over the 3-hr period.
The rating curves from both sites (Figure S6.1) were used to estimate the fluxes.
- Indicates the result is not relevant.

Table S6.3: Power-law river discharge (Q_w, m^3 s^{-1}) to sediment load rating curves at San Pedro gauging station

(g m^{-3})	Equation	r^2
Suspended sediment	= 0.0043 × Q_w $^{3.6763}$	0.75
$POC_{non\text{-}fossil}$ (Q_w > 22)	= 9E-11 × Q_w $^{7.3165}$	0.45
$POC_{non\text{-}fossil}$ (Q_w < 22)	= 0.0072 × Q_w $^{1.5935}$	0.29
POC_{fossil}	= 1E-06 × Q_w $^{4.5346}$	0.71

Table S6.4: Seasonal yields of suspended load for the Kosñipata Valley at San Pedro river gauge

		Wet season (December to March)	Wet-dry transition season (April)	Dry season (May to September)	Dry-wet transition season (October & November)
Suspended sediment	t km^{-2} $month^{-1}$	187+52	97+27	7+2	43+12
	t km^{-2} $month^{-1}$ (range)	187 to 239	97 to 124	7 to 9	43 to 55
	% of annual flux	77.4	10	3.7	8.9
POC_{fossil}	tC km^{-2} $month^{-1}$	0.76+0.28	0.36+0.13	0.02+0.0	0.19+0.07
	tC km^{-2} $month^{-1}$ (range)	0.76 to 1.04	0.36 to 0.49	0.02	0.19 to 0.26
	% of annual flux	78.4	9.2	2.4	10
$POC_{non-fossil}$	tC km^{-2} $month^{-1}$	0.96+0.31	0.52+0.17	0.05+0.02	0.33+0.11
	tC km^{-2} $month^{-1}$ (range)	0.96 to 1.27	0.52 to 0.69	0.05 to 0.07	0.33 to 0.44
	% of annual flux	73.3	9.9	4.3	12.5
Q_w	mm $month^{-1}$ (%)*	340 (50)	296 (11)	137 (25)	190 (14)
Rainfall	mm $month^{-1}$ (%)*	441 (58)	204 (7)	129 (21)	210 (14)

* Seasons were determined from meteorological station rainfall [*Clark et al.*, in review].
Annual breakdown of total flux as a percentage in parenthesis.
Mean seasonal runoff (Q_w; mm $month^{-1}$) and catchment wide tropical rainfall measuring mission (TRMM) calibrated rainfall (mm $month^{-1}$) is derived from *Clark et al.* [in review].
Yield error determined from the rating curve derived error of -28 %, -37 %, and -32 % of suspended sediment, POC_{fossil} and $POC_{non-fossil}$ respectively (Table S6.2).

Table S6.5: Description of the 8 days that contributed to 50 % of the annual $POC_{non-fossil}$ flux

Day rank	Date	Season^	% to annual POC_{nf}	POC_{nf} flux (kg C km^{-2} hr^{-1})	Total stream runoff (mm hr^{-1})	Stream runoff day rank	Q_{max} (m^3s^{-1})	Quickflow (mm d^{-1})^	Baseflow (mm d^{-1})^	Runoff description
1	5/3/2010#	Wet	17.5	38.3	0.85	1	62.8*	10.0	10.2	Falling limb largest storm
2	4/12/2010	Dry-wet	8.1	17.8	0.63	6	55.6	8.6	6.5	3rd largest peak without falling limb, with another storm in the day
3	25/10/2010	Dry-wet	7.2	15.7	0.45	77	61.6	6.2	4.7	2nd largest peak, with another storm in the day
4	4/3/2010#	Wet	6.1	13.4	0.67	3	70.0	5.7	10.2	Largest storm rising limb and peak
5	6/4/2010	Wet-Dry	3.8	8.2	0.64	5	42.8	5.1	10.2	4th largest peak with rising and most of falling limb
6	6/3/2010#	Wet	3.0	6.2	0.69	2	35.2*	6.3	10.3	Falling limb largest storm
7	1/3/2010	Wet	2.5	5.6	0.66	4	35.2	5.7	10.2	Day long storm (rising, peak, and falling limbs)
8	27/4/2010	Wet-dry	2.1	4.7	0.55	26	42.5	5.8	7.3	5th largest peak, flash flood, low baseflow with rising and falling limbs.

Largest annual storm.
* Not from a peak in streamflow.
^ data from [*Clark et al.*, in review].

Table S6.6: Comparison of automatic versus manually derived landslide to river connectivity.

Sub-catch-ment name	Area (km^2)	Mean Slope (°)	Mean Forest Slope (°)	Puna (%)	upslope area of hillslopes ° (m^2)	Automatic - Landslide area that intersects with rivers* (%)	Manual -Landslide area that intersects with rivers" (%)	Error in automatic connectivity ^ (%)
MS2	3.7	42	42	0	108 415	100	100	0
MS1	14.5	37	37	3	159 370	91	95	4
SP3	3.6	38	38	0	40 886	82	87	6
SP4	2.9	43	43	0	96 833	92	100	8
Trocha	4.5	39	39	0	127 097	81	90	10
WQ2	12.8	33	38	32	135 936	83	92	10
WQ	49.3	33	38	49	326 346	87	96	9
Union	3.2	41	41	0	31 068	75	91	18
Max	49	43	43	49	326 346	100	100	0
Min	3	33	37	0	31 068	75	87	13
Mean	12	38	40	10	128 244	86	94	8

Area, mean slope, mean forest slope, mean hillslope upslope area, was determined from a 3m x 3m DEM produced by Carnegie Airborne Observatory (CAO) [*Asner et al.*, 2012; *Asner*, unpublished data].

°The upslope area of hillslopes was determined from a log-log plot of slope (y-axis) to accumulated area (x-axis) with logarithmically spaced bins , following [*Dadson et al.*, 2004; *Meunier et al.*, 2008], where the break in scaling is interpreted as the transition from hillslopes (area < ~128,000 m^2) to fluvial channels (area > ~128,000 m^2).

*Automatic river connectivity was determined using a buffer of 25 m around the stream channels, (> upslope area) for each sub-catchment and then overlap with landslides was determined [*Clark et al.*, in prep].

"Manual inspection of landslides previously mapped with rivers was carried out using high resolution Quickbird (0.6m x 0.6m) orthorectified pan-sharpened image from 2009.

^Error in automatic connectivity was determined as follows: ((auto - manual)/manual) x 100

S6.2. Figures for supplementary information

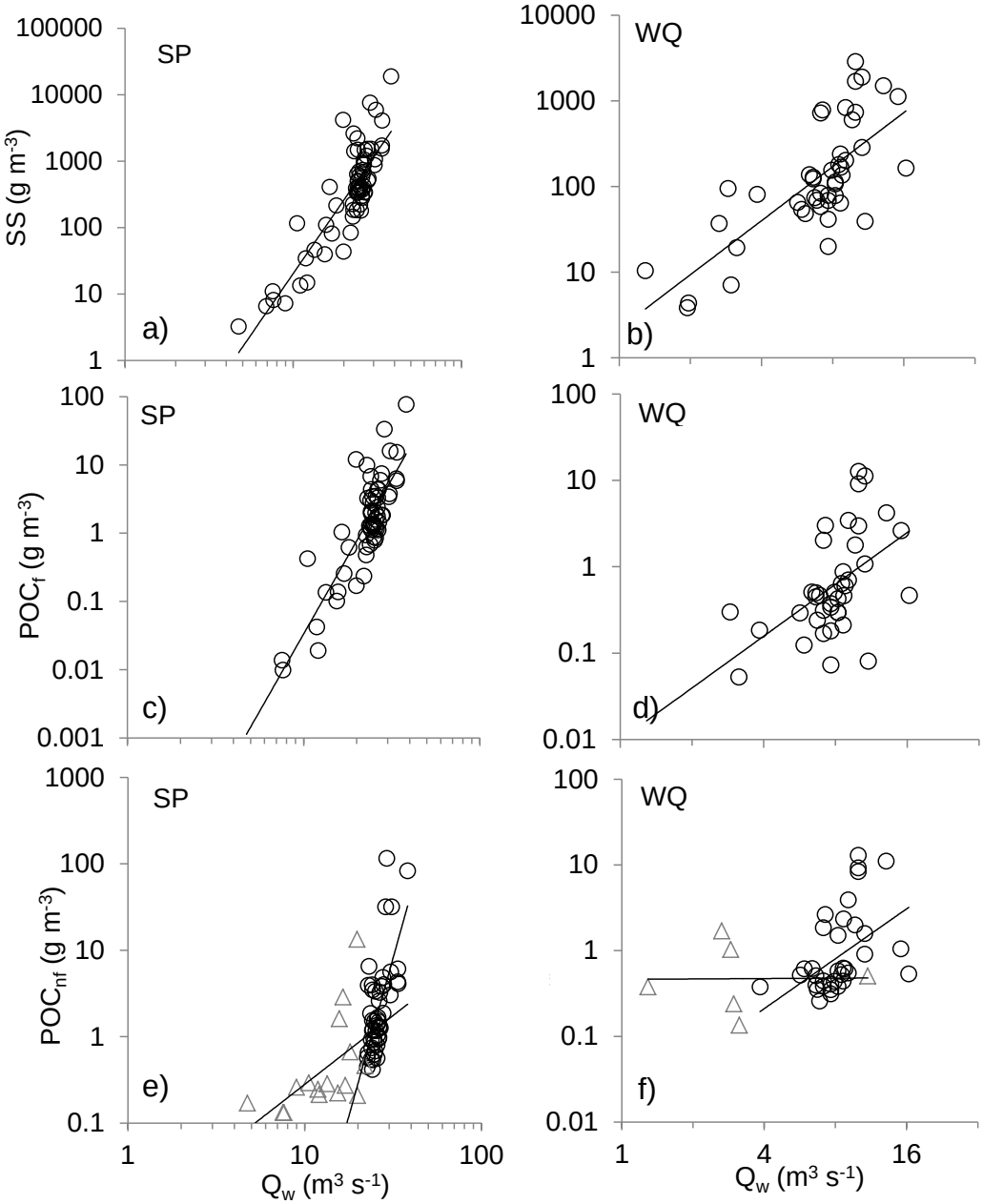


Figure S6.1: Rating curves for a) suspended sediment, c) POC_{fossil}, and e) $POC_{non\text{-}fossil}$ against instantaneous river discharge (Q_w m^3 s^{-1}) at the San Pedro gauging station. The $POC_{non\text{-}fossil}$ data was divided by $Q_w \geq 22$ m^3 s^{-1} as black circles and $Q_w < 22$ m^3 s^{-1} as grey triangles. At the San Pedro gauging station power-law regressions were fit to the data and used to estimate sediment, $POC_{non\text{-}fossil}$ and POC_{fossil} flux over the one year study (Table S6.3, Table 6.2). Rating curves for b) suspended sediment, d) POC_{fossil}, and f) $POC_{non\text{-}fossil}$ against instantaneous Q_w (m^3 s^{-1}) for the Wayqecha gauging station. The $POC_{non\text{-}fossil}$ data was divided up in f) by seasons where mid-April to October was the dry season (black circles) and November to mid-April the wet season (grey triangles). The power-law regressions were fitted to the Wayqecha data, but due to limited onsite runoff values (n = 59) and sediment samples (n = 46) throughout the year, monthly sample means were used to determine fluxes (Table 6.2).

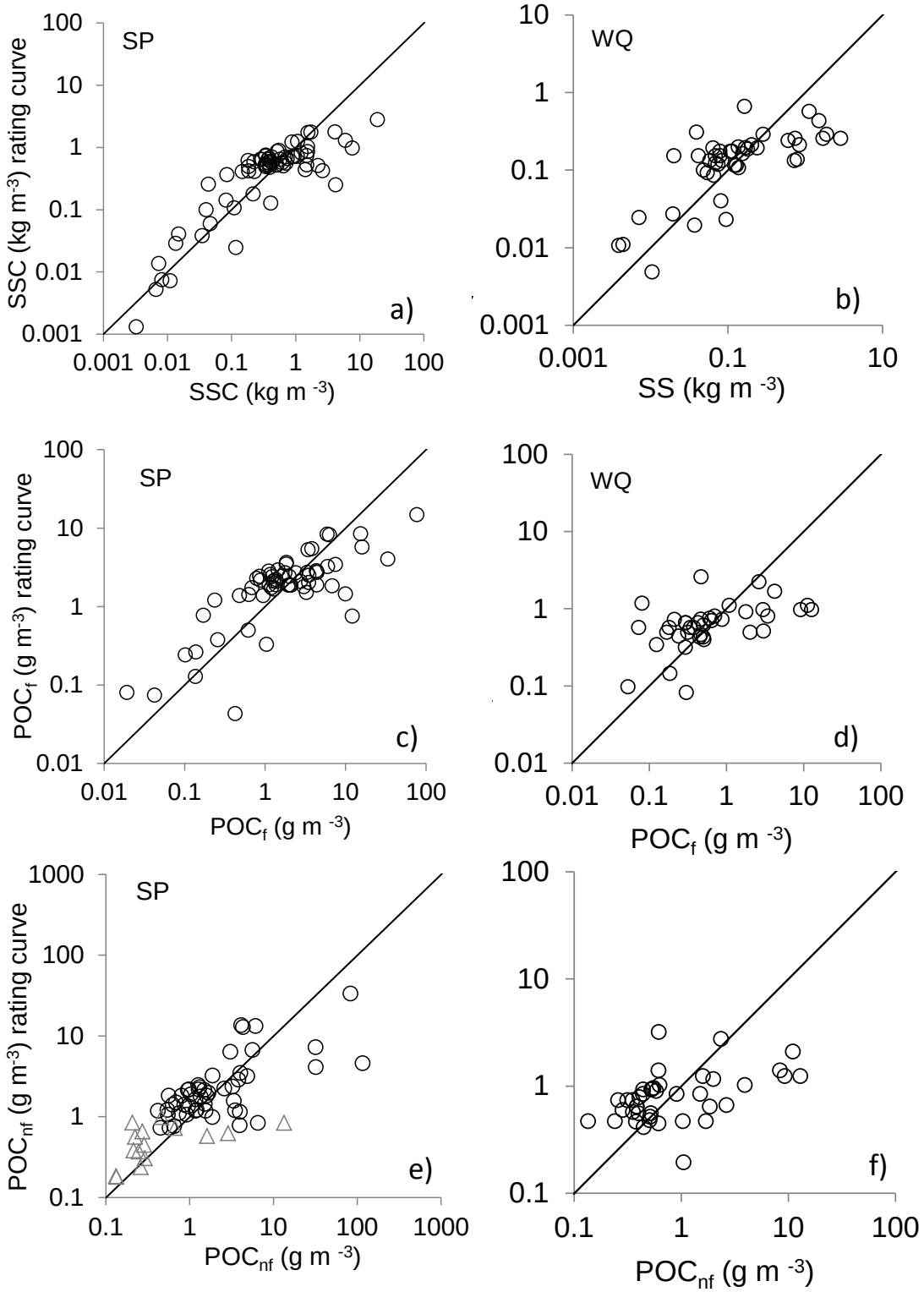


Figure S6.2: Concentrations of a) and b) suspended sediment (kg m^{-3}), c) and d) POC_{fossil} (g m^{-3}), and e) and f) $POC_{non\text{-}fossil}$ (g m^{-3}) for the San Pedro gauging station (a, c, e) and the Wayqecha (b, d, f) gauging station comparing estimates from the rating curves (Figure S6.1) and measured collections (Table S6.1). At high concentrations sediment load is underestimated using the rating curves. Black line indicates the 1:1 ratio.

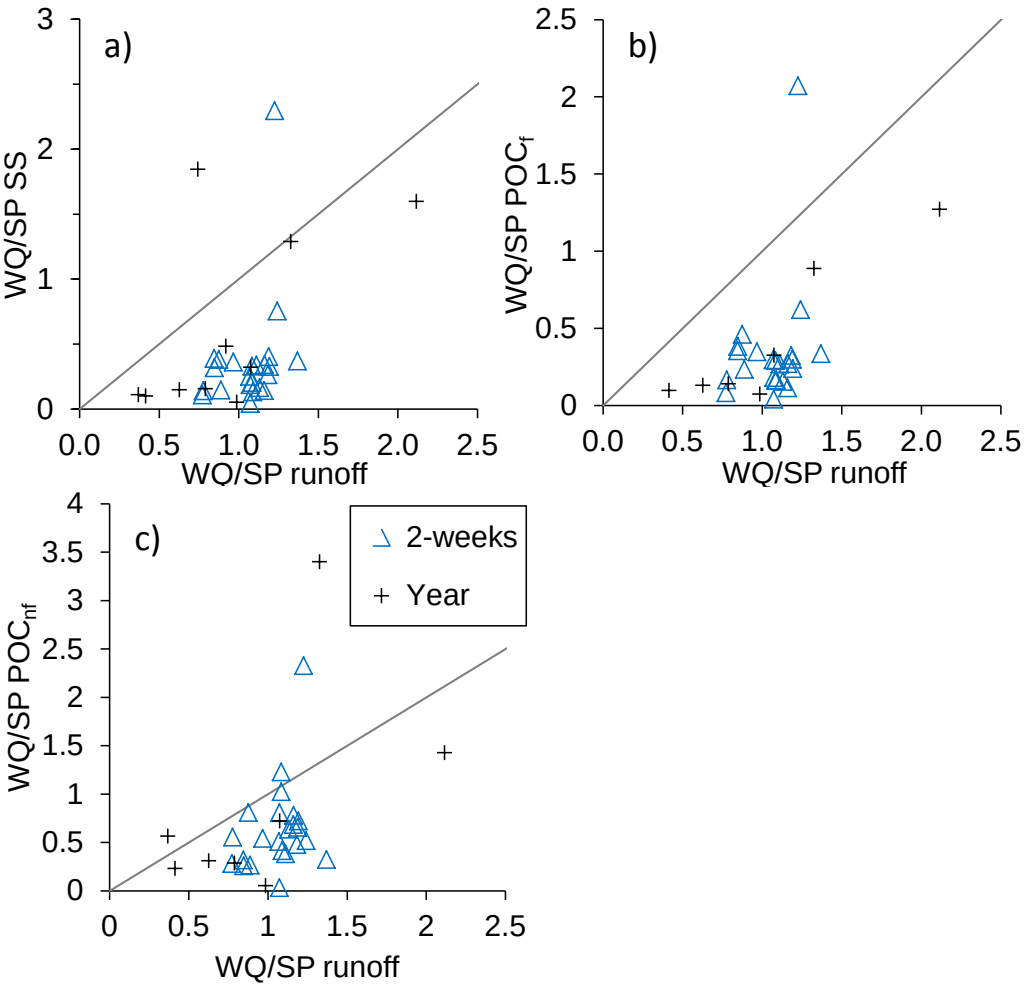


Figure S6.3: Comparison of instantaneous normalised flux (g km^{-2} s^{-1} at WQ / g km^{-2} s^{-1} at SP) for paired measured Wayqecha (WQ) and San Pedro (SP) samples of a) suspended sediment, b) POC_{fossil}, and c) $POC_{non\text{-}fossil}$ versus the runoff ratio. Paired samples were compared from both gauging stations over the 2-week wet season experiment (n = 23) and throughout the year (n = ~11; same day n = 8 and < 3 days n = 3) (Table S6.2).

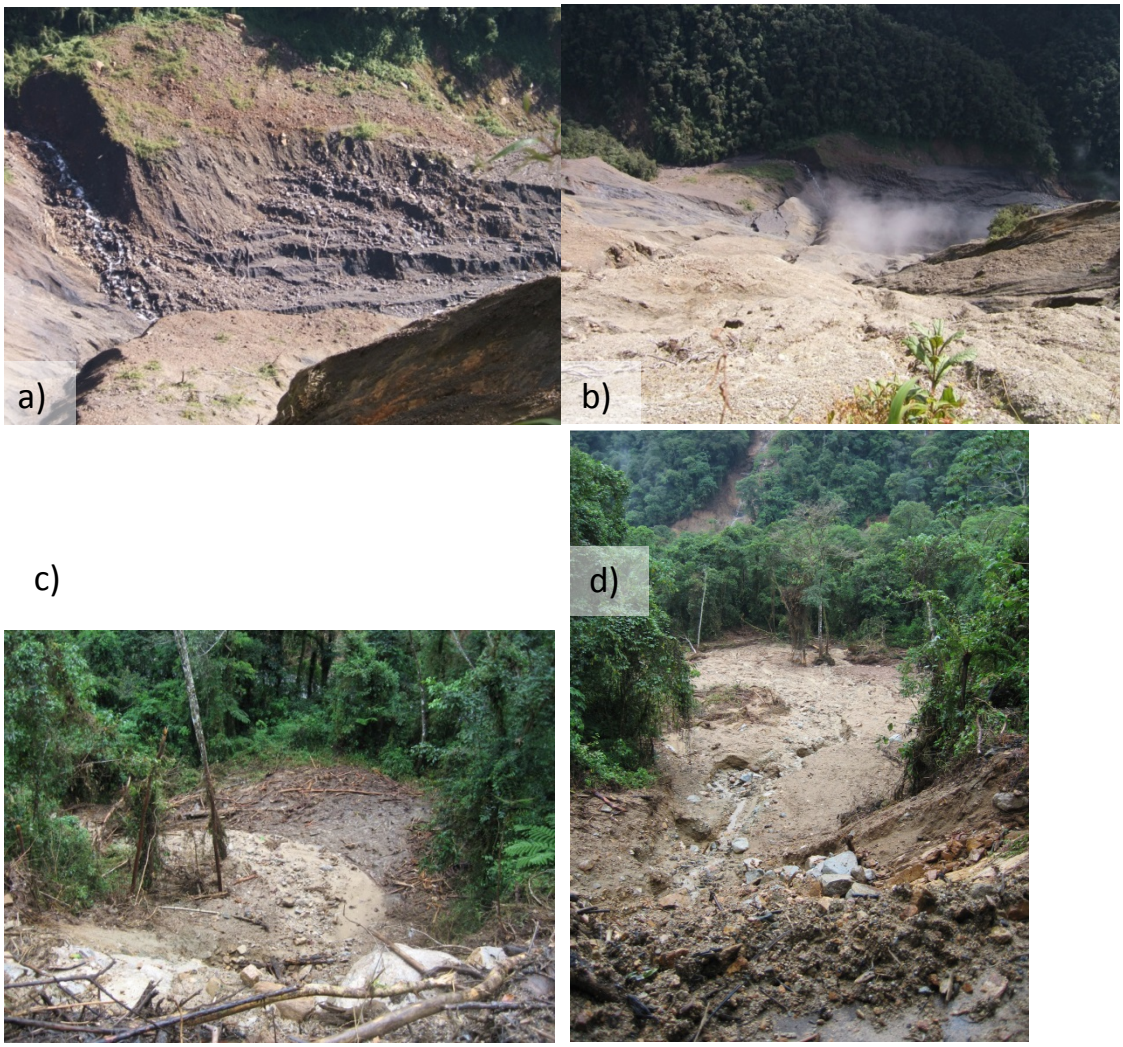


Figure S6.4: a) landslides connected to the river channel, but the supply of eroded material overwhelms the carrying capacity of the stream channel, where b) only a portion is removed by the river and the rest is buried onsite and stored for a period of time. Additionally, c) and d) at lower elevations along the Kosñipata River main stem landslides can deposit material onto a flood plain. The sediment blocks the streams from flowing into the river. Thus, a large proportion of the organic material remains onsite in the river flood plain and may be degassed or buried.

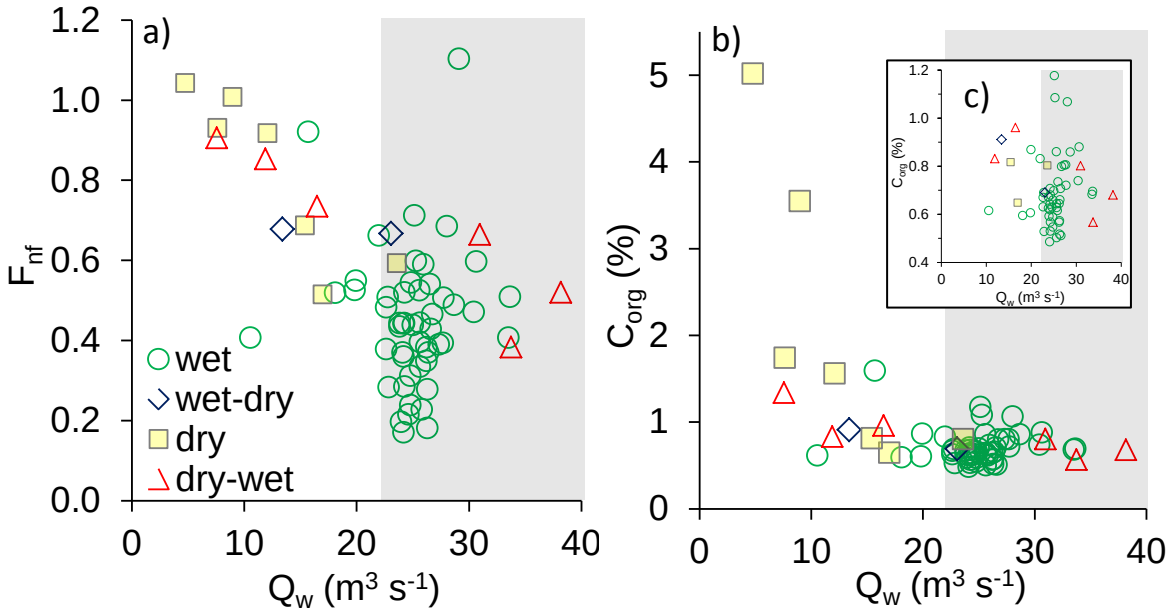


Figure S6.5: a) Fraction non-fossil POC (F_{nf}) versus water discharge (Q_w, m^3 s^{-1}). b) C_{org} (%) versus Q_w, with c) inset at high Q_w. Samples are separated into season and are all from the San Pedro gauging station. The dark band represents the region with elevated concentrations of $POC_{non\text{-}fossil}$ at Q_w > 22 m^3 s^{-1} (Figure S6.1e).

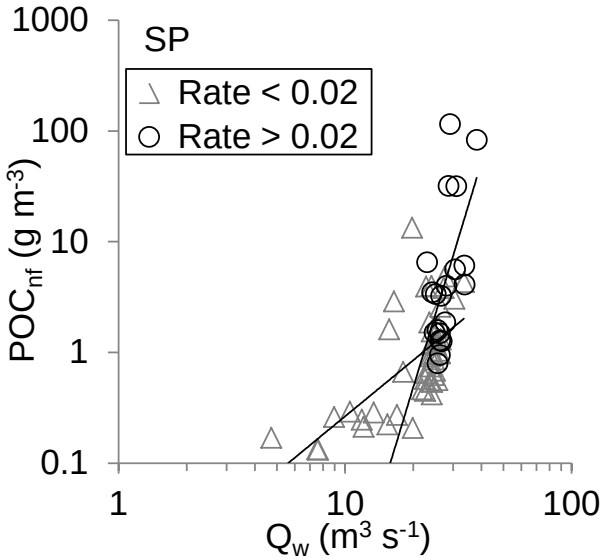


Figure S6.6: $POC_{non\text{-}fossil}$ versus discharge (Q_w) at the San Pedro gauging station. The $POC_{non\text{-}fossil}$ samples were divided by high rate of change (> 0.02) and low rate of change (< 0.02) at a 3hr interval. Rate of change was determined as the difference river height at the time of the sample (with a ± 15 min mean) to the river height 3 hrs previous (with a ± 15 min mean).

S6.3. References for supplementary information

Asner, G. P., Knapp, D. E., Boardman, J., Green, R. O., Kennedy-Bowdoin, T., Eastwood, M., Martin, R. E., Anderson, C., and Field, C. B. (2012), Carnegie Airborne Observatory-2: Increasing science data dimensionality via high-fidelity multi-sensor fusion, *Remote Sensing of Environment, 124*(0), 454-465, doi: http://dx.doi.org/10.1016/j.rse.2012.06.012.

Asner, G. P. (unpublished data).

Clark, K. E., Hilton, R. G., West, A. J., Malhi, Y., Gröcke, D. R., Bryant, C. L., Ascough, P. L., Robles Caceres, A., and New, M. (2013), New views on "old" carbon in the Amazon River: Insight from the source of organic carbon eroded from the Peruvian Andes, *Geochemistry, Geophysics, Geosystems, 14*(5), 1644-1659, doi: http://dx.doi.org/10.1002/ggge.20122.

Clark, K. E., West, A. J., Hilton, R. G., Asner, G. P., Silman, M. R., Saatchi, S. S., Quesada, C. A., Farfan Rios, W., Horwath, A. B., Martin, R. E., New, M., and Malhi, Y. (in prep), Storm-triggered landslides in an Andean Valley: Links to topography, organic carbon, and biodiversity?

Clark, K. E., Torres, M. A., West, A. J., Hilton, R. G., New, M., Horwath, A. B., Fisher, J. B., Rapp, J. M., Robles Caceres, A., and Malhi, Y. (in review), The hydrological regime of a forested tropical Andean valley.

Dadson, S. J., Hovius, N., Chen, H., Dade, W. B., Lin, J.-C., Hsu, M.-L., Lin, C.-W., Horng, M.-J., Chen, T.-C., Milliman, J., and Stark, C. P. (2004), Earthquake-triggered increase in sediment delivery from an active mountain belt, *Geology*, *32*, 733-736, doi: http://dx.doi.org/10.1130/G20639.1

Gröcke, D. R., Hori, R. S., Trabucho-Alexandre, J., Kemp, D. B., and Schwark, L. (2011), An open ocean record of the Toarcian oceanic anoxic event, *Solid Earth*, *2*, 245-257, doi: http://dx.doi.org/10.5194/se-2-245-2011.

Meunier, P., Hovius, N., and Haines, J. A. (2008), Topographic site effects and the location of earthquake induced landslides, *Earth and Planetary Science Letters*, *275*(3), 221-232, doi: http://dx.doi.org/10.1016/j.epsl.2008.07.020.

Chapter 7 : Conclusions

7.1. Review of main findings

This thesis has focused on several research gaps in Andean mountain hydrology, river particulate organic carbon (POC), and landslide carbon dynamics. The main research aims were to quantify the stream runoff in order to determine the POC fluxes (non-fossil and fossil) and compare $POC_{non\text{-}fossil}$ to the soil and vegetation (non-fossil) carbon mobilised by landslides. Understanding the role that soil and vegetation (non-fossil carbon) play in river POC in a mountain catchment in the Andes, opens the door for further understanding of Andean sourced POC in the lowland Amazon and beyond in the Amazon continental shelf. Additionally, beyond the main thesis findings, there is a broader coverage of what earth scientists call the "earth's critical zone" which covers chemical, biological, physical, and geological processes that operate together to support life on the surface of the earth [*Brantley et al.*, 2007]. I have evaluated several key aspects of the critical zone (atmospheric inputs, biological activity, soil dynamics, hillslope dynamics, and stream channel processes) and provided insight into others (bedrock weathering, and fluvial and coastal deposition).

The main findings of the thesis, based in the Kosñipata River Valley can be summarised as:

7.1.1. River hydrology

- Stream runoff was ~3000 mm yr^{-1} for the two montane catchments.
- There is a seasonal lag in runoff at the San Pedro gauging station, where rainfall from the wet season is temporarily stored and then later released as stream runoff in the wet-dry and dry seasons.

- Deep groundwater is most probably responsible for the lag in stream runoff, as soil water storage was insufficient to capture all the variability required.
- The estimated water balance for the Kosñipata Valley at San Pedro over the study period is as follows: rainfall 3028 mm yr^{-1}, cloud water 308 ± 97 mm yr^{-1}, evapotranspiration 909 mm yr^{-1}, runoff 2721 mm yr^{-1}, with a residual of -294 ± 97 mm yr^{-1} (~10 % of total inputs).
- Cloud water contributed 11 ± 4 % of the annual stream runoff and is evenly distributed in streamflow throughout the year.
- Seasonality was very important as 50-56% of the annual water yield was transported in the wet season (over 4 months from December to March) in the San Pedro and Wayqecha gauging stations.
- Wet season rainfall dominated streamflow throughout the dry season (60 ± 7 %), followed by dry season rainfall (25 ± 7 %), and finally by cloud water (12 ± 6 %).

7.1.2. Fossil and non-fossil river POC

- In the Kosñipata Valley, river POC is comprised of non-fossil (soil and vegetation) and fossil (sedimentary bedrock) organic carbon. There was a binary mixing mostly between O_h layer soil and fossil bedrock.
- An end-member mixing model using radiocarbon from a selection of POC samples allowed for partitioning the POC two components as fraction fossil (~ 0.5) and fraction non-fossil (~ 0.5).
- An accurate calibration equation replacing radiocarbon data with N/C ratios (using C_{org} % and N %) was possible. This was an economical alternative to other more costly radiocarbon analysis to accurately estimate the contribution of fossil and non-fossil components in POC.

- At the storm peak there was a higher proportion of soil or vegetation in river POC, suggesting that soil and vegetation input into streamflow is source limited rather than transport limited.

7.1.3. Landslide activity

- The valley wide landslide rate was 0.09 % yr^{-1} with a landslide driven slope turnover of 1200 years.
- Landsat satellite imagery, although moderate resolution (30 x 30 m), provided an annual database from 1988 to 2012 to monitor landslide occurrence. High resolution imagery, such as Quickbird or Worldview, was then used to delineate landslide boundaries and verifying landslide occurrence.
- Landslide probability was highest in the lowest elevations (1200 to 1700 masl) of the study area. This is caused by over-steepened hillslopes created by a knickpoint in the river channel (~1700 masl).
- Landslide activity increased substantially (up to 0.16 % yr^{-1}) above a threshold hillslope angle of 38 °.
- A single extreme rainfall event (mean 44 mm hr^{-1} over 4.5 hrs) in 2010 was the ultimate trigger for ~185 landslides to occur.

7.1.4. Mobilisation of carbon due to landslide activity

- In the forested portion of the valley landslides mobilise ~40 tC km^{-2} yr^{-1} (30 tC km^{-2} yr^{-1} from soil and 10 tC km^{-2} yr^{-1} from vegetation).
- In the whole valley, including the puna grasslands where landslide activity is very low, landslides mobilise ~28 tC km^{-2} yr^{-1} (~21 tC km^{-2} yr^{-1} from soil and ~7 tC km^{-2} yr^{-1} from vegetation).

- Soil and vegetation carbon was more or less evenly distributed throughout elevation. The carbon mobilised by landslides was influenced by spatial trends in landslide rates, where oversampling carbon by landslide of soil and vegetation occurred at lower elevations (< 1800 masl).

7.1.5. River suspended sediment and POC fluxes

- At the San Pedro gauging station, measured POC samples were ~1 % of the suspended sediment load, where $POC_{non\text{-}fossil}$ comprised 0.64 % and POC_{fossil} comprised ~0.33 % of the suspended sediment.
- The year-long rating curve derived $POC_{non\text{-}fossil}$ and POC_{fossil} yields coincided with these measured samples (above), with $POC_{non\text{-}fossil}$ and POC_{fossil} contributing 0.54 % and 0.4 % to suspended sediment respectively.
- The binary mixing between non-fossil (dominated by the O_h soil layer) and fossil (river bed load) POC sources occurred throughout the study year at both the San Pedro and Wayqecha river gauging stations.
- The suspended sediment (SS) yield was 960 to 1230 t km^{-2} yr^{-1} for the San Pedro and Wayqecha catchments respectively. These yields were consistent with Andean estimates of SS for the Madre de Dios Basin.
- The $POC_{non\text{-}fossil}$ yield was 5.2 to 6.9 tC km^{-2} yr^{-1}.
- The POC_{fossil} yield was 3.9 to 5.3 tC km^{-2} yr^{-1} for the San Pedro and Wayqecha catchments respectively.
- ~0.4 – 1.0 % of the annual net primary productivity (NPP) of the Kosñipata Valley is laterally transferred out of the valley via river $POC_{non\text{-}fossil}$.

7.1.6. Climatic and physical forcing of river suspended load

- The wet season contributed 77 %, 73 % and 78 % of the annual suspended sediment, POC_{nf}, and POC_f yields in the Kosñipata valley.
- Storm activity resulting in peak discharges transported most of the POC and SS in the river. The top 8 days contributed 50 % of the annual POC_{nf} flux.
- Landslides are well connected to the river channels and mobilise ~28 tC km^{-2} yr^{-1} of soil and vegetation. The amount of soil and vegetation in the form of river $POC_{non-fossil}$ is less at 5.3 – 6.9 tC km^{-2} yr^{-1}. This suggests that only a portion of the landslide mobilised carbon was removed by the rivers in the form of $POC_{non-fossil}$.

7.2. Implications of findings

The results of this research are far-reaching and provide insight into the study of hydrology, sediment transport, and landslide dynamics. In the Andes that drains into the Amazon, there have been a few studies addressing stream runoff [*Crespo et al.*, 2011], and this study helps to expand this limit knowledge base. In terms of river POC and sediment transport, this is the first study to consider fluxes in the Andes, making this study the basis for future study and reference. Again, only a few studies in the Andes draining into the Amazon have even evaluated landslide rates [*Blodgett and Isacks*, 2007]. In the bigger global picture, various aspects of this research work have been executed in other montane catchments such as in Taiwan, New Zealand, Guatemala, and in the Himalayas [*Hovius et al.*, 1997; *Hilton et al.*, 2008a; *Hilton et al.*, 2008b; *Hilton et al.*, 2010; *Hilton et al.*, 2011; *Andermann et al.*, 2012; *Hilton et al.*, 2012; *Larsen and Montgomery*, 2012; *Muñoz-Villers and McDonnell*, 2012; *Ramos Scharrón et al.*, 2012]. What sets this project apart is that it has brought all of the elements together and that they were measured simultaneously.

This thesis has made several specific contributions to the fields of mountain hydrology, river suspended sediment and POC transport, and landslide dynamics. In chapter 3, a **unique low-**

budget approach to investigating the hydrologic balance of a mountain catchment was carried out and has the potential to be deployed in other remote mountain locations. Innovative river gauging techniques were used at the Wayqecha gauging station, due to river channel migration. In addition, models were used to estimate several components of the Kosñipata Valley water balance (i.e. rainfall, actual evapotranspiration, and cloud water). This is the first study to evaluate the sources of stream discharge in Andean runoff and to demonstrate the **important role of wet season rainfall contribution to streamflow throughout the year**. As well, this is the first study to demonstrate that **a fractured bedrock basement plays an important role in the seemingly impermeable bedrock of the Andes** for the transport of groundwater, providing streamflow well into the dry season. The importance of groundwater in low porosity bedrock in mountain environments has been brought to light very recently [*Tipper et al.*, 2006; *Calmels et al.*, 2011; *Andermann et al.*, 2012], and will continue to be explored.

In chapter 4, it is demonstrated that **fossil carbon is an important component in Andean river POC** [*Meybeck*, 1993; *Blair et al.*, 2003]. This is the first time in the Andes, however, that POC partitioning has been undertaken. Previous work in the Andes has only reported one POC value, reporting that the POC was from non-fossil carbon [*Mayorga et al.*, 2005; *Townsend-Small et al.*, 2007; *Townsend-Small et al.*, 2008]. A two end-member mixing model was developed and it is the first time in river POC that a **$\Delta^{14}C_{org}$ ‰ mixing equation was calibrated to use N/C data** instead of using radiocarbon ($\Delta^{14}C_{org}$ ‰) analysis. The method used in this research was an economical and time saving alternative to solely using radiocarbon analysis which is an expensive and time consuming procedure. Finally, this is the first study to show POC **source switching between soil and vegetation at peak storm discharge**.

Chapter 5 outlines how **Landsat images were used over a continual long-term period to map landslides** and the landslide results were verified in several high resolution images. In past studies, a snap shot approach was carried out using some high resolution images such as air photos possibly with several decades apart to derive landslide rates (i.e. *Hovius et al.* [1997]. Along with unique landslide mapping techniques, this thesis contributed to the growing field of landslide recovery and ecology [*Restrepo et al.*, 2009]. We used **remote sensing to calculate vegetation recovery rates on landslide scars** and we proposed that **landslides rates may influence tree biodiversity**. This would suggest that there is a geomorphic influence on tree species richness in the valley. Finally, this work is the first to compose a **basin-wide carbon stock inventory** of soil, roots (fine and coarse), epiphytes, trees, and coarse woody debris, and then to compare it to landslide rates estimating the **annual mobilisation of carbon due to landslides**.

Chapter 6 outlines the **first study of suspended sediment, $POC_{non\text{-}fossil}$ and POC_{fossil} fluxes in the Andes**. Previous studies have measured various aspects of POC and suspended sediment in the Andes, but have not provided annual fluxes [*Mayorga et al.*, 2005; *Townsend-Small et al.*, 2008]. Additionally, it demonstrates a **distinct seasonal variation in $\delta^{13}C_{org}$ (‰)** showing varying inputs of fossil and non-fossil organic carbon over the year. [*Townsend-Small et al.*, 2008] reported weekly river $\delta^{13}C$ (‰) over the course of a year for the Chorobamba River valley, but because the two Andean catchments are substantially different (ie. the Chorobamba River Valley has less rainfall, lower stream runoff, and less physical erosion), there was no seasonal pattern in $\delta^{13}C$ (‰). This also could have been attributed to the fact that decarbonisation was not carried out to remove inorganic carbon [*Townsend-Small et al.*, 2008].

There were several aspects of this research that produced surprising results. First, the stream runoff, and POC_{nf}, POC_f and suspended sediment fluxes for both the San Pedro and

Wayqecha gauging station were relatively similar, despite the fact that Wayqecha was only measured once a week to once a month. Secondly, even though the Kosñipata Valley consists mostly of tropical montane cloud forest, cloud water comprised a minor but constant portion of water to streamflow. Wet season rainfall dominated streamflow even in the dry season when rainfall was low and cloud immersion of forests is expected to be at its highest. Thirdly, although it is impossible to assign an exact age to the organic matter in the valley, due to atomic bomb testing offsetting atmospheric radioisotope concentrations, the mean age of the river POC_{nf} was very young (mean $\Delta^{14}C_{org}$ ~50 ‰). Fourthly, the maximum concentrations of river POC and SS were greater than what has been reported in the literature for mountain regions [*Hilton et al.*, 2008a; *Hatten et al.*, 2012; *Hilton et al.*, 2012]. Fifthly, the Kosñipata Valley has one of the fastest reported forest slope turnovers due to landslide activity [*Restrepo and Alvarez*, 2006; *Hilton et al.*, 2011], yet the $POC_{non\text{-}fossil}$ flux is one of the lowest compared to those reported in the literature [*Kao and Liu*, 2000; *Hilton et al.*, 2008a; *Hatten et al.*, 2012; *Hilton et al.*, 2012; *Smith et al.*, 2013]. Although 95 % of the landslides are connected to river channels, much of the landslide debris is stored onsite rather than being exported by river POC.

Other aspects of the thesis were as expected, confirming the literature. In chapter 3, annual stream runoff is comparable to other tropical montane forests [*Garcia-Martino et al.*, 1996; *Crespo et al.*, 2011; *Muñoz-Villers et al.*, 2012]. In chapter 4, $POC_{non\text{-}fossil}$ enrichment occurred at peak stormflow. This has been previously demonstrated in Taiwan [*Hilton et al.*, 2008b; *Hilton et al.*, 2012]. Chapter 5 illustrates that landslides in the valley followed a frequency-magnitude curve fitted to an inverse gamma function, as presented in [*Malamud et al.*, 2004]. Landslide coverage was ~2 % of the study site, similar to that found in the Bolivian and Ecuadorian Andes [*Stoyan*, 2000; *Blodgett and Isacks*, 2007]. High resolution LiDAR derived DEM (3 x 3 m) allowed for detailed study of hillslopes, demonstrating a

threshold hillslope angle. This detail was lost, however, when using low resolution SRTM DEM (90 x 90 m), although a 40 x 40 m DEM was sufficient in Taiwan [*Lin et al.*, 2008]. In agreement with the threshold hillslope model, landsliding rates had a higher frequency around a knickpoint in the river channel, as demonstrated in [*Korup*, 2006; *Larsen and Montgomery*, 2012]. In chapter 6, $POC_{non\text{-}fossil}$ flux appears to be coupled with suspended sediment flux, confirming the trend noted by [*Hilton et al.*, 2012]. Storms are important for transporting suspended sediment and POC in mountain catchments [*Hilton et al.*, 2008b] including in the Eastern Andes[*Townsend-Small et al.*, 2008].

7.3. Future research needs

This study underlines how important and scientifically rich the Eastern Andes are; and yet, how they remain comparatively under-studied. I have focused my thesis on monitoring river discharge, river suspended sediment and POC, and landslide activity in the Kosñipata Valley; however, there is a vast range of unanswered questions that could be considered in order to further develop this work.

Evaluating **other aspects of the montane river organic carbon cycle** would be beneficial, as measurements of course woody debris [*West et al.*, 2011] and DOC [*Moreira-Turcq et al.*, 2003] are required to fully understand river carbon transport. In the Eastern Andes draining into the Amazon, nothing is known about the transport of DOC and course woody debris. To fully quantify the non-fossil organic carbon river flux measurements of this type could be carried out at the two gauging stations, focusing on large storm events.

The future of river POC lies in monitoring **mountain carbon routing and its fate in the lowland Amazon River**. The fate of Andean soil and vegetation transported as river POC_{nf} to the Amazon lowlands could be measured in Amazon River sediment by studying riverbed cores at different distances from the Andes, to evaluate depositional rates, source,

and age of sediment. These quantitative values could be included in Amazon carbon budget. POC_{fossil} reburial and oxidation would have to be taken under consideration to produce proper estimates. As well, sediment deposits on the Amazon continental shelf in the Atlantic Ocean could be examined to consider burial rates of POC. As well, similar to approaches in other mountain settings [*Galy et al.*, 2007; *Kao et al.*, 2014], differentiation between non-fossil and fossil components could be attempted. Another avenue could be to examine leaf-wax molecules in POC, as they can help determine the altitudinal source of POC in the Amazon Basin [*Ponton et al.*, in review], based on their water isotopic signatures.

Finally, potential future work lies in the **further exploration of landslide dynamics**. First, the direct contribution from landslides to the river POC needs to be evaluated to quantify the role that landslides play in river POC. For example, detailed landslide analysis could be carried out, quantifying organic carbon content in the landslide deposits and monitoring its change over time (i.e. respired to atmosphere or transport into the river channel) and after rainfall events. As well, onsite measures of soil organic content on the steep landslide prone slopes throughout the basin would be beneficial to verify the valley-wide soil carbon stocks. Secondly, the landslide rate could be measured using a different method to test its accuracy. In chapter 5 regeneration time of forest post-landslide was determined through the use of remote sensing. Another method would be to monitor regeneration onsite visiting several recovered landslides and test the accumulation of soil carbon stocks and vegetation biomass on a chronosequence of landslides. Furthermore, dating landslide regrowth via dendrochronology or dating deposits through the use of lead-210 would be useful to obtain ages of old landslides. Finally, on a broader scope, it would be beneficial to scale up landslide work to the whole of the Eastern Andes. To do this, light detection and ranging (LiDAR) derived datasets of elevation and forest cover over several river valleys in the Eastern Andes could be used to extract landslide coverage, such as in [*van*

den Eeckhaut et al., 2007]. Then, if one assumes carbon stocks are regionally accurate, it would then be possible to estimate the carbon mobilised by landslides for the Eastern Andes.

7.4. Concluding remarks

The Eastern Andes represent a vast expanse of tropical montane forest and puna grasslands and are situated within the largest and most globally important basins in the world. Even though this tropical ecosystem has a surface area 2.5 times the size of the UK and contains a vast biodiversity hotspot with many of the world's endemic species (vascular plants, birds, amphibians, mammals, reptiles and fish) [*Myers et al.*, 2000], the Andes in the Amazon Basin have been studied by only a handful of groups [*Beck et al.*, 2008; *Malhi et al.*, 2010]. The hydrologic cycle of the Andes and Amazon is of global importance [*McClain and Naiman*, 2008] yet understanding of key aspects like river hydrology is limited. The Eastern Andes have a few functioning river gauging stations as opposed to > 1000 river gauging stations in the UK. The steep slopes of the Andes are dynamic with landslides scars predominant in the forested landscape. Little research has gone into the mapping and the study of landslides in the Eastern Andes [*Blodgett and Isacks*, 2007]. The role of landslides in ecology (species richness, soil dynamics, carbon transfer) has been completely understudied throughout the tropics [*Restrepo et al.*, 2009]. In addition to providing further insight into Andean erosional processes, it is hoped that this thesis will promote future geochemical and geomorphological studies in this unique region in South America.

7.5. References

Andermann, C., Longuevergne, L., Bonnet, S., Crave, A., Davy, P., and Gloaguen, R. (2012), Impact of transient groundwater storage on the discharge of Himalayan rivers, *Nature Geoscience*, *5*(2), 127-132, doi: http://dx.doi.org/10.1038/NGEO1356.

Beck, E., Bendix, J., Kottke, I., Makeschin, F., and Mosandl, R. (2008), *Gradients in a tropical mountain ecosystem of Ecuador*, Springer.

Blair, N. E., Leithold, E. L., Ford, S. T., Peeler, K. A., Holmes, J. C., and Perkey, D. W. (2003), The persistence of memory: The fate of ancient sedimentary organic carbon in a modern sedimentary system, *Geochimica et Cosmochimica Acta*, *67*(1), 63-73, doi: http://dx.doi.org/10.1016/s0016-7037(02)01043-8.

Blodgett, T. A., and Isacks, B. L. (2007), Landslide erosion rate in the eastern cordillera of northern Bolivia, *Earth Interactions*, *11*, 1-30, doi: http://dx.doi.org/10.1175/2007EI222.1.

Brantley, S. L., Goldhaber, M. B., and Ragnarsdottir, K. V. (2007), Crossing disciplines and scales to understand the critical zone, *Elements*, *3*(5), 307-314, doi: http://dx.doi.org/10.2113/gselements.3.5.307

Calmels, D., Galy, A., Hovius, N., Bickle, M., West, A. J., Chen, M. C., and Chapman, H. (2011), Contribution of deep groundwater to the weathering budget in a rapidly eroding mountain belt, Taiwan, *Earth and Planetary Science Letters*, *303*(1), 48-58, doi: http://dx.doi.org/10.1016/j.epsl.2010.12.032.

Crespo, P. J., Feyen, J., Buytaert, W., Bücker, A., Breuer, L., Frede, H. G., and Ramírez, M. (2011), Identifying controls of the rainfall–runoff response of small catchments in the tropical Andes (Ecuador), *Journal of Hydrology*, *407*(1), 164-174, doi: http://dx.doi.org/10.1016/j.jhydrol.2011.07.021.

Galy, V., France-Lanord, C., Beyssac, O., Faure, P., Kudrass, H., and Palhol, F. (2007), Efficient organic carbon burial in the Bengal fan sustained by the Himalayan erosional system, *Nature*, *450*(7168), 407-U406, doi: http://dx.doi.org/10.1038/nature06273.

Garcia-Martino, A. R., Warner, G. S., Scatena, F. N., and Civco, D. L. (1996), Rainfall, runoff and elevation relationships in the Luquillo Mountains of Puerto Rico, *Caribbean Journal of Science*, *32*, 413-424.

Hatten, J. A., Goñi, M. A., and Wheatcroft, R. A. (2012), Chemical characteristics of particulate organic matter from a small, mountainous river system in the Oregon Coast Range, USA, *Biogeochemistry*, 1-24, doi: http://dx.doi.org/10.1007/s10533-010-9529-z.

Hilton, R. G., Galy, A., and Hovius, N. (2008a), Riverine particulate organic carbon from an active mountain belt: Importance of landslides, *Global Biogeochemical Cycles*, *22*, BG1017, doi: http://dx.doi.org/10.1029/2006GB002905.

Hilton, R. G., Galy, A., Hovius, N., Chen, M.-C., Horng, M.-J., and Chen, H. (2008b), Tropical-cyclone-driven erosion of the terrestrial biosphere from mountains, *Nature Geoscience*, *1*(11), 759-762, doi: http://dx.doi.org/10.1038/ngeo333.

Hilton, R. G., Galy, A., Hovius, N., Horng, M.-J., and Chen, H. (2010), The isotopic composition of particulate organic carbon in mountain rivers of Taiwan, *Geochimica et Cosmochimica Acta*, *74*(11), 3164-3181, doi: http://dx.doi.org/10.1016/j.gca.2010.03.004.

Hilton, R. G., Meunier, P., Hovius, N., Bellingham, P. J., and Galy, A. (2011), Landslide impact on organic carbon cycling in a temperate montane forest, *Earth Surface Processes and Landforms*, *36*(12), 1670-1679, doi: http://dx.doi.org/10.1002/esp.2191.

Hilton, R. G., Galy, A., Hovius, N., Kao, S.-J., Horng, M.-J., and Chen, H. (2012), Climatic and geomorphic controls on the erosion of terrestrial biomass from subtropical mountain forest, *Global Biogeochemical Cycles*, *26*(3), GB3014, doi: http://dx.doi.org/10.1029/2012gb004314.

Hovius, N., Stark, C. P., and Allen, P. A. (1997), Sediment flux from a mountain belt derived by landslide mapping, *Geology*, *25*(3), 231-234.

Kao, S. J., and Liu, K. K. (2000), Stable carbon and nitrogen isotope systematics in a human-disturbed watershed (Lanyang-Hsi) in Taiwan and the estimation of biogenic particulate organic carbon and nitrogen fluxes, *Global Biogeochem. Cycles*, *14*(1), 189-198, doi: http://dx.doi.org/10.1029/1999gb900079.

Kao, S. J., Hilton, R. G., Selvaraj, K., Dai, M., Zehetner, F., Huang, J. C., Hsu, S. C., Sparkes, R., Liu, J. T., Lee, T. Y., Yang, J. Y. T., Galy, A., Xu, X., and Hovius, N. (2014), Preservation of terrestrial organic carbon in marine sediments offshore Taiwan: mountain building and atmospheric carbon dioxide sequestration, *Earth Surface Dynamics*, *2*(1), 127-139, doi: http://dx.doi.org/10.5194/esurf-2-127-2014.

Korup, O. (2006), Rock-slope failure and the river long profile, *Geology*, *34*(1), 45-48, doi: http://dx.doi.org/10.1130/G21959.1.

Larsen, I. J., and Montgomery, D. R. (2012), Landslide erosion coupled to tectonics and river incision, *Nature Geoscience*, *5*(7), 468-473, doi: http://dx.doi.org/10.1038/ngeo1479.

Lin, G.-W., Chen, H., Hovius, N., Horng, M.-J., Dadson, S., Meunier, P., and Lines, M. (2008), Effects of earthquake and cyclone sequencing on landsliding and fluvial sediment transfer in a mountain catchment, *Earth Surface Processes and Landforms*, *33*(9), 1354-1373, doi: http://dx.doi.org/10.1002/esp.1716.

Malamud, B. D., Turcotte, D. L., Guzzetti, F., and Reichenbach, P. (2004), Landslide inventories and their statistical properties, *Earth Surface Processes and Landforms*, *29*(6), 687-711, doi: http://dx.doi.org/10.1002/esp.1064.

Malhi, Y., Silman, M., Salinas, N., Bush, M., Meir, P., and Saatchi, S. (2010), Introduction: Elevation gradients in the tropics: laboratories for ecosystem ecology and global change research, *Global Change Biology*, *16*(12), 3171-3175, doi: http://dx.doi.org/10.1111/j.1365-2486.2010.02323.x.

Mayorga, E., Aufdenkampe, A. K., Masiello, C. A., Krusche, A. V., Hedges, J. I., Quay, P. D., Richey, J. E., and Brown, T. A. (2005), Young organic matter as a source of carbon dioxide outgassing from Amazonian rivers, *Nature*, *436*(7050), 538-541, doi: http://dx.doi.org/10.1038/nature03880.

McClain, M. E., and Naiman, R. J. (2008), Andean influences on the biogeochemistry and ecology of the Amazon River, *Bioscience*, *58*(4), 325-338, doi: http://dx.doi.org/10.1641/b580408.

Meybeck, M. (1993), C, N, P and S in Rivers: From Sources to Global Inputs, in *Interactions of C, N, P and S Biogeochemical Cycles and Global Change*, edited by R. Wollast, F. Mackenzie and L. Chou, pp. 163-193, Springer Berlin Heidelberg.

Moreira-Turcq, P., Seyler, P., Guyot, J. L., and Etcheber, H. (2003), Exportation of organic carbon from the Amazon River and its main tributaries, *Hydrological Processes, 17*(7), 1329-1344, doi: http://dx.doi.org/10.1002/hyp.1287.

Muñoz-Villers, L. E., Holwerda, F., Gómez-Cárdenas, M., Equihua, M., Asbjornsen, H., Bruijnzeel, L. A., Marín-Castro, B. E., and Tobón, C. (2012), Water balances of old-growth and regenerating montane cloud forests in central Veracruz, Mexico, *Journal of Hydrology, 462*, 53-66, doi: http://dx.doi.org/10.1016/j.jhydrol.2011.01.062.

Muñoz-Villers, L. E., and McDonnell, J. J. (2012), Runoff generation in a steep, tropical montane cloud forest catchment on permeable volcanic substrate, *Water Resources Research, 48*(9), W09528, doi: http://dx.doi.org/10.1029/2011WR011316.

Myers, N., Mittermeier, R. A., Mittermeier, C. G., Da Fonseca, G. A., and Kent, J. (2000), Biodiversity hotspots for conservation priorities, *Nature, 403*(6772), 853-858, doi: http://dx.doi.org/10.1038/35002501.

Ponton, C., West, A. J., Feakins, S. J., and Galy, V. (in review), Biomarkers in transit reveal the nature of fluvial integration.

Ramos Scharrón, C. E., Castellanos, E. J., and Restrepo, C. (2012), The transfer of modern organic carbon by landslide activity in tropical montane ecosystems, *Journal of Geophysical Research: Biogeosciences (2005–2012), 117*(G3), doi: http://dx.doi.org/10.1029/2011JG001838.

Restrepo, C., and Alvarez, N. (2006), Landslides and their contribution to land-cover change in the mountains of Mexico and Central America, *Biotropica, 38*(4), 446-457, doi: http://dx.doi.org/10.1111/j.1744-7429.2006.00178.x.

Restrepo, C., Walker, L. R., Shiels, A. B., Bussmann, R., Claessens, L., Fisch, S., Lozano, P., Negi, G., Paolini, L., and Poveda, G. (2009), Landsliding and its multiscale influence on mountainscapes, *Bioscience, 59*(8), 685-698, doi: http://dx.doi.org/10.1525/bio.2009.59.8.10.

Smith, J. C., Galy, A., Hovius, N., Tye, A. M., Turowski, J. M., and Schleppi, P. (2013), Runoff-driven export of particulate organic carbon from soil in temperate forested uplands, *Earth and Planetary Science Letters, 365*, 198-208, doi: http://dx.doi.org/10.1016/j.epsl.2013.01.027.

Stoyan, R. (2000), Aktivität, Ursachen und Klassifikation der Rutschungen in San Francisco/Süd Ecuador, pp, University of Erlangen-Nuremberg, Germany.

Tipper, E. T., Bickle, M. J., Galy, A., West, A. J., Pomiès, C., and Chapman, H. J. (2006), The short term climatic sensitivity of carbonate and silicate weathering fluxes: insight from seasonal variations in river chemistry, *Geochimica Et Cosmochimica Acta, 70*(11), 2737-2754, doi: http://dx.doi.org/10.1016/j.gca.2006.03.005.

Townsend-Small, A., Noguera, J. L., McClain, M. E., and Brandes, J. A. (2007), Radiocarbon and stable isotope geochemistry of organic matter in the Amazon headwaters, Peruvian Andes, *Global Biogeochemical Cycles, 21*(2), doi: http://dx.doi.org/10.1029/2006gb002835.

Townsend-Small, A., McClain, M. E., Hall, B., Noguera, J. L., Llerena, C. A., and Brandes, J. A. (2008), Suspended sediments and organic matter in mountain headwaters of the Amazon River: Results from a 1-year time series study in the central Peruvian Andes, *Geochimica et Cosmochimica Acta*, *72*(3), 732-740, doi: http://dx.doi.org/10.1016/j.gca.2007.11.020.

van den Eeckhaut, M., Poesen, J., Verstraeten, G., Vanacker, V., Nyssen, J., Moeyersons, J., van Beek, L. P. H., and Vandekerckhove, L. (2007), Use of LIDAR-derived images for mapping old landslides under forest, *Earth Surface Processes and Landforms*, *32*, 754-769, doi: http://dx.doi.org/10.1002/esp.1417.

West, A. J., Lin, C. W., Lin, T. C., Hilton, R. G., Liu, S. H., Chang, C. T., Lin, K. C., Galy, A., Sparkes, R. B., and Hovius, N. (2011), Mobilization and transport of coarse woody debris to the oceans triggered by an extreme tropical storm, *Limnology and Oceanography*, *56*(1), 77-85, doi: http://dx.doi.org/10.4319/lo.2011.56.1.0077.